VISCOSITY COEFFICIENT MEASUREMENT AND THEORETICAL INTERPRETATION FOR HYDROCARBON MIXTURES

KENNETH JOHNSTON YOUNG

A thesis submitted for the degree of

Doctor of Philosophy

of

the University of Glasgow

Department of Physical & Theoretical Chemistry,

The University,

Glasgow G12 8QQ

November, 1980

CONTENTS

TABLES

FIGURES

A C K N O W L E D G M E N T S

The author wishes to express his sincere thanks to Dr. J.H. Dymond and Dr. J.D. Isdale for their continued encouragement, support and constructive criticism throughout this work.

The experimental work at high pressure was carried out in the Properties of Fluids Division at the National Engineering Laboratory, East Kilbride. The author would like to thank the Director, N.E.L., for permission to use the facilities of the Laboratory for this work.

Support from the Chemicals and Minerals Requirements Board of Department of Industry and from Science Research Council through the C.A.S.E. awards scheme is also acknowledged.

DECLARATION

The work described in this thesis was carried out partly at the University of Glasgow and partly at the National Engineering Laboratory, East Kilbride during the period October 1976 to September 1979. It is wholly original except where otherwise indicated in the text.

Some of the results described in Chapters 4 and 5 have been published in the Journal of Chemical Thermodynamics (volume 11, 887-895, 1979) and two papers based on Chapters 3, 4 and 6 have been accepted for publication in volume IV of the International Journal of Thermophysics.

In addition some of the material has been presented at the following Conferences :

(i) Meeting of the Statistical Mechanics and Thermodynamics Group of the Chemical Society, London, April 1980.

(ii) 6th International Conference on Thermodynamics, Merseburg, August, 1980.

(iii) Joint Meeting of the European High Pressure Research Group and the High Pressure Technology Association, Amsterdam, September 1980.

SUMMARY

Accurate measurements of viscosity coefficients have been made for liquid hydrocarbon mixtures over a wide range of temperature and pressure. At saturation pressure, specially designed viscometers were used to measure the viscosity coefficient of binary, ternary and quaternary n-alkane mixtures, of binary mixtures of five n-alkane plus benzene systems and of benzene plus cyclohexane from 283 K to 393 K, with an estimated accuracy of ± 0.5 percent. At elevated pressures, a falling-body viscometer with self-centring sinker was used to measure the viscosity coefficient of n-hexane, n-hexadecane and four binary mixtures with an estimated accuracy of ± 3 percent from 298 K to 373 K at pressures up to 500 MPa or the freezing pressure. To overcome certain weaknesses in design of this instrument, a new viscometer was designed, built and tested. The accuracy of density measurement under elevated pressure was also significantly improved.

The results have been used to make a critical test of current empirical and theoretical relationships. The Hildebrand equation is shown to be valid only up to 90 MPa, and reasons for the failure of the Bertrand extension to this equation for mixtures are determined. The Grunberg and Nissan equation is found to reproduce the present data satisfactorily, provided that the constant is allowed to vary with temperature, pressure and concentration. The limitations of the rough hard-sphere theory are confirmed but a method for correlation of the data, based on this model, is shown to work successfully not only for the pure liquids but also for the mixtures over the whole density range. The results are satisfactorily expressed by a free-volume form of equation which is strongly recommended for the correlation and prediction of viscosity coefficients.

SYMBOLS AND ABBREVIATIONS

Except where specified otherwise the symbols used have the following meaning :

A	*Viscometer Calibration Constant*
B	*Viscometer Calibration Constant*
C	*Chandler Translational-Rotational Coupling Constant*
G	*Grunberg and Nissan Constant*
$\Delta^{*}G^{O}$	*Molar Gibbs Free Energy of Activation for Flow.*
$\Delta^{*}G^{E}$	*Molar Excess Gibbs Free Energy of Activation for Flow.*
H	*Relative Humidity*
K	*Bulk Modulus*
$\bar{K}$	*Secant Bulk Modulus*
L	*Length*
M	*Molecular Weight*
N	*Avogadro's Number*
P	*Pressure*
R	*Universal Gas Constant*
T	*Temperature*
T_c	*Critical Temperature*
V	*Molar Volume*
V_m^E	*Excess Molar Volume*
V_o	*Volume of Close Packing of Hard Spheres*
c_i	*Number of Carbon Atoms in Hydrocarbon Chain of Length i*
$g(\sigma)$	*Hard Sphere Radial Distribution Function at Contact*
h	*Planck's Constant*
n	*Number of Moles*
t	*time*
v_o	*Molar Volume for which Fluidity is Zero*

x	*Mole Fraction*

Subscripts

B	*Benzene*
CH	*Cyclohexane*
D	*n-Decane*
DD	*n-Dodecane*
H	*n-Hexane*
HD	*n-Hexadecane*
MD	*Molecular Dynamics*
O	*n-Octane*
P	*Pressure*
m	*Mixture*
w	*Water*

Superscript

γ	*Volume Fraction*

Greek Symbols

α	*Linear Coefficient of Compressibility of Steel*
β	*Linear Coefficient of Expansion of Steel*
η	*Dynamic Viscosity Coefficient*
η_E	*Enskog Viscosity Coefficient for Hard Spheres*
η_{RHS}	*Rough Hard Sphere Viscosity Coefficient*
η_{SHS}	*Smooth Hard Sphere Viscosity Coefficient*
η_o	*Dilute Gas Hard Sphere Viscosity Coefficient*
ρ , ρ_L	*Liquid Density*
ρ_s	*Sinker Density*
ρ_o	*Liquid Density at Atmospheric Pressure*
σ	*Hard Sphere Diameter*
η/ρ	*Kinematic Viscosity Coefficient*

C H A P T E R 1

INTRODUCTION

CHAPTER 1 - INTRODUCTION

One of the main aims of physical chemistry is the interpretation of macroscopic properties of matter in terms of the behaviour of the constituent molecules. The theory of transport phenomena in dilute gases made up of structureless spherical particles is well developed, and coefficients of diffusion, viscosity and thermal conductivity can be calculated in a straightforward manner based on the Chapman-Enskog solution of the Boltzmann equation[1]. However, detailed knowledge of the intermolecular pair potential energy function is essential for accurate results over a wide temperature range, and it is only recently that the potential energy function has been closely defined for the rare gases[2]. The position concerning mixtures is less satisfactory as even for mixtures of monatomic gases the equations for the transport coefficients become long and unwieldy[3]. The difficulties in predicting transport properties for polyatomic gases are even greater because the pair potential energy functions are not well-defined for these substances and inelastic collisions have to be considered as well as elastic collisions.

For the interpretation of transport properties of dense fluids in terms of molecular behaviour, the problem is much more complex in that account must now be taken of triple collisions, quadruple collisions, and higher many-body interactions. Only the triple collision case has been solved and then only for the simplest of molecular interactions, the hard-sphere model[4]. In addition, whereas in equilibrium theory thermodynamic properties can be expanded in a power series in the density, in the expansion of the transport coefficients it has been shown[5] that logarithmic terms appear after the linear term. For these reasons, the density expansion method cannot be used to calculate transport coeffici-

ents for dense fluids.

An alternative approach is therefore required for calculating transport coefficients of dense gases and liquids. One approximate molecular theory is the Enskog theory[6] for dense hard-sphere systems which takes into account the fact that there is an increased collision rate and also collisional transfer of flux in a dense system. This theory has been extended to binary hard-sphere mixtures by Thorne[6] and to multicomponent systems by Tham and Gubbins[7]. Real molecules are not hard-spheres, however, but Enskog showed how the theory could be applied in an ad hoc manner to real systems so that transport coefficients can be calculated for real dense gases from equation-of-state data alone. This modified Enskog Theory has been fully investigated by Hanley, McCarty and Cohen[8], and Ely and McQuarrie[9] have shown how to incorporate a theoretical equation of state to remove the need for experimental PVT data in cases where the pair potential energy function is accurately known. The disadvantages of this approach, although it leads to reasonable agreement with experimental transport property data for simple fluids at densities up to one and a half times the critical density, are that it is an ad hoc theory and that extensive accurate equilibrium data are required for the calculation. Furthermore, these modified theories are based on the Enskog expressions which are derived on the basic assumption of molecular chaos. In fact, as shown by Alder, Gass and Wainwright[10], molecular motions in a dense hard-sphere system are correlated. Dymond[11] has applied this corrected Enskog theory to real dense fluids, and shown that the predicted density dependence of the viscosity coefficient and thermal conductivity coefficient for the rare gases at a constant temperature is practically identical to that found experimentally for densities down to 1.2 times the critical density, for viscosity, and

to 0.8 times the critical density, for thermal conductivity. In the case of the diffusion coefficient where there are no extensive data for the rare gases, the density dependence of the experimental measurements on methane along an isotherm were shown to be in close agreement with the predicted values at densities down to 0.7 times the critical density. For polyatomic molecules there is the possibility of translational-rotational coupling which has been treated by Chandler[12] and forms the basis of the rough hard-sphere theory. This theory has been applied to viscosity coefficient data[13] and diffusion coefficient data[14] for benzene and tetramethylsilane with limited success. It is not possible at present to calculate the translational-rotational coupling constant, and the theory cannot be applied at high densities.

Another approach to the problem of relating transport properties to the properties of the molecules themselves is by the technique of computer simulation known as molecular dynamics which is becoming more widely used[15-20]. By this method, transport properties are calculated for a system of molecules which interact according to a given form of intermolecular pair potential energy function, which is supposed to represent the interactions of argon atoms, chlorine molecules, water molecules or whatever system is being simulated. However, the results of such computations do not represent experimental data for real systems but only provide information on the transport coefficients of systems interacting with the assumed form of intermolecular potential energy function. One further important point is that even if the computed transport coefficients were for real systems the computer time involved in such calculations is so great, especially for calculation of viscosity coefficients and thermal conductivity coefficients, that other methods of calculation and prediction are still required.

In view of the many problems associated with the exact calculation of transport properties of dense polyatomic gases and liquids and their mixtures on a molecular basis, at the present time it is only possible to correlate and predict transport coefficients for such systems using purely empirical relationships or semi-empirical relationships, that is those which have a molecular model as their basis, but which involve certain approximations in their application. Some of the most important of these relationships are discussed in Chapter 2.

In order to provide a severe test of existing expressions for viscosity coefficients of binary mixtures, it is essential that experimental measurements be made over a wide range of temperatures and pressures. Most data available at present for mixtures extends only over a very limited temperature range, generally no more than 25 K, and practically all measurements are at saturation pressure. For this reason, and to provide accurate data for the development of molecular theories of transport properties, viscosity coefficient measurements have been made from 285 K to 378 K for n-hexane plus n-hexadecane mixtures; for a three-component n-alkane mixture with n-hexane, n-octane and n-hexadecane; and a four-component n-alkane mixture with n-decane as the fourth component. Measurements were also made from 283 K to 393 K for a series of benzene plus n-alkane binary systems, where the n-alkane was n-hexane, n-octane, n-decane, n-dodecane and n-hexadecane, and for benzene plus cyclohexane. The suspended-level viscometers used for the experimental determination of kinematic viscosity were designed specially so that measurements could be made above the normal boiling point for relatively simple liquids such as benzene. The viscometer and the volume-change apparatus developed for the determination of liquid densities above 298 K are described in Chapter 3, where the results obtained for the

systems described above are presented.

Such measurements as have been made in the past on binary hydrocarbon mixtures at elevated pressures generally extend to no more than a few hundred atmospheres[21,22] but in order to provide a more critical test of mixture equations it is vital to have data over a wider range of molar volumes, by extending the measurements to much higher pressures. Some progress in this direction has been made and the n-hexane plus cyclohexane system has recently been studied from atmospheric pressure to 500 MPa at temperatures up to 373 K[23].

In this present study, the viscosity coefficients of n-hexane, n-hexadecane and four binary mixtures were measured from 298 K to 373 K up to 500 MPa using a similar falling cylinder viscometer to that designed and built by Isdale and Spence[24]. This apparatus is described in Chapter 4 and values obtained for the densities and viscosity coefficients of n-hexane, n-hexadecane and four binary mixtures are presented. During the course of operation of this viscometer, certain weaknesses in design became apparent and a new viscometer was designed, built and tested. The accuracy of density measurement under elevated pressure was also significantly improved.

The experimental data obtained in this work were used to test both the semi-empirical relationships discussed in Chapter 2, and recently recommended empirical expressions. The results of these tests are given in Chapter 6, and summarised in Chapter 7.

C H A P T E R 2

THEORIES OF VISCOSITY COEFFICIENTS FOR DENSE FLUIDS

2.1 *EXACT SMOOTH HARD-SPHERE THEORY, AND THE ROUGH HARD-SPHERE THEORY*

The simplest molecular model of a real dense fluid is an assembly of hard-spheres. This is a not unrealistic representation with regard to transport properties at high density because the attractive interactions between real molecules give a practically uniform attractive energy surface throughout the fluid and the molecules move in fairly straight lines between core collisions. The pair intermolecular potential energy function for real molecules is not infinitely steep and so in applying the hard-sphere theory it is to be expected that derived values for the molecular core size will decrease as the temperature is raised.

However, the advantage of this simple molecular theory is that transport coefficients can be treated exactly. Enskog[6] *obtained an approximate theory of transport in dense hard-sphere fluids by modifying the Boltzmann equation to take into account the importance of collisional transfer of flux and the fact that the frequency of collisions in a dense fluid is greater than in a dilute gas. The derived expression for the viscosity coefficient* η_E *in terms of the dilute gas hard-sphere value* η_o *is*

$$\frac{\eta_E}{\eta_o} = \left[\frac{1}{g(\sigma)} + 0.8\,\frac{b}{V} + 0.761\; g(\sigma) \left(\frac{b}{V}\right)^2 \right] \qquad (2.1)$$

where V *is the molar volume, and* $b = 2\pi N\sigma^3/3$ *for spheres of diameter* σ. *For the dilute gas in the first approximation*[6],

$$\eta_o = \left[\frac{5}{16\sigma^2}\right]\left[\frac{mkT}{\pi}\right]^{\frac{1}{2}} \qquad (2.2)$$

Values of $g(\sigma)$, *the radial distribution function at contact, can be determined from the Carnahan-Starling equation*[25] *which gives*

$$g(\sigma) = (1 - 0.5\xi)(1 - \xi)^{-3} \qquad (2.3)$$

where $\xi = b/4V$.

The Enskog viscosity coefficients have to be corrected for the effects of correlated molecular motions[26,27] and the exact dense hard-sphere coefficients are given with respect to the low density values by

$$\eta/\eta_o = (\eta_E/\eta_o)(\eta/\eta_E)_{MD} \qquad (2.4)$$

where $(\eta/\eta_E)_{MD}$ is the computed correction to Enskog theory[10]. In order to evaluate the transport coefficients for any given substance at conditions of known temperature and pressure, it is necessary to specify a value for the core size σ. However, Dymond[28] was able to make a comparison of experimental results with the predictions of the hard-sphere theory without prior estimation of the core size, by consideration of η^* defined as

$$\eta^* = (\eta/\eta_o)(V/V_o)^{2/3} \qquad (2.5)$$

where V_o is the volume of close-packing of hard-spheres.

On the basis of exact hard-sphere theory, values of η^* can be calculated from the above equations; they depend only on (V/V_o). Values can also be calculated from experimental data since on substitution for the hard-sphere expressions for η_o and V_o,

$$\eta^* = 6.035 \times 10^8 \, \eta V^{2/3}/(MRT)^{\frac{1}{2}}. \qquad (2.6)$$

The experimentally derived η^* values are thus a function of molar volume at constant temperature.

The applicability of this smooth hard-sphere model was tested by

superimposing plots of η^* versus log (V/V_o) from theory and η^* versus log V from experiment for a given temperature. Dymond[28] has shown that for the rare gases at any given temperature the density dependence of the viscosity coefficient found experimentally is in very close agreement with the results given by the hard-sphere theory at densities down to 1.2 times the critical density.

Values of V_o derived from the curve fitting procedure were found to decrease with increase in temperature as expected from the fact that real molecules undergo steep, but not infinitely steep, repulsive interactions.

Now for polyatomic fluids it is necessary to take into account the effects of non-spherical shape and the possibility of coupling of translational and rotational motion. The latter effect has been discussed by Chandler[12] and the viscosity coefficient for a rough hard-sphere system η_{RHS} shown to be directly proportional to a good approximation to that for a smooth hard-sphere system, η_{SHS}. Thus,

$$\eta_{RHS} \simeq C\, \eta_{SHS} \qquad (2.7)$$

where $C \geq 1$, and C is expected to be temperature and density independent. Values for C were determined by matching along isotherms, the logarithmic derivative of the experimental viscosity coefficient with respect to the density with that predicted by the theory. This approach has the serious limitation that it should not be applied at densities corresponding to V_o/V greater than 0.66, because the smooth hard-sphere system becomes metastable in this region[29]. Even at densities close to V_o/V equals 0.66 it is found[13] that the model predicts lower values for the fluidity of benzene and tetramethylsilane than are found experimentally. This was interpreted as due to a

density dependence of the core diameter. This approach is therefore only valid for the interpretation of viscosity coefficient data for liquids over a restricted density range. Even at these densities it is necessary to have viscosity coefficient data at different pressures at each temperature in order to determine the molecular core size and the translational-rotational coupling constant.

In order to correlate experimental viscosity coefficient data for a polyatomic liquid at all densities and temperatures Dymond and Brawn[30] therefore suggest that, until results of computer studies of transport properties of dense polyatomic fluids become available, a method analogous to that described above for monatomic fluids be used.

Accordingly, they defined η' as equal to $\eta V^{2/3}/(MT)^{\frac{1}{2}}$. Values for η' can thus be calculated from experimental data. For polyatomic liquids composed of spherical molecules, η' will be directly proportional to $(\eta_{SHS}/\eta_o)(V/V_o)^{2/3}$ providing that the factor C in equation (2.7) is at most only very weakly temperature dependent. Thus, η' will depend only upon V/V_o and curves of η' (or log η') versus log V for each temperature will be superimposable by adjustment along the log V axis.

Dymond and Brawn[30] found this approach very satisfactory for pseudo-spherical molecules such as carbon tetrachloride and tetramethylsilane and also for larger aspherical polyatomic liquids whose molecular shape was not expected to vary much with temperature. These results demonstrated that for a dense fluid composed of fairly rigid molecules, experimental viscosity coefficient data at different temperatures and pressures can be correlated very satisfactorily by a plot of log η' versus log V', where $V' \equiv V.V_o(T_R)/V_o(T)$. This has great practical

importance for accurate prediction of viscosity coefficient data for such fluids at any density and temperature. All that is required is the η' or log η' versus log V' curve, established from data at any one temperature, together with the atmospheric pressure viscosity coefficient and density at the temperature of interest. These curves also have theoretical significance in that they give the results in a form suitable for direct comparison with theoretical results for systems of hard rough aspherical molecules.

Furthermore, the curves illustrate the important point that the magnitude of the viscosity coefficient of a dense fluid composed of fairly rigid molecules depends upon the volume, specifically on the volume relative to some reference volume which in the case of the hard-sphere system is the close packed volume.

2.2 FREE-VOLUME THEORIES

Several relationships have been proposed between the viscosity coefficient of a fluid and the volume in which the molecules are free to move around. For example, the Batschinski equation[31], recently modified by Hildebrand[32], relates fluidity, $1/\eta$ to the relative expansion from v_o, the molar volume for which the fluidity is zero :

$$\frac{1}{\eta} = B\left(\frac{V - v_o}{v_o}\right) \qquad (2.8)$$

In this equation, the parameter v_o is a 'corresponding states fraction' of the critical molar volume and parameter B is a measure of the extent to which the external momentum that produces viscous flow is absorbed by the molecules of the liquid resulting from molecular mass, flexibility or rotational inertia. For data at atmosphere pressure at different temperatures, this expression gives a satisfactory fit provided the temperature range does not go near the freezing point[33,34]. Ertl and Dullien[35] have shown that deviations from equation (2.8) normally occur at reduced temperatures $\frac{T}{T_c}$, where T_c is the critical temperature, below 0.46.

Bertrand[36] has extended the Hildebrand equation in an attempt to enable mixture fluidity to be predicted from the fluidities of the pure components. He proposed the equation

$$\frac{1}{\eta} = (B_1V_1)^{\gamma_1}\ (B_2V_2)^{\gamma_2} \ldots \left[(x_1v_{o_1} + x_2v_{o2} + \ldots)^{-1} - (x_1V_1 + x_2V_2 + \ldots)^{-1} \right] \qquad (2.9)$$

where γ is volume fraction, V is molar volume, x is mole fraction and B and v_o are parameters in the original Hildebrand equation. This equation was limited in applicability to mixtures where the ex-

perimental temperature was above 0.46 T_c for each of the pure components and was derived from experimental results in the range of temperature 293 K to 298 K. Equation (2.9) predicted the viscosity coefficients of mixtures from the viscosity coefficients of the pure components to within 2 percent for eight of the thirteen systems studied with the mixture viscosity coefficients of the remaining five systems predicted to within an average of 4 percent.

Another empirical relationship which accurately described atmospheric viscosity coefficients of many pure liquids is the Doolittle[37] equation which can be written as :

$$\ln\eta = A + \frac{C\ V^*}{V - V^*} \qquad (2.10)$$

where A, C are constants for a given liquid and V^* was defined initially as the specific volume of the liquid extrapolated to absolute zero but later[38] was considered as another adjustable constant. This relationship has a similar form to the Cohen-Turnbull equation[39,40] derived for a hard-sphere fluid from consideration of the statistical redistribution of the free volume :

$$\ln\ (\eta/T^{\frac{1}{2}}) = A' + C'/V_f \qquad (2.11)$$

where V_f is the free volume assumed to be equivalent to a thermal expansion from a reference temperature T_o to the experimental temperature T.

The Doolittle[37] and Cohen-Turnbull[39,40] equations are equivalent when applied to viscosity coefficient data at elevated pressures by considering data at each temperature in turn. It was found[41] that an excellent fit was obtained for many liquids, although in the form of equation used the three parameters were all found to be temperature dependent.

It is of interest to compare these expressions with the exact smooth hard-sphere theory. Dymond and Brawn[30] have shown that for smooth hard-spheres η^* is a function of the reduced volume V/V_o, where V_o here refers to the volume of close packing, and that when results are plotted as log η^* vs $V_o/(V - V_o)$ a linear plot is obtained whose equation is :

$$\log \eta^* = 0.49 + 0.58 \frac{V_o}{V - V_o} \qquad (2.12)$$

which is equivalent to :

$$\ln \eta' = -0.762 + 1.335 \frac{V_o}{V - V_o} \qquad (2.13)$$

with η' defined as above, using the c.g.s. system of units with η in 10^{-4} g $cm^{-1}s^{-1}$. This has a similar form to the Doolittle and Cohen-Turnbull equations, but contains only one adjustable parameter. Dymond found that for monatomic fluids and simple polyatomic fluids such as oxygen, fluorine, ethane and propane which have been shown[42,43] to behave in respect of their viscosity coefficients as smooth hard-sphere systems rather than rough hard-sphere systems, the experimental data[44-48] are correlated very satisfactorily by this equation.

For rough aspherical molecules this equation will not be valid because of effects of non-spherical molecular shape and of translational-rotational coupling. However, since the viscosity coefficient data for such molecules at different temperatures and pressure can be correlated on the basis of a single curve in a manner analogous to that used for monatomic fluids, then this form of equation should apply. Accordingly Dymond and Brawn[30] have fitted the experimental viscosity coefficient data for certain pseudo-spherical molecules and relatively rigid ring hydrocarbons to the equation

$$\ln \eta V^{2/3}/(MT)^{\frac{1}{2}} = A + BV_o/(V - V_o) \qquad (2.14)$$

where A and B are now adjustable constants.

In order to fit the data within the estimated experimental uncertainty, it was found that A could have a range of values but when viscosity coefficient data were available up to high pressure (360 MPa) A was then given within fairly close limits. For the liquids considered A was temperature independent. Furthermore for the liquids of closely similar molecular structure namely cis- and trans-decahydronaphthalene, spiro(4,5)decane, spiro(4,5)undecane, and cis- and trans-octahydroindene, they found A had the same value of -1.0. This value also gave a good fit to the data for carbon tetrachloride and tetramethylsilane, but for perhydrochrysene A was definitely positive.

Values of B were temperature independent and very similar for the bicyclic ring hydrocarbons. Equation (2.14) is worthy of further investigation as to its effectiveness in representing liquid viscosity coefficient data for polyatomic molecules at elevated pressures.

2.3 EYRING ACTIVATION MODEL AND THE THEORY OF CONGRUENCE

Eyring[49] has considered the problem of transport processes in dense fluids based on the theory of absolute reaction rates.

This theory is based on the assumption that in a pure liquid at rest the individual molecules are constantly in motion but because of close packing the motion is largely confined to vibration of each molecule within a 'cage' formed by its nearest neighbours. The 'cage' is represented by a potential energy barrier of height $\Delta^* G^o$ where $\Delta^* G^o$ is the molar free energy of activation. Eyring[49] has suggested that a liquid at rest continually undergoes rearrangement in which one molecule at a time escapes from its 'cage' into an adjoining hole. In a fluid which flows the frequency of molecular rearrangements is increased. For Newtonian flow the coefficient of viscosity is given[50] by the expression

$$\eta = \left(\frac{\delta}{a}\right)^2 \frac{Nh}{V} \exp\left[\Delta^* G^o/RT\right] \qquad (2.15)$$

where a is the distance travelled per jump, δ is the distance between separate layers, N is Avogadro's number, h is the Planck constant, R is the gas constant, V is the molar volume and T the temperature. Theories such as this suffer from the criticism that they introduce one or more constants which cannot be calculated from molecular data, but which may be related to macroscopic properties. In this theory (δ/a) is often taken as unity, and $\Delta^* G^o$ is empirically found[51] to be about forty percent of the internal energy of vaporisation of the liquid. This equation predicts a linear dependence of the logarithm of the viscosity coefficient on reciprocal temperature as is found experimentally in many cases. However, as shown recently by Hildebrand and Alder[52] it is not necessary to assume an activation model to derive a linear

relationship between ln η and reciprocal temperature. Indeed computer simulation studies[53] on simple molecular models have shown that the underlying assumption of diffusion as occurring by a small number of jumps is in fact incorrect and that there is a co-operative motion with a large number of small molecular displacements.

Nevertheless, this approach is of great interest in that it can be readily extended to mixtures. If the ideal viscosity of a mixture is defined by

$$\Delta^* G^{ideal} = \Sigma_i x_i \Delta^* G_i \qquad (2.16)$$

then a molar excess Gibbs free energy of activation for flow, $\Delta^* G^E$, which is given by

$$\Delta^* G^E = \Delta^* G - \Delta^* G^{ideal} \qquad (2.17)$$

can be derived from experimental viscosity coefficient data, according to :

$$\Delta^* G^E = RT \left[\ln(\eta V) - \Sigma_i x_i \ln(\eta_i V_i) \right]. \qquad (2.18)$$

This expression has been used by various workers[54,55] in the description of mixture viscosity. Coursey and Heric[56] have suggested that the principle of congruence originally proposed by Bronsted and Koefoed[57] for the molar excess Gibbs free energy of mixing can be applied to the molar excess Gibbs free energy of activation for flow and used to predict viscosity coefficients for n-alkane mixtures at 298 K knowing the viscosity coefficients of the pure components at the same temperature.

C H A P T E R 3

VISCOSITY COEFFICIENTS AND DENSITIES FOR HYDROCARBONS AND HYDROCARBON MIXTURES AT SATURATION PRESSURE

3.1 INTRODUCTION

Newton[58] in 1685 proposed that an internal resistance to flow is present in liquids when relative motion exists between the particles of the liquid. This can be expressed as :

$$F = \eta A\left(\frac{dv}{dz}\right) \qquad (3.1)$$

where A is the area of contact of two liquid laminae and F is the force necessary to maintain a velocity gradient (dv/dz) between these laminae. η is a characteristic constant for each liquid and is called the coefficient of viscosity. However, it was not until 1842 and the exacting studies of Poiseuille[59] on the flow of liquids through capillary tubes that a firm understanding of liquid flow through such tubes was established.

In 1923 the British Standards Institution published its first British Standard Method for the Determination of the Viscosity of Liquids and since then four revised editions have been published. Various methods of determining the viscosity of liquids have been devised but the British Standards Institution is concerned with only two of these methods which are based on

(a) the resistance to motion of a liquid passing through the capillary of a glass viscometer, and

(b) the resistance to motion of a sphere falling through a liquid.

Since the method using the falling sphere is suitable only for liquids with a kinematic viscosity of 2000 $mm^2\ s^{-1}$ and upwards the method using capillary glass viscometers was adopted for this research on hydrocarbons and hydrocarbon mixtures at saturation pressure. However, since the object of this research was to measure viscosity coefficients

of pure liquids and mixtures over a wide temperature range, extending the measurements above the normal boiling point the viscometers described in the present British Standards Institution publication[60] are unsuitable. They require suction to fill the measuring section and are open to the atmosphere, both of which limit the temperature range which can be studied if boiling and change in liquid mixture composition due to evaporation of the more volatile component are to be avoided.

These problems can be overcome by having a closed system. To return the liquid to its original position to make measurements of flow times, hydrogen can be admitted at a slight excess pressure[61] but in order to overcome the possibility of solution of gas in the liquids, an alternative procedure whereby the closed viscometer could be simply inverted and then returned to its original position was preferred.

Of the various types of viscometers described in the British Standards Institution publication[60] the suspended level viscometer, type BS/IP/SL, was chosen as being most suitable for adapting to the present needs. A diagram of this viscometer and the modified version used in this research are shown in Figure 3.1.

The main difference between the British Standards Institution design and the present one is that limb L used for charging the viscometer has been discarded and limbs N and M joined to enable viscosity coefficients to be measured under saturated vapour pressure. The modified viscometer is charged through limb M and sealed by means of an S13 Rotaflo tap. A fuller description of the modified suspended level viscometer and the method of operation is given in Section 3.2. In

all 11 of these modified viscometers were constructed and ready for use.

Kestin, Sokolov and Wakeham[62] *have recently re-examined the theory of the capillary viscometer to create a rigorous foundation for the accurate evaluation of recent precise measurements on the kinematic viscosity coefficients of water*[61,63]*, and to provide easily accessible improved working formulae. Their final working formula is of*

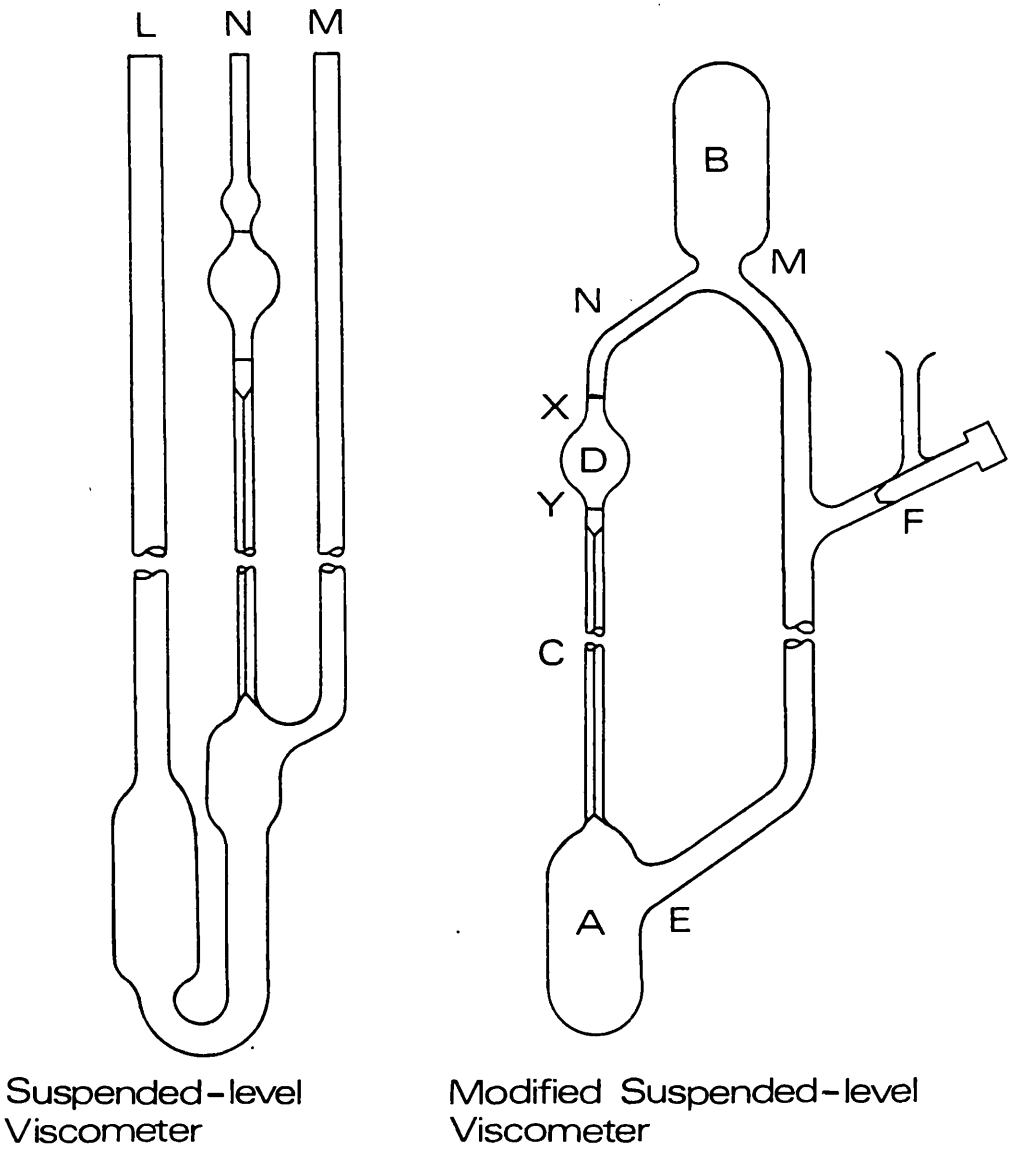

Figure 3.1 Comparison between the British Standards Institution Suspended-level Viscometer and the Modified Version used in this Research.

the form

$$\eta = \frac{\pi a^4 \rho}{8(L + na)} \left[\frac{\Delta p}{\dot{m}} - \frac{m_o \dot{m}}{\rho \pi^2 a^4} \right] \qquad (3.2)$$

where a is capillary radius, ρ is liquid density, L is the capillary length, m_o and n are constants which arise due to an attempt to take into account the complex conditions which exist at the inlet to the capillary and $\dot{m}$ is the mass flow rate. The factor (L + na) was first suggested by Couette[64] on an entirely experimental basis. Whereas previously[65,66] values for n and m_o were determined from experiment, Kestin, Sokolov and Wakeham[62] were able to calculate values for liquid flow in square ended capillaries at Reynolds numbers from 0.5 to 100. With the arrangement considered by Kestin, Sokolov and Wakeham[62], it is therefore possible to obtain absolute values for viscosity coefficients. However, the experimental arrangement considered in this research does not correspond to this ideal situation and so, in common with most recent experimenters[67,68], the corrections were grouped together and the following general formula was used.

$$\eta/\rho = A(1 - \rho_v/\rho)(1 + \alpha\Delta T)t - B/t^n \qquad (3.3)$$

where A and B are apparatus constants for a particular viscometer, ρ_v and ρ are densities for vapour and liquid respectively and α is the coefficient of linear expansion of glass. ΔT is the difference between the experimental temperature and a reference temperature taken as 313 K. The value of n depends on whether the Couette correction factor is a constant when n = 1, or a function of Reynolds number[69,70], when it has the value 2. In this work it has been assigned the value 1. In using equation (3.3), it is assumed that surface tension effects balance[67,68,71,72]. A recent paper[73] has made a new analysis of the factors affecting the driving head within a capillary

viscometer and concluded that errors of a few parts of a percent may arise by neglect of surface tension corrections, when a viscometer is calibrated with water and then used for measurements of viscosity coefficients of organic liquids. However, there are uncertainties in determining one of the surface tension terms, the magnitude of the effect depends on the shape of the viscometer bulb, and the analysis itself was for a non volatile liquid. For these reasons, plus the absence of organic liquid standards for which the viscosity coefficient, surface tension and density are accurately known, equation (3.3) has been used for the kinematic viscosity coefficient. The viscometers were calibrated with organic liquids with accurately known kinematic viscosity coefficients as described in Section 3.2.6.

Since the viscometers measure kinematic viscosity coefficients separate determinations of density have to be made to enable dynamic viscosity coefficients to be calculated. An apparatus which measures the change in liquid volume caused by a change in temperature was developed to obtain densities at temperatures above ambient temperature. The design and method of use are described in Sections 3.3.4 and 3.3.5.

For accurate values of kinematic viscosity coefficients and densities to be obtained it is essential that the liquids used are of the highest purity possible. A list of the liquids used in this research, together with their source and purity, and a comparison with recent literature values of density and refractive index at 298.15 K, are given in Section 3.4.1.

3.2 MEASUREMENT OF KINEMATIC VISCOSITY COEFFICIENTS

Standard capillary viscometer techniques were used whereby the time for a definite volume of liquid to flow through a capillary tube was measured under an accurately reproducible head of liquid and at a closely controlled temperature. Kinematic viscosity coefficients were calculated after first determining the apparatus constants A and B for a particular viscometer as described in Section 3.2.6. In order to make viscosity coefficient measurements in the range 283 K to 393 K viscometers were developed which completely enclosed the liquid or liquid mixture under study. This ensured that the composition of the liquid did not change appreciably at the higher temperatures as would be the case if the viscometer was open to the atmosphere. Furthermore, it also allowed viscosity coefficient determinations to be made above the normal boiling point, and eliminated the possibility of solution of gas at higher pressure in the liquid as occurs in other measurements[61].

A diagram of the viscometer is shown in Figure 3.1. The viscometer consisted of two reservoir bulbs A and B of 15 cm^3 capacity connected on one side by a measuring section consisting of a capillary C, made from precision bore Veridia tubing and bulb D, whose volume depended on the size of the capillary bore. Two circular marks X and Y were etched on the glass above and below this bulb and these marks defined an exact volume for timing. Reservoirs A and B were connected on the other side by a side arm and filler section and sealed by an S13 Rota-flo tap F. This tap was capable of withstanding internal pressures of about four to five atmospheres before the seal between the tap and the glass was broken and vapour escaped. Care was taken during manu-

facture to ensure that the capillary tube opened smoothly in a bell shape into the bulbs at either end, and that the straight section of tubing above the bulb D was long enough to allow the liquid meniscus to reach a constant velocity before passing mark X. The glass tubing at the entry to and exit from this bulb had the same diameter to minimise surface tension effects. The viscometers were made in the University Glass Blowing workshops and three different capillary bore sizes and measuring volume D were used in the construction. In all a total of eleven viscometers, the important dimensions of which are given in Table 3.1, were calibrated and available for use.

The viscometer bath could hold two viscometers and it was usual to make measurements on a given mixture using two viscometers of different dimensions to obtain a more reliable estimate of the precision of the kinematic viscosity coefficients. Flow times for a particular viscometer were found to be reproducible to $\pm$ 0.1 percent.

Table 3.1

Characteristics of the Viscometers Used

Viscometer number	Calibration range ($mm^2 s^{-1}$)	Capillary bore (mm)	Capillary length (mm)	Volume D (cm^3)
1	1.15 - 3.97	0.61	55	6
2	1.15 - 3.97	0.61	55	6
3	0.46 - 3.97	0.50	75	9
4	0.46 - 3.97	0.50	55	9
5	0.46 - 3.97	0.50	75	9
6	0.46 - 3.97	0.50	55	9
7	0.46 - 1.82	0.30	115	2
8	0.46 - 1.82	0.30	115	2
9	0.46 - 3.97	0.30	115	2
10	0.46 - 1.82	0.30	115	2
11	0.46 - 1.82	0.30	115	2

3.2.1. Cleaning the Viscometers

Scrupulous cleanliness of the apparatus was essential for consistent results. The viscometers were initially cleaned by filling with chromic acid and leaving for two hours at 298 K. They were then rinsed several times with freshly distilled water followed by two rinses with AnalaR acetone, and drying was accelerated by evacuating the viscometers on a vacuum line. Between viscosity coefficient experiments the viscometers were given two rinses with petroleum ether followed by three rinses with AnalaR acetone and dried as before. During initial experiments problems were encountered with small wool or tissue fibres being lodged in the capillary bore, but this was overcome by filtering all liquids entering the viscometer through a millipore syringe filter. The above procedure ensured that previous solvents, grease and dust were removed from the apparatus.

3.2.2 Preparation of Mixtures

Mixtures were made up as follows. The volumes of the components required to make up a total volume of about 75 cm^3 of mixture of given composition were calculated from values for the densities at room temperature and one of the constituents was run from a burette into a bottle of known weight which was then stoppered and weighed. The second component was added to the bottle from a burette, and the bottle again stoppered to prevent evaporation losses. (For ternary and quaternary mixtures, additional components were added, and the weight taken). The total weight was recorded and the exact mole fraction calculated from the weight of the constituents. The total volume of liquid in the bottle was such that there was only a small vapour space remaining in the bottle. The pyknometer, volume change apparatus and viscometers were filled within ten minutes of making up the mixture.

In this way any slight change in the composition of the mixture transferred to the experimental apparatus was minimised.

3.2.3 Filling the Viscometers

To commence an experiment the viscometers were filled with a suitable volume (approximately 10 cm^3) of specially prepared liquid or liquid mixture using a 20 cm^3 syringe fitted with a millipore syringe filter to prevent dust particles entering. When filling the viscometers, care was taken to ensure that the liquid level in the reservoir bulb A was below the side arm entrance E when the viscometer was in the position shown in Figure 3.1 so that during an experiment the liquid flow would depend only on the head of liquid.

To enable flow time measurements to be made under saturated vapour pressure most of the air in the viscometers was removed as follows. The liquid in the viscometer was first cooled to 273 K by immersion of the viscometer in an ice/water slurry. This reduced the vapour pressure to a low level. The viscometer was then attached to a vacuum line and the vacuum pump isolated. The viscometer tap was opened for two seconds and then closed, the line re-evacuated and the procedure repeated. The change in mixture composition was minimised by cooling, and isolation of the vacuum pump when opening the viscometer tap.

3.2.4 Measurement and Control of Temperature

Two Townson and Mercer Bridge Controlled Thermostat Baths, E 270 Series 3, were used to cover the temperature range from 283 K to 393 K. Bath 1, containing distilled water, was used in the range of temperature 283 K to 368 K, with a refrigeration unit used for temperatures below

293 K. Bath 2 was filled with Shell Risella 33 oil and used in the temperature range 333 K to 393 K. The temperature control was rated as $\pm$ 0.01 K. Temperature in the range 293 K to 378 K was measured by one of two Total Immersion Zeal mercury-in-glass thermometers which had been calibrated at the National Physical Laboratory, Teddington, England. They were graduated every 0.1 K and temperatures could be estimated to 0.02 K using an eyepiece. The maximum calibration correction to be applied was at 333.15 K where the temperature indicated was 0.15 K less than the corrected temperature. (The calibration corrections over the range 298 K to 378 K were the same for both thermometers to within 0.01 K). A total immersion bomb calorimeter thermometer was used for temperatures below 293 K. This was graduated every 0.01 K and temperatures could be estimated to 0.002 K. This thermometer was compared with one of the Zeal thermometers and agreed to within 0.02 K at 283.15 K and 288.15 K. At 393 K a total immersion alcohol thermometer was used which was graduated every 0.2 K and temperatures could be estimated to 0.05 K. This thermometer was found to agree with the Zeal thermometers at 373.18 K to within 0.05 K.

With a total immersion thermometer the entire liquid column should be immersed in the medium such that the top of the mercury column is just visible above the surface of the medium. However, due to the experimental arrangement as shown in Figure 3.2 this was not possible as the mercury meniscus had to be just above the bath lid to enable accurate readings of temperature to be made using an eyepiece. This necessitated emergent stem corrections to the temperature read and these were calculated in the standard way[74]. They range from 0.00 K at 298.19 K to + 0.11 K at 378.18 K. Table 3.2 presents the difference between the observed thermometer reading and the actual temperature. Between

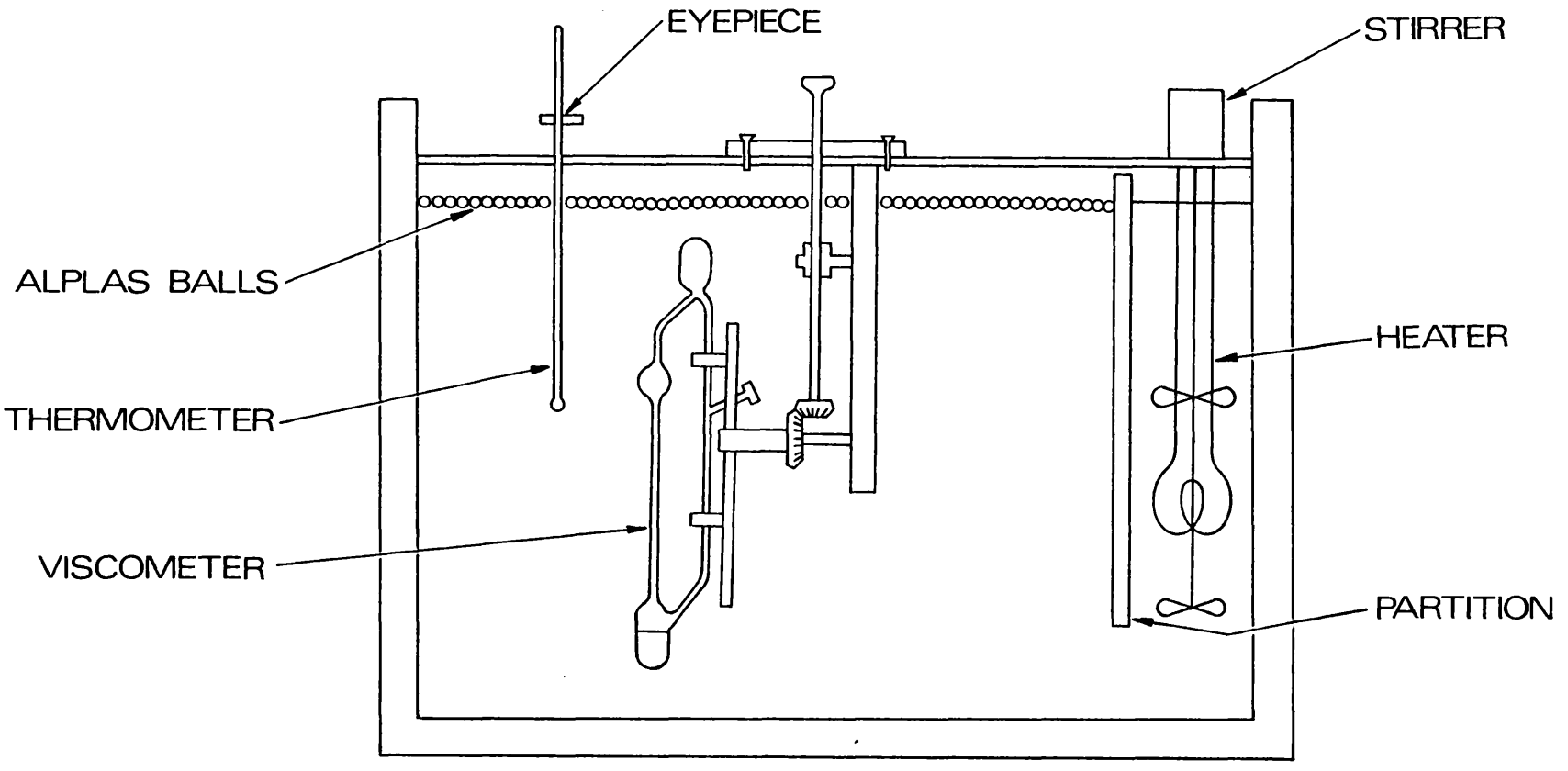

Figure 3·2 Constant Temperature Bath and Viscometer Assembly.

283.15 K and 373.28 K a reliable estimate of the uncertainty of a temperature reading is ± 0.02 K.

From temperature measurements in different regions of the thermostat baths it was found that the temperature was constant to within the estimate of ± 0.02 K in this range. It was not possible to detect fluctuations less than this with the Zeal thermometers.

Table 3.2

Corrected Temperatures for Zeal Thermometers

Thermometer reading (K)	Calibration graph corrected temperature (K)	Emergent stem correction (K)	Actual temperature (K)
298.15	298.19	0.00	298.19
303.15	303.19	0.01	303.20
308.15	308.20		308.21
313.15	313.21	0.02	313.23
318.15	318.23		318.26
323.15	323.25	0.04	323.29
328.15	328.28		328.33
333.15	333.30	0.06	333.36
338.15	338.29		338.36
343.15	343.26	0.07	343.33
348.15	348.23		348.30
353.15	353.21	0.08	353.29
358.15	358.20		358.28
363.15	363.19	0.09	363.28
368.15	368.18		368.27
373.15	373.18	0.10	373.28
378.15	378.18	0.11	378.29

3.2.5 Measurement of Flow Time

Each constant temperature bath was capable of having two viscometers operating simultaneously so during kinematic viscosity coefficient determinations two viscometers with different capillary bore sizes were used. The viscometers were mounted on stands which were attached to the bath lid and these allowed free rotation of the viscometers in the bath. The experimental arrangement is shown in Figure 3.2. Before measurements were made sufficient time was allowed to elapse for thermal equilibrium to be established. This generally took about thirty minutes. To start a run the viscometer was first inverted to fill the top reservoir bulb and then returned to the position shown in Figure 3.1 where the liquid fell under gravity into bulb D. As the liquid meniscus was falling towards the mark X the viscometer was vertically aligned by means of a plumb line using two cathetometers at right angles to each other. In the vertical position the top of the viscometer was 2 cm to 3 cm below the bath liquid surface.

The time taken for the liquid meniscus to move from the mark X above bulb D to the lower mark Y was measured to the nearest 0.1 s using a Junghaus stop watch or a Racal Instruments Universal Counter 9835. Periodically both the counter and the stopwatch were used to record the flow time and a comparison of the times showed agreement to within 0.2 s.

Initial flow times for a particular viscometer very occasionally differed by more than 0.1 percent which generally indicated that thermal equilibrium had not yet been established. Flow time readings were recorded when three successive determinations agreed to within $\pm$ 0.1 percent of their mean. Since flow times were measured for two viscometers simul-

taneously, kinematic viscosity coefficient results quoted are the average of the results from two viscometers with different capillary bore sizes.

3.2.6 Viscometer Calibration

In order to calibrate the viscometers, pure liquids were required whose kinematic viscosity coefficients were accurately known, preferably over a wide range of temperature.

The magnitude of the kinematic viscosity coefficients had to be such as to cover the range of values likely to be obtained with the mixtures to be investigated.

Problems were encountered using water in the viscometers because of surface tension effects and so benzene, cyclohexane, n-dodecane and n-hexadecane were used as the calibration liquids. Values for the kinematic viscosity coefficients of these liquids are available in API 44 tables[75] produced by the American Petroleum Institute, but recent measurements on n-hexane[68] cast some doubt on the accuracy of these values. It was therefore decided to measure the kinematic viscosity coefficients for these liquids in a Master Viscometer. The viscometer, a Technico BS/IP/SL/MV number 2511, had a capillary bore of 0.38 mm and a capillary length of 40 cm. It was calibrated with freshly distilled water at 298.11 K and 333.14 K.

At 298.15 K and 333.15 K the National Bureau of Standards[76,77] recommended values of dynamic viscosity coefficients are 0.8903 mPa s and 0.4666 mPa s. More recent effort towards the establishment of standard values of well defined accuracy has been made under the guid-

ance of the International Association for the Properties of Steam[78,79]. In particular, a consensus of experimental evidence and opinion with regard to the viscosity of water at 293.15 K and a pressure of 0.1 MPa has led to the recommendation that the value η(293.15 K) = 1.0020 mPa s be adopted as a standard[78,80,81]. It is adjudged that this standard value has an accuracy of 0.1 percent. In the case of viscosity coefficient data at low pressure and other temperatures the recommended correlation[78] has been based on a number of extremely precise recent measurements in the range 273.15 K to 373.15 K[61,63,77,82]. The raw data from the most precise of these by Korson, Drost-Hansen and Millero[63] in the range 283.15 K to 343.15 K and Eicher and Zwolinski[82] in the range 264.87 K to 313.15 K has recently been re-analysed by Kestin, Sokolov and Wakeham[72] in an effort to derive the maximum benefit from the precision of these measurements. Kestin, Sokolov and Wakeham[72] obtain values of 0.889 mPa s and 0.467 mPa s at 298.15 K and 333.15 K using reference (63) data and a value of 0.8902 mPa s at 298.15 K using reference (82) data. Using values for the density of water of 997.0751 kg m^{-3} at 298.15 K and 983.24 kg m^{-3} at 333.15 K, they obtain kinematic viscosity coefficients of 0.892 mm^2 s^{-1} and 0.475 mm^2 s^{-1} at 298.15 K and 333.15 K respectively using reference (63) data and 0.8928 mm^2 s^{-1} at 298.15 K using reference (82) data. The values 0.8928 mm^2 s^{-1} and 0.475 mm^2 s^{-1} were used to calibrate the Master Viscometer.

The Master Viscometer has been designed such that flow times are sufficiently long to make the B/t term in equation (3.3) insignificant relative to At. Flow times for freshly distilled water together with the calibration constant obtained from equation (3.3) are given in Table 3.3.

Table 3.3

Master Viscometer Calibration

Temperature (K)	*Flow time (s)*	η/ρ $(mm^2\ s^{-1})$	A $(mm^2\ s^{-2})$
298.11	*470.0*		
	470.1		
	469.8		
	470.1		
average	*470.0*	*0.8928*	*0.0019019*
333.14	*250.0*		
	250.4		
	250.0		
	250.1		
average	*250.1*	*0.475*	*0.0019011*

The table shows that for flow times of 250 s and 470 s the values of A derived at the two temperatures agree to within 0.04 percent. This confirms that for flow times of 250 s and above any errors in η/ρ *introduced by ignoring the B/t term will be less than 0.04 percent. The value 0.0019015* $mm^2\ s^{-2}$ *was taken for A.*

Measurements were made of the flow times for the calibration liquids benzene, cyclohexane, n-dodecane and n-hexadecane. The source and purity of these liquids together with a comparison with literature densities and refractive indices at 298.15 K is given in Section 3.4.1. Flow times for these liquids in the Master Viscometer were measured at 298.12 K and 333.14 K for benzene and cyclohexane and at 298.12 K and 313.14 K for n-dodecane and n-hexadecane. The experimental results are given in Table 3.4. The table also gives kinematic viscosity coefficients calculated from average flow times using the value of A

Table 3.4

Comparison of the Experimental Kinematic Viscosity Coefficients of the Calibration Liquids with Reference (75)

Liquid	Temperature (K)	Flow time (s)	Average flow time (s)	η/ρ ($mm^2 s^{-1}$)	Ref (75) η/ρ ($mm^2 s^{-1}$)	Δ* (percent)
Benzene	298.12	363.7	363.8	0.6906	0.6878	0.41
		363.9				
		363.7				
		363.8				
	333.14	245.6	245.8	0.4662	0.466	0.04
		245.7				
		246.0				
		245.8				
		245.7				
c-hexane	298.12	610.6	610.6	1.1591	1.157	0.18
		610.6				
		610.8				
		610.5				
	333.14	376.7	376.9	0.7149	0.712	0.41
		376.9				
		376.9				
		377.1				
n-dodecane	298.12	959.1	960.6	1.8240	1.843	-1.04
		961.4				
		963.5				
		961.0				
		959.3				
		959.3				
	313.14	760.7	761.0	1.4450	1.465	-1.38
		761.1				
		761.4				
n-hexadecane	298.11	2092.7	2092.6	3.9735	4.008	-0.87
		2092.6				
	313.14	1537.1	1536.5	2.9175	2.953	-1.22
		1536.6				
		1535.9				

*$\Delta = 100 \left(\frac{\text{expt.} - \text{ref.}}{\text{expt.}}\right)$

given above and compares these results with values given in API 44[75] tables.

For benzene and cyclohexane at these temperatures the agreement with the API 44[75] tables is within the combined estimated uncertainties. There is significant disagreement in the case of n-dodecane and n-hexadecane however, the API 44[75] values being higher by 1.1 percent on average. A similar discrepancy exists between the results of Eicher and Zwolinski[68] for n-hexane and the API 44[75] values at temperatures around 313 K. Further support for the present results is given by Heric and Brewer[54] who obtained a value of 3.9723 $mm^2 s^{-1}$ for the kinematic viscosity coefficient of n-hexadecane at 298.15 K.

Using the kinematic viscosity coefficients determined in the Master viscometer, the apparatus constants for the eleven viscometers were determined from flow time measurements on the same four hydrocarbon liquids at the same temperatures. The calculation of the optimum A and B values for each viscometer was performed on a Univac computer using a least squares linear regression program written for this purpose. The values of A and B for each viscometer together with the calculated kinematic viscosity coefficients and a comparison with the kinematic viscosity coefficients obtained from the Master Viscometer are given in Table 3.5. The agreement with the Master Viscometer values is generally within 0.3 percent, and the deviations appear to be random as shown in Figure 3.3. From this is concluded that provided the viscometers are used for liquids whose kinematic viscosity coefficients fall within the limits given, the results obtained using values for the apparatus constants A and B given in Table 3.5 should be accurate to within $\pm$ 0.5 percent.

Table 3.5

Viscometer Calibration and Comparison of Kinematic Viscosity Coefficients with Master Viscometer Values

Viscometer number	Calibration liquid	Temperature (K)	Average flow time (s)	η/ρ ($mm^2\ s^{-1}$)	$\Delta^{\neq}$ (percent)	$A \times 10^3$ ($mm^2\ s^{-2}$)	B (mm^2)
1	n-hexadecane	298.19	477.1	3.9766	+0.12	8.355	4.607
		313.23	350.7	2.9170	+0.02		
	n-dodecane	298.19	220.6	1.8223	-0.06		
		313.23	176.0	1.4443	-0.02		
	c-hexane	298.19	142.7	1.1593	+0.05		
2	n-hexadecane	298.19	458.1	3.9756	+0.08	8.700	4.581
		313.23	337.1	2.9193	+0.10		
	n-dodecane	298.19	211.8	1.8211	-0.12		
		313.23	169.1	1.4441	-0.03		
	c-hexane	298.19	137.2	1.1596	+0.08		
3	n-hexadecane	298.19	1374.4	3.9798	+0.18	2.898	4.410
		313.23	1007.7	2.9159	-0.02		
	n-dodecane	298.19	631.5	1.8231	-0.01		
		313.23	501.5	1.4445	-0.01		
	c-hexane	298.19	403.6	1.1580	-0.06		
		333.36	253.3	0.7151	+0.06		
	benzene	298.19	244.2	0.6893	-0.16		
		333.36	170.0	0.4658	-0.03		
4	n-hexadecane	298.19	1413.0	3.9787	+0.16	2.819	5.811
		313.23	1039.3	2.9239	+0.25		
	n-dodecane	298.19	650.2	1.8238	+0.02		
		313.23	516.1	1.4435	-0.08		
	c-hexane	298.19	416.1	1.1582	-0.04		
		333.36	261.5	0.7134	-0.19		
	benzene	298.19	252.4	0.6880	-0.33		
		333.36	177.5	0.4667	+0.16		
5	n-hexadecane	298.19	1545.3	3.9821	+0.24	2.580	7.065
		313.23	1134.0	2.1914	+0.10		
	n-dodecane	298.19	709.7	1.8210	-0.13		
		313.23	564.4	1.4436	-0.07		
	c-hexane	298.19	455.2	1.1581	-0.05		
		333.36	287.4	0.7154	+0.09		
	benzene	298.19	277.0	0.6887	-0.23		
		333.36	195.0	0.4660	0		
6	n-hexadecane	298.19	1313.4	3.9765	+0.10	3.031	6.402
		313.23	967.0	2.9247	+0.28		
	n-dodecane	298.19	604.9	1.8231	-0.02		
		313.23	480.0	1.4417	-0.20		
	c-hexane	298.19	387.7	1.1580	-0.06		
		333.36	244.8	0.7144	-0.13		
	benzene	298.19	236.5	0.6895	-0.12		
		333.36	166.7	0.4661	+0.02		
7	n-dodecane	296.19	1509.9	1.8258	+0.13	1.209	-0.467
		313.23	1195.5	1.4457	+0.08		
	c-hexane	298.19	956.5	1.1562	-0.22		
		333.36	590.7	0.7134	-0.18		
	benzene	298.19	571.5	0.6915	+0.15		
		333.36	384.9	0.4658	-0.06		
8	n-dodecane	298.19	1688.9	1.8235	+0.01	1.079	-0.984
		313.23	1338.6	1.4455	+0.07		
	c-hexane	298.19	1073.0	1.1583	-0.03		
		333.36	662.6	0.7152	+0.06		
	benzene	298.19	637.6	0.6884	-0.14		
		333.36	430.2	0.4658	+0.06		
9	n-hexadecane	298.19	3865.6	3.9579	-0.36	1.024	0.5174
		313.23	2846.3	2.9142	-0.08		
	n-dodecane	298.19	1781.3	1.8236	+0.01		
		313.23	1413.8	1.4472	+0.19		
	c-hexane	298.19	1137.1	1.1631	+0.38		
		333.36	700.4	0.7149	+0.02		
	benzene	298.19	674.9	0.6899	-0.06		
		333.36	456.4	0.4654	-0.14		
10	n-dodecane	298.19	1764.8	1.8229	-0.03	1.033	-0.377
		313.23	1399.8	1.4460	+0.10		
	c-hexane	298.19	1123.1	1.1696	+0.07		
		333.36	692.4	0.7142	+0.08		
	benzene	298.19	667.2	0.6893	-0.15		
		333.36	451.2	0.4660	+0.01		
11	n-dodecane	298.19	1701.0	1.8276	+0.22	1.074	-2.173
		313.23	1345.8	1.4466	+0.14		
	c-hexane	333.36	662.6	0.7132	-0.22		
	benzene	298.19	637.6	0.6877	-0.39		
		333.36	430.8	0.4668	+0.16		

$\neq$ Reference values taken as the Master Viscometer values in Table 3.4, $\Delta = 100\ (\frac{\text{expt.} - \text{ref.}}{\text{expt.}})$

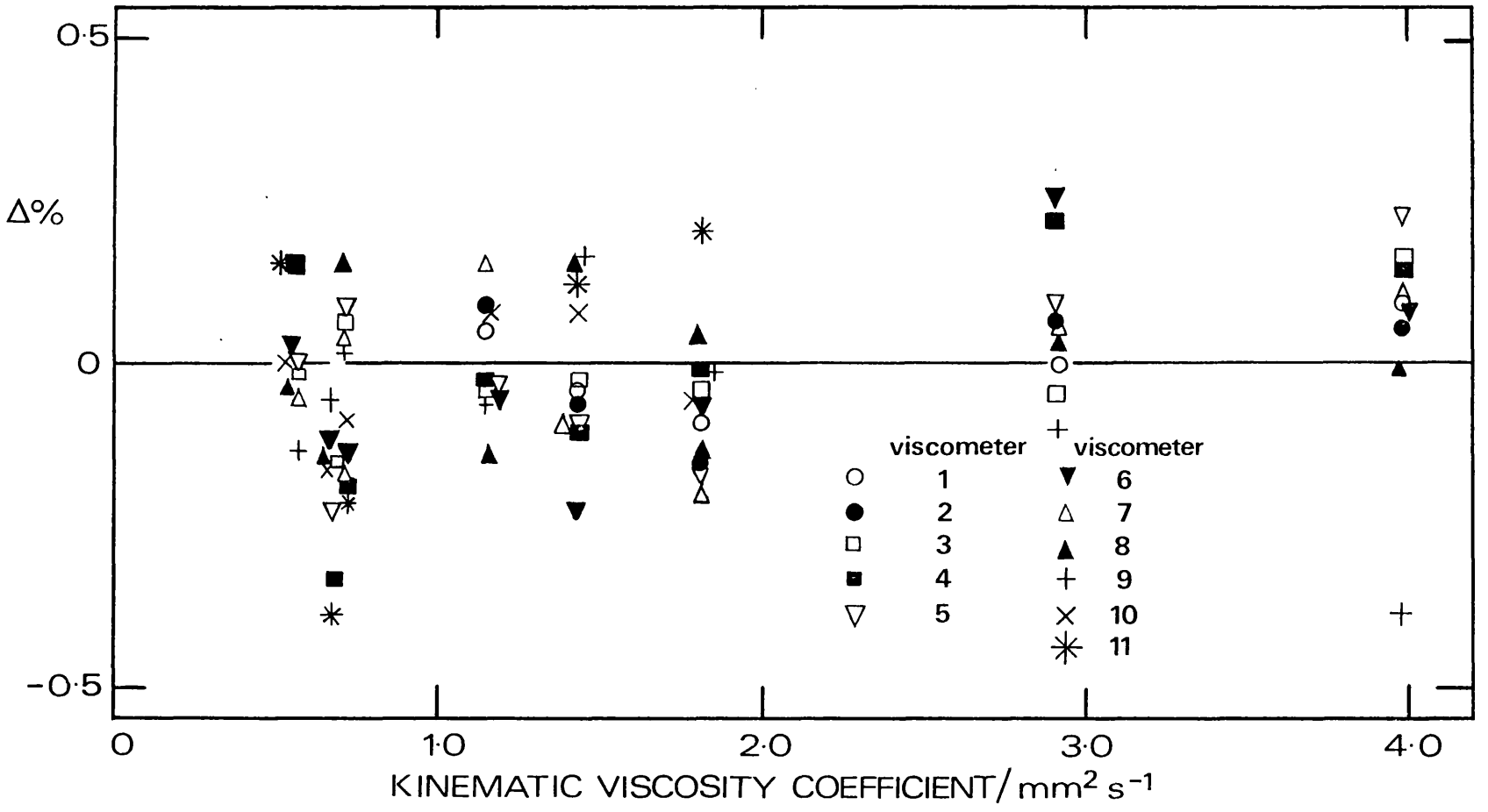

Figure 3.3 Deviation of the Kinematic Viscosity Coefficients Measured using the Saturation Pressure ***Viscometers*** *from the Values Measured using the Master Viscometer.*
$\Delta = 100\ [((\eta/\rho)_{SPV} - (\eta/\rho)_{MV})/(\eta/\rho)_{MV}]$

Support for this estimate of the accuracy is given by the fairly recent results obtained for n-hexane by Eicher and Zwolinski[68]. Kinematic viscosity coefficients derived from flow time measurements on n-hexane are given in Table 3.6, and compared with literature values[68,75] in

Table 3.6

Kinematic Viscosity Coefficients for n-Hexane

Temperature (K)	Viscometer nos.	η/ρ ($mm^2\ s^{-1}$)
298.19	3,4,5,6,7,8.	0.4504 ± 0.0014
313.23	7,8.	0.3994 ± 0.0012
318.26	3,11.	0.3843 ± 0.0009

Figure 3.4.

Agreement with the results of Eicher and Zwolinski[68] shown by the solid line, is within 0.5 percent, the combined experimental uncertainties, even at temperatures where the kinematic viscosity coefficient is somewhat lower than the lower limit of 0.46 $mm^2\ s^{-1}$ mentioned above. The results given by API 44[75] tables deviate at higher temperatures, becoming higher than the Eicher and Zwolinski[68] values by 1.4 percent at 313 K. This discrepancy is practically the same as that found between the results of the present work and the values reported in API 44[75] tables for n-hexadecane and n-dodecane.

Viscometers 1 and 2 were calibrated for the range 1.15 $mm^2\ s^{-1}$ to 3.97 $mm^2\ s^{-1}$. For liquids with lower kinematic viscosity coefficients the flow times in viscometers 1 and 2 become less than 140 seconds and the B/t term becomes very significant. For viscometers 3, 4, 5, 6 and 9 all eight flow times were used for the calibrations, although for viscometer 9 the flow times became inconveniently large for n-hexadecane.

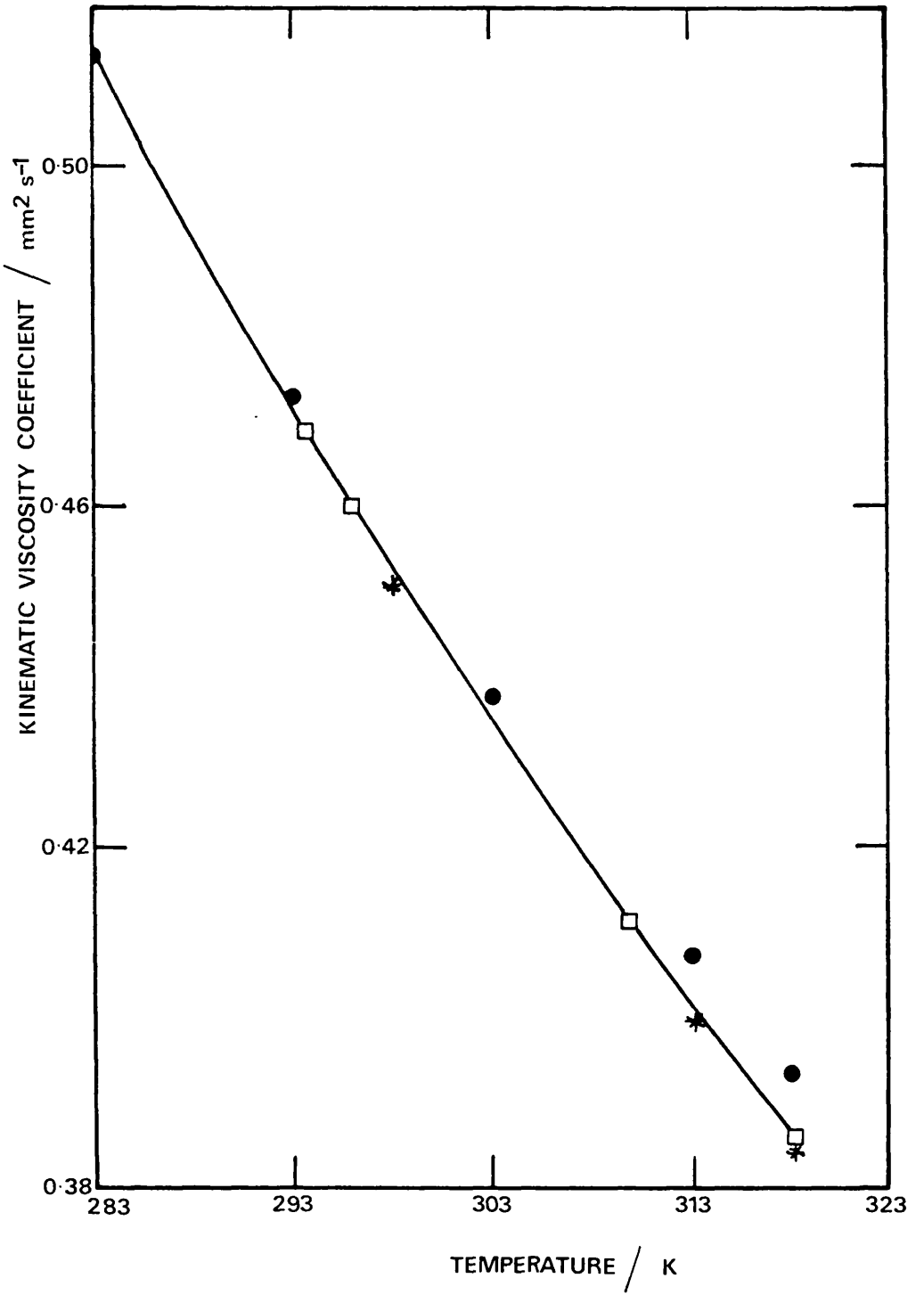

Figure 3.4 Comparison of Kinematic Viscosity Coefficients for n-Hexane with Results of □ Eicher and Zwolinski (68) and ● API 44 Tables (75). ✳ This work.

For this reason, for viscometers 7, 8, 10 and 11 this liquid was not included in the calibration liquids.

It should be noted that for viscometers 7, 8, 10 and 11 the calibration produces negative values of B, which is contrary to expectation. However, the contribution of the B/t term is generally very much less than 0.5 percent for these viscometers. The kinematic viscosity coefficients of the reference liquids can be fitted to within their estimated uncertainty with a negative value for B and a larger A value, except for viscometer 11 where the agreement is slightly less satisfactory. Although this may be of physical significance, data of greater accuracy would be required to determine B precisely, and for practical purposes the values of A and B given in Table 3.5 have been used in this work.

3.3 MEASUREMENT OF DENSITIES

3.3.1 Description and Use of Pyknometer

There are many different kinds of pyknometer used for the determination of liquid densities[83]. In order to achieve an accuracy approaching 0.01 percent a calibrated Lipkin pyknometer, illustrated in Figure 3.5 was used. It consisted of a reservoir R of capacity about 5 cm^3 and two graduated capillary limbs A and B of length about 8 cm. Caps C fit on to the cones at the top of the limbs and prevent evaporation losses.

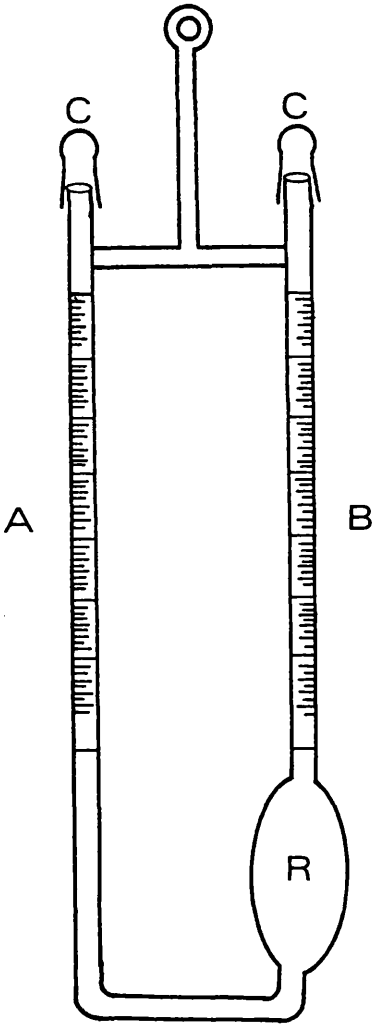

Figure 3.5 Pyknometer.

Before use, the pyknometer was thoroughly cleaned in the manner specified in Section 3.2.1, dried on a vacuum line and weighed empty. Since the weight of a glass object can change appreciably as a result of changes in the amount of water adsorbed from the atmosphere on to the glass the weighing procedure was standardised by waiting till the change in weight with time was practically zero, a delay of about ten minutes. Measurements of weight were made using a Stanton Unimatic Balance, model CL1.

3.3.2 Calibration of Pyknometer

The pyknometer was filled with freshly distilled water of accurately known density[72] using a syringe with a 15 cm long stainless steel needle which was inserted into limb A. The pyknometer was filled to about half way up the capillary limbs, the caps were fitted and the pyknometer was then suspended in a thermostatically controlled water bath at 298.19 K to just below the level of the caps. Sufficient time was allowed for thermal equilibrium to be established. In practice thirty minutes was found to be sufficient. The reading on each capillary arm was recorded and an average of these noted. The pyknometer was then removed from the bath, carefully dried and then weighed after sufficient time had elapsed. A small amount of water was then withdrawn, the caps replaced and the pyknometer again placed in the bath. This procedure was repeated twice and then the pyknometer was emptied, dried and refilled and a second calibration run made. Values for volume of water in the pyknometer corresponding to different meniscus heights could then be calculated accurately using a value of 997.07[72] kg m^{-3} for the density of water. The results are given in Table 3.7 and plotted in Figure 3.6 as average capillary height versus liquid volume. This linear plot was the calibration curve

for the pyknometer since, given the height of any liquid in the capillaries, the corresponding volume can be obtained.

Table 3.7

Pyknometer Calibration: Volume at Different Meniscus Heights

Calibration number	*Height of liquid (cm)*	*Weight (g)*	*Volume (cm^3)*
1	*6.55*	*4.9937*	*5.0084*
	4.24	*4.9571*	*4.9717*
	1.70	*4.9157*	*4.9301*
2	*5.93*	*4.9825*	*4.9971*
	4.08	*4.9541*	*4.9687*
	1.08	*4.9049*	*4.9193*

The average slope shown in Figure 3.6 reproduces the density of water to within $\pm$ 0.05 kg m^{-3} for particular values of capillary height and liquid volume. For other liquids, however, buoyancy corrections and vapour corrections have to be made to the measured densities as described in the next section.

3.3.3 Buoyancy and Vapour Pressure Corrections to Density

There are standard corrections[83] for the effects of buoyancy and vapour pressure of the liquid but they are discussed in this section because of their importance in obtaining accurate (1 part in 10^4) density values.

(a) Buoyancy Correction

It is necessary to make corrections to the recorded weights to give the weights in vacuo. This correction depends on the weight of air

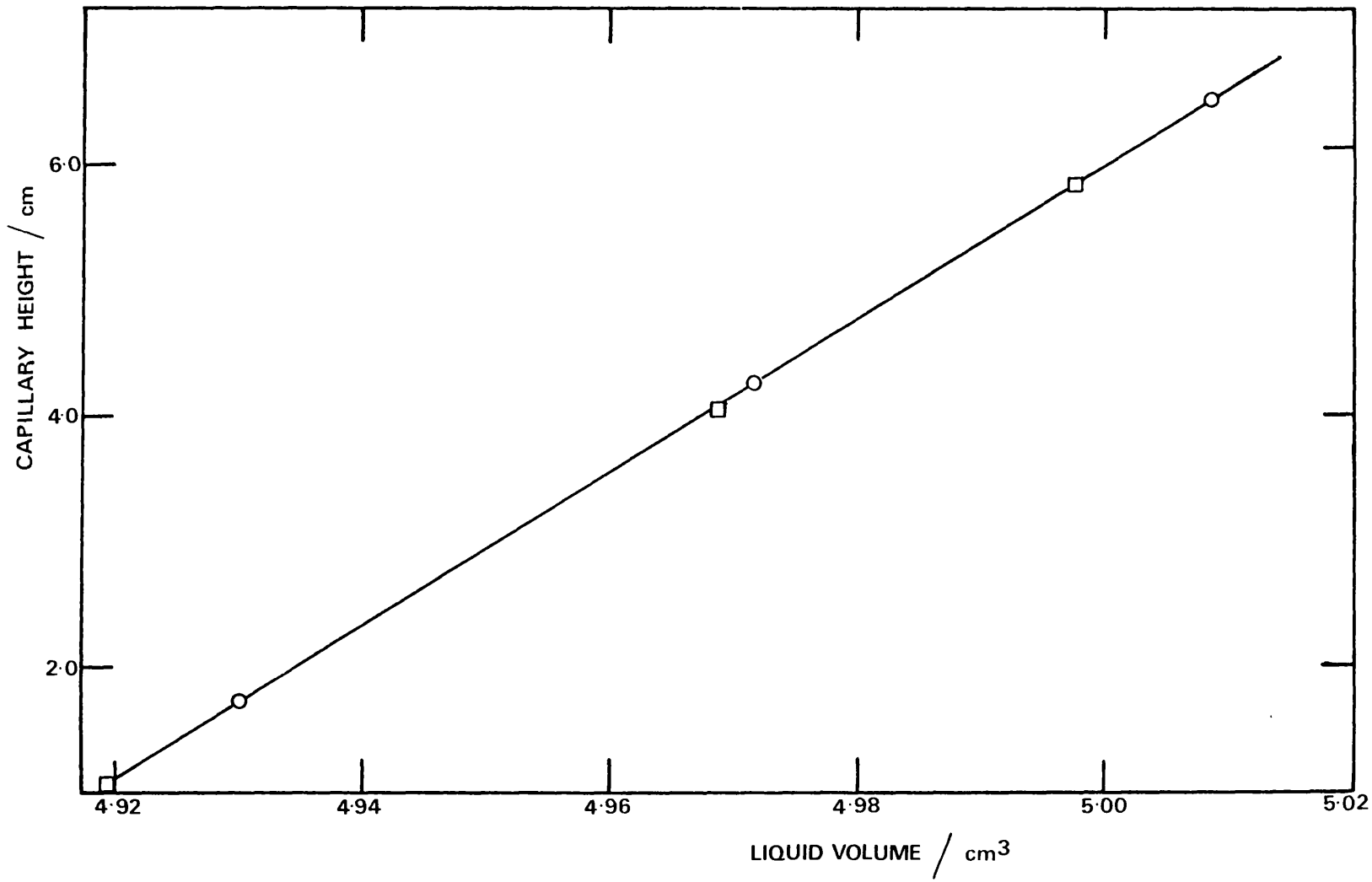

Figure 3.6 Pyknometer Calibration Curve. O *Calibration Number 1,* □ *Calibration Number 2.*

displaced by the object being balanced. Its magnitude is determined by the volume of the object and the density of the air. These corrections are based on Archimedes' Principle which states that every object receives an upthrust equal to the weight of medium displaced.

The downward force on the balance pans is decreased on one side by the weight of air displaced by the weights and on the other side by the weight of air displaced by the object. Let W be the true weight of the pyknometer and contents and W^* be the apparent weight. Then,

$$W = W^* + V_p\rho_{air} - V_W(\rho_{air} - 1.2) \qquad (3.4)$$

where V_p and V_W refer to the volume of the pyknometer (glass only) and volume of the weights. ρ_{air} is the density of the air in kg m^{-3}. It is not necessary, even for an accuracy of 0.01 percent, to apply this equation separately to each weighing. Instead a correction term can be added to ρ_m, the measured density, to give

$$\rho = \rho_m + \rho_{air}(1 - \rho_m/\rho_o) \qquad (3.5)$$

where ρ_o is the density of the calibrating liquid, in this case water. ρ_{air} may be calculated from the formula[83]

$$\rho_{air} = \frac{1.293(P - 0.0038\ HP^T_{H_2O})}{760(1 + 0.00367T)} \qquad (3.6)$$

H is the observed relative humidity in percent and $P^T_{H_2O}$ is the vapour pressure of water given in standard tables, for example[84]. Typical values of the correction are in the range 0.02 kg m^{-3} to 0.3 kg m^{-3}.

(b) Vapour Pressure Corrections

This correction takes into account the fact that the space above the menisci in the pyknometer is filled with a mixture of air and solvent

vapour. The more volatile the solvent, the larger this correction will be. If V_g is the enclosed gas space above the capillaries (2.54 cm^3 in this case), the adjustment to the weight of the filled pyknometer is

$$\Delta W = V_g \, (\rho_{air} - \rho_{air + vapour}) \qquad (3.7)$$

where

$$\rho_{air + vapour} = \frac{P_V M_V}{RT} + \frac{(P - P_V)}{P} \rho_{air} \qquad (3.8)$$

and where P_V is the vapour pressure of the liquid, R is the gas constant, T is the absolute temperature, M_V is the molecular weight of the vapour and P is the barometric pressure.

Calculation of the buoyancy and vapour pressure corrections to the measured density of benzene is shown in Table 3.8.

Table 3.8

Buoyancy and Vapour Pressure Corrections to the Density of Benzene at 298.19 K

Buoyancy Correction

T (K)	P (mm Hg)	$P^T_{H_2O}$ (mm Hg)	H (%)	ρ_{air} (kg m^{-3})	$\rho_{air}(1 - \rho_m/\rho_{air})$ (kg m^{-3})
294	738	18.65	45	1.16	0.14

Vapour Pressure Correction

P (Nm^{-2})	P_V (Nm^{-2})	$10^3 M_V$ (kg)	R (kJ/kmol K)	$10^7 \Delta W$ (kg)	$10^3 W$ (kg)	$100 \frac{\Delta W}{W}$ (%)	$\Delta\rho$ (kg m^{-3})
98390	10665	78.108	8.314	5.3	4.25	0.013	-0.11

Table 3.8 - continued

Corrected Density

T (K)	ρ_m (kg m^{-3})	$\rho_{air}(1 - \rho_m/\rho_{air})$ (kg m^{-3})	$\Delta\rho$ (kg m^{-3})	ρ (kg m^{-3})
298.19	873.61	0.14	-0.11	873.64

3.3.4 *Description and Use of the Volume Change Apparatus*

In order to obtain accurate densities at temperatures in the region of the boiling point and for mixtures it is essential to have a sealed apparatus and so the volume change apparatus, illustrated in Figure 3.7, was developed. Basically this leads to a measurement of the change in volume for a given change in temperature. If the density and volume at a reference temperature, T_R, (298.19 K in this case) are known and the volume at T is determined then, from the relationship

$$V_{T_R} \rho_{T_R} = V_T \rho_T \qquad (3.9)$$

the density at T can be calculated. The apparatus consisted of a 60 cm long capillary tube made from precision bore Veridia glass tubing shaped as illustrated in Figure 3.7, and connected to bulbs A and B and Rotaflo taps R as shown. It was mounted on a perspex stand with an engraved scale. Bulb A had a volume of about 0.4 cm^3. The lower bulb B was filled completely with liquid from a syringe.

The Volume Change Apparatus was immersed in a thermostatically controlled water bath at 298.19 K and the height of the liquid meniscus was measured. The temperature of the bath was then changed and a new meniscus height recorded. This procedure was continued until the whole temperature range was covered.

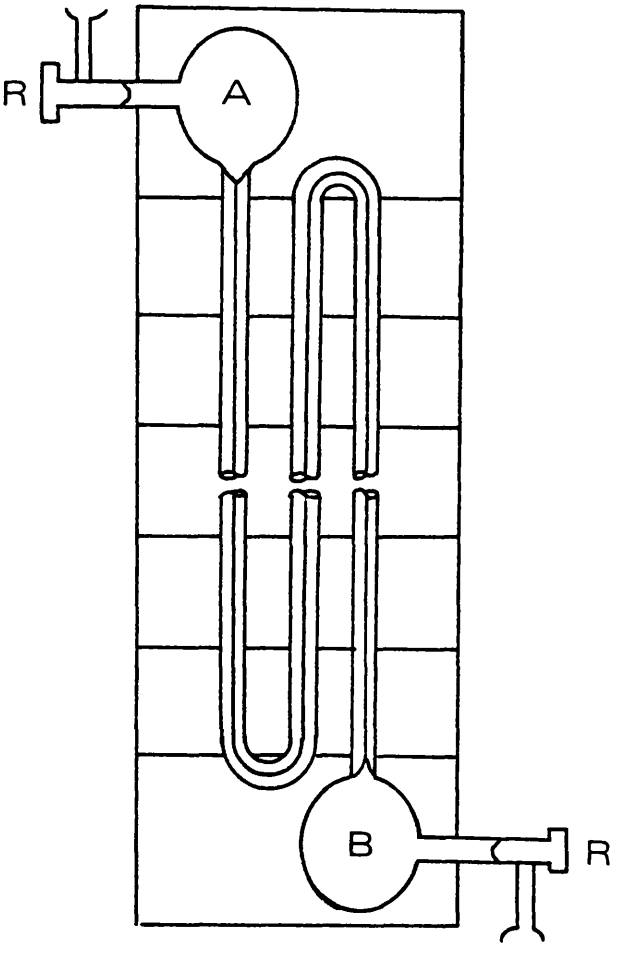

Figure 3·7 Volume Change Apparatus.

Since the volume of the apparatus was unknown, it required calibration using a liquid of known density.

3.3.5 *Calibration of Volume Change Apparatus*

Benzene was chosen as the calibration liquid as recent measurements have been made on the density up to 490 K by Hales and Townsend[85] *to an accuracy of* $\pm$ *0.1 kg* m^{-3}. *Meniscus heights were recorded over the temperature range 298 K to 368 K. Since density was accurately known, it was possible to determine the volume of the reservoir B in terms of equivalent lengths of capillary tubing as follows.*

The density ρ_T, height h_T and volume V_T are related to their respective values at 298.19 K (subscript R) by the formula

$$\frac{\rho_T}{\rho_{T_R}} = \frac{h_{T_R} + V_O}{h_T + V_O} = \frac{V_{T_R}}{V_T} \qquad (3.10)$$

when the meniscus height is below the upper bend. In this expression V_O is the volume of the lower reservoir B including the tubing up to the 0 cm mark on the scale. Since ρ_T and ρ_{T_R} are known and h_{T_R} and h_T are measurable, V_O can be determined.

However, equation (3.10) does not account for expansion of the glass or evaporation of some of the liquid into the gas phase. Both of these effects will reduce h_T for T greater than 298 K so densities calculated using this formula will be too high.

The diminution of height due to evaporation is calculated as follows.

The number of moles of gas in the vapour phase can be taken as PV/RT since the pressure is low and so the change in the number of moles, Δn, with increasing temperature is given by

$$\Delta n = \frac{P_T V_T}{RT} - \frac{P_{T_R} V_{T_R}}{RT_R} \qquad (3.11)$$

V_T and V_{T_R} the gas volumes at temperature T and the reference temperature are obtained experimentally and P_T and P_{T_R} the corresponding vapour pressures are calculated from the Antoine Equation[75] with coefficients given in API 44 Tables[75].

The change in weight, ΔW, is given by $\Delta W = \Delta n\ M$ where M is the molecular weight of the liquid and the corresponding change in liquid volume, ΔV, is given by $\Delta W/\rho'$ where ρ' is the approximate liquid

density. The change in length of the liquid column, ΔL_T, is therefore given by

$$\Delta L_T = \frac{\Delta n \; M}{\rho' \; C} \qquad (3.12)$$

where C is the volume per unit length. The change in volume due to the expansion of the glass is given by $(1 + \gamma\,(T - T_R))(V_O + h_T)$ where γ is the coefficient of cubical expansion of glass[86]*. The density corrected for these effects is given by*

$$\rho_T = \frac{(V_O + h_{T_R})\;\rho_{T_R}}{(1 + \gamma(T - T_R))(V_O + h_T + \Delta L_T)} \qquad (3.13)$$

Due to limitation in height of the bath the capillary tube had to be bent back on itself causing a small section on the bend to change its internal dimensions. This necessitated a calculation of volume V_B between some arbitrary point before the bend and one after the bend. For convenience the 21 cm scale mark on each side was taken as the point as illustrated in Figure 3.8.

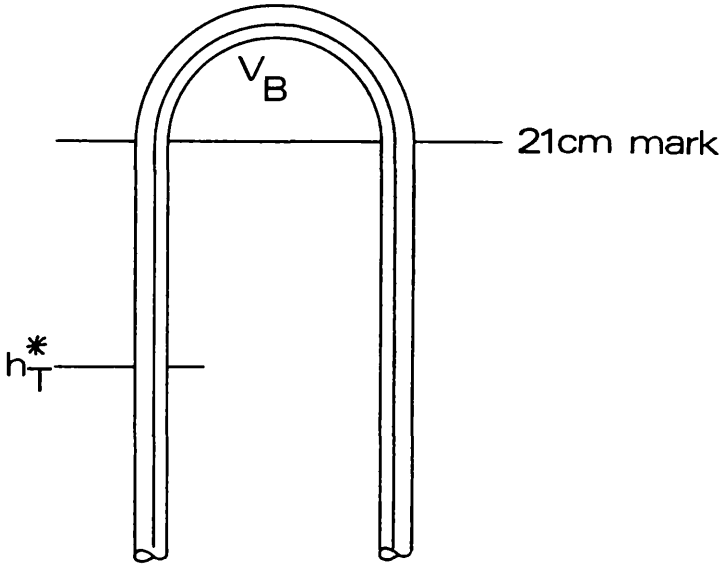

Figure 3.8 Volume Change Apparatus: Bend Volume.

The density at temperature T where the liquid meniscus is beyond the bend is now given by

$$\rho_T = \frac{(V_O + h_{T_R})\ \rho_{T_R}}{(1 + \gamma(T - T_R))(V_O + V_B + 2l + (2l - h_T^*) + \Delta L_T)} \qquad (3.14)$$

Data of Hales and Townsend[85] for benzene were used to determine V_O and V_B from measured meniscus heights of benzene in the apparatus at different temperatures. Two sets of volume change apparatus were used. Five separate calibration runs were carried out using the first apparatus and two calibration runs for the second apparatus, using redistilled Ultra R benzene from Hopkin and Williams Ltd. The values derived for V_O and V_B in units of capillary length for each set of apparatus are given in Table 3.9 together with a comparison of experimental densities with the values of Hales and Townsend[85] interpolated to the same temperatures. The experimental results are reproducible to better than $\pm$ 0.1 kg m^{-3} in the range 298.19 K to 343.33 K and $\pm$ 0.3 kg m^{-3} in the range 348.30 K to 368.27 K. Equations (3.13) and (3.14) were also used to obtain the densities of the other liquids used in this research.

Where measurements were made at regular temperature intervals it was found that the difference in density between successive readings varied linearly with average temperature and graphs of $\Delta\rho$ vs $\frac{1}{2}(T_n + T_{n+1})$ allowed density at temperatures above 363 K and below 298 K to be calculated. It is estimated that density values calculated in this way are accurate to $\pm$ 0.5 kg m^{-3}.

Table 3.9

Comparison of Experimental Benzene Densities with Reference (85)

Temperature (K)	Apparatus VA1 V_O = 332.5, V_B = 3.29 Density (kg m^{-3})					Apparatus VA2 V_O = 339.0 V_B = 5.10 Density (kg m^{-3})		Density (kg m^{-3})	
	1	2	3	4	5	1	2	Average	Reference (85)
(298.19	873.6	873.6	873.6	873.6	873.6	873.6	873.6	873.6	873.6)[a]
303.20					868.2	868.2		868.2	868.2
308.21					862.8	862.9		862.8	862.8
313.23	857.4	857.4	857.4	857.4	857.4	857.5		857.4	857.4
318.26					852.0	852.1	852.1	852.1	852.0
323.29	846.6	846.5	846.5	846.5		846.5	846.6	846.5	846.5
328.33					841.1	841.1	840.9	841.1	841.0
333.36	835.6	835.6	835.7	835.5	835.5	835.7	835.5	835.6	835.5
338.35						830.1	830.0	830.0	830.0
343.33	824.7		824.5	824.3			824.5	824.5	824.6
348.30					818.8	818.8	818.9	818.8	819.0
353.29	813.2	813.3	813.5	813.2		813.2	813.4	813.3	813.4
358.28		807.7					807.9	807.8	807.8
363.28	802.1	802.2	802.3	802.1	801.9		802.2	802.1	802.1
368.27							796.6	796.6	796.3

[a] Reference values for density at high temperatures.

3.4 RESULTS

In this section results are presented for densities and kinematic and dynamic viscosity coefficients at saturation pressure for the pure hydrocarbons and hydrocarbon mixtures listed in Table 3.10.

Table 3.10

Hydrocarbon Systems Investigated in this Work

System	Mole fraction of first (second, third) component at 298 K	Temperature range (K)
Binary Systems		
n-hexane + n-hexadecane	0.200, 0.378, 0.599, 0.799	285.15 - 378.29
benzene + n-hexane	0.500	283.15 - 373.28
benzene + n-octane	0.254, 0.504, 0.675, 0.826	283.15 - 393.2
benzene + n-decane	0.499	283.15 - 393.2
benzene + n-dodecane	0.251, 0.499, 0.750	283.15 - 393.2
benzene + n-hexadecane	0.121, 0.286, 0.598, 0.850	298.19 - 393.2
benzene + cyclohexane	0.199, 0.402, 0.600, 0.795, 0.878	283.15 - 393.2
Ternary System		
n-hexane + n-octane + n-hexadecane	0.110 (0.115) 0.329 (0.330)	288.15 - 378.29 298.19 - 358.28
Quaternary System		
n-hexane + n-octane + n-dodecane + n-hexadecane	0.260 (0.300, 0.251)	288.15 - 358.27

Results are given first for the pure components and the densities and dynamic viscosity coefficients are compared with literature values in Section 3.4.2 and 3.4.3. An analysis of the mixture composition change at elevated temperatures due to evaporation within the experi-

mental apparatus is given in Section 3.4.4. Sections 3.4.5 and 3.4.6 present densities and kinematic and dynamic viscosity coefficients for the mixtures.

3.4.1 Source and Purity of Liquids Used

With the exception of benzene and n-decane the liquids used in this research were purchased from British Drug Houses Limited, Poole, England. The benzene and n-decane used were purchased from Hopkin & Williams Limited, Romford, Essex, England. Benzene, cyclohexane, n-hexane and n-octane were fractionally distilled in a 70 cm Vigreux column before use.

n-decane, n-dodecane and n-hexadecane were used as received. Freezing point determinations on the n-hexadecane indicated its purity was 99.6 mole percent. The purity of these liquids together with a comparison with recent literature values of density and refractive index at 298.15 K is given in Table 3.11. Densities were measured by pyknometry as described in Section 3.3.1 and refractive indices were measured on a Bellingham and Stanley precision Abbé refractometer.

3.4.2 Density Results for Pure Components

Experimental density results are presented and compared with values given in API 44[75] tables and other references for n-hexane in Table 3.12, n-octane in Table 3.13, n-decane in Table 3.14, n-dodecane in Table 3.15, n-hexadecane in Table 3.16 and cyclohexane in Table 3.17.

The agreement is generally very satisfactory and within the estimated uncertainties based on the benzene results. In a few instances

Table 3.11

Comparison of the Experimental Densities and Refractive Indices with Literature Values at 298 K

Liquid	Stated purity (mole percent)	Density (kg m^{-3})		Refractive Index n (D 298.15 K)	
		This work (298.19K)	Literature (298.15 K)	This work (298.15K)	Literature (298.15 K)
n-hexane	99.7	655.0	654.79[a], 655.32[b]	1.37240	1.37229[c]
n-octane	>99.5	698.9	698.61[d], 698.62[e]	1.39507	1.39505[e]
n-decane	>98	726.3	726.25[d], 726.35[e]	1.40956	1.40967[e]
n-dodecane	>99	745.5	745.37[a], 745.18[e]	1.41956	1.41949[e]
n-hexadecane	99.6*	770.2	769.96[f], 770.79[g]	1.43244	1.43250[e]
cyclohexane	>99.8	773.8	773.598[h], 773.95[b]	1.42355	1.42350[j]
benzene	>99	873.6	873.60[k], 873.68[a]	1.49790	1.49793[c]

* By freezing point analysis; [a] Ref (87); [b] Ref (88); [c] Ref (89); [d] Ref (90); [e] Ref (75); [f] Ref (91); [g] Ref (54); [h] Ref (92); [j] Ref (93); [k] Ref (94).

usually at temperatures where results have been extrapolated the agreement is outside these estimates.

Table 3.12

Densities for n-Hexane
(in Volume Change Apparatus 2)

Temperature (K)	Meniscus height (cm)	Density (kg m^{-3})		
		This work	Literature values	
			(g)	
283.15		668.6[a]	668.2	
288.15		664.1[a]		
298.19	2.42	655.0	654.84	655.13[b], 654.8[c], 654.85[d]
303.20	4.76	650.4	650.15	
308.21	7.13	645.8		646.07[b], 645.78[e], 645.8[f]
313.23	9.61	641.1	640.9	
318.26	12.11	636.3		636.79[b], 636.39[e]
328.33	17.30	626.7		
333.36	19.98	621.8	622.0	622.21[b], 622.10[e]
	———			
343.33	21.37	611.6	612.3	
348.30	18.48	606.6		
353.29	15.52	601.6	602.4	
358.28	12.19	596.0		
368.27		585.8[a]		
373.28		580.4[a]	581.7	
378.29		574.9[a]		
393.2		558.4[a]	559.4	

[a] Extrapolated values, ——— bend
[b] Ref (95); [c] Ref (89); [d] Ref (96); [e] Ref (90); [f] Ref (97);
[g] Ref (75).

Table 3.13

Densities for n-Octane

(in Volume Change Apparatus 1)

Temperature (K)	Meniscus height (cm)	Density (kg m^{-3})		
		This work	Literature values	
283.15		710.9[a]	710.7[b]	
288.15		706.9[a]		
298.19	2.76	698.9	698.62	698.61[c], 698.67[d]
303.20	4.66	694.9	694.54	
308.21	6.60	690.8		690.54[c]
313.23	8.59	686.7	686.3	
318.26	10.60	682.5		682.32[c]
323.29	12.68	678.3	678.0	
328.33	14.75	674.2		
333.36	16.86	670.0	669.7	669.88[e]
338.36	18.90	666.0		
343.33	21.18	661.6	661.2	
353.29		653.1[a]	652.6	
363.28		644.4[a]	643.9	
373.28		635.7[a]	635.0	
393.2		617.8[a]	616.8	

[a] Extrapolated values

[b] Ref (75); [c] Ref (95); [d] Ref (98);

[e] Ref (90).

Table 3.14

Densities for n-Decane

(in Volume Change Apparatus 2)

Temperature (K)	Meniscus height (cm)	Density (kg m^{-3})		
		This work	Literature values	
			(b)	
283.15		737.4[a]	737.6	
288.15		733.7[a]		
298.19	2.19	726.3	726.35	726.06[c], 726.25[d]
303.20	3.90	722.6	722.57	
308.21	5.69	718.7		718.72[d]
313.23	7.48	714.9	715.0	
318.26	9.31	711.1		711.09[d]
323.29	11.16	707.2	707.3	
328.33	13.02	703.4		
333.36	14.90	699.6	699.6	699.55[d]
338.36	16.80	695.7		
343.33	18.73	691.9	691.7	
348.30	20.72	688.0		
353.29		684.2[a]	683.8	
363.28		676.2[a]	675.8	
373.28		668.1[a]	667.8	
393.2		651.6[a]	651.8	

[a] *Extrapolated values*

[b] *Ref (75);* [c] *Ref (99);* [d] *Ref (90).*

Table 3.15

Densities for n-Dodecane

(in Volume Change Apparatus 1)

Temperature (K)	Meniscus height (cm)	Density (kg m^{-3})		
		This work	Literature values	
283.15		756.4[a]	755.9 (b)	
288.15		752.8[a]		
298.19	2.39	745.5	745.18	745.27[c], 745.17[d]
303.20	3.99	741.9	741.60	
308.21	5.61	738.2		737.92[d]
313.23	7.25	734.6	734.4	
318.26	8.91	730.9		730.66[d]
323.29	10.59	727.2	727.2	
328.33	12.30	723.5		
333.36	13.99	719.9	719.9	719.66[d]
338.36	15.71	716.2		
343.33	17.47	712.6	712.5	
348.30	19.22	708.9		
353.29	21.00	705.3	705.1	
363.28		697.9[a]	697.6	
373.28		690.5[a]	690.0	
393.2		675.8[a]	674.7	

[a] Extrapolated values

[b] Ref (75); [c] Ref (100); [d] Ref (90).

Table 3.16

Densities for n-Hexadecane

(in Volume Change Apparatus 2)

Temperature (K)	Meniscus height (cm)	Density (kg m^{-3})		
		This work	Literature values	
			(b)	
298.19	2.22	770.2	769.94	770.79[c], 769.97[d]
303.20	3.72	766.7	766.42	
308.21	5.23	763.3		763.05[d]
313.23	6.77	759.8	759.5	
318.26	8.31	756.3		756.14[d]
323.29	9.86	752.9	752.8	
328.33	11.41	749.4		
333.36	12.99	746.0	746.1	745.82[d]
338.36	14.57	742.5		
343.33	16.17	739.1	739.3	
348.30	17.78	735.7		
353.29	19.40	732.3	732.5	
358.28	21.02	728.9		
363.28		725.4[a]	725.4	
373.28		718.5[a]	718.0	
378.29		715.1[a]		
393.2		704.7[a]	702.0	

[a] Extrapolated values

[b] Ref (75); [c] Ref (54); [d] Ref (90).

Table 3.17

Densities for Cyclohexane
(in Volume Change Apparatus 2)

Temperature (K)	Meniscus height (cm)	Density ($kg\ m^{-3}$)		
		This work	Literature values	
			(b)	
283.15		787.9[a]	787.8	
288.15		783.2[a]		
298.19	2.36	773.8	773.89	773.598[e], 773.92[d]
303.20	4.40	769.1	769.3	
308.21	6.49	764.3		764.51[d]
313.23	8.60	759.5	759.8	759.9[c], 759.7[f]
318.26	10.77	754.6		754.85[d]
323.29	12.98	749.7	750.1	
328.33	15.20	744.9		
333.36	17.47	739.9	740.5	740.5[c], 740.36[d]
338.36	19.75	735.1		
343.33	22.12	730.0	730.9	
348.30	22.45	724.8		
353.29	19.99	719.7	721.2	
358.28	17.50	714.6		
363.28	14.96	709.5		
373.28		699.4[a]		
393.2		678.2[a]		

[a] Extrapolated values, ——— bend

[b] Ref (75); [c] Ref (101); [d] Ref (95);

[e] Ref (92); [f] Ref (97).

3.4.3 Viscosity Coefficient Results for Pure Components

Experimental kinematic viscosity coefficients and calculated dynamic viscosity coefficients are presented and compared with API 44[75] values corrected to the same temperature and other references for n-hexane in Table 3.18, n-octane in Table 3.19, n-decane in Table 3.20, n-dodecane in Table 3.21, n-hexadecane in Table 3.22, cyclohexane in Table 3.23 and benzene in Table 3.24. The viscosity coefficients in this work have an estimated accuracy of $\pm$ 0.5 percent except for n-hexane above 298.19 K where the results lie below the lower limit of kinematic viscosity coefficient used for the viscometer calibration. For n-hexane the uncertainty is estimated to increase from $\pm$ 0.5 percent at 298.19 K to $\pm$ 1 percent at 393.2 K. Apart from n-hexane, measurements have not previously been made over a wide temperature range for the liquids studied. However, Isdale[102] has recently considered general expressions for representing viscosity coefficients for all the n-alkanes and has shown that a good representation of the data from the melting point to 0.9 times the critical temperature is given by the equation

$$\ln \eta/D = A\,(\Theta - 1)^{1/3} + B\,(\Theta - 1)^{4/3} \qquad (3.15)$$

$$\text{where } \Theta = \frac{T_c - C}{T - C}$$

C and D are calculated from critical properties, and A and B are obtained by fitting the equation to viscosity coefficient data and correlated with values for other members in the series. The recommended viscosity coefficient values agree with the present results to well within the quoted minimum uncertainties of the tabulated values.

Table 3.18

Viscosity Coefficients for n-Hexane

Temperature (K)	η/ρ ($mm^2\ s^{-1}$)	η (mPa s)		
		This work	Literature values	
283.15	0.5141	0.3437	0.3426 [a]	
288.15	0.4911	0.3261	0.3265 [a]	
298.19	0.4504	0.2950	0.2976 [a]	0.2961 [b], 0.2958 [c]
313.23	0.3994	0.2561	0.2609 [a]	
318.26	0.3843	0.2448	0.2502 [a]	
333.36	0.3450	0.2146	0.2212 [a]	
338.36	0.3348	0.2064	0.2124 [a]	
353.29	0.3028	0.1821		0.190 [d]
358.28	0.2971	0.1771		
373.28	0.2672	0.1550		0.158 [d]
374.55				0.1562 [e]
378.29	0.2648	0.1522		
393.2	0.2403	0.1341		0.132 [d]
395.25				0.1324 [e]

[a] Ref (75); [b] Ref (54); [c] Ref (103); [d] Ref (104); [e] Ref (105).

Table 3.19

Viscosity Coefficients for n-Octane

Temperature (K)	η/ρ ($mm^2\ s^{-1}$)	η (mPa s)		
		This work	Literature values	
			(a)	
283.15	0.8646	0.6146	0.6184	
288.15	0.8154	0.5764	0.5798	
298.19	0.7255	0.5070	0.5134	
313.23	0.6272	0.4307	0.4351	
333.36	0.5231	0.3505	0.3569	
353.29	0.4461	0.2913	0.2992	
373.28	0.3869	0.2459	0.2544	
393.2	0.3420	0.2113	0.2187	

[a] Ref (75)

Table 3.20

Viscosity Coefficients for n-Decane

Temperature (K)	η/ρ ($mm^2\ s^{-1}$)	η (mPa s)		
		This work	Literature values	
			(a)	
283.15	1.4595	1.076	1.087	
288.15	1.3502	0.9906	1.001	
298.19	1.1718	0.8511	0.8583	
313.23	0.9669	0.6912	0.6981	
333.36	0.7750	0.5422	0.5489	
353.29	0.6418	0.4391	0.4457	
373.28	0.5428	0.3626	0.3700	
393.2	0.4686	0.3053	0.3127	

[a] Ref (75)

Table 3.21

Viscosity Coefficients for n-Dodecane

Temperature (K)	η/ρ ($mm^2\ s^{-1}$)	η (mPa s)		
		This work	Literature values	
			(a)	
283.15	2.3954	1.812	1.828	
288.15	2.1740	1.637	1.653	
298.19	1.8231	1.359	1.373	1.363[b]
313.23	1.4446	1.061	1.077	1.062[b]
333.36	1.1128	0.8011	0.8102	
353.29	0.8928	0.6297	0.6368	
373.28	0.7379	0.5095	0.5162	
393.2	0.6235	0.4214	0.4277	

[a] Ref (75); [b] Ref (106).

Table 3.22

Viscosity Coefficients for n-Hexadecane

Temperature (K)	η/ρ ($mm^2\ s^{-1}$)	η (mPa s)		
		This work	Literature values	
			(a)	
298.19	3.9799	3.065	3.083	3.0620[b]
313.23	2.9210	2.219	2.239	
318.26	2.6675	2.017	2.034	
333.36	2.0763	1.549	1.563	
338.36	1.9292	1.432	1.444	
353.29	1.5721	1.151	1.160	
358.28	1.4769	1.076	1.085	
373.28	1.2396	0.8906	0.8979	
378.29	1.1752	0.8404	0.8466	
398.2	1.0159	0.7159	0.7178	

[a] Ref (75); [b] Ref (54).

Table 3.23

Viscosity Coefficients for Cyclohexane

Temperature (K)	η/ρ ($mm^2 s^{-1}$)	η (mPa s)		
		This work	Literature values	
			(a)	
283.15	1.4991	1.181	1.176	
288.15	1.3719	1.074	1.070	1.065[b]
298.19	1.1587	0.8966	0.894	0.8856[c], 0.892[d]
313.23	0.9252	0.7027	0.701	0.701[b]
333.36	0.7143	0.5285	0.525	
353.29	0.5737	0.4129	0.409	
373.28	0.4728	0.3306		
393.2	0.4008	0.2719		

[a] Ref (75); [b] Ref (107); [c] Ref (108); [d] Ref (109).

Table 3.24

Viscosity Coefficients for Benzene

Temperature (K)	η/ρ ($mm^2 s^{-1}$)	η (mPa s)		
		This work	Literature values	
			(a)	
283.15	0.8564	0.7620	0.7574	0.7604[b]
288.15	0.7916	0.6998	0.6983	0.699[c]
298.19	0.6893	0.6021	0.6007	0.603[d], 0.5996[e], 0.602[f]
313.23	0.5739	0.4921	0.4903	0.4922[b], 0.493[c]
333.36	0.4661	0.3894	0.388	
353.29	0.3903	0.3174	0.317	0.317[g]
373.28	0.3344	0.2644		0.262[g]
393.2	0.2946	0.2263		0.218[g]

[a] Ref (75); [b] Ref (110); [c] Ref (107); [d] Ref (111); [e] Ref (108); [f] Ref (109); [g] Ref (112).

3.4.4 Calculation of Composition Changes Due to Evaporation

In both the volume change apparatus and the viscometers, liquid is in contact with vapour and for the mixtures these two phases are of different composition. The liquid composition in the experimental apparatus differs slightly from the original composition prepared even at 298 K, and as the temperature is altered the change in composition becomes greater because of the different vapour pressures of the components. The change in composition is calculated by finding the number of moles of each component in the vapour phase at each temperature and subtracting this from the number of moles of each component originally present in the liquid phase. Since these systems of hydrocarbons do not exhibit significant large deviations from Raoults Law, the number of moles, n_i, of each component in the vapour phase is calculated on the basis of Raoults Law from

$$n_i = \frac{x_i P_i V}{RT} \qquad (3.16)$$

where V is the volume of the vapour space, P_i the vapour pressure of pure i at temperature T calculated from the Antoine Equation, and x_i is the mole fraction of i in the liquid originally present. The true mole fraction of component 1 in a binary liquid mixture is now given by

$$x_1 = \frac{n_1(L) - n_1(G)}{(n_1(L) - n_1(G)) + (n_2(L) - n_2(G))} \qquad (3.17)$$

where $n_i(L)$, $n_i(G)$ represent the number of moles of component i in the liquid and vapour phase respectively. For ternary and quaternary mixtures the denominator will contain further terms to take account of the additional components present. The true mole fractions were computed using a modification of a Fortran program written by Robertson[113].

For the volume change apparatus the vapour volume is approximately 0.8 cm^3 compared to a vapour volume of 30 cm^3 in the viscometers. Thus for a particular mixture, although the original composition in the two sets of apparatus is the same on injecting the sample, the liquid composition will be slightly different when equilibrium has been established. As temperature is increased, this divergence in composition will become more marked. For example, for the n-hexane plus n-hexadecane system, the mixture with the composition $x_H = 0.5993$ becomes $x_H = 0.5992$ in the volume change apparatus and $x_H = 0.5983$ in the viscometers when equilibrium has been attained at 298 K. At 378 K $x_H = 0.5975$ in the volume change apparatus and $x_H = 0.5864$ in the viscometers.

This composition difference at the higher temperature means that the liquid density is different for the two sets of apparatus even though the temperatures are the same. In the example considered above, the density of the liquid in the volume change apparatus is 662.8 kg m^{-3} and the liquid in the viscometer has a density of 664.2 kg m^{-3} at this temperature, a difference of 0.2 percent. This means that before the dynamic viscosity coefficients can be calculated from the corresponding kinematic viscosity coefficients, it is necessary to calculate the density of the mixture in the viscometer from the density in the volume change apparatus. Mixture densities in the viscometers were interpolated from 'volume change apparatus density' versus 'volume change apparatus mole fraction'. A Hewlett Packard 9810 Desktop Calculator was used to interpolate these densities using the Lagrangian interpolation method.

3.4.5 *Density Results for Mixtures*

Density results for the n-hexane plus n-hexadecane system are given in Table 3.25 and for two three component n-alkane mixtures and one four component n-alkane mixture in Table 3.26. Results for a series of binary benzene plus n-alkane mixtures are given in Tables 3.27 (plus n-hexane), 3.28 (plus n-octane), 3.29 (plus n-decane), 3.30 (plus n-dodecane), and 3.31 (plus n-hexadecane). Results for benzene plus c-hexane are given in Table 3.32.

Table 3.25

Densities and Corrected Liquid Compositions for the n-Hexane plus n-Hexadecane System at Saturated Vapour Pressure

Temperature (K)	$x_H^* \sim 0.2$		$x_H \sim 0.4$		$x_H \sim 0.6$		$x_H \sim 0.8$	
	ρ (kg m^{-3})	x_H	ρ (kg m^{-3})	x_H	ρ (kg m^{-3})	x_H	ρ (kg m^{-3})	x_H
298.19	759.5	0.1995	747.0	0.3782	726.4	0.5992	699.0	0.7987
303.20	755.9		743.3		722.5		694.9	
308.21	752.3		739.5		718.6		690.8	
318.26	745.1	0.1993	732.1	0.3780	710.8	0.5990	682.3	0.7986
328.33	737.9		724.6		702.9		673.9	
338.36	730.8	0.1990	717.2	0.3777	695.1	0.5987	665.3	0.7985
348.30	723.7		709.7		687.0			
353.29	720.0		706.0				651.9	
358.28	716.4	0.1986	702.2	0.3771	678.4	0.5982	647.5	0.7982
363.28					674.2		643.1	
368.27			695.8					
378.29	701.7[a]	0.1980[a]	686.9[a]	0.3763[a]	662.8[a]	0.5975[a]	630.0[a]	0.7978[a]

[a] Extrapolated

* subscript H - n-hexane

Table 3.26

Densities and Corrected Liquid Compositions for Two Ternary and One Quaternary n-Alkane System at Saturated Vapour Pressure

Temperature (K)	$x_H^* \sim x_O \sim x_{HD} \sim 0.33$			$x_H \sim x_O \sim 0.1$, $x_{HD} \sim 0.8$			$x_H \sim x_{DD} \sim 0.25$, $x_O \sim 0.3$, $x_{HD} \sim 0.2$			
	ρ (kg m^{-3})	x_H	x_O	ρ (kg m^{-3})	x_H	x_O	ρ (kg m^{-3})	x_H	x_O	x_{DD}
298.19	727.4	0.3294	0.3294	759.5	0.1098	0.1151	726.5	0.2600	0.2995	0.2504
303.20	723.6			755.9			722.7			
308.21	719.7			752.3			718.9			
313.23	715.9	0.3293	0.3294	748.8	0.1098	0.1151	715.0	0.2599	0.2995	0.2504
318.26	712.0			745.2			711.1			
323.29	708.1			741.6			707.2			
328.33	704.2			738.0			703.3			
333.36	700.3	0.3291	0.3295	734.4	0.1096	0.1151	699.5	0.2597	0.2996	0.2505
338.36	696.4			730.9			695.6			
343.33	692.4			727.4			691.7			
348.30	688.5			723.8			687.7			
353.29	684.5[a]	0.3287	0.3296	720.3	0.1094	0.1151	683.5[a]	0.2594	0.2996	0.2807
358.28	680.4[a]			716.7			679.4			
363.28	676.3			713.2[a]			675.4			
368.28	672.0			709.7[a]			671.3			
373.28	668.0[a]	0.3281	0.3298	706.1[a]	0.1090	0.1150	667.1[a]	0.2590	0.2997	0.2509

* Subscript H - n-hexane; O - n-octane; DD - n-dodecane; HD - n-hexadecane.

[a] Extrapolated.

Table 3.27

Densities and Corrected Liquid Compositions for the Benzene plus n-Hexane System at Saturated Vapour Pressure

Temperature (K)	$x_B^* \sim 0.5$	
	ρ (kg m^{-3})	x_B
283.15	755.4	
288.15	750.6	
298.19	741.0	0.4995
303.20	736.2	
308.21	731.3	
313.23	726.4	0.4996
318.26	721.4	
323.29	716.4	
328.33	711.3	
333.36	706.3	
338.36	700.7	
343.33	695.7	
348.30	690.6	
353.29	685.3	0.4997
358.28	680.0	
363.28	674.7	
368.27	669.3	
373.28	663.9[a]	
393.2	641.4[a]	0.4999[a]

[a] *Extrapolated.*

* *Subscript B - benzene*

Table 3.28

Densities and Corrected Liquid Compositions for the Benzene plus n-Octane System at Saturated Vapour Pressure

Temperature (K)	$x_B^* \sim 0.25$		$x_B \sim 0.5$		$x_B \sim 0.67$		$x_B \sim 0.82$	
	ρ (kg m^{-3})	x_B	ρ (kg m^{-3})	x_B	ρ (kg m^{-3})	x_B	ρ (kg m^{-3})	x_B
283.15	736.0		769.6		800.2		835.5	
288.15	731.8		765.1		795.5		830.6	
298.19	723.4	0.2539	756.2	0.5040	786.2	0.6746	820.8	0.8255
303.20	719.1		751.8		781.4		815.8	
308.21	714.9		747.2		776.7		810.9	
313.23	710.6	0.2538	742.7	0.5040	772.0	0.6745	805.9	0.8255
318.26	706.3		738.1		767.2		800.8	
323.29	702.0		733.5		762.4		795.8	
328.33	697.6		728.9		757.5		790.7	
333.36	693.2	0.2537	724.3	0.5039	752.8	0.6744	785.7	0.8254
338.36	688.8		719.8		747.9		780.6	
343.33	684.4		715.1		743.1		775.5	
348.30	679.6							
353.29	675.1	0.2536	705.0	0.5037	733.0	0.6743	764.9	0.8253
358.28	670.6		700.4		728.1		759.7	
363.28	666.1		696.0				754.5	
373.28	657.4[a]		687.1[a]		712.9[a]		743.9[a]	
393.2	638.8[a]	0.2531[a]	667.9[a]	0.5032[a]	692.1[a]	0.6739[a]	722.2[a]	0.7251[a]

[a] *Extrapolated.*

* *Subscript B - benzene*

Table 3.29

Densities and Corrected Liquid Compositions for the Benzene plus n-Decane System at Saturated Vapour Pressure

Temperature (K)	$x_B^* \sim 0.5$	
	ρ (kg m^{-3})	x_B
283.15	780.5	
288.15	776.3	
298.19	768.0	0.4990
303.20	763.8	
308.21	759.5	
313.23	755.3	0.4990
318.26	751.0	
323.29	746.7	
328.33	742.4	
333.36	738.0	0.4988
338.36	733.7	
343.33	729.3	
353.29	720.2	
358.28	715.8	
363.28	711.3	
368.27	706.8	
373.28	702.4[a]	
393.2	683.8[a]	0.4977[a]

[a] Extrapolated.

* Subscript B - benzene

Table 3.30

Densities and Corrected Liquid Compositions for the Benzene plus n-Dodecane System at Saturated Vapour Pressure

Temperature (K)	x_B^* ~ 0.25		x_B ~ 0.50		x_B ~ 0.75	
	ρ (kg m^{-3})	x_B	ρ (kg m^{-3})	x_B	ρ (kg m^{-3})	x_B
283,15	769.4		789.1		822.0	
288.15	765.7		785.0		817.5	
298.19	758.1	0.2508	776.9	0.4993	808.6	0.7498
303.20	754.4		772.8		804.1	
308.21	750.5		768.7		799.6	
313.23	746.6	0.2508	764.6	0.4993	795.1	0.7497
318.26	742.7		760.5		790.5	
323.29	738.9				785.9	
328.33	735.0		752.3		781.4	
333.36	731.1	0.2506	748.1	0.4991	776.8	0.7496
338.36	727.3		744.0		772.2	
343.33	723.4		739.8		767.6	
348.30	719.6		735.7			
353.29		0.2504	731.5	0.4988	757.8	0.7495
358.28	711.3				753.2	
363.28	707.3		722.6		748.4	
373.28	700.0[a]		714.7[a]		739.6[a]	
393.2	684.0[a]	0.2494[a]	697.7[a]	0.4978[a]	720.5[a]	0.7489[a]

[a] *Extrapolated* * *Subscript B - benzene*

Table 3.31

Densities and Corrected Liquid Compositions for the Benzene plus n-Hexadecane System at Saturated Vapour Pressure

Temperature (K)	x_B^* ~ 0.12		x_B ~ 0.29		x_B ~ 0.60		x_B ~ 0.85	
	ρ (kg m^{-3})	x_B	ρ (kg m^{-3})	x_B	ρ (kg m^{3})	x_B	ρ (kg m^{-3})	x_B
298.19	773.6	0.1243	779.5	0.2880	798.0	0.5998	829.6	0.8495
303.20			775.9		794.1			
313.23	763.0	0.1243	768.6	0.2879	786.1	0.5997	815.9	0.8494
323.29			761.2		778.0		806.7	
333.36	748.8	0.1242	753.9	0.2877	770.0	0.5996	797.5	0.8494
343.33			746.7		761.9		788.2	
353.29	734.7	0.1240	739.2	0.2874	753.7	0.5993	778.4	0.8493
358.28	731.2		735.6				773.7	
363.28					745.1		768.9	
368.28					740.9			
373.28	720.5[a]		724.6[a]		736.9[a]		759.5[a]	
393.2	706.4[a]	0.1232[a]	709.9[a]	0.2862[a]	719.9[a]	0.5982[a]	740.0[a]	0.8489[a]

[a] *Extrapolated*

* *Subscript B - benzene*

Table 3.32

Densities and Corrected Liquid Compositions for the Benzene plus Cyclohexane System at Saturated Vapour Pressure

Temperature (K)	x_B^* ∿ 0.19, ∿ 0.80		x_B ∿ 0.40, ∿ 0.88		x_B ∿ 0.60	
	ρ (kg m^{-3})	x_B	ρ (kg m^{-3})	x_B	ρ (kg m^{-3})	x_B
283.15	801.3		819.1		839.0	
288.15	796.6		814.2		834.0	
298.19	787.0	0.1952	804.4	0.4020	823.9	0.6006
303.20			799.5		818.8	
313.23	772.4	0.1951	789.5	0.4019	808.7	0.6005
323.29	762.6		779.4		798.4	
333.36	752.6	0.1951	769.3	0.4018	788.1	0.6004
343.33			759.0			
348.30	737.2					
353.29	732.1	0.1950	748.2	0.4016	766.6	0.6003
358.28	726.9		743.0		761.3	
363.28	721.8		737.7		756.0	
373.28	711.0[a]		727.0[a]		745.1[a]	
393.2	689.9[a]	0.1945[a]	705.1[a]	0.4009[a]	723.2[a]	0.5996[a]
283.15	861.3		872.2			
288.15	856.2		867.0			
298.19	845.9	0.7952	856.5	0.8783		
303.20	840.7		851.3			
313.23	830.3	0.7951	840.7	0.8783		
323.29	819.7		830.0			
333.36	809.2	0.7951	819.3	0.8782		
343.33	798.4		808.4			
353.29	787.2	0.7950	798.2	0.8782		
363.28	776.2		787.2			
373.28	765.0[a]		775.7[a]			
393.2	742.1[a]	0.7946[a]	753.3[a]	0.8779[a]		

[a] *Extrapolated*

[*] *Subscript B - benzene*

3.4.6 *Viscosity Coefficient Results for Mixtures*

Kinematic viscosity coefficient results together with corrected composition densities and calculated dynamic viscosity coefficients are presented in Table 3.33 for n-hexane plus n-hexadecane, Table 3.34 for two ternary and one quarternary n-alkane systems, Table 3.35 for benzene plus n-hexane, Table 3.36 for benzene plus n-octane, Table 3.37 for benzene plus n-decane, Table 3.38 for benzene plus n-dodecane, Table 3.39 for benzene plus n-hexadecane and Table 3.40 for benzene plus cyclohexane.

Figures 3.9 to 3.13 plot dynamic viscosity coefficients versus mole fraction at various temperatures for the n-hexane plus n-hexadecane (Figure 3.9), benzene plus n-octane (Figure 3.10), benzene plus n-dodecane (Figure 3.11), benzene plus n-hexadecane (Figure 3.12) and benzene plus cyclohexane (Figure 3.13) systems.

The estimated accuracy of the dynamic viscosity coefficients is $\pm$ 0.5 percent, except for the system benzene plus n-hexane above 313 K where the uncertainty is larger possibly increasing to $\pm$ 1 percent at 393 K and for benzene plus n-octane and benzene plus cyclohexane above 353 K where the uncertainty may rise possibly to $\pm$ 0.7 percent at 393 K.

Heric and Brewer[54] have measured viscosity coefficients at 298.15 K for the n-hexane plus n-hexadecane system and the benzene plus n-hexadecane system and these values are compared with the present values in Figure 3.9 for n-hexane plus n-hexadecane and in Figure 3.12 for benzene plus n-hexadecane.

Table 3.33

Viscosity Coefficients for the n-Hexane plus n-Hexadecane System at Saturated Vapour Pressure

Temperature (K)	x_H*	η/ρ ($mm^2\ s^{-1}$)	ρ ($kg\ m^{-3}$)	η (mPa s)	x_H	η/ρ ($mm^2\ s^{-1}$)	ρ ($kg\ m^{-3}$)	η (mPa s)
285.15		Frozen			0.3784	2.7381	756.8	2.072
288.15	0.1996	3.6300	766.8	2.784	0.3784	2.5823	754.5	1.948
298.19	0.1987	2.9422	759.5	2.235	0.3772	2.1514	747.1	1.607
318.26	0.1976	2.0586	745.2	1.534	0.3758	1.5778	732.3	1.155
338.36	0.1958	1.5433	731.0	1.128	0.3734	1.2197	717.6	0.8753
358.28	0.1929	1.2153	716.8	0.8711	0.3695	0.9862	702.9	0.6932
378.29	0.1885	0.9878	702.4	0.6938	0.3637	0.8172	688.1	0.5623
285.15	0.5993	1.6757	738.0	1.237	0.7988	0.9883	709.7	0.7014
288.15	0.5993	1.5969	734.1	1.172	0.7988	0.9530	707.2	0.6740
298.19	0.5983	1.3785	726.5	1.001	0.7982	0.8487	699.1	0.5933
318.26	0.5971	1.0676	711.0	0.7591	0.7975	0.6903	682.5	0.4712
338.36	0.5949	0.8616	695.5	0.5993	0.7963	0.5776	665.7	0.3845
358.28	0.5916	0.7178	679.8	0.4880	0.7944	0.4938	648.6	0.3203
378.29	0.5864	0.6109	664.2	0.4058	0.7915	0.4293	631.3	0.2710

*Subscript H - n-hexane

Table 3.34

Viscosity Coefficients for Two Ternary and One Quaternary n-Alkane System at Saturated Vapour Pressure

Temperature (K)	Ternary						Quaternary						
	x_H*	x_O	x_{HD}	η/ρ ($mm^2\ s^{-1}$)	ρ ($kg\ m^{-3}$)	η (mPa s)	x_H	x_O	x_{DD}	x_{HD}	η/ρ ($mm^2\ s^{-1}$)	ρ, ($kg\ m^{-3}$)	η (mPa s)
288.15	0.1097	0.1152	0.7751	3.5656	766.6	2.733	0.2596	0.2996	0.2506	0.1902	1.4768	734.1	1.084
298.19	0.1093	0.1152	0.7755	2.8891	759.5	2.194	0.2593	0.2997	0.2507	0.1903	1.2747	726.5	0.9261
318.26	0.1086	0.1151	0.7763	2.0287	745.2	1.512	0.2584	0.2997	0.2510	0.1909	0.9902	711.1	0.7041
338.36	0.1076	0.1151	0.7773	1.5241	730.9	1.114	0.2569	0.3004	0.2517	0.1910	0.7988	695.6	0.5556
358.28	0.1058	0.1149	0.7793	1.1996	716.7	0.8598	0.2545	0.3009	0.2529	0.1917	0.6657	679.4	0.4523
378.29	0.1032	0.1146	0.7822	0.9780	702.5	0.6870							
298.19	0.3286	0.3297	0.3417	1.3427	727.4	0.9767							
318.26	0.3276	0.3300	0.3424	1.0392	712.0	0.7399							
338.36	0.3259	0.3303	0.3438	0.8381	696.4	0.5836							
358.28	0.3229	0.3317	0.3454	0.6975	680.4	0.4746							

* Subscript H - n-hexane; O - n-octane; DD - n-dodecane; HD - n-hexadecane

Table 3.35

Viscosity Coefficients for the Benzene plus n-Hexane System at Saturated Vapour Pressure

Temperature (K)	x_B^*	η/ρ $(mm^2\ s^{-1})$	ρ $(kg\ m^{-3})$	η *(mPa s)*
283.15	*0.4995*	*0.5550*	*755.4*	*0.4193*
288.15	*0.4995*	*0.5280*	*750.6*	*0.3963*
298.19	*0.4997*	*0.4806*	*741.0*	*0.3561*
313.23	*0.4999*	*0.4214*	*726.5*	*0.3062*
333.36	*0.5002*	*0.3603*	*706.4*	*0.2545*
353.29	*0.5007*	*0.3156*	*685.5*	*0.2163*
373.28	*0.5013*	*0.2796*	*664.2*	*0.1857*

* *Subscript B - benzene*

Table 3.36

Viscosity Coefficients for the Benzene plus n-Octane System at Saturated Vapour Pressure

Temperature (K)	x_B *	η/ρ ($mm^2\ s^{-1}$)	ρ ($kg\ m^{-3}$)	η (mPa s)	x_B	η/ρ ($mm^2\ s^{-1}$)	ρ ($kg\ m^{-3}$)	η (mPa s)
283.15	0.2539	0.7932	736.0	0.5838	0.5041	0.7501	769.6	0.5773
288.15	0.2539	0.7503	731.8	0.5491	0.5041	0.7076	765.1	0.5414
298.19	0.2536	0.6723	723.4	0.4863	0.5037	0.6351	756.2	0.4803
313.23	0.2533	0.5815	710.5	0.4132	0.5034	0.5478	742.6	0.4068
333.36	0.2527	0.4881	693.1	0.3383	0.5027	0.4606	724.1	0.3335
353.29	0.2518	0.4184	675.3	0.2825	0.5016	0.3949	705.6	0.2786
373.28	0.2503	0.3644	657.1	0.2394	0.4999	0.3441	686.6	0.2363
393.2	0.2482	0.3214	638.2	0.2051	0.4975	0.3063	667.2	0.2044
283.15	0.6746	0.7421	800.2	0.5938	0.8255	0.7609	835.5	0.6357
288.15	0.6746	0.6998	795.5	0.5567	0.8255	0.7153	830.6	0.5941
298.19	0.6743	0.6255	786.1	0.4917	0.8253	0.6345	820.7	0.5207
313.23	0.6741	0.5377	771.9	0.4151	0.8252	0.5410	805.8	0.4359
333.36	0.6735	0.4509	752.6	0.3393	0.8249	0.4485	785.6	0.3524
353.29	0.6726	0.3852	732.7	0.2823	0.8243	0.3822	764.8	0.2923
373.28	0.6713	0.3354	712.4	0.2390	0.8236	0.3306	743.5	0.2458
393.2	0.6694	0.2982	691.3	0.2062	0.8224	0.2917	721.6	0.2105

* Subscript B - benzene

Table 3.37

Viscosity Coefficients for the Benzene plus n-Decane System at Saturated Vapour Pressure

Temperature (K)	x_B*	η/ρ $(mm^2\ s^{-1})$	ρ $(kg\ m^{-3})$	η *(mPa s)*
283.15	*0.4991*	*1.0360*	*780.5*	*0.8086*
288.15	*0.4991*	*0.9693*	*776.3*	*0.7525*
298.19	*0.4986*	*0.8544*	*767.9*	*0.6561*
313.23	*0.4982*	*0.7224*	*755.2*	*0.5456*
333.36	*0.4972*	*0.5948*	*737.6*	*0.4387*
353.29	*0.4956*	*0.5023*	*720.0*	*0.3617*
373.28	*0.4931*	*0.4319*	*701.8*	*0.3031*
393.2	*0.4895*	*0.3785*	*682.9*	*0.2585*

* *Subscript B - benzene*

Table 3.38

Viscosity Coefficients for the Benzene plus n-Dodecane System at Saturated Vapour Pressure

Temperature (K)	x_B*	η/ρ ($mm^2\ s^{-1}$)	ρ ($kg\ m^{-3}$)	η (mPa s)	x_B	η/ρ ($mm^2\ s^{-1}$)	ρ ($kg\ m^{-3}$)	η (mPa s)
283.15	0.2509	1.8759	769.4	1.443	0.4994	1.4301	789.1	1.129
288.15	0.2509	1.7204	765.7	1.317	0.4994	1.3245	785.0	1.040
298.19	0.2504	1.4611	758.1	1.108	0.4988	1.1478	776.9	0.8917
313.23	0.2500	1.1851	746.6	0.8848	0.4983	0.9494	764.5	0.7258
333.36	0.2490	0.9321	731.0	0.6814	0.4973	0.7624	748.0	0.5703
353.29	0.2473	0.7609	715.6	0.5445	0.4954	0.6327	731.2	0.4626
373.28	0.2446	0.6374	699.7	0.4460	0.4925	0.5368	714.3	0.3834
393.2	0.2408	0.5469	683.6	0.3739	0.4882	0.4652	697.1	0.3243
283.15	0.7498	1.0700	822.0	0.8795				
288.15	0.7498	0.9961	817.5	0.8143				
298.19	0.7495	0.8756	808.5	0.7079				
313.23	0.7492	0.7364	795.0	0.5854				
333.36	0.7485	0.6011	776.6	0.4668				
353.29	0.7474	0.5054	758.0	0.3831				
373.28	0.7457	0.4330	739.1	0.3200				
393.2	0.7431	0.3785	719.8	0.2725				

* Subscript B - benzene

Table 3.39

Viscosity Coefficients for the Benzene plus n-Hexadecane System at Saturated Vapour Pressure

Temperature (K)	x_B*	η/ρ ($mm^2\ s^{-1}$)	ρ ($kg\ m^{-3}$)	η (mPa s)	x_B	η/ρ ($mm^2\ s^{-1}$)	ρ ($kg\ m^{-3}$)	η (mPa s)
298.19	0.1211	3.4668	773.5	2.682	0.2858	2.8086	779.4	2.189
313.28	0.1207	2.5790	762.9	1.968	0.2852	2.1496	768.5	1.652
333.36	0.1199	1.8675	748.7	1.398	0.2839	1.5880	753.8	1.197
353.29	0.1186	1.4313	734.6	1.051	0.2817	1.2387	739.0	0.9154
373.28	0.1165	1.1399	720.4	0.8212	0.2782	1.0043	724.3	0.7274
393.2	0.1134	0.9417	706.2	0.6650	0.2730	0.8359	709.6	0.5932
298.19	0.5976	1.7153	797.8	1.369	0.8497	1.0139	829.6	0.8411
313.23	0.5971	1.3715	785.9	1.078	0.8495	0.8330	815.9	0.6797
333.36	0.5960	1.0632	769.8	0.8185	0.8491	0.6711	797.4	0.5351
353.29	0.5940	0.8647	753.4	0.6514	0.8483	0.5592	778.4	0.4353
373.28	0.5910	0.7197	736.5	0.5300	0.8472	0.4780	759.2	0.3630
393.2	0.5864	0.6367	719.4	0.4580	0.8454	0.4153	739.5	0.3071

*Subscript B - benzene

Table 3.40

Viscosity Coefficients for the Benzene plus Cyclohexane System at Saturated Vapour Pressure

Temperature (K)	x_B*	η/ρ ($mm^2\ s^{-1}$)	ρ ($kg\ m^{-3}$)	η (mPa s)	x_B	η/ρ ($mm^2\ s^{-1}$)	ρ ($kg\ m^{-3}$)	η (mPa s)
283.15	0.1991	1.1662	801.6	0.9348	0.4020	0.9834	819.1	0.8055
288.15	0.1991	1.0858	796.9	0.8653	0.4020	0.9172	814.2	0.7468
298.19	0.1989	0.9330	787.3	0.7346	0.4017	0.7990	804.4	0.6427
313.23	0.1987	0.7656	772.7	0.5916	0.4014	0.6672	789.5	0.5268
333.36	0.1982	0.6092	752.8	0.4586	0.4007	0.5410	769.2	0.4161
353.29	0.1975	0.5011	732.1	0.3668	0.3995	0.4515	748.0	0.3377
373.28	0.1969	0.4203	711.1	0.2989	0.3977	0.3836	726.7	0.2788
393.2	0.1944	0.3628	689.9	0.2503	0.3950	0.3332	704.5	0.2348
283.15	0.6004	0.8857	839.0	0.7431	0.7949	0.8440	861.3	0.7269
288.15	0.6004	0.8277	834.0	0.6903	0.7949	0.7865	856.2	0.6734
298.19	0.6001	0.7255	823.8	0.5977	0.7947	0.6887	845.8	0.5825
313.23	0.5998	0.6095	808.6	0.4928	0.7945	0.5793	830.2	0.4809
333.36	0.5991	0.4979	788.0	0.3923	0.7941	0.4737	809.1	0.3832
353.29	0.5980	0.4179	766.4	0.3203	0.7934	0.3976	787.0	0.3129
373.28	0.5963	0.3574	744.8	0.2662	0.7922	0.3411	764.7	0.2608
393.2	0.5936	0.3141	722.7	0.2270	0.7905	0.3003	741.6	0.2227
283.15	0.8779	0.8391	872.2	0.7319				
288.15	0.8779	0.7818	867.0	0.6778				
298.19	0.8778	0.6841	856.4	0.5859				
313.23	0.8777	0.5741	840.6	0.4826				
333.36	0.8774	0.4688	819.2	0.3840				
353.29	0.8769	0.3946	797.5	0.3147				
373.28	0.8762	0.3396	775.4	0.2633				

* Subscript B - benzene

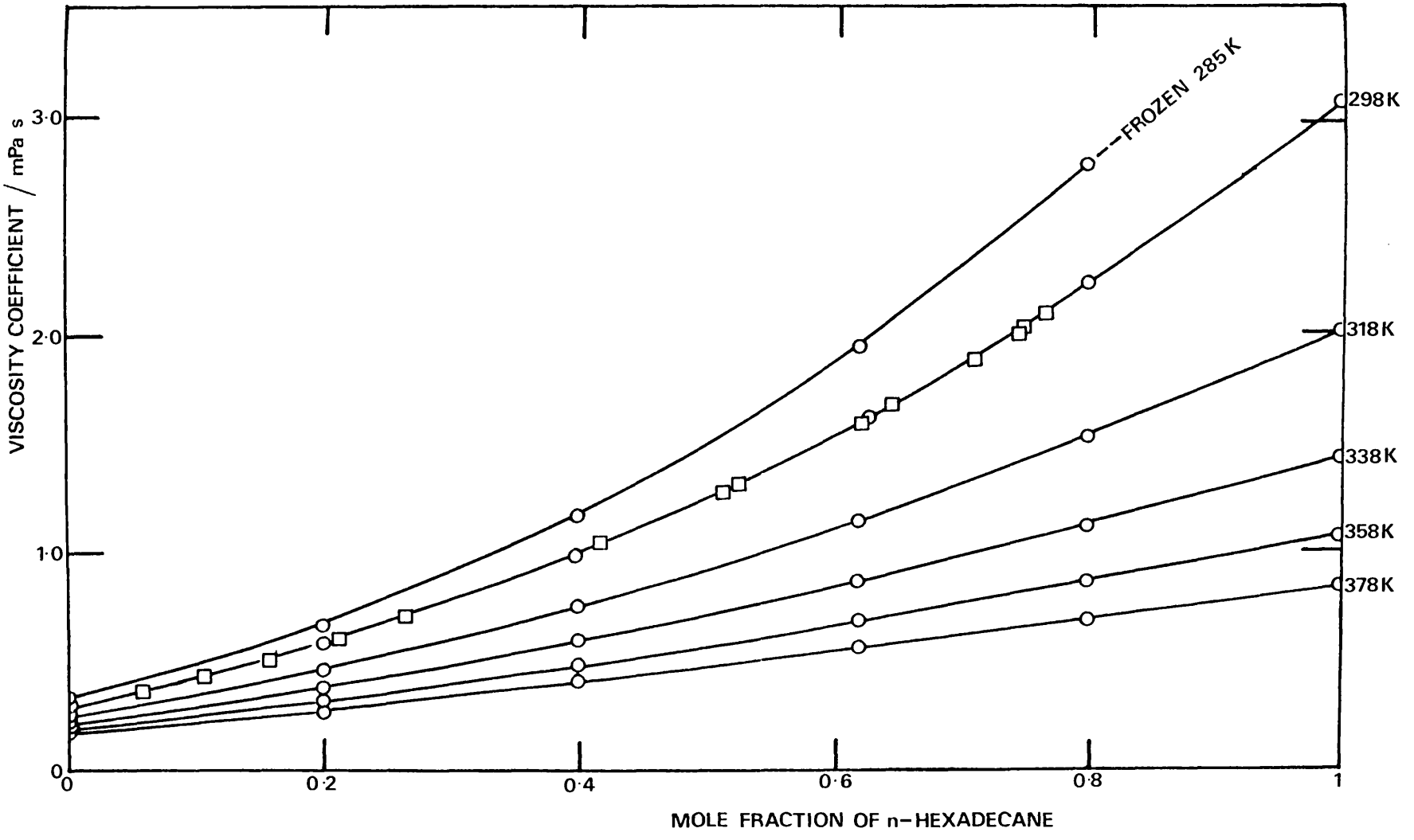

Figure 3.9 Dynamic Viscosity Coefficients for the n-Hexane plus n-Hexadecane System at Saturated Vapour Pressure. □ Results of Heric and Brewer (54) at 298 K.

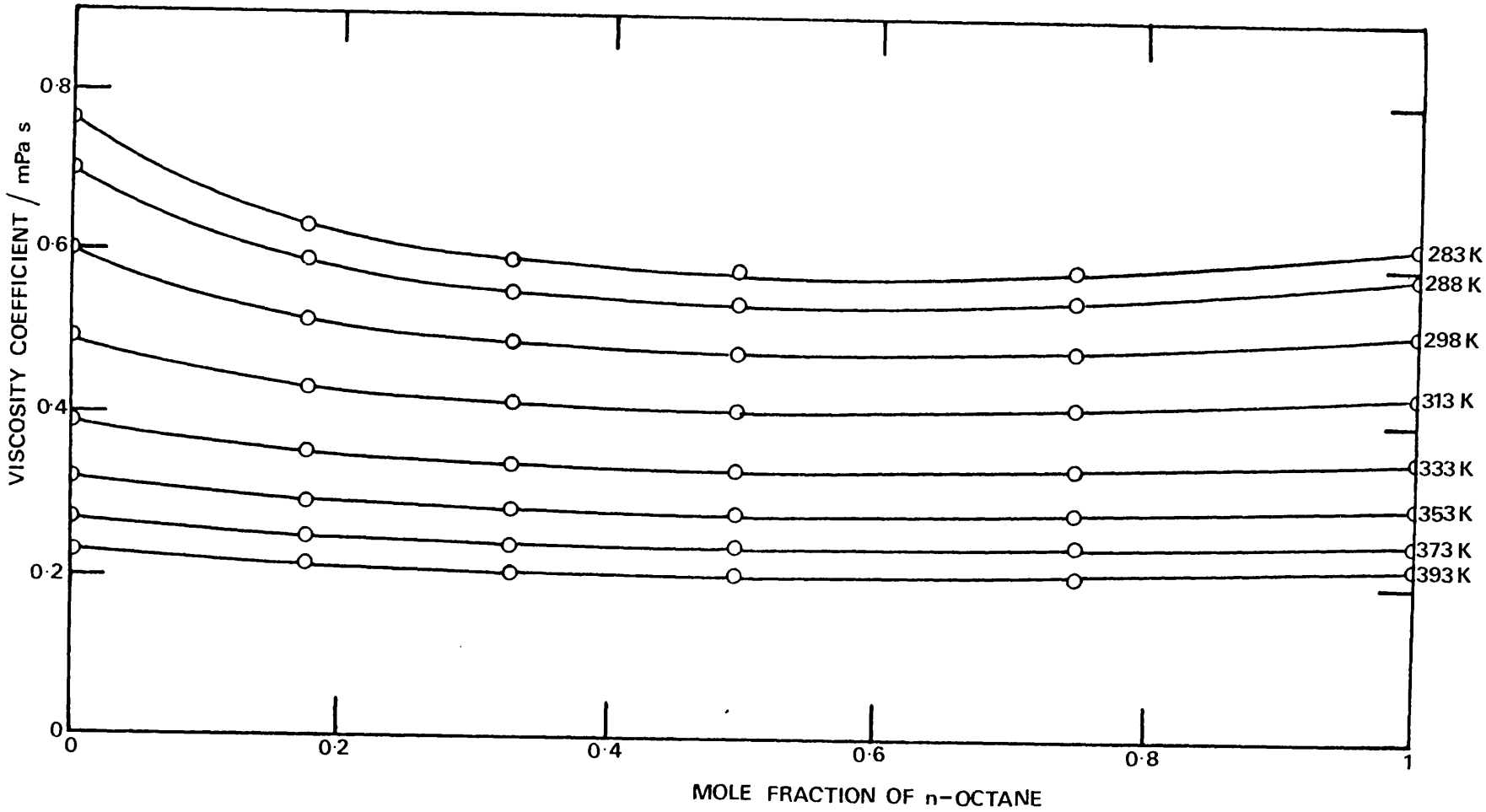

Figure 3.10 Dynamic Viscosity Coefficients for the Benzene plus n-Octane System at Saturated Vapour Pressure.

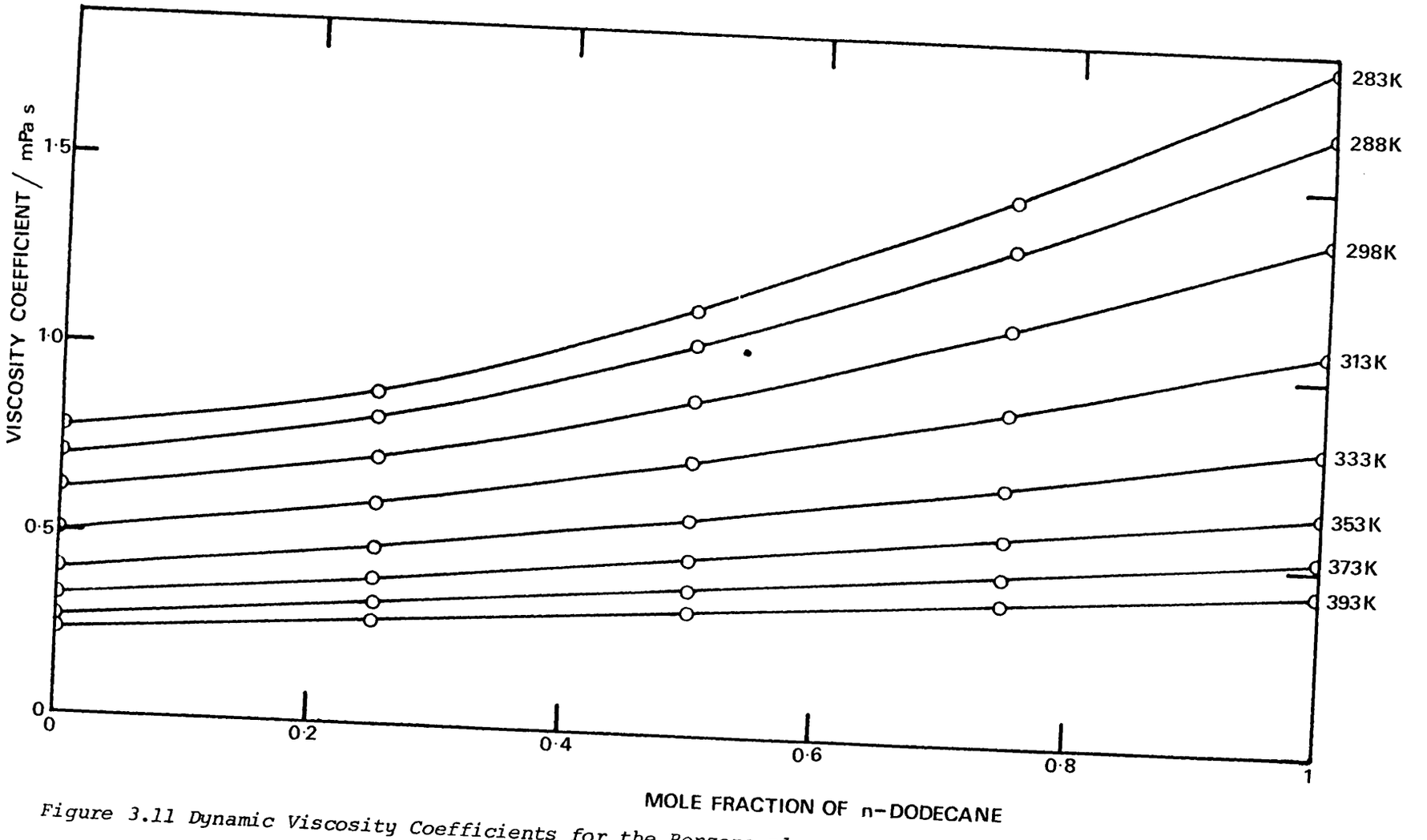

Figure 3.11 Dynamic Viscosity Coefficients for the Benzene plus n-Dodecane System at Saturated Vapour Pressure.

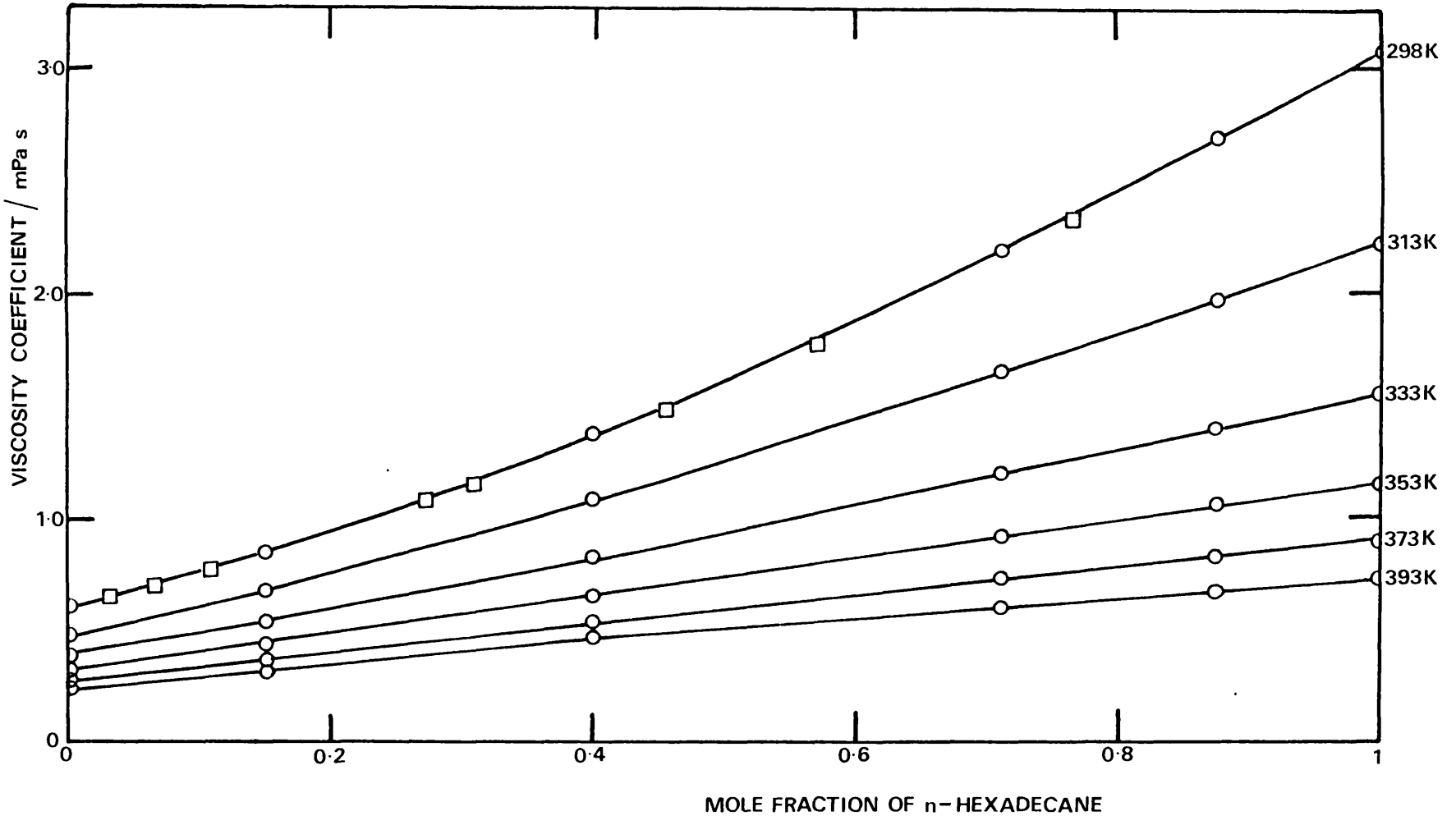

Figure 3.12 Dynamic Viscosity Coefficients for the Benzene plus n-Hexadecane System at Saturated Vapour Pressure. □ *Results of Heric and Brewer (54) at 298 K.*

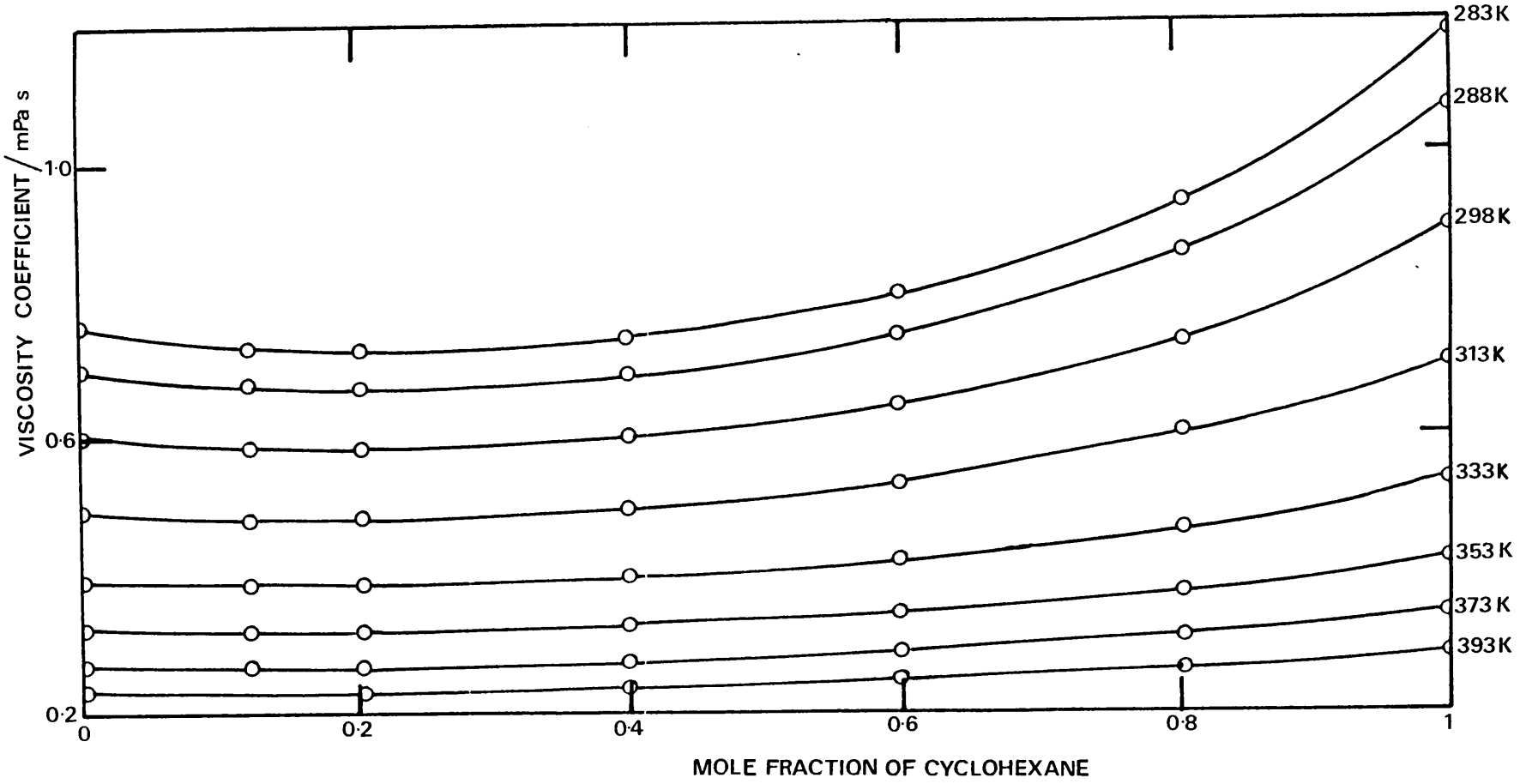

Figure 3.13 Dynamic Viscosity Coefficients for the Benzene plus Cyclohexane System at Saturated Vapour Pressure.

C H A P T E R 4

DENSITIES AND VISCOSITY COEFFICIENTS FOR THE n-HEXANE PLUS n-HEXADECANE SYSTEM AT ELEVATED PRESSURES

4.1 INTRODUCTION

Viscosity coefficients at atmospheric and elevated pressures were obtained using a high pressure falling body viscometer at the National Engineering Laboratory, East Kilbride, Glasgow. This apparatus was built and used by Isdale[114] for the investigation of the pressure dependence of the viscosity coefficient of certain pure liquids at temperatures from 298 K to 373 K up to 500 MPa pressure. In the viscometer the terminal velocity of a hemispherically nosed cylindrical sinker is measured as it falls axially down the centre of a vertical circular tube containing the liquid whose viscosity coefficient is to be measured. More recently the viscometer has been used by Brawn[23] for measurements, under similar conditions of temperature and pressure, of the viscosity coefficients of n-hexane plus cyclohexane mixtures. He recommended a number of general improvements to the design of the viscometer and these suggestions, together with other modifications, have been incorporated in a new viscometer which was designed, built and tested during the period of this research. Discussion of the new viscometer is given in Section 4.5. Because of the length of time involved to develop this new viscometer, measurements on the n-hexane plus n-hexadecane system were made in the original tube, but with a sinker chosen to suit the viscosity coefficient range to be measured. Before measurements could be made, however, it was necessary to calibrate the manganin pressure gauge on several occasions over a period of time to check for any change in gauge characteristics, and to calibrate the viscometer tube/sinker combination to cover the viscosity coefficient range of the system studied. The liquid density under the same experimental conditions is also required to make buoyancy corrections to the falling sinker and improvements have been made to the

density measuring apparatus increasing the accuracy from 0.5 percent to 0.2 percent. These improvements are discussed in Section 4.3.1.

4.2 DESCRIPTION OF THE HIGH PRESSURE APPARATUS

For the measurement of viscosity coefficients and densities under elevated pressure, it is essential to be able to generate and maintain such pressure for a sufficiently long time to enable experimental measurements to be made. It is also important that the temperature be kept constant to within 0.02 K as both density and viscosity coefficients change with changing temperature. This section deals with the control and measurement of pressure and temperature necessary for accurate determination of densities and viscosity coefficients.

4.2.1 Pressure Generation

The pressurising system is shown in Figure 4.1. The system consisted of a Madan Airhydro Pump supplied by an air line, pressure intensifier, pressure gauge block with pressure release valve and a pressure vessel which was enclosed in an oil bath. The pressurising fluid used was a mixture of two parts kerosine to one part Tellus 21 oil. This mixture provided a high freezing pressure fluid with good lubricating properties. Pressures from 0.1 MPa to 200 MPa were obtained using the priming circuit. With taps B and C open and A closed, fluid could be transferred to the pressure vessel via non-return valves D and E.

These valves were only effective at pressures greater than about 20 MPa to 30 MPa so for pressures below this a backing pressure had to be maintained by the air pump to compensate for slight leakage of hydraulic fluid. This was satisfactory and after equilibrium was reached pressure could be held constant. In practice this technique was used for pressures up to 100 MPa. For pressures between 100 MPa and 200 MPa when the desired pressure was reached tap A was opened very quickly slamming

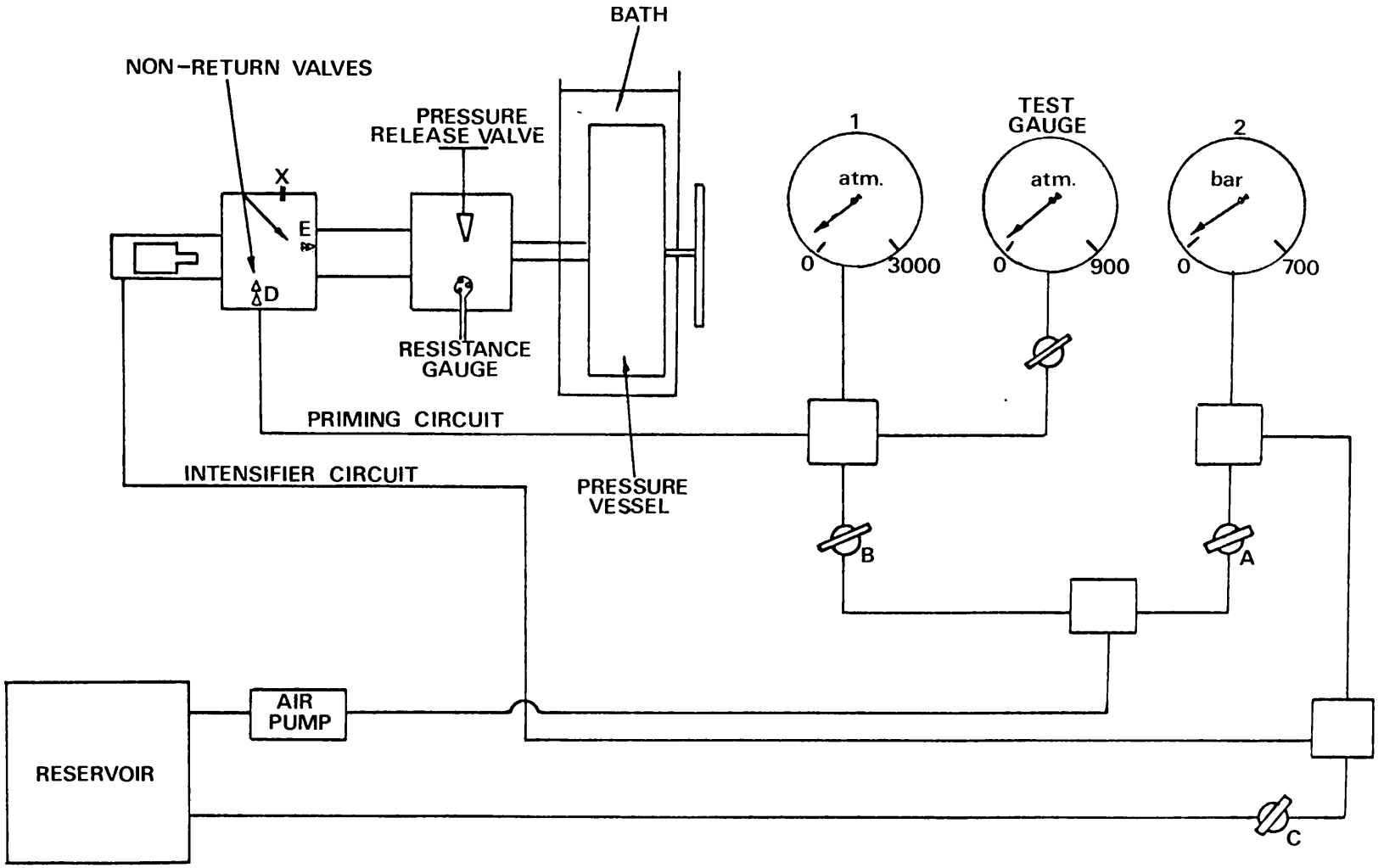

Figure 4.1 High Pressure Apparatus.

the non-return valve D home. For pressures above 200 MPa taps B and C were then closed. With A open fluid was pumped in behind the intensifier piston and when the pressure behind the piston was slightly greater than that in front, non-return valve E opened and hydraulic fluid was transferred to the gauge block and pressure vessel. When the desired pressure was reached valve C was quickly opened slamming non-return valve E closed.

One stroke of the intensifier piston gave a pressure increase of about 100 MPa so if higher pressures than 300 MPa were desired the intensifier piston was first returned to its starting position by using the priming circuit as previously described and the intensifier circuit was then used as before.

4.2.2 Pressure Measurement

Values of pressure were determined by measuring the change in resistance of a length of manganin wire immersed in the pressurising fluid relative to a similar wire at atmospheric pressure attached to the outside of the gauge block. The wires, which were about 3 metres long with a nominal resistance of 100 Ω, were wound loosely and non inductively on ptfe spools. The manganin coil in the pressure line was sufficiently far from the constant temperature bath for it to remain close to room temperature over most of the experimental temperature range. However, heating of the coil was observed at temperatures in excess of 348 K. Wang[115] has shown that the resistance of manganin wire remains effectively constant with increasing temperature up to 323 K but decreases rapidly with temperature above this. To enable the temperature coefficient of resistance to be eliminated the resistance ratio technique was used with both manganin

coils close enough together to ensure that they were at approximately the same temperature. The change in resistance ratio was then solely due to the effect of pressure on one of the coils. The resistance ratio was measured using a Rosemount Engineering Co. Ltd Precision Comparison Bridge, type VLF 51A.

Both the resistance ratio of the pressurised to unpressurised and unpressurised to pressurised wires were measured and an average value obtained by taking the reciprocal of one and adding it to the other. The reciprocal differed from the other by between 0.000 030 and 0.000 050. This procedure was recommended by the manufacturers to obtain maximum accuracy from the Bridge.

It was also found that the averaged atmospheric resistance ratio, R_o, was subject to an increase of 0.000 025/day. Since R_o was measured before each run this did not constitute any serious problem as no significant change occurred during the period of a run. The continual increase was thought to be due to the kerosine/oil environment of one of the wires. Boren, Babb, Jr. and Scott[116] have noted a similar effect with manganin wire immersed in petroleum ether. They have noted a drift in atmospheric resistance of 0.0065 Ω in a period of two months.

Pressures up to 200 MPa could be set roughly with gauge 1 (Figure 4.1) and then measured accurately with the manganin resistance gauge. For pressures above 200 MPa the resistance ratio was calculated, the resistance gauge set, and hydraulic fluid pumped in till the desired resistance ratio was obtained. Gauge 2 was used to follow the travel of the high-pressure piston during the generation of pressures above

200 MPa. When the piston had reached the end of its stroke the pressure indicated by gauge 2 increased from about 10 MPa to approximately 30 MPa.

During experiments, after a desired pressure was reached, ten to fifteen minutes were allowed for the system to regain thermal equilibrium and the two ratios measured. The average value then gave a measure of the pressure.

4.2.3 Pressure Gauge Calibration

The manganin pressure gauge was calibrated using a Budenberg Dead Weight Tester. A facility was provided at position X on the high pressure apparatus (see Figure 4.1) for attaching a high pressure line to the Budenberg Dead Weight Tester and this line was filled with the recommended mixture of brake fluid and castor oil in the ratio 2:1. Pressure was generated as described in Section 4.2.1, using first the priming circuit and then the intensifier circuit.

The Budenberg Dead Weight Tester consisted of a small close fitting piston and sleeve assembly on which weights were hung and when the pressure below the piston was slightly greater than the pressure due to the weight above, the piston lifted. Slow leakage of fluid between the piston and sleeve caused the weights with the piston to fall slowly again and at the exact balance point a reading of resistance ratio was taken. A further weight was then added, the fluid pressure increased and the resistance ratio taken at the balance point. This procedure was repeated till a set of readings covering the range of pressure from 100 MPa to 500 MPa was obtained. The slow leakage of the castor oil/brake fluid mixture past the piston eventually resulted

in hydraulic fluid reaching the piston, at which point the rate of fall of the weights was considerably increased as the hydraulic fluid was less viscous. It was then necessary to dismantle and refill the line with more castor oil/brake fluid mixture. In general, two runs were completed before this occurred. Five calibrations of the pressure gauge were carried out using the Budenberg Dead Weight Tester. Two calibrations were made before the density measurements were commenced and two after, with the final calibration on completion of the viscosity coefficient measurements. The measurements covered a period of about eight months so any change in the manganin gauge characteristics would show up as differences between the calibrations.

The manganin pressure gauge is widely used in hydrostatic pressure systems. The electrical resistance of a coil of manganin wire was employed on a pressure gauge by Bridgman[117] and subsequent investigations[116,118-121] have characterised the properties and seasoning techniques for manganin coil pressure gauges. It was found that the electrical resistance change with pressure was linear to 800 MPa.

Since as has already been discussed the temperature coefficient of resistance has been eliminated by using a ratio technique the resistance ratio results were fitted to an equation of the form

$$P = A\ (R_p/R_o) - B \qquad (4.1)$$

where R_o is the atmospheric pressure resistance ratio and R_p the resistance ratio at pressure, P, and A and B are constants.

The calibration results are given in Table 4.1, with A and B obtained by least squares fit. In the final two columns pressures were calculated for specific values of the resistance ratio and these show

Table 4.1

Calibration of Manganin Pressure Gauge

Calibration number	*DWT pressure (MPa)*	R_P/R_o	*Maximum deviation (MPa)*	*A (MPa)*	*B (MPa)*	*Pressure at* $R_P/R_o = 1.002$ *(MPa)*	*Pressure at* $R_P/R_o = 1.012$ *(MPa)*
1	*0.101*	*1.0*	*0.1*	*40407.460*	*40407.362*	*80.9*	*485.0*
	100.134	*1.002476*					
	200.157	*1.004950*					
	300.180	*1.007427*					
	400.202	*1.009900*					
2	*0.101*	*1.0*	*0.4*	*40440.807*	*40440.450*	*81.2*	*485.7*
	100.134	*1.002457*					
	200.157	*1.004931*					
	300.180	*1.007426*					
	400.202	*1.009892*					
	500.225	*1.012357*					
3	*0.101*	*1.0*	*0.1*	*40329.683*	*40329.587*	*80.8*	*484.1*
	100.134	*1.002479*					
	150.146	*1.003719*					
	200.157	*1.004963*					
	250.169	*1.006199*					
	300.180	*1.007444*					
	350.192	*1.008682*					

- continued -

Table 4.1 (continued)

Calibration of Manganin Pressure Gauge

Calibration number	*DWT pressure (MPa)*	R_P/R_o	*Maximum deviation (MPa)*	*A (MPa)*	*B (MPa)*	*Pressure at R_P/R_o = 1.002 (MPa)*	*Pressure at R_P/R_o = 1.012 (MPa)*
	400.202	*1.009923*					
	450.214	*1.011159*					
	500.225	*1.012399*					
4	*0.101*	*1.0*	*0.5*	*40291.833*	*40291.845*	*80.6*	*483.5*
	100.134	*1.002481*					
	200.157	*1.004969*					
	300.180	*1.007463*					
	400.202	*1.009937*					
	500.225	*1.012405*					
5	*0.101*	*1.0*	*0.2*	*40493.722*	*40493.510*	*81.2*	*486.1*
	150.146	*1.003697*					
	200.157	*1.004936*					
	300.180	*1.007414*					
	400.202	*1.009876*					
					Average pressure	*80.9*	*484.9*
					Maximum difference	*0.6*	*2.2*

that all five calibrations give pressures which agree to within 0.5 percent of the mean over the pressure range 80 MPa to 480 MPa. It was therefore concluded that the manganin gauge characteristics did not vary significantly with time. From Table 4.1 it is seen that within the accuracy of measurements the maximum deviation from equation (4.1) is only 0.5 MPa in any one calibration showing that the resistance ratio is indeed linearly related to pressure between 80 MPa and 480 MPa. The main difficulty in the calibration experiments was, as already mentioned, the depletion of castor oil/brake fluid mixture allowing hydraulic fluid to enter the Dead Weight Tester piston/sleeve assembly. Calibrations 1 and 3 were free from this problem and coefficients were averaged to give A = 40368.572 MPa and B = 40368.475 MPa. These averaged A and B values were used to calculate all experimental pressures and based on the comparison of calibration runs the maximum errors incurred by this technique are estimated to be 0.6 MPa at low pressures (80 MPa) and 2 MPa at high pressures (500 MPa).

It was not possible to use the Budenberg Dead Weight Tester below 100 MPa but a comparison between pressures measured using the test gauge and those measured using the resistance gauge showed that the calibrations could be linearly extrapolated down to 0.1 MPa. The results of this calibration are shown in Table 4.2.

The test gauge, which could be read to $\pm$ 0.3 MPa had an accuracy of $\pm$ 0.3 MPa as determined by calibration using a different Dead Weight Tester. The resistance gauge was accurate to better than $\pm$ 0.6 MPa so within experimental error both the test gauge and the resistance gauge give the same pressure readings.

Table 4.2

Calibration of Manganin Pressure Gauge Below 100 MPa

Test gauge pressure (MPa)	*Resistance gauge pressure (MPa)*	*Difference (MPa)*
0.1	*0.1*	*0*
0.6	*0.3*	*0.3*
3.1	*2.5*	*0.6*
15.6	*15.0*	*0.6*
22.2	*21.6*	*0.6*
25.3	*24.7*	*0.6*
37.7	*36.9*	*0.8*
42.2	*41.8*	*0.4*
57.6	*57.2*	*0.4*
0.1	*0.1*	*0*
5.2	*4.6*	*0.6*
11.1	*10.6*	*0.5*
19.2	*19.5*	*-0.3*
32.1	*32.0*	*0.1*
40.9	*40.7*	*0.2*
50.7	*50.7*	*0*
61.8	*61.9*	*-0.1*
70.6	*70.8*	*-0.2*
81.7	*82.0*	*-0.3*

4.2.4 Temperature Measurement

The temperature of the pressure vessel was controlled by immersion in a bath containing Marlotherm S heating oil. The bath was insulated on all sides with Fibreglass and heat loss from the surface minimised by using Alplas insulating spheres.

The temperature of the bath fluid was controlled by a 3 kW Grant Instruments controller with mercury contact thermometer. Additional stirring (and movement of the pressure vessel during viscosity coefficient experiments) ensured good circulation of the bath fluid. The arrangement is shown in Figure 4.2. Temperature control was found to be better than $\pm$ 0.03 K over the whole temperature range.

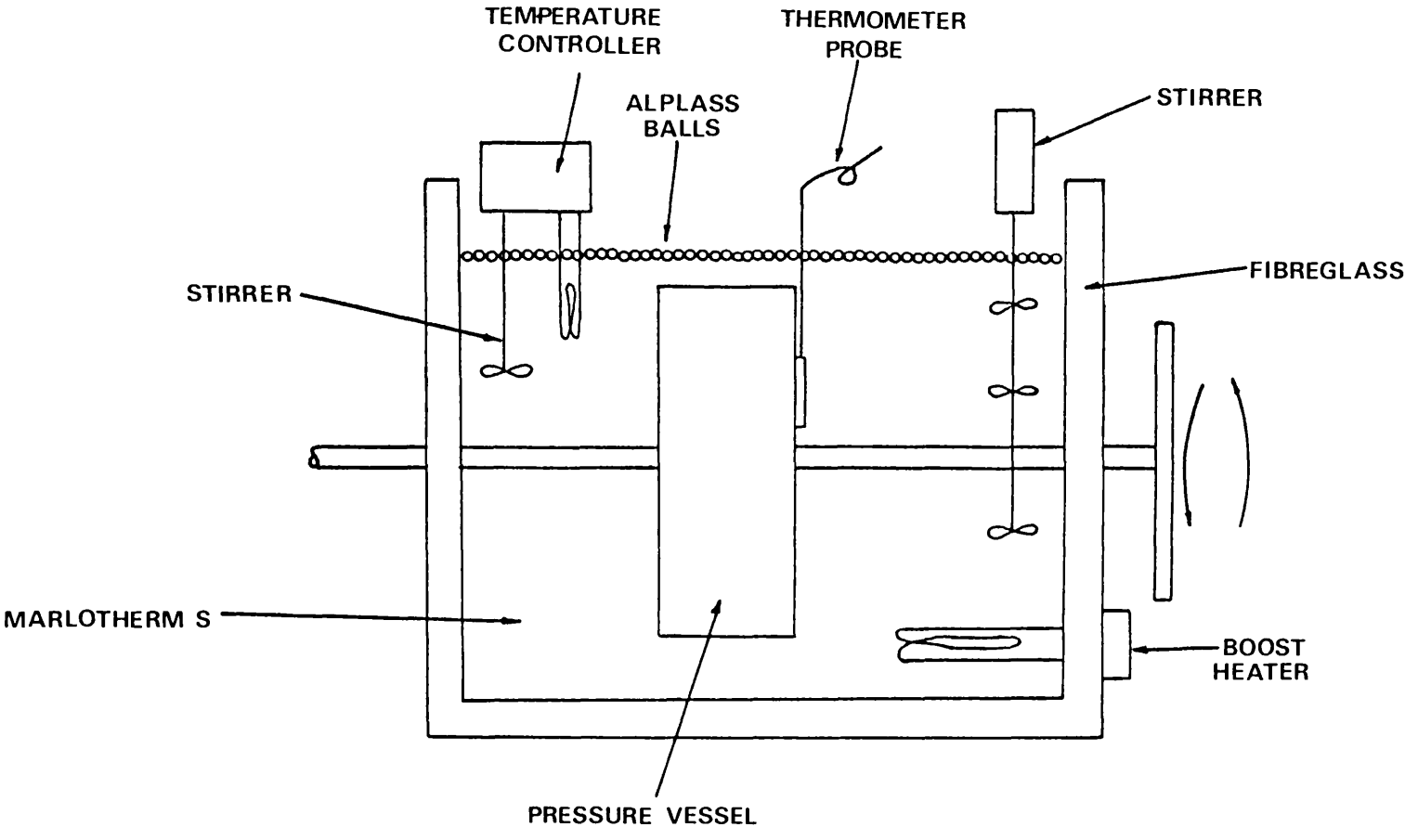

Figure 4.2 Constant Temperature Bath.

Temperature was measured using a Hewlett Packard 2801A quartz thermometer which had a stated accuracy of ± 0.02 K. A calibration chart was provided with the quartz probe and temperatures were corrected using this chart.

The quartz thermometer was checked at four temperatures by measuring the temperature at a particular point in the bath with both the quartz thermometer and a National Physical Laboratory calibrated platinum resistance thermometer coupled to the Rosemount Engineering Company Precision Comparison Bridge. The results are shown in Table 4.3.

Table 4.3

Calibration of Quartz Thermometer

Quartz (measured temperature) (K)	*Calibration correction (K)*	*Quartz (corrected temperature) (K)*	*Platinum resistance temperature (K)*
303.039	*-0.03*	*303.01*	*303.04*
323.880	*-0.04*	*323.84*	*323.87*
348.490	*-0.02*	*348.47*	*348.50*
373.329	*+0.03*	*373.36*	*373.39*

The stated accuracy of the Rosemount Engineering Company Precision Comparison Bridge with a ratio of 0.2 was ± 0.000 020. This is equivalent to ± 0.02 K. The stated accuracy of the platinum resistance thermometer calibration was ± 0.01 K. This lead to an uncertainty of ± 0.03 K in the temperature measured by the platinum resistance thermometer. Table 4.3 illustrates that measurements with the platinum resistance thermometer are in agreement with the quoted accuracy of ± 0.02 K for the quartz thermometer.

Throughout the viscosity coefficient and density experiments a continual check on the reading given by the quartz thermometer at the ice point was carried out. This ensured that the calibration given above remained valid.

Though bath temperature fluctuations of $\pm$ *0.03 K were observed during a run corresponding variations in sample temperature were much smaller due to the very high thermal inertia of the pressure vessel. It is therefore estimated that the sample temperatures quoted are within* $\pm$ *0.02 K of the absolute temperature.*

4.3 DENSITIES

Values of density at elevated pressure are required to make buoyancy corrections to the falling sinker in the viscosity coefficient experiments. This requires a separate experiment where density is measured as a function of pressure. For measurements under pressure one of the simplest methods is to fill a flexible metal bellows with a known mass of liquid at atmospheric pressure and then measure the change in length produced by an increase in pressure. Density at pressure, ρ_p, is then given by

$$\rho_p = \frac{M}{M/\rho_o - A\Delta L} \qquad (4.2)$$

M/ρ_o, the liquid mass, M, divided by liquid density at atmospheric pressure, ρ_o, is the initial liquid volume and the product of bellows area, A, and change in length of the bellows, ΔL, gives the change in volume under pressure. This is the method employed in this work and is similar to that described by Bridgman[122]. The mass of liquid, its density at atmospheric pressure, the bellows area and the change in length of the bellows with increase in pressure were all measured separately and values combined to give the density under particular conditions of temperature and pressure. A significant improvement in the accuracy of the density measurements was made by improving the method of measuring the change in length of the bellows under an applied pressure. The method used is fully described in Section 4.3.1.

4.3.1 Experimental Measurements

The bellows were made by Isdale[114] from stainless steel. They were 14 cm long and 2 cm in diameter and had a total of 50 convolutions. At either end of the flexible section were two caps one of which had

a screw which could be removed to allow filling and the other a threaded portion to enable a rod to be attached which was used to measure the change in length of the bellows under an applied pressure as described later. The bellows could accommodate a reduction in length of about 3 cm before distorting and held a volume of approximately 25 cm^3.

Determination of Liquid Mass and Initial Volume

The bellows were cleaned with AnalaR acetone and dried by hanging up-side-down, while heating with a blower and tapping the sides to release acetone vapour condensing at the outlet.

When the bellows were completely dry, the weight was taken immediately, as dry steel adsorbs moisture from the atmosphere thus altering the weight. After weighing, the liquid whose density was to be measured was inserted by syringe, allowing the weight of the plunger alone to force the liquid through the syringe needle, so reducing the possibility of air bubbles being trapped on the bellows' walls. The bellows were immersed to the neck in an ultrasonic bath while filling was taking place. This freed any air bubbles trapped by the filling procedure.

After filling, the bellows were sealed with a 'dowty' seal and were again washed with acetone and dried. The weight was measured and the difference between the two gave the sample mass, M.

The initial volume, V_o, was obtained from the mass and the density of the liquid at atmospheric pressure and the temperature at which the experiment was to be run. This density was measured as described in Section 3.3.

Determination of Bellows Area

A 30 cm length of uniform 1.93 mm bore capillary glass tubing with markings etched every 10 cm was calibrated by weighing a slug of mercury which had been run from the tubing after measuring its length in the glass. This was repeated with the mercury in a different portion of the glass to ensure that the bore was uniform and this gave the internal volume of the tube per unit length, v.

The bellows were attached to the tubing by means of flexible PVC hose and held as shown in Figure 4.3. To obtain a value of bellows area the micrometer was screwed in till the liquid meniscus was on the first calibration mark in the glass tubing and a micrometer reading, R, was taken. The micrometer was then screwed further till the meniscus reached the next mark and a second reading of R was taken. This was repeated for all four calibration marks after which the liquid meniscus was returned to the first calibration mark and the procedure repeated five times till 20 results of bellows area, A, were obtained from the equation

$$A = \frac{v(H_k - H_j)}{(R_k - R_j)} \qquad (4.3)$$

where R is the micrometer reading and H the height of the liquid in the glass tubing at marks j and k. The average value found for A was $(2.20 \pm 0.03) \times 10^{-4}\ m^2$. *This uncertainty of* $\pm$ *1.5 percent in bellows area was higher than is desired as this alone can lead to an uncertainty of about 0.3 percent in density. The major source of error was considered to be due to slight movement of the flexible hose producing large changes in* $(R_k - R_j)$ *for particular calibration marks from one run to the next.*

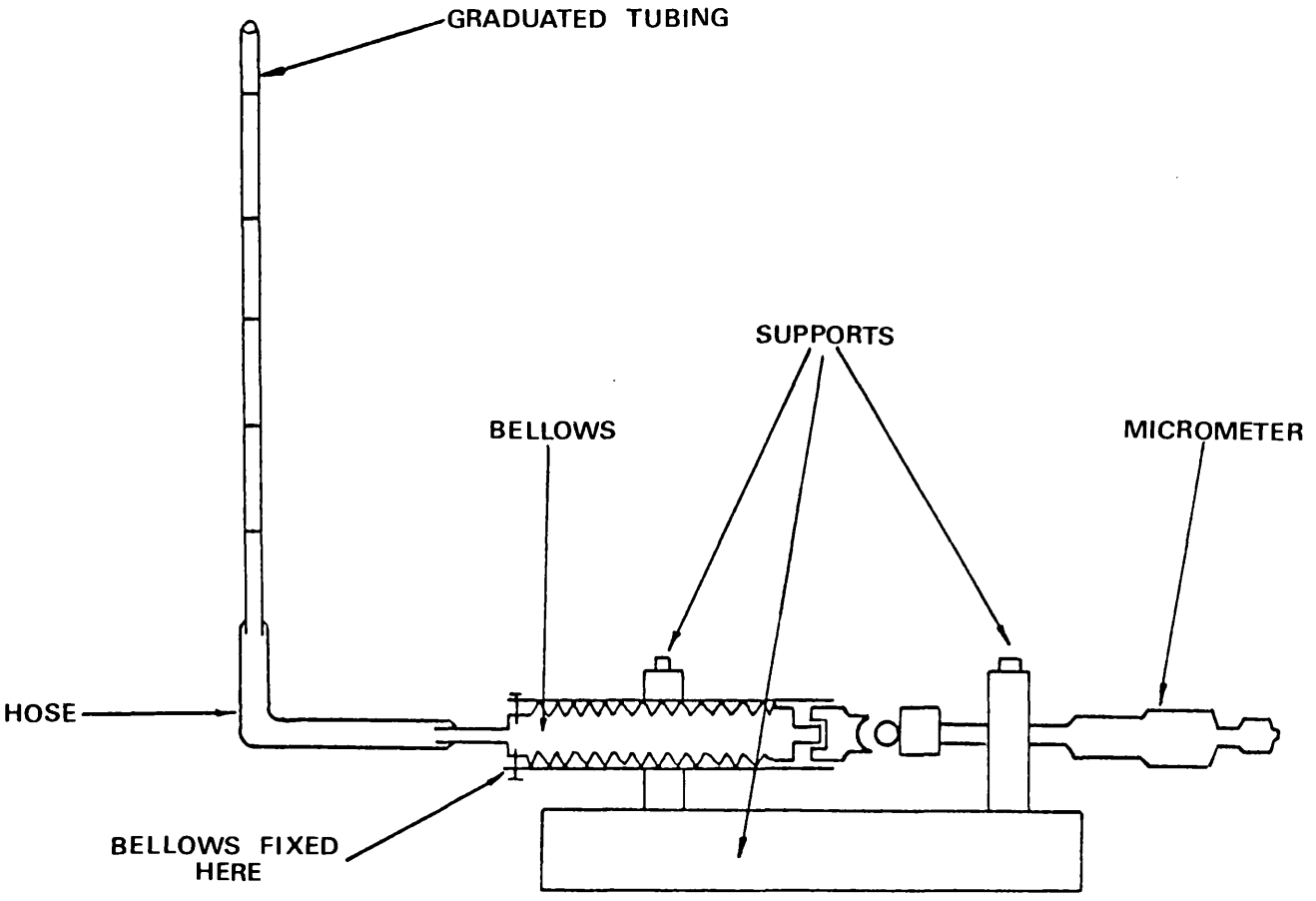

Figure 4.3 Apparatus for Measuring Bellows Area.

The uncertainty caused by the flexible hose could be eliminated by using a different method. If the liquid expelled by the bellows was run through microbore capillary tubing straight into a container on an accurate balance, measurement of the change in weight produced by a change in length of the bellows should produce a more accurate value for the bellows area. However, if this method was used a separate fill would be required for each run.

A 0.5 percent uncertainty in density leads to only a 0.1 percent uncertainty in the viscosity coefficient and so it was decided to accept the value of 2.20×10^{-4} m^2 for A which agreed to within 0.5 percent with the value of 2.21×10^{-4} m^2 previously found by Isdale[114] for the same bellows using a different calibration method.

Determination of Change in Length of Bellows under Applied Pressure

The method used by Isdale[114] for determining the change in length of the bellows gave an estimated uncertainty of 0.1 mm on each reading which led to a contribution of $\pm$ 0.2 percent to the total uncertainty in the calculated density. This uncertainty arose because the micrometer used to measure the change in length of the bellows was attached to the thermostat bath and slight movement of the pressure vessel with respect to the micrometer was thus possible. In order to reduce this uncertainty a new technique was devised in conjunction with Brawn[123]. The experimental set up is shown in Figure 4.4. The main advantage of this design over that of Isdale[114] was that the micrometer was fixed directly to the AMINCO high pressure tubing thus eliminating any uncertainty caused by movement of the pressure vessel. This arrangement minimised any angular error between the micrometer and the ferrite tip and the use of perspex in the construction of

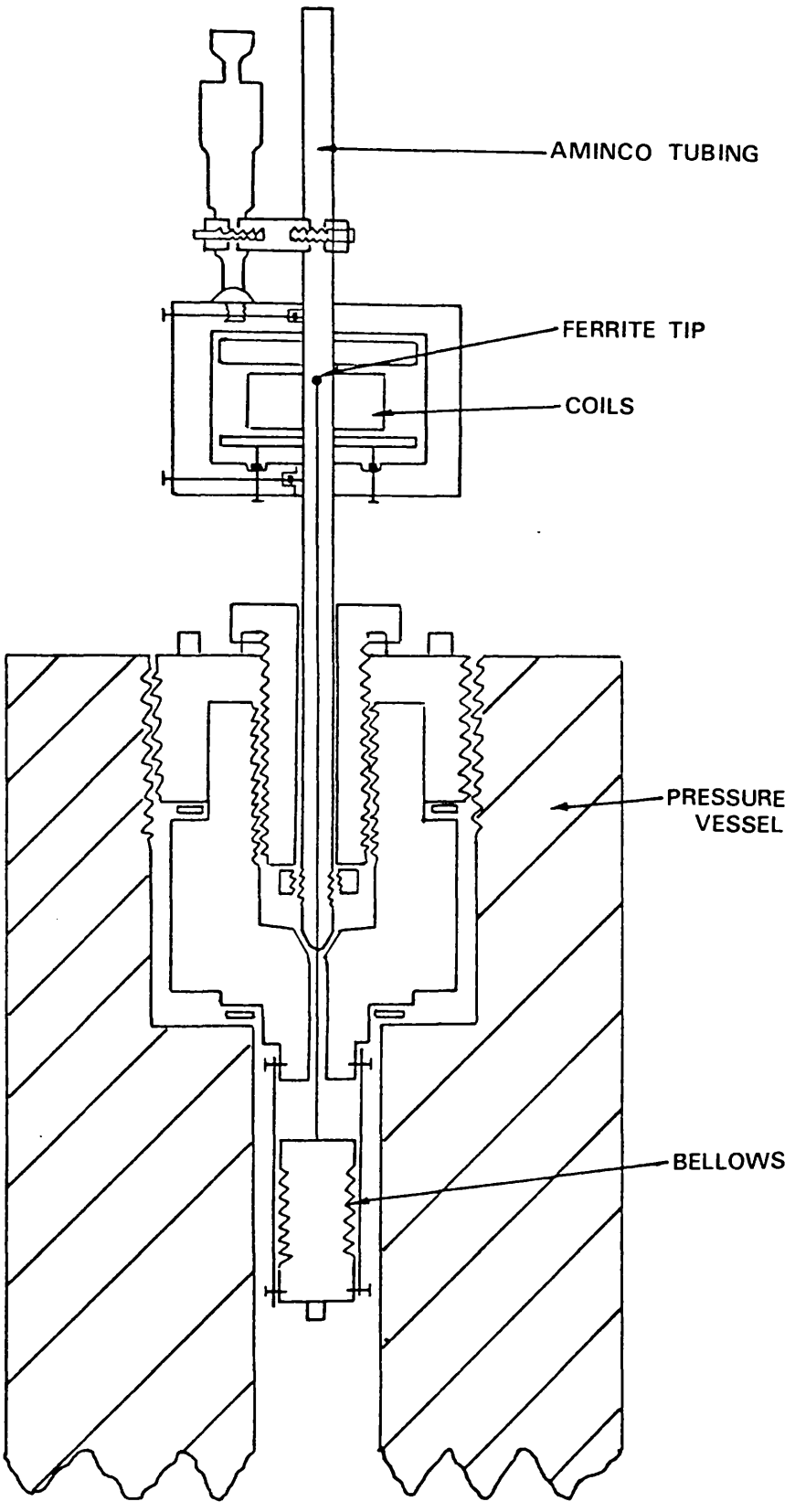

Figure 4.4 Apparatus for Measuring Density at Elevated Pressure.

the coil block also minimised the amount of iron around or close to the coils. A steel dome-headed screw attached to the perspex provided a solid surface on which the micrometer could bear and the coil block was held tight to the AMINCO tubing by means of adjustable screws bearing on a copper sheath.

To measure the change in length of the bellows under pressure the following procedure was carried out. After weighing the bellows, one end was screwed to a rigid housing which ensured linear movement of the bellows. A length of non-magnetic stainless steel rod with a ferrite tip was screwed into the free end of the bellows and the housing was then attached to the pressure vessel end cap and the end cap tightened to the pressure vessel. The free end of the rod projected through the end cap of the pressure vessel into the length of non-magnetic high-pressure AMINCO tubing which was sealed at its extremity. The coil block, containing a pair of coils, could be moved along the length of the tube and these coils together with a second pair of coils in an insulated box mounted in a fixed position remote from unwanted temperature and magnetic influences, were connected to form a bridge circuit and electrical connections completed at a bridge unit. The exact position of the ferrite tip was detected by these coils by observing the operation of a Schmitt trigger as the bridge circuit was unbalanced by the ferrite tip entering the detector coils. The trigger operated when the ferrite tip was midway between the two detector coils. The bridge unit circuits are shown in Figure 4.5.

The bridge was balanced initially with the detector coils remote from the influence of the ferrite tip. The detector block was then moved manually up the tubing till the coils had just passed the ferrite tip.

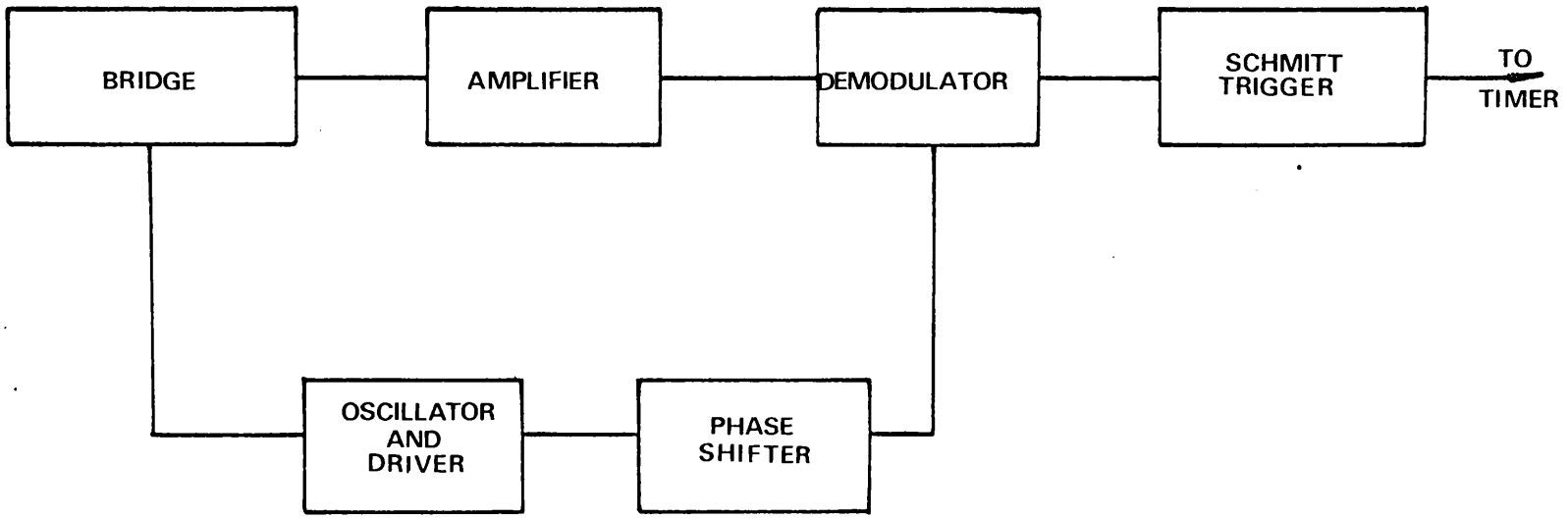

Figure 4.5 Bridge Unit.

The micrometer attached to the tubing was then used to move the block slowly down again till the position of the tip was detected by the Schmitt trigger operating. A micrometer reading, R, the temperature and the pressure were recorded. This procedure was carried out till three consecutive micrometer readings agreed to within $\pm$ 0.005 mm. Pressure was then applied and the system left for ten minutes to regain thermal equilibrium. The bridge was then rebalanced and a further set of readings taken. This was continued till all the desired points along the isotherm had been measured. $(R_o - R_p)$, where R_o is the micrometer reading at atmospheric pressure and R_p the reading at pressure P, then gave a measure of the change in length of the bellows. Pressure and temperature were measured using a manganin wire resistance gauge and a Hewlett Packard thermometer as previously described.

Freezing of the liquid sample in the bellows was detected by increasing values of $(R_o - R_p)$ after thermal equilibrium should have been reached. When this situation had been detected, the pressure was reduced to reverse the freezing process thus avoiding possible damage to the bellows. A gradual decrease in pressure was also observed as the bellows contracted under freezing.

4.3.2 Calibration of the Density Apparatus

Absolute Measurement of Density

The equation used to calculate density under pressure, ρ_p, which was given earlier as equation (4.2) is

$$\rho_p = \frac{M}{M/\rho_o - A\Delta L}$$

where A is the bellows area, M the liquid mass, ρ_o the density at atmospheric pressure and ΔL the measured change in length. Both A and ΔL are pressure dependent because of the effect of pressure on the various components. Allowing for the compression of steel, the bellows area is now given by $A_p = A_o(1 - 2\alpha P)$ where A_o is the bellows area at atmospheric pressure, A_p is the bellows area at pressure, P, and α is the linear coefficient of compressibility. ΔL which was measured as $(R_o - R_p)$ is correctly given by $(R_o - R_p) - \{l_o - l_o(1 - \alpha P)\} - kP$ where l_o is the initial length of the rod between the bellows and the ferrite tip and R_o, R_p, α and P defined as above.

This equation arises from the fact that under an applied pressure the rod contracts while the high pressure AMINCO tubing expands.

$(R_o - R_p) - \{l_o - l_o(1 - \alpha P)\}$ gives the change in length of the steel components and kP gives a measure of the effect of the pressurising fluid on the high-pressure tubing to which the micrometer is attached. k is calculated from

$$k = \frac{L_p r_1^2}{E(r_2^2 - r_1^2)} \qquad (4.4)$$

where L_p is the length from pressure vessel cap to micrometer, E is Young's modulus, r_1 is the outside pipe diameter and r_2 the inside diameter.

The full equation used to calculate density is

$$\rho_p = \frac{M}{M/\rho_o - A_o\,[(R_o - R_p) - kP(1 - 2\alpha P) - \alpha P\{2(R_o - R_p) + l_o(1 - 2\alpha P)\}]} \qquad (4.5)$$

Values assigned to the constants l_o, α and k were 0.4 m, 2×10^{-12} m^2N^{-1} and 6.773×10^{-14} m^3N^{-1} respectively. At 500 MPa $l_o - l_o(1 - \alpha P) = 0.4 \times 10^{-3}$ m. The new value of $A\Delta L$ at 500 MPa reduces the density by 0.4 percent so unless compression of steel under pressure is considered density will be out by 0.4 percent at the highest pressure (at low pressures the corrections will be negligible).

In principle, it should therefore be possible to measure density absolutely. Distilled water, for which accurate density data[124,125] are available within the present pressure and temperature range, was used to check the accuracy of equation (4.5) in calculating density. The results are shown in Table 4.4.

It was found that water densities calculated using equation (4.5) differed from the literature data by up to 0.8 percent at 500 MPa and that there was a systematic trend in all cases towards negative deviation to a maximum of 0.8 percent at the highest pressure. This suggested some other effect with pressure whose origin was unknown. A possible explanation was that the reduction in l_o with pressure was offset by movement of the whole assembly in the opposite direction. This is not unlikely as the bellows, cage, rod and pressure vessel end cap are screwed together, movement at the screw holes being possible on applying pressure. A similar effect has been reported by Scaife, Vij Lyons and Ruttle[126] who found unexpected temperature and pressure effects which made their bellows area effectively constant for different temperatures and pressures.

From the comparison of experimental and literature water data, it seems that density cannot be measured absolutely to a greater accuracy

Table 4.4

Comparison of Experimental Water Densities with References (124)* and (125)* Using Equation (4.5)

Pressure (MPa)	298.15 K			333.15 K			348.15 K		
	Density ($kg\ m^{-3}$)		Percentage difference	Density ($kg\ m^{-3}$)		Percentage difference	Density ($kg\ m^{-3}$)		Percentage difference
	Experimental	Literature		Experimental	Literature		Experimental	Literature	
10	1001.7	1001.5	+0.01	987.9	987.5	+0.04	979.2	979.1	+0.01
20	1005.8	1005.9	-0.00	991.9	991.8	+0.01	983.3	983.4	-0.01
50	1017.8	1018.4	-0.06	1003.6	1003.9	-0.03	995.0	995.7	-0.07
100	1036.4	1037.8	-0.14	1021.6	1022.8	-0.12	1013.1	1014.7	-0.16
200	1069.0	1072.1	-0.29	1053.0	1055.8	-0.26	1044.5	1047.8	-0.31
300	1096.6	1101.4	-0.44	1079.6	1084.2	-0.42	1071.0	1076.3	-0.49
400	1120.5	1127.1	-0.59	1102.9	1109.4	-0.59	1094.2	1101.6	-0.67
500	1141.9	1150.1	-0.72	1124.5	1132.0	-0.66	1115.7	1124.2	-0.76

* Reference (125) - 10 - 50 MPa and Reference (124) - 100 - 500 MPa.

than 0.8 percent without a major improvement in rigidity.

Calibration using Literature Water Data at Elevated Pressure

If the apparatus is calibrated using a literature value for the density of water at a particular temperature and pressure a better fit can be obtained.

Equation (4.5) was approximated by

$$\rho_p = \frac{M}{M/\rho_o - A_o(R_o - R_p) + BP} \qquad (4.6)$$

By introducing the term BP any uncertainty in the value of A_o is eliminated since the constant B allows for the constant A_o being slightly out. B was calculated as the number necessary to give an exact fit with literature data[124] at 298.15 K and 500 MPa, and found to have a value of 7.768×10^{-17} $m^5 N^{-1}$. Experimental density results for water at the other temperatures and pressures of measurement were recalculated on the basis of this equation, and a comparison with literature values is given in Table 4.5. At pressures above 100 MPa, only two results deviate by more than 0.05 percent and consideration of all the results shows that the fit is better than $\pm$ 0.15 percent.

4.3.3 Accuracy of Density Measurements

The accuracy to which density can be measured depends on the sum of the uncertainties of the various measurements made. These uncertainties are in the micrometer reading, bellows area, liquid mass, atmospheric density, temperature and pressure. An estimate of the various contributions to the combined uncertainty in a density is as follows.

Table 4.5

Comparison of Experimental Water Densities with References (124) and (125)* Using Equation (4.6)*

Pressure (MPa)	298.15 K			333.15 K			348.15 K		
	Density ($kg\ m^{-3}$)		Percentage difference	Density ($kg\ m^{-3}$)		Percentage difference	Density ($kg\ m^{-3}$)		Percentage difference
	Experimental	Literature		Experimental	Literature		Experimental	Literature	
10	1001.7	1001.5	+0.02	988.4	987.5	+0.09	979.2	979.1	+0.01
20	1005.9	1005.9	0	992.5	991.8	+0.07	983.4	983.4	0
50	1018.3	1018.4	-0.01	1004.3	1003.9	+0.04	995.6	995.7	-0.01
100	1037.6	1037.8	-0.02	1022.7	1022.8	-0.01	1014.3	1014.7	-0.04
200	1071.8	1072.1	-0.04	1055.5	1055.8	-0.03	1047.2	1047.8	-0.06
300	1101.1	1101.4	-0.03	1083.9	1084.2	-0.03	1075.2	1076.3	-0.10
400	1126.7	1127.1	-0.04	1109.1	1109.4	-0.03	1100.1	1101.6	-0.14
500	1150.1	1150.1	0	1132.4	1132.0	-0.03	1123.6	1124.2	-0.05

* Reference (125) - 10 - 50 MPa and Reference (124) - 100 - 500 MPa

The micrometer could be read $\pm$ 0.002 mm, but sideways movement of the coil block led to an uncertainty of $\pm$ 0.005 mm. Added to this the micrometer and the tubing to which it was attached were not exactly parallel. Experiment showed the deviation to be less than $\pm$ 1^{o} leading to an uncertainty of 0.01 mm at the maximum pressure of 500 MPa. This uncertainty will, of course, be negligible at low pressures. The major source of uncertainty in the micrometer reading was a drift of the balance point of the bridge circuit causing the trigger to operate at different points on the ferrite tip. It was found that the micrometer reading at the triggering point after rebalancing was in some cases different by 0.05 mm, but in 95 percent of the measurements the difference was only 0.02 mm. The uncertainty was kept to this by rebalancing the bridge after each pressure increase. The average uncertainty on a micrometer reading was therefore $\pm$ 0.03 mm leading to an uncertainty of $\pm$ 0.06 mm in $(R_o - R_p)$. Typical values of $(R_o - R_p)$ were 1.91 mm and 20.78 mm at 100 MPa and 500 MPa respectively. The uncertainty was thus 3 percent at 100 MPa and 0.3 percent at 500 MPa leading to an uncertainty in density of the order of 0.05 to 0.005 percent in the range 100 MPa to 500 MPa. As previously stated the uncertainty in bellows area was estimated to be $\pm$ 1.5 percent leading to an uncertainty of $\pm$ 0.3 percent in density if density was measured absolutely. However, by using equation (4.6) and calibrating the bellows with water this uncertainty was eliminated relative to the absolute error in the calibration data. The liquid mass could be measured to $\pm$ 0.0002 g but because of possible adsorption of atmospheric moisture, a better estimate was $\pm$ 0.001 g producing an uncertainty of $\pm$ 0.006 percent in density. The atmospheric densities measured as described in Section 3.3 were accurate to within $\pm$ 0.05 percent. The temperature was estimated to be accurate to $\pm$ 0.02 K giving

an uncertainty of ± 0.0005 percent in density. The pressure was estimated to be accurate to ± 0.7 percent leading to an uncertainty of ± 0.04 percent in density.

Since the error in the bellows area was effectively eliminated using equation (4.6) the error in density from the other sources mentioned should be less than ± 0.15 percent. This is in good agreement with the fit obtained for water shown in Table 4.5 using literature water data[124,125] which was estimated to be accurate to ± 0.02 percent. The sum of the estimated experimental uncertainty and the uncertainty of 0.02 percent in the reference data leads to an expected accuracy of better than ± 0.2 percent for density calculated using equation (4.6). Measurements for other liquids and a comparison with literature data is given in Sections 4.6.1 and 4.6.2.

4.4 VISCOSITY COEFFICIENTS

A falling body viscometer was used to measure viscosity coefficients at atmospheric and elevated pressure. In the viscometer the terminal velocity of a self centering sinker was measured as it fell axially down the centre of a vertical circular tube containing the liquid whose viscosity coefficients were being measured. The sinker and the tube were made from the same non-magnetic En 58J stainless steel thus minimising compressibility and thermal expansion effects. The sinker had a small cylinder of ferrite embedded in the core and its position was detected by the change in inductance it caused as it passed through two pairs of coils wound on the outside of the tube. Pressure was transmitted to the liquid by flexible metal bellows attached to one end of the tube.

In the course of operation certain practical problems previously experienced by Brawn[123] became apparent. It was also obvious that the bellows used gave a limit on the pressure range that could be covered with more compressible liquids. Therefore, a new viscometer was designed and built to overcome these shortcomings and this is described fully in Section 4.5. Because of the time taken to have this new viscometer manufactured measurements on the n-hexane plus n-hexadecane system were made using the old viscometer tube but with a different sinker to cover the viscosity coefficient range of the chosen system. A brief description of this viscometer is given in the following section.

4.4.1 Viscometer Description

The high pressure viscometer consisted of four main components - the viscometer tube, viscometer end cap, bellows and sinker. A section through the viscometer is shown in Figure 4.6. The viscometer tube was approximately 23 cm in length with an external diameter of 24 mm and an internal diameter of 7.645 mm. The internal diameter of the tube was constant to within $\pm$ 0.005 mm and deviated from circularity by less than 0.005 mm.

The detector coils each consisted of approximately 550 turns of 44 SWG insulated copper wire with a nominal resistance of 80 ohms. They were trimmed to the same inductance within 0.2 mH and to the same resistance within 0.5 ohms. The ends were soldered to individual points on a collar attached to a narrow section of the viscometer tube and connecting wires from this collar were led along axial grooves to a pin connector at the end of the bellows support cage. The viscometer end cap was screwed to one end of the viscometer tube and sealing effected by 0.1 mm thick copper washers which were tightly clamped in a recess in the end cap by raised sections of the viscometer tube.

The pressure transmitting bellows were of 0.1 mm stainless steel seamless tubing with 12 convolutions and fully compressed they could expel 25 percent of the total sample volume. Sealing between the bellows and viscometer tube was effected with copper washers in the same way as between the tube and end cap. The relative amount of liquid expelled by the bellows could be increased by decreasing the liquid volume with the addition of solid fillers, one in the bellows and the other in the viscometer tube remote from the measuring section. During experiments the filler in the bellows section gave an indication of the

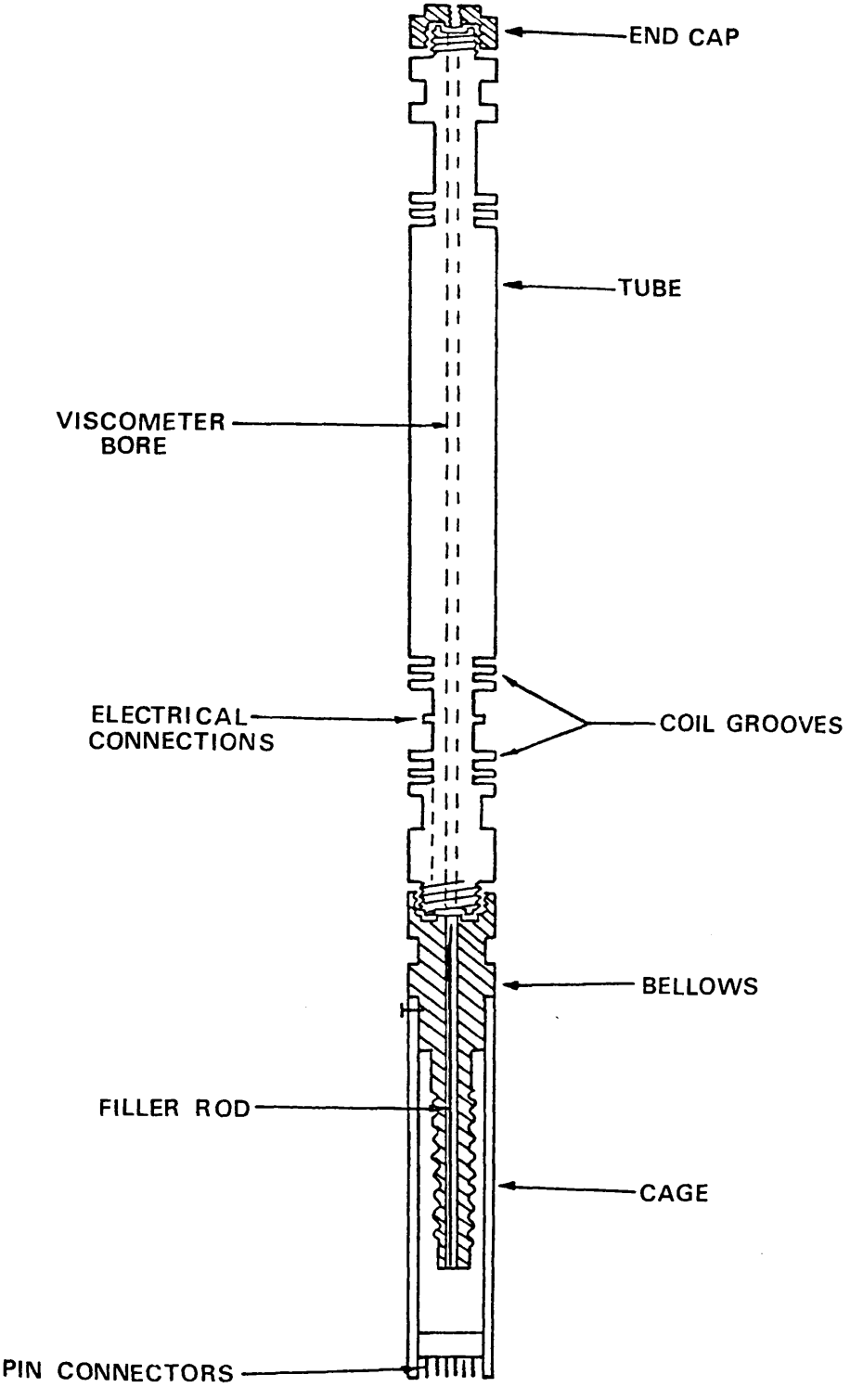

Figure 4.6 High Pressure Viscometer.

state of compression of the bellows as, when fully compressed, the filler rod prevented the sinker from leaving the bottom pair of detector coils. Linear deformation of the bellows was ensured by a brass support cage which had holes drilled to allow free passage of the pressurising fluid. A pin/socket connector between the bellows support cage and the pressure vessel end cap provided for electrical connections to the viscometer bridge unit and also allowed the viscometer to be held to the pressure vessel end cap as shown in Figure 4.7.

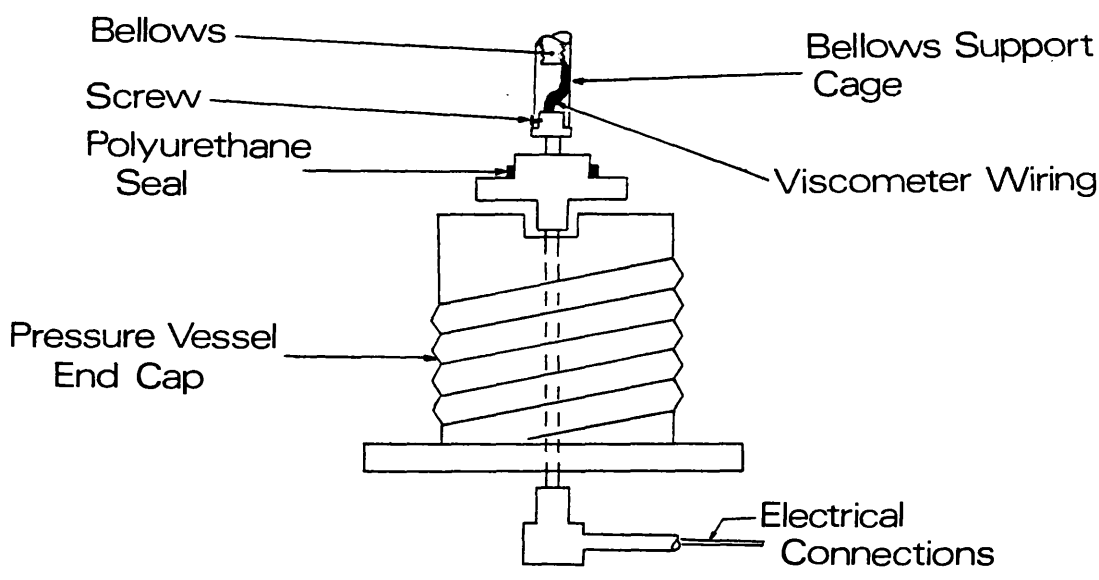

Figure 4:7 Pressure Vessel End Cap.

The sinker was 14 mm long and 7.549 mm in diameter leaving an annulus of 0.048 mm between the tube and the sinker. The diameter of the sinker was constant to within ± 0.005 mm and deviated from circularity by less than 0.005 mm. This particular type of sinker was designed by Isdale[114] who has shown it to be self centering. A section through the sinker is shown in Figure 4.8.

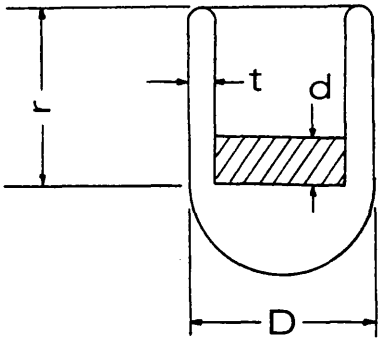

t	0·06L-0·08L
d	0·20L-0·26L

Figure 4:8 Section Through Sinker.

4.4.2 Viscometer Assembly and Filling

Before filling, the viscometer was completely dismantled and cleaned thoroughly with AnalaR acetone filtered through a millipore syringe filter to avoid dust entering the viscometer. The individual components were then rinsed several times with filtered n-hexane and allowed to dry in air. Heat was applied to the outside of the

bellows section to accelerate drying which would otherwise take several hours.

The filling procedure took place in three stages the first being to fill the bellows section without trapping air in the convolutions. This was done by filtering the test liquid through a syringe filter into the bellows. As the bellows were being filled the sides were tapped gently and air bubbles could be seen to rise to the surface. When filled the bellows were stretched, compressed and tapped for about a minute till no more air could be seen to rise to the surface. The viscometer tube was then attached and filled by running the filtered liquid down the inside wall to avoid splashing. When filled the sinker was inserted nose first. The sinker was always placed in the same orientation relative to the tube. With the sinker in position the end cap was connected and the tube topped up through the small vent at the top of the end cap. Finally a small copper seal was placed in the vent and a grub screw inserted to give a seal between the test liquid and the hydraulic pressurising fluid.

After filling, the bellows support cage was attached and the wires from the pin connector soldered to the appropriate points on the collar. The coil section was then wound with thin ptfe tape to protect the delicate wiring and the viscometer was then ready to be inserted in the pressure vessel.

The pin connector at the end of the bellows housing was connected to the corresponding socket connector on the pressure vessel end cap and a screw inserted to hold the viscometer rigidly to the end cap as shown in Figure 4.7.

The viscometer was then inserted in the bore of the pressure vessel after first screwing a small spacer onto the viscometer end cap to ensure that the viscometer was held rigidly in the pressure vessel bore. The pressure vessel end cap was then screwed down to a torque of about 4×10^{3} *N m with the aid of a hydraulic spanner. This compressed a polyurethane seal between the pressure vessel end cap and the pressure vessel providing an effective seal for the hydraulic fluid. Electrical connections were brought through the pressure vessel end cap by ceramic cone insulators to a viscometer bridge unit. When all electrical connections were made the viscometer coils were connected as shown in Figure 4.9. This Wheatstone bridge arrangement could be balanced by the bridge unit shown in Figure 4.5 and an output signal was led to an oscilloscope to aid balancing.*

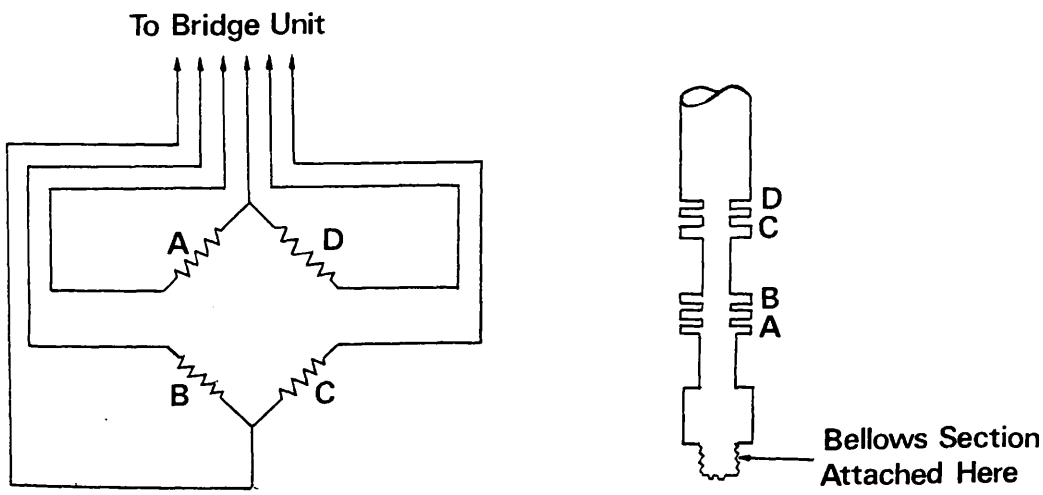

Figure 4:9 Viscometer Wiring Diagram.

4.4.3 Measurement of Fall Time

The terminal velocity of the sinker was determined by measuring its time of fall between the two pairs of coils on the viscometer. The four coils formed a Wheatstone bridge circuit which was connected externally to a bridge unit. A block diagram of the bridge unit is shown in Figure 4.5. As the sinker with its ferrite core entered the first coil an out-of-balance signal was produced in the bridge which was then amplified. The demodulator working in conjunction with the phase shifter then reduced this 300 Hz signal to a d.c. level which first rose and then fell as the sinker approached the second coil, reaching zero at the mid-point. At this point the d.c. signal operated a Schmitt trigger which produced a sharp pulse to start a Hewlett Packard Counter Timer, type 5223L. The input level at which the trigger operated was offset slightly from zero to avoid false triggering caused by background noise in the circuit. This process was repeated as the sinker went through the second pair of coils and this time the pulse from the Schmitt trigger stopped the timer.

4.4.4 Measurement of Sinker Density

A value for sinker density is required to make buoyancy corrections to the fall time. The density of the sinker was obtained by weighing it firstly while suspended in air, w_a and secondly while suspended in water, w_w. When suspended in water care was taken to ensure that no air was trapped inside the sinker and that sufficient time was allowed for the system to come to equilibrium. Care was also taken to avoid errors due to the effects of surface tension and upthrust on the immersed portion of the wire from which the sinker was suspended.

The temperature of the water was measured and the density of water at this temperature, ρ_w, obtained from API 44 Tables[75]. Sinker density, ρ_s, was calculated from the equation

$$\rho_s = \frac{w_a \rho_w}{w_a - w_w} \qquad (4.7)$$

The sinker was found to have a density of 7401 kg m^{-3} at 298.15 K.

4.4.5 Viscometer Performance

In general between five and ten fall time measurements were made for each point on an isotherm and the mean and standard deviation calculated. Although standard deviations are not very significant for numbers as small as 10, it is of interest to note that out of a total 230 points only 10 had a standard deviation which was greater than 1 percent of the mean, the average of these being 1.5 percent of the mean. For the other 220 points the standard deviation was an average of about 0.6 percent of the mean. For fall times below 3 seconds the fall time standard deviation was less than 0.3 percent of the mean.

Factors which may affect the repeatability of fall time are :

(a) centering of the sinker,

(b) entry and exit effects,

(c) possible rotation of the sinker,

(d) surface imperfections on the tube or sinker,

(e) temperature fluctuations, and

(f) pressure fluctuations.

(a) Isdale[114] has shown that provided the sinker is allowed to fall backwards for a distance equal to the measuring section, then on

returning to the forward direction the sinker will have centred before entering the coils. The sinker was allowed to fall this distance each time so it is unlikely that non-centering is the cause of the deviation.

(b) Isdale[114] has also shown that entry and exit effects are negligable as theoretical and experimental viscometer constants are in close agreement.

(c) It was possible that the sinker was catching slightly at its extremities of travel causing it to rotate slightly with each run. If the sinker was not perfectly symmetrical and this was occuring then it would be expected that the fall times would oscillate fairly regularly. This did not always occur but it was observed on some runs. Figure 4.10 shows the oscillation of the atmospheric fall time for the n-hexane plus n-hexadecane mixture with a mole fraction of n-hexane of 0.400 at 348.31 K.

(d) Surface imperfections of the sinker were visible as small axial scratches and these may have caused slight turbulence in the annulus between the sinker and tube causing the deviation in the fall time.

(e) Temperature control of the bath fluid was better than $\pm$ 0.03 K and due to the thick walls of the pressure vessel the temperature inside would effectively be constant. Fluctuations of the bath temperature would not be expected to affect the fall times to a greater extent than about 0.04 percent.

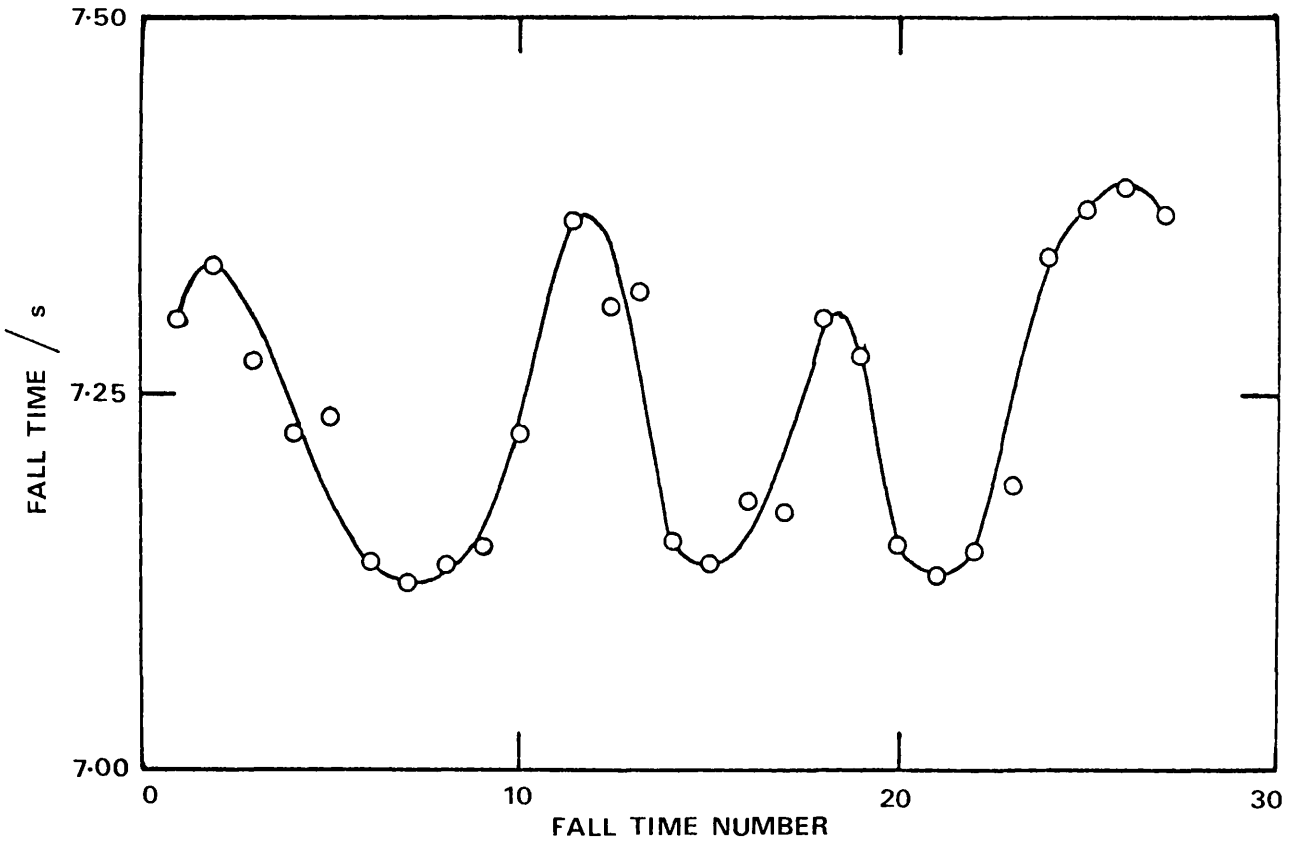

Figure 4.10 Oscillation of Sinker Fall Time at Atmospheric Pressure for the n-Hexane plus n-Hexadecane Mixture with a Mole Fraction of n-Hexane of 0.400 at 348.31 K.

(f) Loss of pressure due to slight leakage of hydraulic fluid was not always observed. When this did occur the pressure change was always less than 0.5 MPa over the time taken to collect a set of fall time readings. As pressure decreased constantly it is unlikely that this could lead to oscillation in the fall time which in any case was also observed at atmospheric pressure.

It was not possible to tie down the source of these variations in fall time with any certainty although surface imperfections and/or rotation of the sinker seemed the most likely causes. Interestingly atmospheric pressure fall times below about 5 seconds had an uncertainty which fell off to less than 0.1 percent at the shortest fall times. The fall time standard deviation also became smaller under pressure as the fall times increased. The overall uncertainty on fall time was of the order of $\pm$ 0.5 percent and this was confirmed by repeating some experimental points. This was an acceptable figure in terms of the error it produced in viscosity coefficients. Exact quantification of the effects from all of the various sources would clearly be required for the most precise measurements or for use in an absolute instrument, however the uncertainties obtained are sufficiently small to meet the objective of measuring viscosity coefficients to an accuracy of better than 2 percent.

The balance point of the bridge circuit was sensitive to changes in temperature of the viscometer coils so this provided an indication of the time taken for the temperature of the bath and viscometer to equilibrate. It was found necessary to allow one hour after the thermostat bath reached a steady temperature, for the temperature of the viscometer to become constant. This was due to the thick walls of the pressure vessel.

Several experiments were carried out to find out how long the test liquid takes to re-equilibrate after increasing or decreasing pressure. The results of two of these tests are shown in Figure 4.11.

Measurement of fall time versus time after pressure change gave an indication of the state of the test liquid. It was found that five minutes was sufficient time to allow before recording fall times at the new pressure. During experiments however, ten to fifteen minutes were allowed to give a safe margin.

4.4.6 Viscometer Calibration

Fall times recorded in the falling body viscometer have to be corrected for the buoyancy effects of the test liquid on the sinker. Further corrections due to compressibility and thermal expansion of the components are also necessary before viscosity coefficients can be calculated from fall time measurements. The equation used to calculate viscosity coefficients from fall time measurements was that derived by Isdale[114] for a similar viscometer from a consideration of the physical dimensions of the viscometer and is of the form

$$\eta_P = \frac{t(1 - \rho_L/\rho_s')}{A\{1 + 2\beta(T - T_o)\}(1 - 0.666\ \alpha P)} \qquad (4.8)$$

where η_p is the viscosity coefficient at pressure P, t the fall time, ρ_L and ρ_s' the density of the liquid and sinker at pressure P, A the viscometer constant, T the experimental temperature, T_o a reference temperature taken as 298.15 K, β the linear coefficient of thermal expansion and α the compressibility coefficient.

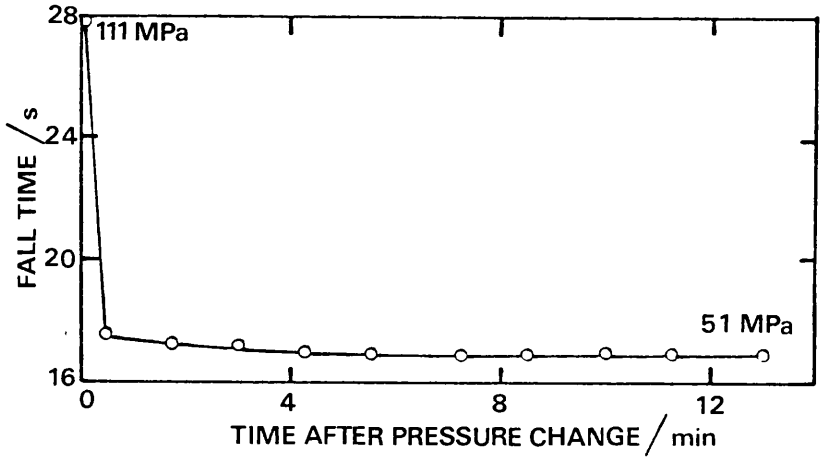

(a) x_{HD} = 0.6 at 323 K

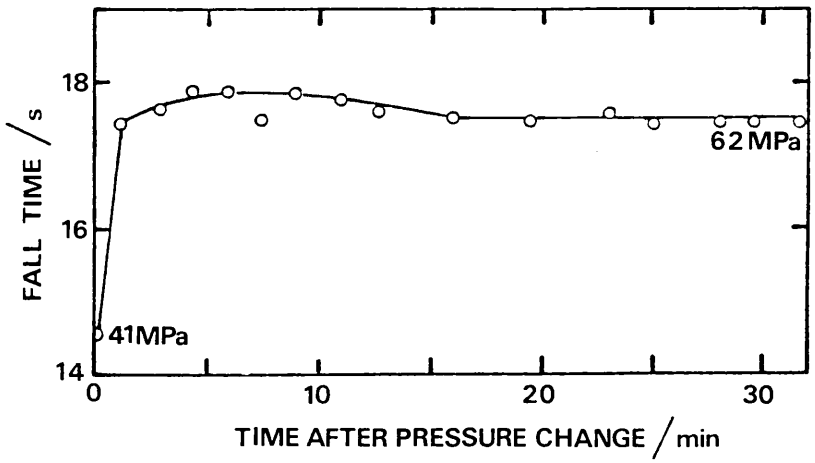

(b) x_{HD} = 0.4 at 298 K

Figure 4.11 Equilibration Time after Changing Pressure During Viscosity Coefficient Experiments. HD - n-Hexadecane.

ρ_s' the corrected sinker density is calculated from

$$\rho_s' = \rho_s \left[\frac{1}{\{1 + 3\beta(T - T_o)\}(1 - 0.666\alpha P)} \right] \qquad (4.9)$$

where ρ_s is the sinker density at 298.15 K and atmospheric pressure. The other symbols are as defined for the previous equation. This equation is obtained by considering the sinker to be a simple cylinder and studying the effect of temperature and pressure on its volume.

Values of viscometer constant A, in the range 0.16 mPa s to 24.78 mPa s were obtained via equation (4.8) by measuring sinker fall times at atmospheric pressure in liquids of accurately known densities and viscosity coefficients. A series of liquids were chosen whose viscosity coefficients at atmospheric pressure covered the full range of viscosity coefficients likely to be encountered with the n-hexane plus n-hexadecane system at all temperatures and pressures. Liquids used in the calibration were n-hexane, n-hexadecane, mixtures of n-hexane plus n-hexadecane and Shell Vitrea 21 calibration oil. The kinematic viscosity coefficients of Shell Vitrea 21 at the various temperatures were measured in National Physical Laboratory calibrated U-tube viscometers and the densities in a calibrated Lipkin pyknometer. Saturation pressure kinematic viscosity coefficients and densities for n-hexane, n-hexadecane and mixtures of n-hexane plus n-hexadecane were measured in sealed viscometers and pyknometer as described in Sections 3.2 and 3.3. The viscosity coefficients at saturation pressure have been measured at different temperatures from the high pressure viscometer measurements. However viscosity coefficients were obtained at the required temperature by interpolation from a quadratic fit of ln η versus 1/T for the experimental points. Figure 4.12 shows the variation of the calibration constant, A, with increasing viscosity coefficient. As the fall time decreases the calibration constant, A,

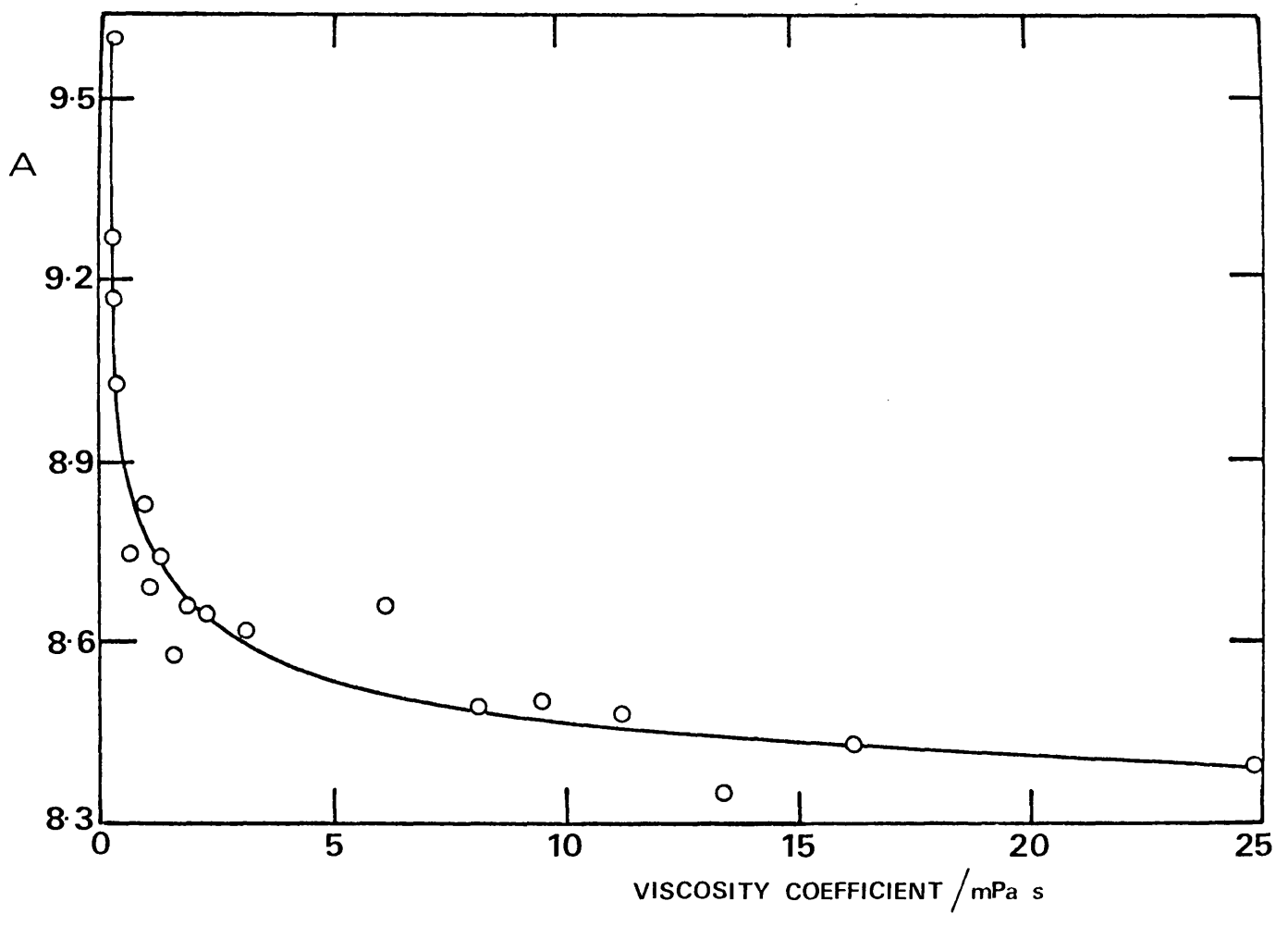

Figure 4.12 High Pressure Viscometer Calibration Curve.

increases possibly indicating that the flow of liquid past the sinker is becoming non laminar at low viscosity coefficients . Below 0.29 mPa s the increase in A is very rapid.

To enable A to be calculated when the liquid viscosity coefficients are unknown the experimental A values above 0.29 mPa s were fitted by the equation

$$A = A_o + B\,[(t^*)^{-N}] \qquad (4.10)$$

where A_o is the calibration constant at infinite viscosity coefficient and t* corresponds to $t(1 - (\rho_L/\rho_s'))$. A comparison between the experimental and fitted values of A is given in Table 4.6. In this table $\gamma = 1 + 2\beta(t - t_o)$. The fitted A values are represented in Figure 4.12 as a solid line corresponding to equation (4.10) with the values $A_o = 7.994$, $B = 1.168$ and $N = 0.2$ substituted. The maximum deviation from the experimental A values is 1.59 percent with a mean deviation of $\pm$ 0.5 percent. Below 0.29 mPa s A values were fitted by a graphical method. Agreement with experimental A values was within $\pm$ 0.2 percent. The viscometer tube/sinker combination is thus calibrated in the range 0.16 mPa s to 24.78 mPa s (1.6 to 235.5 seconds).

Subsequent independent experiments on oils with fall times of 369 and 386 seconds at atmospheric pressure gave experimental A values of 8.37 and 8.41 respectively. These agreed with the calculated A value of 8.36 from the above calibration to 0.1 and 0.6 percent respectively. confirming the calibration for high viscosity coefficients.

Table 4.6

Calibration of High Pressure Viscometer

Calibration liquid	Temperature (K)	Fall time (s)	Liquid density ($kg\ m^{-3}$)	Sinker density ($kg\ m^{-3}$)	t^* (s)	Viscosity coefficient (mPa s)	Υ	$(t^*)^{-0.2}$	A (experimental)	A (fitted)	Percentage difference
Shell Vitrea 21	303.15	235.45	859.2	7399.8	208.11	24.78	1.0001	0.3438	8.40	8.40	0
	313.15	154.32	852.7	7397.7	136.53	16.19	1.0003	0.3741	8.43	8.43	0
	318.15	126.27	849.5	7396.5	111.77	13.38	1.0004	0.3893	8.35	8.45	-1.18
	323.15	107.07	846.3	7395.5	94.82	11.18	1.0005	0.4023	8.48	8.46	0.18
	328.15	90.95	843.1	7394.3	80.58	9.47	1.0006	0.4156	8.50	8.48	0.24
	333.15	77.61	839.9	7393.2	68.79	8.10	1.0007	0.4290	8.49	8.50	-0.06
	343.15	59.53	833.4	7391.0	52.82	6.09	1.0009	0.4523	8.66	8.52	1.59
n-Hexadecane	298.15	29.506	770.2	7401.0	26.4354	3.068	1.0000	0.5195	8.62	8.60	0.22
	323.15	17.790	753.0	7395.5	15.9786	1.843	1.0005	0.5745	8.66	8.67	-0.05
	348.15	12.033	735.8	7389.9	10.8349	1.239	1.0010	0.6209	8.74	8.72	0.23
	373.15	8.722	718.6	7384.3	7.8732	0.8910	1.0015	0.6619	8.83	8.77	0.72
x_{Hd}^* = 0.800	298.15	21.501	759.5	7401.0	19.2945	2.231	1.0000	0.5532	8.65	8.64	0.11
x_{Hd} = 0.600	298.15	14.670	745.3	7401.0	13.1926	1.537	1.0000	0.5969	8.58	8.69	-1.30
x_{Hd} = 0.400	298.15	9.619	726.3	7401.0	8.6751	0.9978	1.0000	0.6491	8.69	8.75	-0.72
x_{Hd} = 0.200	298.15	5.705	698.8	7401.0	5.1663	0.5903	1.0000	0.7200	8.75	8.84	-0.97
n-Hexane	298.15	2.927	655.0	7401.0	2.6680	0.2951	1.0000	0.8218	9.04	8.95	1.00
	323.15	2.357	631.6	7395.5	2.1557	0.2350	1.0005	0.8576	9.17		
	348.15	1.928	606.7	7389.9	1.7697	0.1905	1.0010	0.8921	9.28		
	373.15	1.620	580.5	7384.3	1.4926	0.1551	1.0015	0.9230	9.61		

* Subscript HD - n-hexadecane

4.4.7 Accuracy of Viscosity Coefficient Measurements

Measurements of fall time t, liquid density ρ_L, sinker density ρ_s, viscometer constant A, temperature T and pressure P have to be made and the degree of accuracy with which each can be measured will determine the contribution to the total uncertainty in a viscosity coefficient. An estimate of the uncertainty is as follows. Temperature control of the bath was better than $\pm$ 0.03 K. This will produce an uncertainty of 0.03 percent in fall time for low viscosity coefficients and 0.06 percent in fall time at the highest viscosity coefficient measured.

Pressure may change by up to 0.5 MPa over the time taken to collect the set of fall times at a particular point on an isotherm. This effect will be more significant at low pressures and short fall times. For n-hexane at 298 K between 50 MPa and 80 MPa this could produce an uncertainty of 0.3 percent in the fall time. However, since the pressure change occurs constantly and slowly, as a result of slow leakage of pressurising fluid, the mean value of fall time at the average pressure should be repeatable to better than this. Pressure changes of this magnitude were found only at a few points and usually where fall times are longer resulting in a longer time to collect the five or ten fall time values at a particular pressure.

The uncertainty in the fall time t, was found in Section 4.4.5 to be $\pm$ 0.5 percent. This figure will have contributions from the temperature and pressure fluctuations already mentioned and also contributions from other sources such as sinker imperfections. This figure of $\pm$ 0.5 percent will appear directly as uncertainty in the viscosity coefficients.

The major sources of uncertainty in calculating experimental A values are the uncertainty in fall time and the uncertainty in the viscosity coefficient measured in the capillary viscometer.

Viscosity coefficient measurements at saturation pressure have been found in Section 3.2 to be accurate to $\pm$ 0.5 percent so adding the uncertainty in fall time gives a total uncertainty of $\pm$ 1.0 percent on the A values. This agrees well with the difference between experimental and fitted A values given in Table 4.6.

From equation (4.8) it is seen that the maximum contribution to uncertainty in viscosity coefficient arising from uncertainty in liquid density, ρ_L, will be at maximum density. The maximum density encountered is for n-hexadecane at 373 K and 425 MPa. Density at pressure is accurate to $\pm$ 0.2 percent and this will produce an error of 0.03 percent in viscosity coefficient.

The estimated uncertainty in sinker density, ρ_s', is $\pm$ 0.2 percent and the maximum error this will produce in a viscosity coefficient is for n-hexadecane at 373 K and 425 MPa. The error in viscosity coefficient here is $\pm$ 0.02 percent. However, since the sinker is used to calibrate the viscometer initially this value will be reduced.

The estimated uncertainty in the viscosity coefficient for pure liquids obtained by summing these individual contributions is better than $\pm$ 2 percent. For mixtures, there is the additional uncertainty arising from composition changes while filling the viscometer. This is difficult to quantify but could contribute $\pm$ 1 percent.

4.5 DESIGN, PREPARATION AND TESTING OF THE NEW VISCOMETER

4.5.1 Design

While using the high pressure viscometer it soon became apparent that there were some features of the design which, if modified, would increase the pressure range and the reliability while making the viscometer easier to fill and operate. To this end the experience gained together with some suggestions made by Brawn[123] were incorporated in a new viscometer design.

One of the major limitations of the old viscometer was that the metal bellows only allowed a reduction in liquid volume of about 25 percent when fully compressed. This reduction was only large enough to accommodate the reduction in volume experienced by n-hexane when pressurised to about 250 MPa. If higher pressures than this had been attempted damage to the bellows would have resulted. The relative amount of liquid expelled by the bellows could be increased by adding a solid filler rod to the bellows to decrease the 'dead volume' of liquid not expelled by the bellows when compressed and by inserting a second filler rod into the viscometer bore before attaching the end cap. However, the reduction in volume under an applied pressure which could be accommodated was still very close to the deformation limit of the bellows and it was only possible to pressurise n-hexane to a maximum of 400 MPa before this limit was reached.

The new viscometer design overcame this problem in two ways. The first of these was the reduction in the overall length of the viscometer tube from 23 cm to 12 cm and the second a redesign of the bellows section to enable a larger liquid volume to be expelled.

A sketch of the new viscometer tube design is given in Figure 4.13. The new tube has an outside diameter of 24 mm, an internal diameter of 7.562 mm and a capacity of 5 cm^3.

Another design change incorporated was the new viscometer end cap sealing arrangement. This new arrangement is an improved method of sealing the test liquid as it was difficult to ensure that the copper washer was properly seated before tightening the grub screw in the old arrangement. With this new arrangement a conical plug is tightened into a seat by means of a nut which is screwed onto the viscometer tube.

The bellows section was replaced in the new viscometer design by a collapsible tube section with an overall length of 16 cm and a diameter of 2 cm at the collapsible tube. It has a capacity of 16 cm^3 and the expected decrease in volume which can be accommodated is 13 cm^3 or 62 percent of the total liquid volume in the viscometer tube and collapsible tube. This compares favourably with the 25 percent reduction obtained with the original bellows/tube combination. A sketch of this new section is shown in Figure 4.14. The reduction in liquid volume is taken up by a collapsible ptfe tube. This tube was clamped at either end by the connector and tube base piece and the tube end piece and cap. The connector was attached to the viscometer as described in Section 4.4.1. The tube base piece was vented to allow trapped air to escape when filling.

The electrical wiring of the old viscometer had some limitations the most serious of these being that, after assembly, electrical connections were made by soldering wires to a collar which also had the

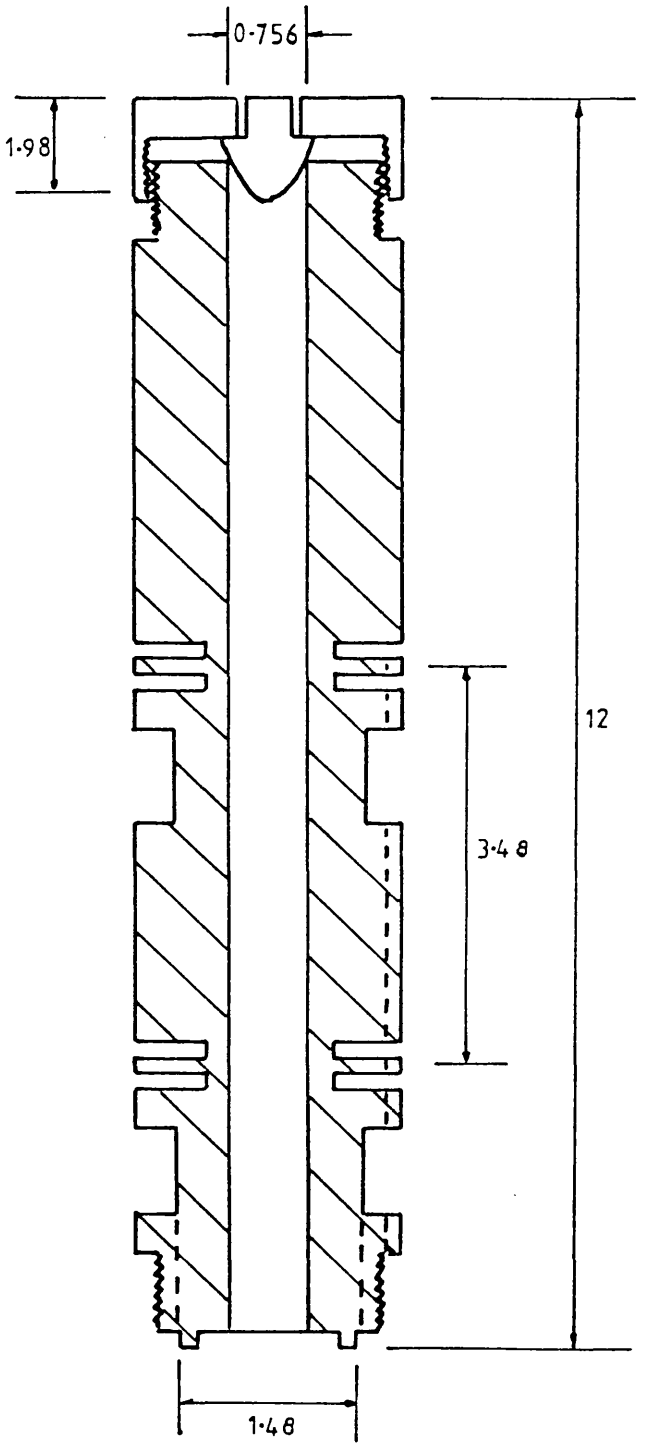

Figure 4.13 New Viscometer Tube Design.
Dimensions in cm.

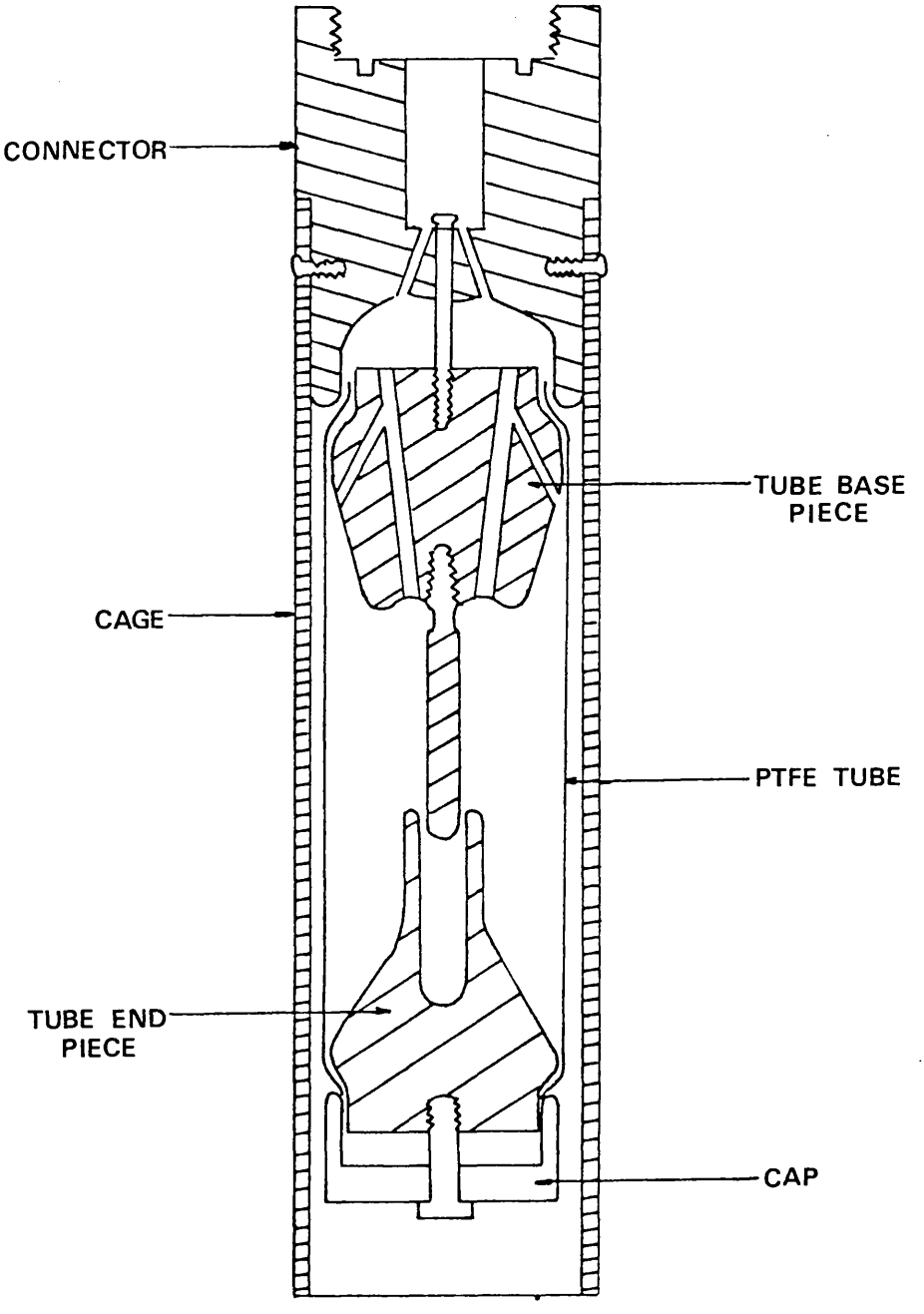

Figure 4.14 New Viscometer Collapsible End Tube Design.

fragile detector coil wires attached. This occasionally led to breaking of the coil wires and desoldering of the connections when heat was applied. It was also a disadvantage to use the pin/socket connector at the base of the bellows cage to hold the viscometer to the pressure vessel end cap connector as slight flexing of this joint on turning the pressure vessel over and back caused changes in the lead resistance to the Wheatstone Bridge thus changing the balance point of the circuit. In the new design the pin/socket connector is discarded and the bellows cage screwed directly to the pressure vessel end cap connector. A small tufnol connector with pins situated at the base of the collapsible end tube is used as a point remote from the coils which takes over as the point of connection and disconnection of the electrical wiring.

The final design change was to alter the sealing arrangement between the pressure vessel and the pressure vessel end cap. The use of a polyurethane seal between the pressure vessel and the pressure vessel end cap in the old arrangement necessitated the use of a cumbersome hydraulic press to tighten the pressure vessel end cap. The new design is shown in Figure 4.15. The initial seal is provided by a tight fitting 'O' ring and higher pressures maintained by extrusion of a phosphor bronze ring into the bore of the pressure vessel.

The new viscometer tube and the pressure vessel end cap sealing arrangement were designed such that they would be interchangeable with the corresponding old components. This meant that each could be tested separately.

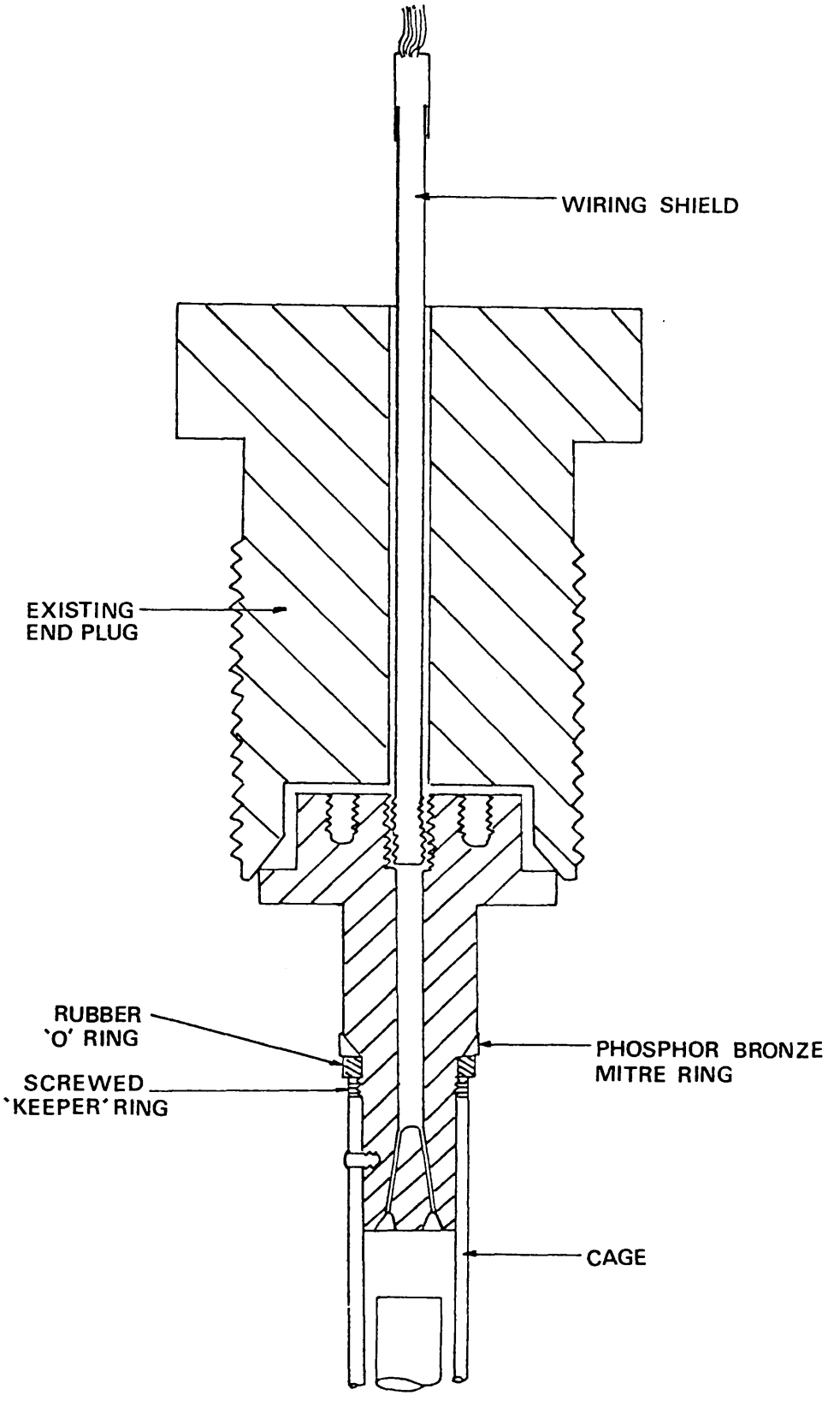

Figure 4.15 New Viscometer Pressure Vessel Seal Design.

4.5.2. Preparation of the Viscometer Tube

The first stage in the preparation of the new tube ready for use was to file off the rough edges around the coil grooves as these could damage or cut the coil wire while it was being wound into the groove. The coil grooves were then lined by stretching ½ inch ptfe tape into the groove. Although the coil wire to be used was silk wound this additional protection against electrical shorting was thought advisable. Approximately 700 turns of 44 SWG insulated copper wire were wound into each groove by turning the viscometer tube with an electric motor. The tension on the wire was kept constant by using the makeshift apparatus shown in Figure 4.16. The figure shows a coil in the initial stages of being wound. When the four coils had been wound the approximate resistance of each wire was measured using an Avometer and three of the coils trimmed back till all four gave the same resistance reading. Resistance ratios were then measured accurately using the Rosemount Engineering Company VLF Precision Comparison Bridge and one of the wires shortened as its resistance was higher than the other three. The mean final resistance was $57.9 \pm 0.8\ \Omega$. A tufnol ring with six pins was glued to the centre of the viscometer tube using Araldite and the four coils were then connected to these pins in such a way as to form the Wheatstone Bridge arrangement described for the old viscometer in Section 4.4.2. The tube was temporarily wired to the viscometer bridge unit and the Wheatstone Bridge balanced using this unit. A small piece of ferrite was then pushed slowly up the tube and was found to operate the Schmitt trigger at the appropriate points. The coils were then temperature cycled by heating to approximately 373 K with a hot air blower and allowing to cool. This cycle was repeated a further five times and

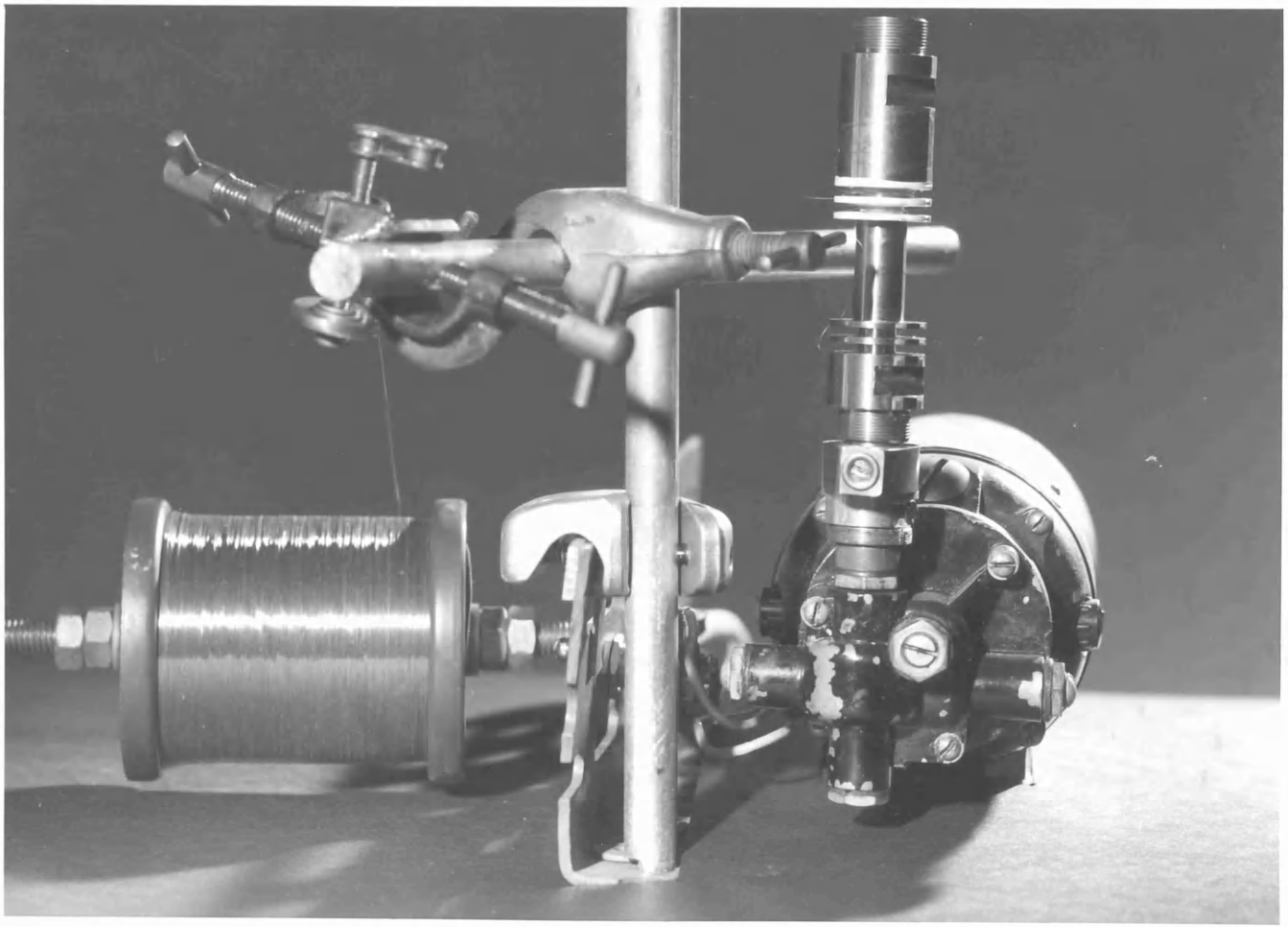

Figure 4.16 Winding of Viscometer Coil

the viscometer tube was then ready for use.

4.5.3 Preparation of the Collapsible Tube Section

The individual components of the collapsible tube section were cleaned by immersion in an ultrasonic bath for 30 minutes and then assembled using a piece of nylon tubing in place of the ptfe tubing which had not yet arrived from the manufacturers. The complete assembly was then filled with acetone to see if any leaks could be detected. No leaks could be found and so the collapsible tube section was dried ready for filling and connection to the viscometer tube. The collapsible tube section prior to assembly is shown in Figure 4.17. Twelve 0.01 mm thick copper washers were cut from a copper sheet using dies. They were then heated over a bunsen flame to soften them after which they were placed in the seat in the collapsible tube section and bedded in by tightening the viscometer tube into position. The washers then acted as a seal between the collapsible tube section and the viscometer on assembly.

4.5.4 Testing the Viscometer Assembly

Before testing, a new sinker with a suitable diameter was selected from a stock with different diameters. The new sinker was 14 mm long and 7.500 mm in diameter. The sinker density was measured as described in Section 4.4.4 and had a value of 6843.6 kg m^{-3} at 298.15 K. This time the annulus between the sinker and the tube was 0.031 mm. Since the annulus was smaller than with the previous viscometer tube/ sinker combination and the distance between the detector coils was the same, the sinker fall time for a particular liquid should be greater

Figure 4.17 Collapsible Tube Section Prior to Assembly

than that in the old viscometer at the same temperature and pressure. n-Hexane was chosen as the test liquid as it was the most compressible and least viscous of the two liquids studied in the old viscometer and so provided the best test of the collapsible tube section. It also provided a check on the accuracy of the viscosity coefficients obtained using the old viscometer particularly for low viscosity coefficients where the calibration constant is strongly dependent on the fall time and consequently may be subject to a higher degree of uncertainty. A view of the complete viscometer prior to assembly is shown in Figure 4.18.

The collapsible tube section was first filled then the viscometer tube was attached and filled, the sinker inserted, and the viscometer end plug tightened down. No leaks were detected on compressing the collapsible tube by hand so the viscometer assembly was connected to the existing pressure vessel end cap, the electrical connections made and the viscometer inserted in the pressure vessel and the pressure vessel end cap tightened down.

Initially at 298 K the viscometer behaved very well with fall times for a particular point on the isotherm agreeing to within $\pm$ 0.4 percent. However, on increasing the temperature to 323 K, allowing to cool overnight and reheating to 323 K the next day, it was not possible to obtain consistent fall time results. The viscometer was removed from the pressure vessel and when the electrical connections were desoldered and the bellows cage removed the collapsible tube was seen to be almost empty. The remaining liquid was contaminated with the pressurising fluid and the screws which clamped the nylon tubing were slack. It seemed that expansion of the metal components as temperature

Figure 4.18 Complete Viscometer Prior to Assembly

increased or the effect of temperature on the nylon tubing caused a gap between the metal and the tubing allowing n-hexane to escape and hydraulic fluid to enter. The viscometer assembly was cleaned and the collapsible tube section refilled and this time the screws were further tightened after heating with a hot air blower. Again the same problem was experienced on increasing the temperature after a successful run at a lower temperature. After several attempts to remedy the situation the collapsible tube section was discarded till the ptfe tubing arrived from the manufacturers as it was thought that the origin of the problem was the nylon tubing deforming at the joint with the metal as the temperature was increased. However, since the new viscometer tube was designed to be compatible with the old bellows section it was possible to continue testing the viscometer tube using the original metal bellows and bellows cage. This eliminated the problem of leaking and no additional problems were encountered.*

Due to a limitation in the time available for further experimental work the new pressure vessel end cap sealing arrangement was not tested.

---

* *Unfortunately the tubing did not arrive before this research was completed but subsequent testing by Robertson[113] proved successful with pressures up to 500 MPa being obtained with no leaking of contents occurring over a wide range of temperature.*

4.5.5 Calibration

The new viscometer tube/sinker combination was calibrated in the same manner as described in Section 4.4.6 for the old viscometer tube/sinker calibration using equations (4.8) and (4.10). Saturation pressure fall times for n-hexane at 323 K and for n-hexadecane at 298 K, 323 K, 348 K and 373 K provided six calibration points over the viscosity coefficient range 0.24 mPa s to 3.07 mPa s. Although this calibration was fairly limited the main interest was to compare viscosity coefficient results for a particular liquid with those from the old viscometer both as a test of the estimated accuracy of the quoted viscosity coefficients and as a test of the new viscometer. This range was sufficient to cover n-hexane viscosity coefficients obtained at 323 K and 348 K up to 500 MPa. The calibration results are given in Table 4.7 and shown in Figure 4.19. Again the solid line represents the values calculated using equation (4.10). The constants in equation (4.10) for this particular viscometer tube/sinker combination are $A = 103.479$, $B = 10.881$ and $N = 0.2$. Using these constants equation (4.10) fits the data to within one percent.

Table 4.7

Calibration of High Pressure Viscometer 2

Liquid	*Temperature (K)*	η *(mPa s)*	ρ_L *(kg m^{-3})*	ρ_s' *(kg m^{-3})*	*t (s)*	*t* (s)*	$(t^*)^{-0.2}$	Υ	*A (experimental)*	*A (fitted)*	*Percentage difference*
n-hexane	323.15	0.2350	631.6	6838	28.44	25.813	0.5220	1.0005	109.8	109.2	0.5
n-hexadecane	298.15	3.068	770.2	6844	373.55	331.51	0.3133	1.0000	108.0	106.9	1.0
	298.15	3.068	770.2	6844	366.10	324.90	0.3145	1.0000	105.9	106.9	-0.9
	323.15	1.843	753.0	6838	221.46	197.07	0.3476	1.0005	106.8	107.3	-0.5
	348.15	1.239	735.8	6833	149.15	133.09	0.3760	1.0010	107.3	107.6	-0.3
	373.15	0.8910	718.6	6828	107.83	96.48	0.4010	1.0015	108.3	107.8	0.5

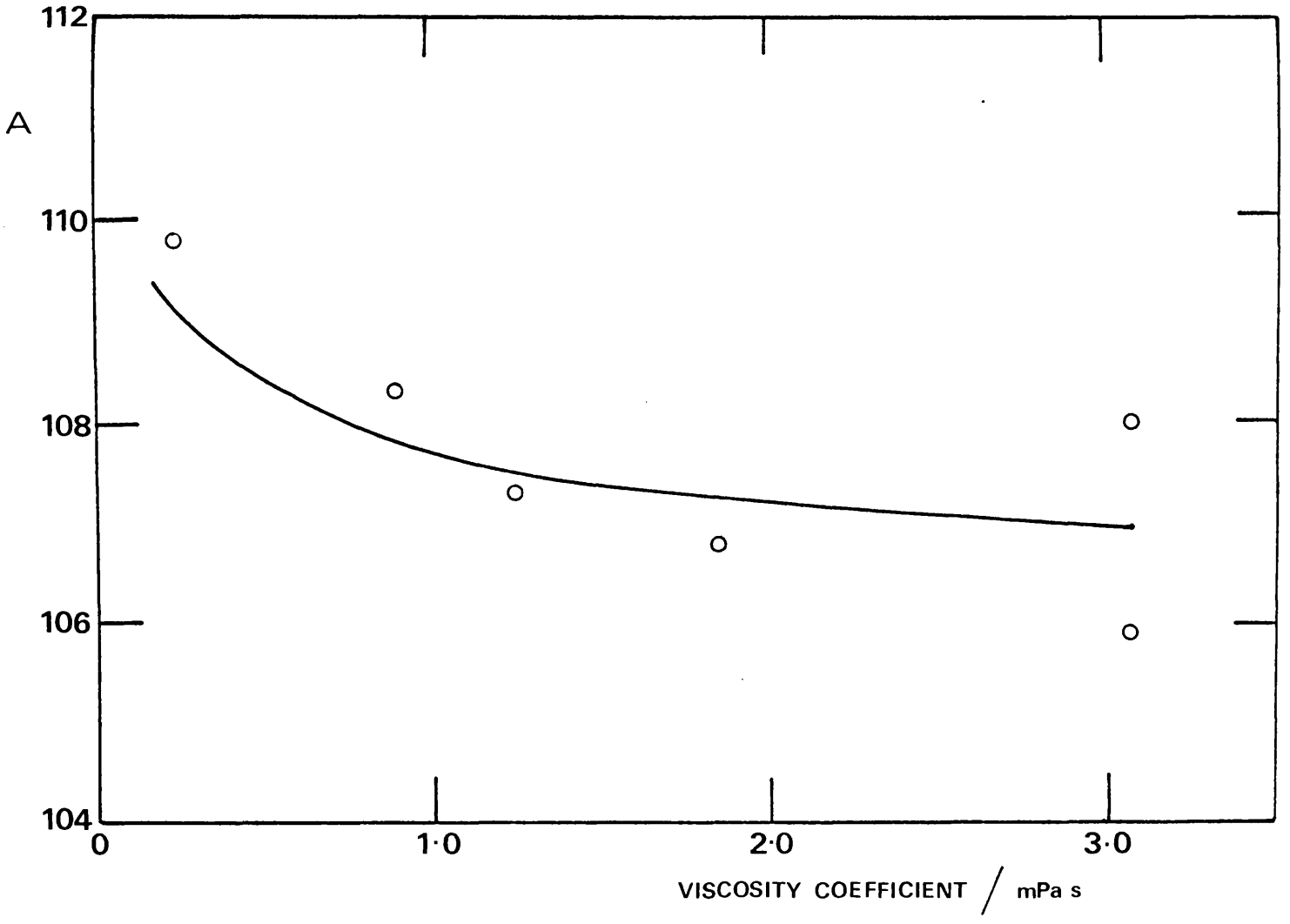

Figure 4.19 High Pressure Viscometer 2 Calibration Curve.

4.6 RESULTS FOR THE n-HEXANE PLUS n-HEXADECANE SYSTEM

4.6.1 Experimental Density Results

Densities for n-hexane, n-hexadecane and four mixtures of n-hexane plus n-hexadecane have been measured at 298.15 K, 323.15 K, 348.15 K and 373.15 K up to the freezing pressure or a maximum of approximately 500 MPa. Equation (4.6) was used to calculate density and the experimental results are given in Table 4.8 and plotted as density versus pressure in Figures 4.20 to 4.25.

During measurement of density the formation of a solid phase became evident when the position of the coil block at the balance point continued to change after thermal equilibrium had been established. When the micrometer readings for the full pressure range were plotted against pressure, the curve showed a sharp change in slope at this point corresponding to the phase boundary. This is illustrated in Figure 4.26 for the mixture with a mole fraction of n-hexadecane of 0.200 at 298.15 K. The approximate position of the solid/liquid equilibrium line derived from such measurements at 298.15 K, 323.15 K, 348.15 K and 373.15 K is shown in Figure 4.27. No attempt was made to determine exact freezing pressures. These will lie between the lowest pressure at which freezing was detected and the previous pressure reading. The uncertainty is illustrated in Figure 4.27 by vertical lines. The freezing pressure for mixtures containing a small mole fraction of n-hexadecane is significantly lower than the freezing pressure of n-hexane itself at the same temperature, but addition of n-hexane to n-hexadecane results in only a relatively small change in freezing pressure, even up to a mole fraction of n-hexane of 0.600.

Table 4.8

Experimental Elevated Pressure Densities for the n-Hexane plus n-Hexadecane System

Mole fraction of n-hexadecane	298.15 K		323.15 K		348.15 K		373.15 K	
	Pressure (MPa)	Density ($kg\ m^{-3}$)	Pressure (MPa)	Density ($kg\ m^{-3}$)	Pressure (MPa)	Density ($kg\ m^{-3}$)	Pressure (MPa)	Density ($kg\ m^{-3}$)
0	0.1	655.0	0.1	631.6	0.1	606.7	0.1	580.5
	50.5	695.9	49.0	678.2	69.4	674.2	48.5	642.5
	92.1	718.3	100.8	708.1	146.1	714.3	101.7	678.7
	153.1	744.0	201.5	748.7	221.5	742.5	201.2	723.1
	224.3	767.6	299.6	777.4	311.7	769.5	303.1	755.8
	312.0	792.1	404.0	800.7	401.4	791.2	330.2	762.6
	394.5	811.0	500.3	819.3	487.6	809.2	400.0	780.2
	533.8	838.1			564.0	823.3	425.0	785.9
0.200	0.1	698.8	0.1	678.0	0.1	656.3	0.1	634.4
	20.2	716.1	37.9	713.8	48.4	702.1	49.6	687.2
	41.2	729.7	83.1	738.2	102.2	733.4	101.2	719.1
	62.2	741.7	121.6	755.8	202.7	773.6	153.0	742.9
	83.2	751.9	163.7	772.0	295.1	801.3	204.3	762.2
	102.7	760.7	204.2	785.6	394.4	825.6	297.2	790.4
	123.4	769.1	229.9	793.6	490.8	847.9	349.8	803.6
	143.4	776.5	251.0	799.6	500.0[a]		399.4	815.1
	148.0[a]		274.8	806.1			436.5	823.2
			301.3	812.9				
			321.8[a]					

[a] *Lowest pressure at which freezing was detected*

Table 4.8 (continued)

Mole fraction of n-hexadecane	298.15 K		323.15 K		348.15 K		373.15 K	
	Pressure (MPa)	Density ($kg\ m^{-3}$)	Pressure (MPa)	Density ($kg\ m^{-3}$)	Pressure (MPa)	Density ($kg\ m^{-3}$)	Pressure (MPa)	Density ($kg\ m^{-3}$)
0.400	0.1	726.3	0.1	706.9	0.1	687.0	0.1	666.9
	49.4	759.1	50.1	744.2	51.8	730.3	49.6	714.8
	89.1	777.8	87.2	763.4	88.2	750.2	100.2	744.2
	100.9[a]		152.2	789.2	151.7	777.3	200.5	785.1
			202.0	806.3	201.4	794.5	300.0	812.2
			245.8[a]		256.8	811.1	400.0	836.6
					309.0	824.9	450.0	848.3
					352.1	835.7		
					402.5[a]			
0.600	0.1	745.3	0.1	726.7	0.1	707.9	0.1	688.9
	17.2	758.6	21.4	744.4	51.3	747.5	49.8	731.6
	39.9	771.7	40.2	755.7	101.6	773.2	101.3	759.6
	61.6	782.5	61.3	767.2	200.7	809.9	199.7	798.0
	70.4[a]		84.1	777.9	300.7	838.0	300.3	827.1
			100.4	785.1	329.7	845.1	402.3	851.2
			121.5	793.8	352.0	850.4	452.5	861.3
			145.9	802.6	369.0[a]		486.0[a]	
			161.9	808.2				
			185.4	815.8				
			203.3[a]					

[a] Lowest pressure at which freezing was detected

Table 4.8 (continued)

Mole fraction of n-hexadecane	298.15 K		323.15 K		348.15 K		373.15 K	
	Pressure (MPa)	Density (kg m^{-3})	Pressure (MPa)	Density (kg m^{-3})	Pressure (MPa)	Density (kg m^{-3})	Pressure (MPa)	Density (kg m^{-3})
0.800	0.1	759.5	0.1	741.6	0.1	723.8	0.1	705.5
	20.8	774.0	40.7	769.5	49.2	759.7	49.3	746.0
	29.6	778.9	70.3	784.4	100.5	784.8	100.0	772.8
	34.7	781.5	98.1	796.5	150.0	804.2	152.5	794.4
	39.9	784.1	118.7	804.5	199.9	820.7	200.7	810.9
	46.0	787.3	139.4	812.1	251.7	836.1	301.6	840.0
	50.0[a]		158.3	818.9	304.3	849.7	400.7	862.6
			179.4[a]		322.5[a]		450.1	872.8
							500.0[a]	
1	0.1	770.2	0.1	753.0	0.1	735.8	0.1	718.6
	12.0	778.7	29.0	773.2	48.8	770.3	51.4	758.1
	19.4	783.4	59.5	789.1	99.4	794.6	100.6	783.3
	25.2	786.4	89.2	802.4	150.2	814.2	151.8	804.3
	30.3	789.0	120.0	814.5	199.4	830.6	200.2	820.7
	35.2[a]		139.4	821.3	253.5	845.9	302.2	849.7
			148.9	824.7	290.0	855.2	399.8	871.7
			158.4[a]		305.5[a]		450.5	882.2
							469.3[a]	

[a] *Lowest pressure at which freezing was detected*

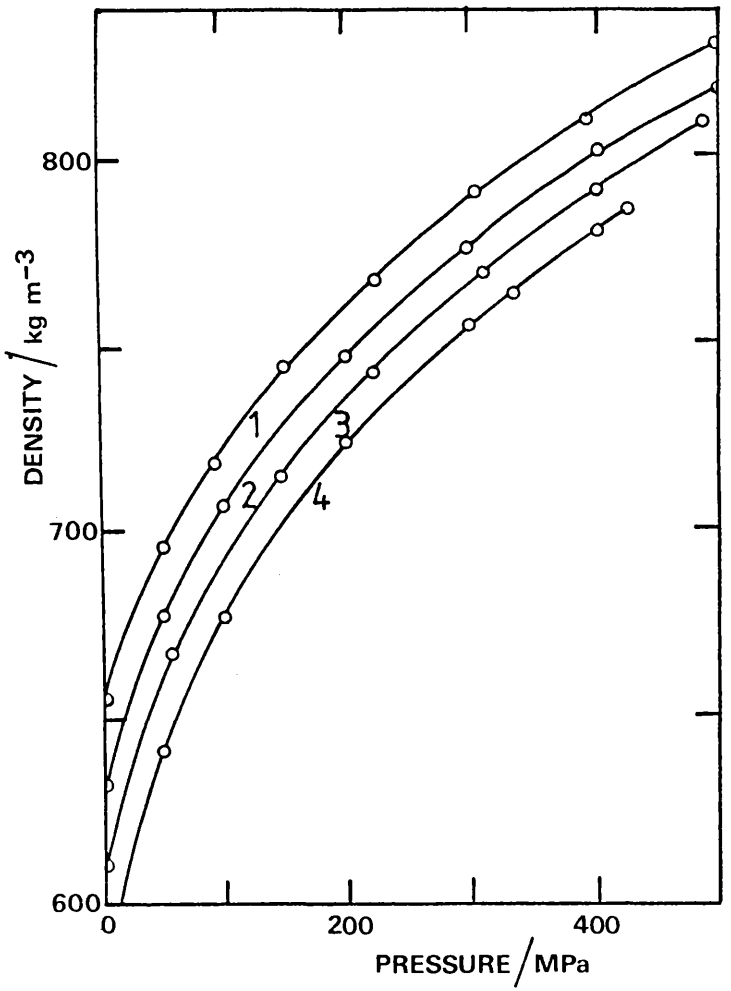

Figure 4.20 Densities for n-Hexane.
1 = 298.15 K, 2 = 323.15 K,
3 = 348.15 K, 4 = 373.15 K.

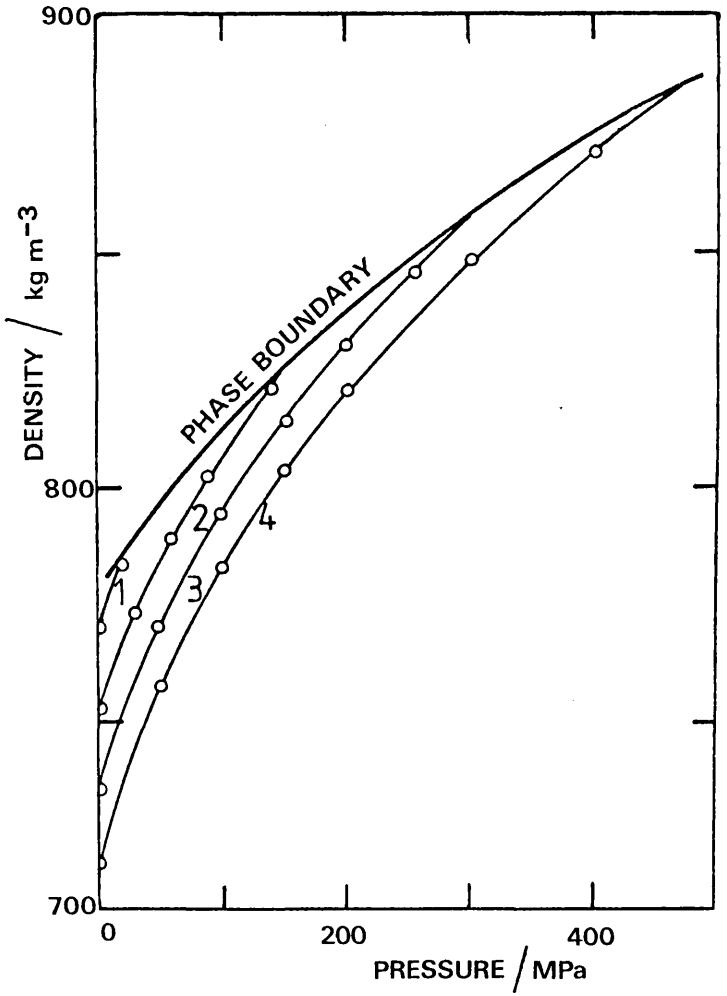

Figure 4.21 Densities for n-Hexadecane.
1 = 298.15 K, 2 = 323.15 K,
3 = 348.15 K, 4 = 373.15 K.

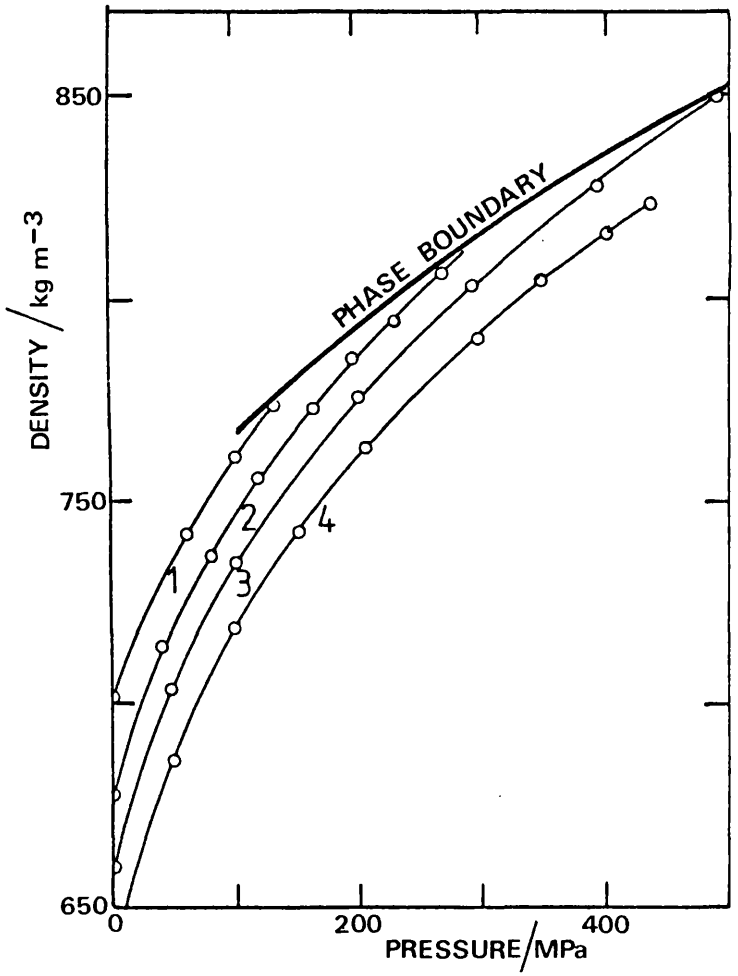

Figure 4.22 Densities for the Mixture with a Mole Fraction of n-Hexadecane of 0.200. 1 = 298.15 K, 2 = 323.15 K, 3 = 348.15 K, 4 = 373.15 K.

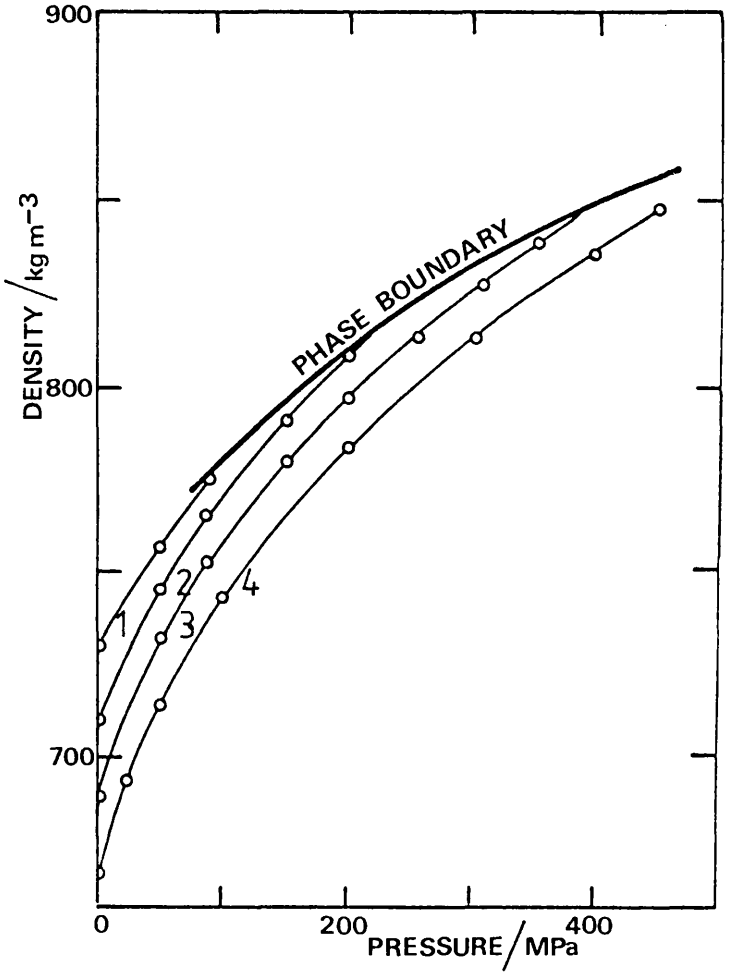

Figure 4.23 Densities for the Mixture with a Mole Fraction of n-Hexadecane of 0.400. 1 = 298.15 K, 2 = 323.15 K, 3 = 348.15 K, 3 = 373.15 K.

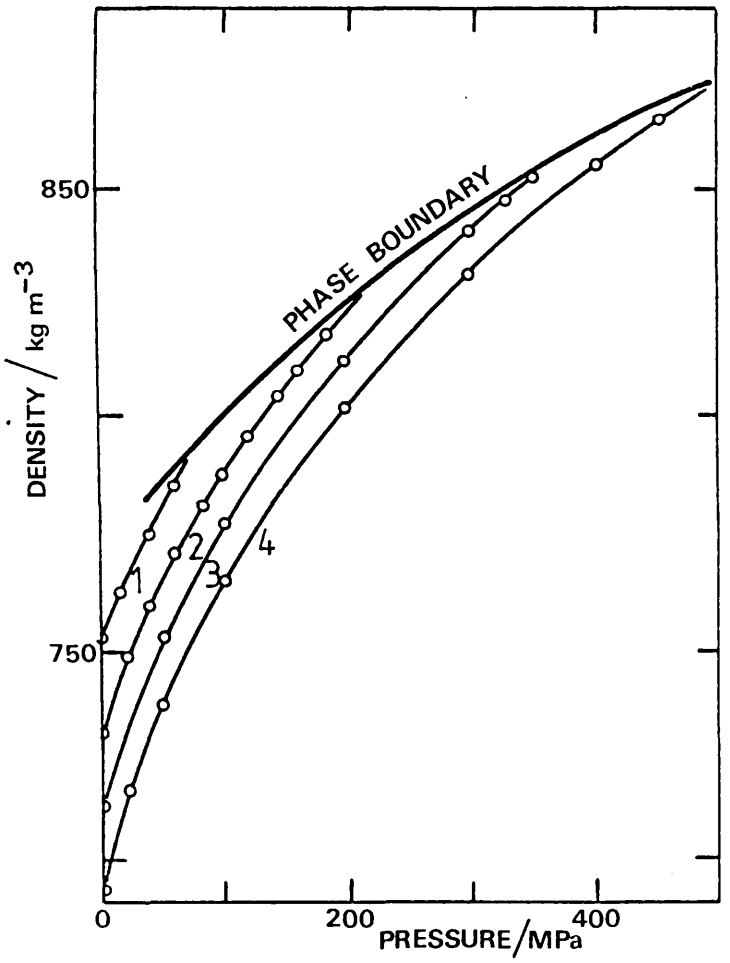

Figure 4.24 Densities for the Mixture with a Mole Fraction of n-Hexadecane of 0.600. 1 = 298.15 K, 2 = 323.15 K, 3 = 348.15 K, 4 = 373.15 K.

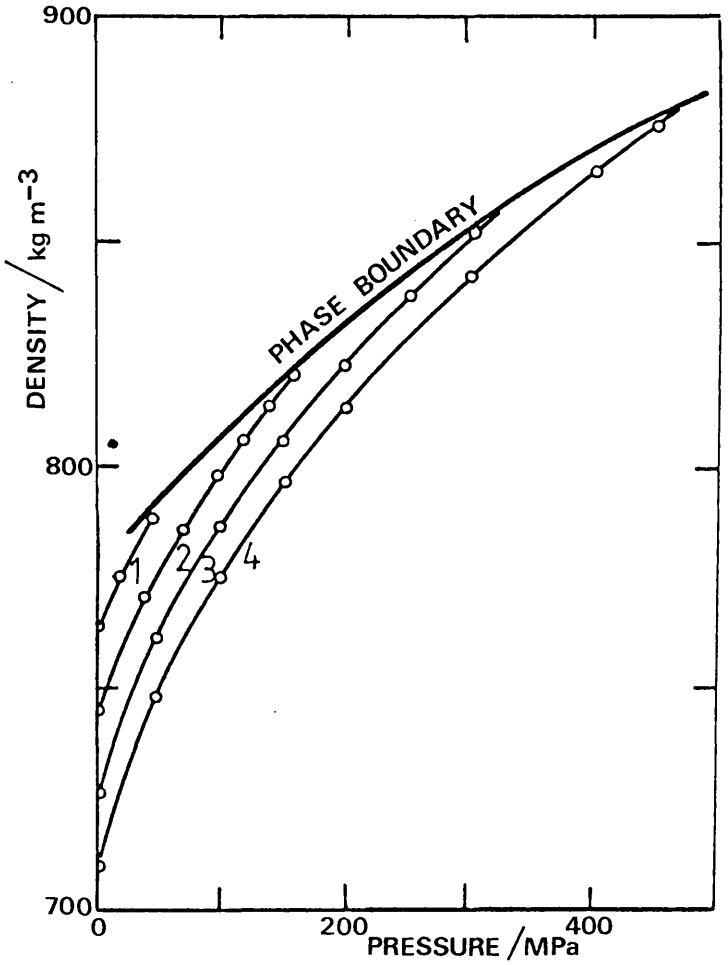

Figure 4.25 Densities for the Mixture with a Mole Fraction of n-Hexadecane of 0.800. 1 = 298.15 K, 2 = 323.15 K, 3 = 348.15 K, 4 = 373.15 K.

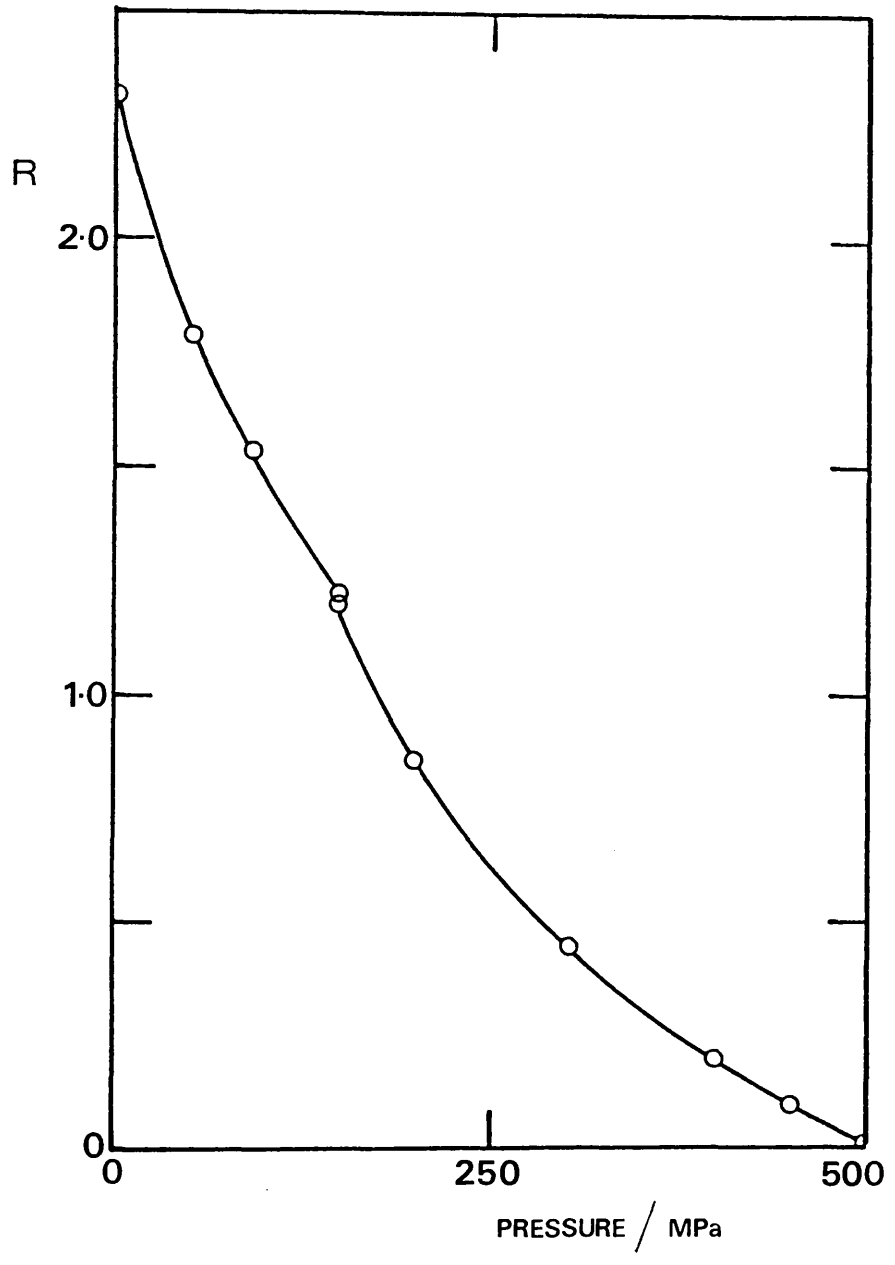

Figure 4.26 Equilibrium Micrometer Reading of the Coil Block Position at Different Pressures for the Mixture with a Mole Fraction of n-Hexadecane of 0.200 at 298.15 K.

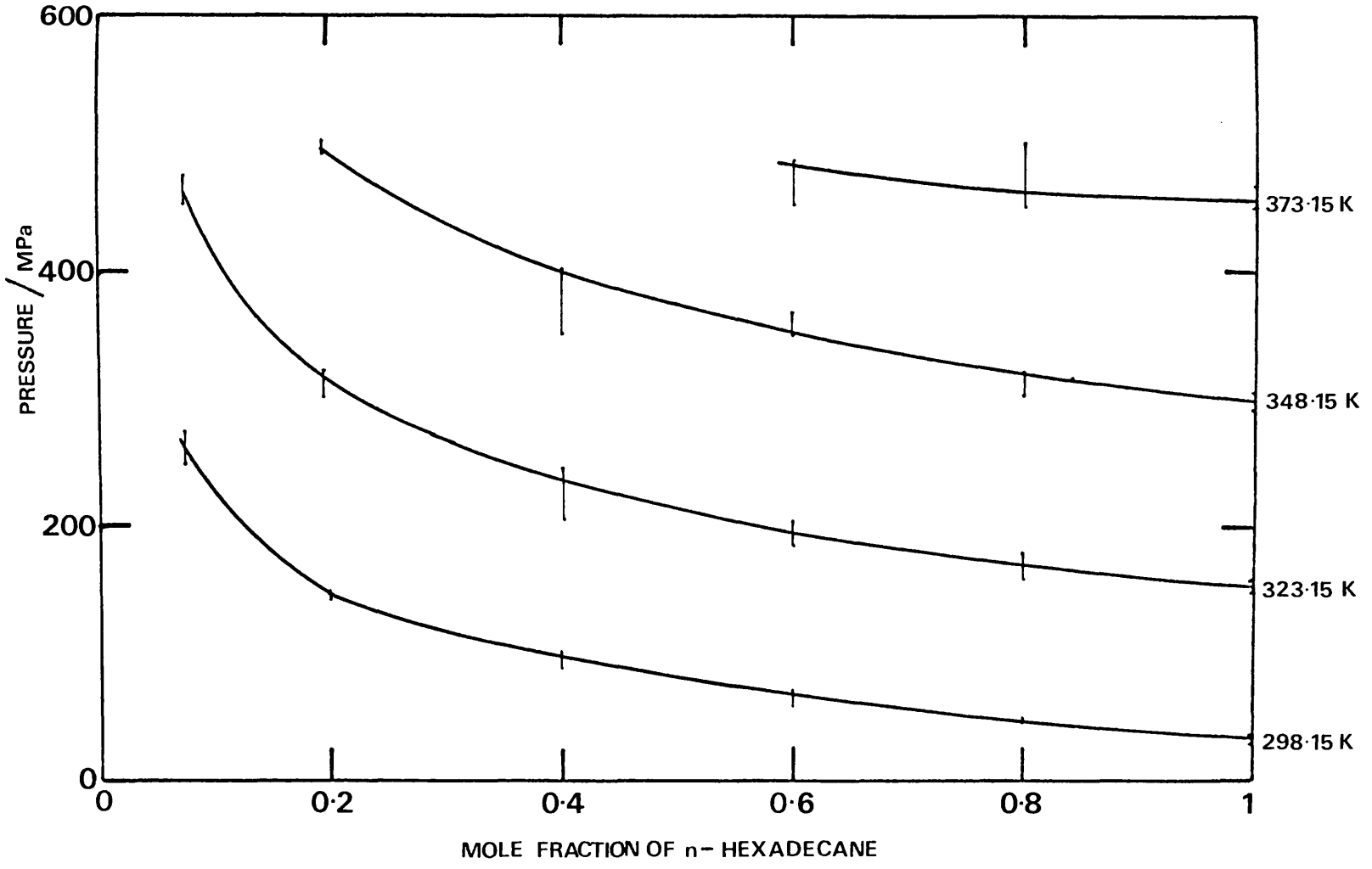

Figure 4.27 Freezing Pressures for the n-Hexane plus n-Hexadecane System at Different Temperatures.

Few data are available for the factors affecting the freezing pressure of liquid mixtures under pressure. Bridgman[127] was mainly concerned with measuring the freezing pressure of pure liquids and other workers[128] have assumed a linear relationship with mole fraction between the freezing pressures of the pure components which is certainly not the case for this system.

4.6.2 Comparison of Density Results with Literature Values

At atmospheric pressure the density of n-hexane at 298.15 K was found to be 655.0 kg m^{-3} which can be compared with literature values of 655.13[95], 655.18[54], 654.8[89] and 654.85[96] kg m^{-3}. For n-hexadecane at 298.15 K and atmospheric pressure the experimental density of 770.2 kg m^{-3} can be compared with 770.79[54] and 769.97[90] kg m^{-3}. At higher pressures, density measurements on n-hexane have been made by Mopsik[129], Eduljee, Newitt and Weale[130], Bridgman[122] and Isdale, Dymond and Brawn[23], and the present results agree with the values reported by these authors generally to within 0.1 percent at 298.15 K. The maximum difference is 0.21 percent. At 323.15 K, agreement with the results of Bridgman[122] is within 0.18 percent up to 500 MPa, and at 348.15 K the agreement with Isdale, Dymond and Brawn[23] is within 0.2 percent over this pressure range. For n-hexadecane, the experimental densities at 323.15 K and 373.15 K agree to within 0.12 percent, over the whole liquid range, with values calculated from tables of specific volumes given by Doolittle[131]. The densities given in A.S.M.E. Pressure Viscosity Report, 1953[132] agree with the present values to within 0.2 percent. This general agreement to $\pm$ 0.2 percent confirms the estimate of the accuracy of $\pm$ 0.2 percent for the density data calculated in Section 4.3.3.

4.6.3 Calculation of Densities at other Pressures

To enable viscosity coefficients to be calculated from sinker fall times measured in the high pressure viscometer, values of densities at the same temperatures and pressures are required. Experimental densities were measured in a separate experiment and the results were obtained at slightly different temperatures and different pressures. To enable densities to be obtained at the same pressure as the fall time experiments the experimental densities were fitted by a polynomial equation. An equation of the form

$$\rho = A + BP + CP^2 + DP^3 + EP^4 + \ldots \qquad (4.11)$$

was tried but this required five or six terms to reproduce the densities to the required accuracy. Since the maximum number of experimental points on each isotherm was only eight or nine an equation of this type was overfitting the data. It was therefore decided to use some form of the secant bulk modulus equation suggested by Hayward[133].

Isothermal compressibility is defined as the fractional volume change per unit pressure at constant temperature and its reciprocal, the bulk modulus, is defined as

$$K = -V\left(\frac{\partial P}{\partial V}\right)_T \qquad (4.12)$$

It is much easier however to derive the average value of the bulk modulus from P_o to P where P_o is atmospheric pressure. This average value is called the secant bulk modulus and is defined as

$$\bar{K} = \frac{V_o(P - P_o)}{V_o - V} \qquad (4.13)$$

It follows that

$$V = V_o \frac{\bar{K} - (P - P_o)}{\bar{K}} \qquad (4.14)$$

and hence

$$\rho = \frac{\rho_o \bar{K}}{\bar{K} - (P - P_o)} \qquad (4.15)$$

where ρ and ρ_o are the densities at pressure P and P_o.

From equation (4.15) it follows that

$$\bar{K} = \left[\frac{\rho}{\rho - \rho_o}\right] P \qquad (4.16)$$

where P_o is negligible compared to P.

This equation was used to calculate $\bar{K}$ from experimental pressure-density data and a quadratic equation of the form

$$\bar{K} = K_o + mP + nP^2 \qquad (4.17)$$

was used to calculate secant bulk modulus and hence density at other pressures. Table 4.9 gives the values of the coefficients derived using equation (4.17) for the n-hexane plus n-hexadecane system. This representation has the advantage of requiring fewer empirical constants than a polynomial equation of density. The secant bulk modulus data was fitted by equation (4.17) to within $\pm$ 2.3 percent which is equivalent to $\pm$ 0.21 percent in density. The general fit was significantly better than this, the mean deviation for all isotherms being within $\pm$ 0.07 percent in density. At 298.15 K the pressure range over which mixtures having a mole fraction of n-hexadecane greater than 0.200 remain liquid was too small to warrant a quadratic fit. For these a linear fit of the experimental secant bulk

Table 4.9

Values of Coefficients Used in Equation (4.17) for Secant Bulk Modulus

Mole fraction of n-hexadecane	Temperature (K)	K_o (MPa)	m	$-10^3 n$ (MPa^{-1})
0	298.15	668.2	4.156	1.580
	323.15	531.2	4.016	1.442
	348.15	454.8	3.636	1.156
	373.15	332.4	3.731	1.636
0.200	298.15	717.6	6.337	9.597
	323.15	572.8	5.487	4.649
	348.15	547.2	4.275	1.976
	373.15	455.1	4.104	1.832
0.400	298.15	891.3	5.090	
	323.15	729.3	5.666	5.763
	348.15	638.9	4.798	2.844
	373.15	528.9	4.462	2.137
0.600	298.15	866.6	7.089	
	323.15	781.3	6.617	9.271
	348.15	730.0	4.872	2.803
	373.15	645.3	4.458	1.992
0.800	298.15	955.9	7.781	
	323.15	873.5	6.521	9.118
	348.15	797.2	5.224	3.644
	373.15	695.4	4.656	2.221
1	298.15	978.3	9.649	
	323.15	926.8	6.773	10.065
	348.15	848.3	5.256	3.566
	373.15	764.8	4.614	2.066

modulus-pressure data reproduced the density results to within 0.05 percent.

The coefficients given in Table 4.9 can be used to calculate secant bulk modulus at any pressure up to the maximum experimental pressure and the corresponding density can then be obtained from equation (4.15). Values for density at rounded pressure steps of 50 MPa have been calculated in this way and these are given in Table 4.10.

4.6.4 Experimental Viscosity Coefficient Results

Viscosity coefficients for n-hexane, n-hexadecane and four mixtures of n-hexane plus n-hexadecane have been measured in the old viscometer, hereafter referred to as viscometer 1, at 298 K, 323 K, 348 K and 373 K up to just below the freezing pressure or a maximum of 500 MPa. The precaution of keeping the pressure below the freezing pressure was taken as if the liquid or liquid mixture had frozen, the viscometer tube could buckle at the thin coil section due to the pressure difference at the viscometer wall. This precaution was taken even though Hogenboom, Webb and Dixon[40] found that the liquids they studied, which included n-alkanes, could be superpressed above the equilibrium freezing point and were very stable despite agitation of the sample by the falling ball. Equation (4.8) was used to calculate viscosity coefficients and the results are given in Table 4.11 and plotted as viscosity coefficient versus pressure in Figure 4.28 to 4.33. Fall times quoted for n-hexane at 348 K and 373 K at 0.1 MPa and for the mixture with the mole fraction of n-hexane of 0.200 at 373 K and 0.1 MPa were extrapolated from fall times measured at pressures between 0.5 MPa and 10 MPa since it was necessary to apply a small pressure at these temperatures as the samples were above the normal boiling

Table 4.10

Densities (in kg m^{-3}) for the n-Hexane plus n-Hexadecane System at 50 MPa Intervals

Pressure (MPa)	Mole fraction of n-hexadecane					
	0	0.200	0.400	0.600	0.800	1
Temperature : 298.15 K						
0.1	655.0	698.8	726.3	745.3	759.5	770.2
50.0	694.8	735.2	759.4	777.1		
100.0	722.7	759.3				
150.0	743.8					
200.0	761.0					
250.0	775.5					
300.0	788.4					
350.0	800.2					
400.0	811.2					
450.0	821.7					
500.0	831.9					
Temperature : 323.15 K						
0.1	631.6	678.0	706.9	726.7	741.6	753.0
50.0	678.2	721.2	744.2	761.7	774.5	784.6
100.0	708.8	747.5	769.0	784.8	797.2	806.7
150.0	731.2	767.1	788.5	803.7	815.9	
200.0	748.9	783.6	805.6			
250.0	763.7	798.7				
300.0	776.7	813.6				
350.0	788.4					
400.0	799.3					
450.0	809.7					
500.0	819.7					
Temperature : 348.15 K						
0.1	606.7	656.3	687.0	707.9	723.8	735.8
50.0	658.7	702.8	728.8	746.5	760.0	770.8
100.0	692.5	733.1	756.4	772.9	785.0	795.2
150.0	717.1	755.3	777.0	793.0	804.3	814.3
200.0	736.4	773.2	794.0	809.6	820.6	830.3
250.0	752.3	788.4	808.8	824.1	835.1	844.7
300.0	766.1	802.0	822.4	837.5	848.9	
350.0	778.5	814.6	835.5	850.1		
400.0	790.0	826.7				
450.0	800.7	838.5				
500.0	811.1					

Table 4.10 (continued)

Pressure (MPa)	Mole fraction of n-hexadecane					
	0	0.200	0.400	0.600	0.800	1
Temperature 373.15 K						
0.1	580.5	634.4	666.9	688.9	705.5	718.6
50.0	642.9	686.8	714.8	731.3	745.9	756.8
100.0	679.0	719.3	745.0	759.8	773.4	783.6
150.0	704.0	742.6	766.9	781.2	794.1	804.1
200.0	723.3	760.9	784.3	798.5	811.0	820.9
250.0	739.5	776.4	799.1	813.2	825.4	835.3
300.0	753.9	790.2	812.4	826.4	838.4	848.2
350.0	767.3	803.0	824.7	838.5	850.5	860.2
400.0	780.2	815.2	836.6	850.1	862.1	871.5
450.0	792.9	827.1	848.3	861.3	873.4	882.5

Table 4.11

Experimental Elevated Pressure Viscosity Coefficients for the n-Hexane plus n-Hexadecane System

Mole fraction of n-hexadecane	Temperature (K)	Pressure (MPa)	Fall time (s)	Calculated density ($kg\ m^{-3}$)	Viscosity coefficient (mPa s)
0	298.29	0.1	2.923	655.0	0.2976
		21.1	3.559	673.8	0.3628
		42.2	4.18	698.6	0.4265
		59.8	4.75	701.0	0.4850
		82.6	5.48	713.9	0.5601
		102.2	6.20	723.7	0.6342
		203.4	10.49	762.0	1.077
		298.7	15.89	788.1	1.637
		358.2	20.35	802.0	2.100
0	323.15	0.1	2.357	631.6	0.2357
		48.4	3.598	677.0	0.3665
		101.5	5.01	709.6	0.5109
		144.5	6.31	729.0	0.6448
		198.4	8.11	748.4	0.8202
		252.0	10.19	764.3	1.045
		301.7	12.45	777.1	1.279
		350.7	14.91	788.5	1.533
		402.0	17.77	799.7	1.829
0	348.38	0.1	1.925	606.7	0.1902
		3.9	2.018	611.8	0.2001
		7.4	2.104	616.2	0.2094
		49.8	3.032	658.5	0.3084
		100.9	4.168	693.0	0.4246
		155.0	5.50	719.2	0.5611
		204.5	6.82	737.9	0.6967
		248.9	8.15	752.0	0.8335
		299.3	9.84	766.0	1.008
		349.8	11.75	778.5	1.205
		401.1	13.85	790.2	1.421
0	373.36	0.1	1.618	580.5	0.1549
		4.8	1.722	588.6	0.1669
		10.0	1.837	596.7	0.1803
		52.5	2.662	645.2	0.2672
		102.2	3.613	680.3	0.3675
		153.1	4.657	705.3	0.4743
		202.7	5.75	724.2	0.5865
		250.0	6.90	739.5	0.7048
		300.0	8.24	753.9	0.8422
		350.1	9.73	767.3	0.9955
		400.7	11.31	780.4	1.158
		419.6	12.07	785.2	1.236

Table 4.11 (continued)

Mole fraction of n-hexadecane	Temperature (K)	Pressure (MPa)	Fall time (s)	Calculated density ($kg\ m^{-3}$)	Viscosity coefficient (mPa s)
0.200	298.22	0.1	5.70	698.8	0.5842
		1.4	5.84	700.2	0.5987
		9.0	6.30	707.0	0.6462
		18.5	6.91	714.7	0.7091
		41.4	8.53	730.2	0.8767
		61.2	9.94	741.2	1.023
		80.9	11.50	750.8	1.184
		103.9	13.61	760.9	1.404
0.200	323.19	0.1	4.33	678.0	0.4426
		1.6	4.41	679.9	0.4508
		8.4	4.76	687.3	0.4868
		48.5	6.84	720.2	0.7009
		98.7	9.76	747.0	1.002
		127.9	11.73	759.0	1.206
		152.5	13.52	768.0	1.392
		204.5	18.00	785.0	1.857
		230.4	20.77	792.9	2.145
0.200	348.07	0.1	3.432	656.3	0.3501
		3.1	3.560	660.0	0.3632
		9.4	3.823	667.0	0.3902
		48.3	5.40	701.5	0.5521
		101.1	7.85	733.6	0.8043
		152.7	10.54	756.4	1.082
		202.5	13.63	774.0	1.401
		248.7	16.86	788.0	1.736
		296.0	20.74	800.9	2.138
		351.1	25.96	814.9	2.680
		401.8	32.03	827.1	3.310
		450.4	38.50	838.6	3.982
		482.2	42.52	846.2	4.399
0.200	373.12	0.1	2.779	634.4	0.2803
		48.6	4.48	685.7	0.4572
		101.8	6.46	720.3	0.6605
		151.6	8.53	743.2	0.8736
		201.4	10.81	761.4	1.109
		249.5	13.32	776.3	1.368
		302.2	16.62	790.8	1.709
		351.5	20.02	803.3	2.061
		398.3	23.74	814.8	2.446
		447.7	28.09	826.6	2.896
		501.9	33.90	839.6	3.498

Table 4.11 (continued)

Mole fraction of n-hexadecane	Temperature (K)	Pressure (MPa)	Fall time (s)	Calculated density ($kg\ m^{-3}$)	Viscosity coefficient (mPa s)
0.400	298.12	0.1	9.62	726.3	0.9913
		4.6	9.97	730.0	1.027
		10.6	10.75	734.5	1.109
		19.6	11.89	741.0	1.227
		32.0	13.52	749.0	1.396
		40.7	14.52	754.3	1.500
		50.7	15.92	759.8	1.646
		61.9	17.46	765.6	1.806
		70.8	19.11	769.9	1.978
		82.0	20.86	774.9	2.161
0.400	323.33	0.1	6.85	706.9	0.7032
		5.3	7.30	711.9	0.7498
		10.5	7.64	716.4	0.7848
		26.2	9.02	728.8	0.9276
		50.7	11.18	744.6	1.151
		75.0	13.71	757.6	1.414
		101.5	16.75	769.7	1.730
		121.5	19.40	777.8	2.006
		153.8	23.95	789.9	2.479
		172.1	26.67	796.3	2.763
		199.2	31.79	805.4	3.297
0.400	348.29	0.1	5.10	687.0	0.5219
		2.6	5.23	689.8	0.5353
		4.3	5.32	691.5	0.5445
		9.2	5.67	696.4	0.5807
		51.1	8.43	729.5	0.8653
		101.4	12.48	757.0	1.284
		153.0	17.16	778.1	1.770
		202.7	23.11	794.8	2.388
		249.7	29.31	808.7	3.033
		298.4	37.00	822.0	3.834
		341.7	45.48	833.3	4.717
0.400	373.24	0.1	4.06	666.9	0.4147
		5.2	4.35	673.2	0.4445
		10.5	4.65	679.3	0.4753
		49.8	6.70	714.6	0.6860
		103.3	9.89	746.7	1.015
		152.3	13.16	767.8	1.353
		203.7	17.45	785.5	1.797
		251.9	21.86	799.7	2.254
		303.3	27.62	813.2	2.852
		351.3	33.87	825.0	3.502
		402.3	41.77	837.1	4.323
		451.7	50.45	848.7	5.225
		478.3	56.81	855.0	5.888
		502.8	61.11	860.8	6.334

Table 4.11 (continued)

Mole fraction of n-hexadecane	Temperature (K)	Pressure (MPa)	Fall time (s)	Calculated density ($kg\ m^{-3}$)	Viscosity coefficient (mPa s)
0.600	298.15	0.1	14.67	745.3	1.518
		4.3	15.92	748.9	1.649
		9.0	16.77	752.6	1.737
		15.7	18.15	757.5	1.881
		21.6	19.40	761.4	2.011
		31.6	21.67	767.5	2.248
		36.9	21.95	770.5	2.277
		41.8	24.01	773.1	2.493
		46.2	24.99	775.3	2.595
		57.2	27.54	780.4	2.862
0.600	323.13	0.1	9.98	726.7	1.028
		25.8	13.36	747.1	1.379
		52.1	16.92	762.8	1.749
		77.6	21.15	775.3	2.190
		111.0	27.87	789.2	2.891
		126.9	31.28	795.3	3.248
		153.2	37.67	804.9	3.915
		178.4	44.96	813.8	4.678
0.600	348.31	0.1	7.34	707.9	0.7540
		4.9	7.77	712.5	0.7984
		8.7	8.11	716.0	0.8335
		49.8	12.28	746.4	1.265
		102.0	18.21	773.8	1.881
		137.1	22.80	788.2	2.358
		167.3	27.76	799.1	2.874
		202.6	34.37	810.4	3.563
		249.9	44.94	824.1	4.666
		297.1	59.79	836.7	6.219
0.600	373.18	0.1	5.55	688.9	0.5684
		4.3	5.81	693.4	0.5952
		9.6	6.24	698.7	0.6396
		49.9	9.34	731.2	0.9596
		91.4	12.80	755.6	1.317
		140.9	17.69	777.7	1.824
		202.2	25.13	799.2	2.597
		298.9	41.32	826.1	4.282
		400.0	65.37	850.1	6.791
		418.4	71.19	854.2	7.398

Table 4.11 (continued)

Mole fraction of n-hexadecane	Temperature (K)	Pressure (MPa)	Fall time (s)	Calculated density ($kg\ m^{-3}$)	Viscosity coefficient (mPa s)
0.800	298.09	0.1	21.53	759.5	2.236
		4.3	22.40	762.8	2.327
		10.2	24.35	767.1	2.531
		19.8	27.57	773.3	2.868
		30.1	31.45	779.2	3.275
		34.3	32.65	781.4	3.400
		39.5	34.10	764.0	3.552
0.800	323.21	0.1	13.63	741.6	1.409
		5.0	14.39	745.7	1.488
		9.8	15.34	749.4	1.587
		39.0	20.91	768.5	2.167
		61.4	25.93	780.3	2.691
		79.0	30.38	788.4	3.156
		101.3	37.32	797.7	3.882
		123.4	45.26	806.2	4.714
		142.9	52.59	813.4	5.483
		156.6	57.66	818.3	6.014
0.800	348.09	0.1	9.60	723.8	0.9884
		4.5	10.04	727.8	1.034
		9.7	10.70	732.2	1.102
		48.9	15.77	759.4	1.628
		99.4	24.61	784.7	2.549
		148.2	35.27	803.7	3.661
		201.8	49.84	821.1	5.184
		246.8	64.65	834.2	6.733
		300.4	89.57	849.0	9.344
0.800	373.17	0.1	7.10	705.5	0.7287
		48.2	11.74	744.8	1.208
		100.1	17.78	773.5	1.835
		158.5	26.24	797.2	2.714
		202.2	33.94	811.7	3.515
		251.0	44.60	825.7	4.627
		302.1	59.31	838.9	6.163
		351.4	75.46	850.8	7.851
		401.0	94.67	862.3	9.859
		446.1	116.47	872.5	12.139

Table 4.11 (continued)

Mole fraction of n-hexadecane	Temperature (K)	Pressure (MPa)	Fall time (s)	Calculated density ($kg\ m^{-3}$)	Viscosity coefficient (mPa s)
1	298.08	0.1	29.55	770.2	3.078
		0.7	29.84	770.8	3.109
		4.5	31.44	773.6	3.276
		15.1	36.03	780.7	3.758
		27.9	42.10	787.8	4.395
1	323.09	0.1	17.81	753.0	1.845
		0.8	18.07	753.7	1.872
		4.3	18.87	756.4	1.956
		27.3	24.86	772.1	2.581
		52.4	32.56	785.8	3.387
		78.6	41.79	797.9	4.354
		103.4	52.75	808.0	5.504
		139.1	71.70	821.2	7.495
1	348.11	0.1	12.04	735.8	1.242
		0.9	12.15	736.6	1.254
		4.1	12.69	739.3	1.310
		50.6	20.92	771.1	2.166
		102.5	32.93	796.3	3.419
		154.2	48.72	815.7	5.070
		204.9	69.06	831.8	7.200
		273.1	106.25	851.0	11.102
1	373.24	0.1	8.71	718.6	0.9854
		51.1	15.04	757.5	1.551
		103.1	23.15	785.0	2.394
		201.8	44.62	821.5	4.631
		330.1	90.82	855.5	9.462
		398.8	127.77	871.3	13.331
		425.1	144.42	877.1	15.075

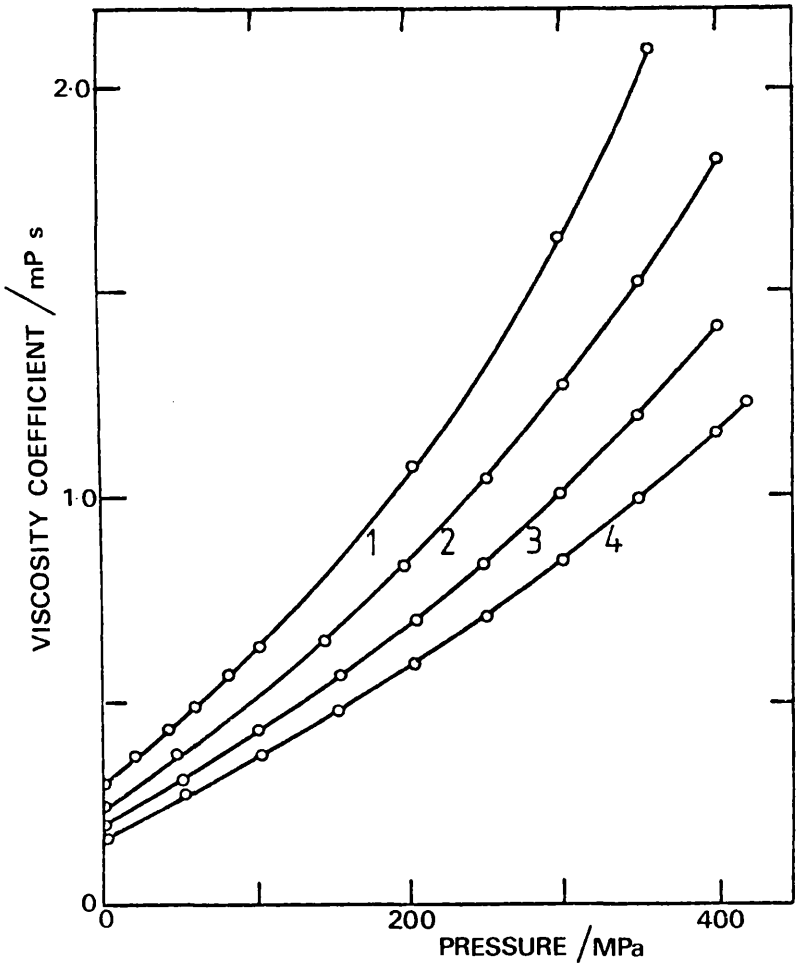

Figure 4.28 Viscosity Coefficients for n-Hexane.

1 = 298.29 K, 2 = 323.15 K,
3 = 348.38 K, 4 = 373.36 K.

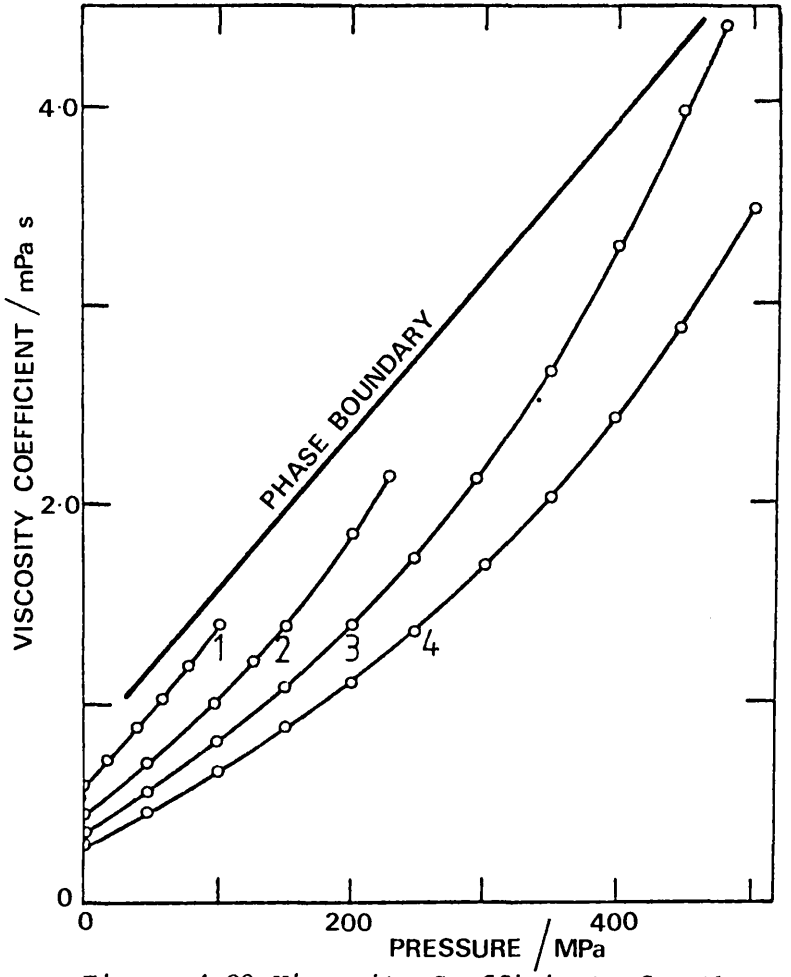

Figure 4.29 Viscosity Coefficients for the Mixture with a Mole Fraction of n-Hexadecane of 0.200.
1 = 298.22 K, 2 = 323.19 K,
3 = 348.07 K, 4 = 373.12 K.

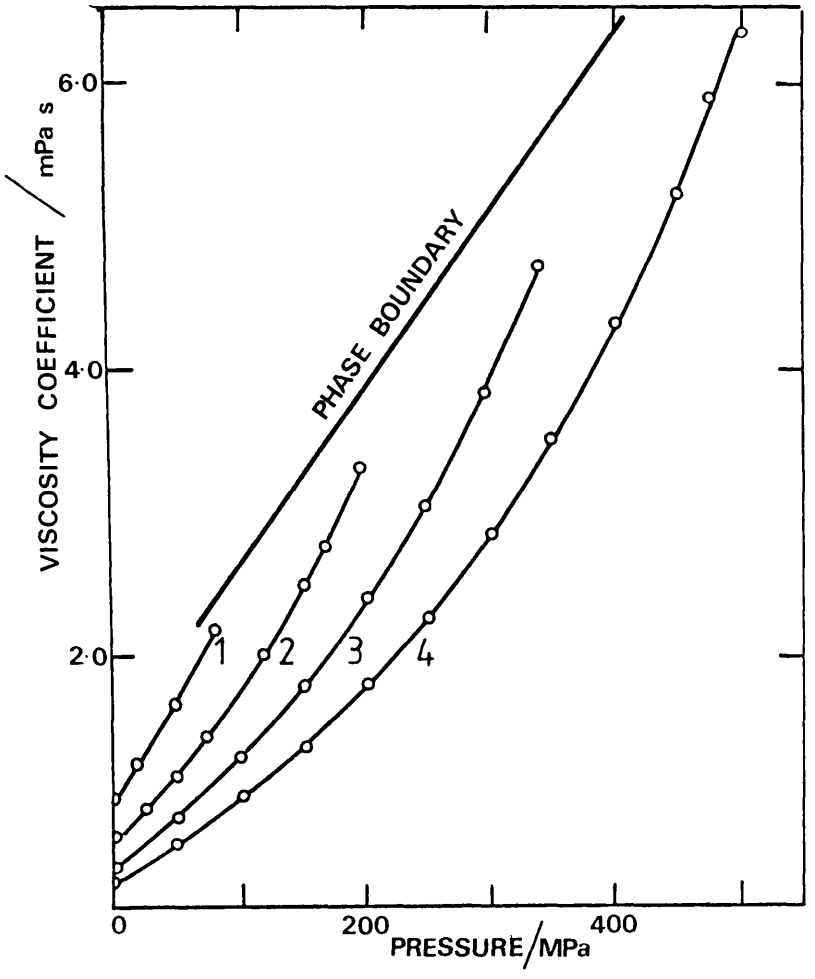

Figure 4.30 Viscosity Coefficients for the Mixture with a Mole Fraction of n-Hexadecane of 0.400. 1 = 298.12 K, 2 = 323.33 K, 3 = 348.29 K, 4 = 373.24 K.

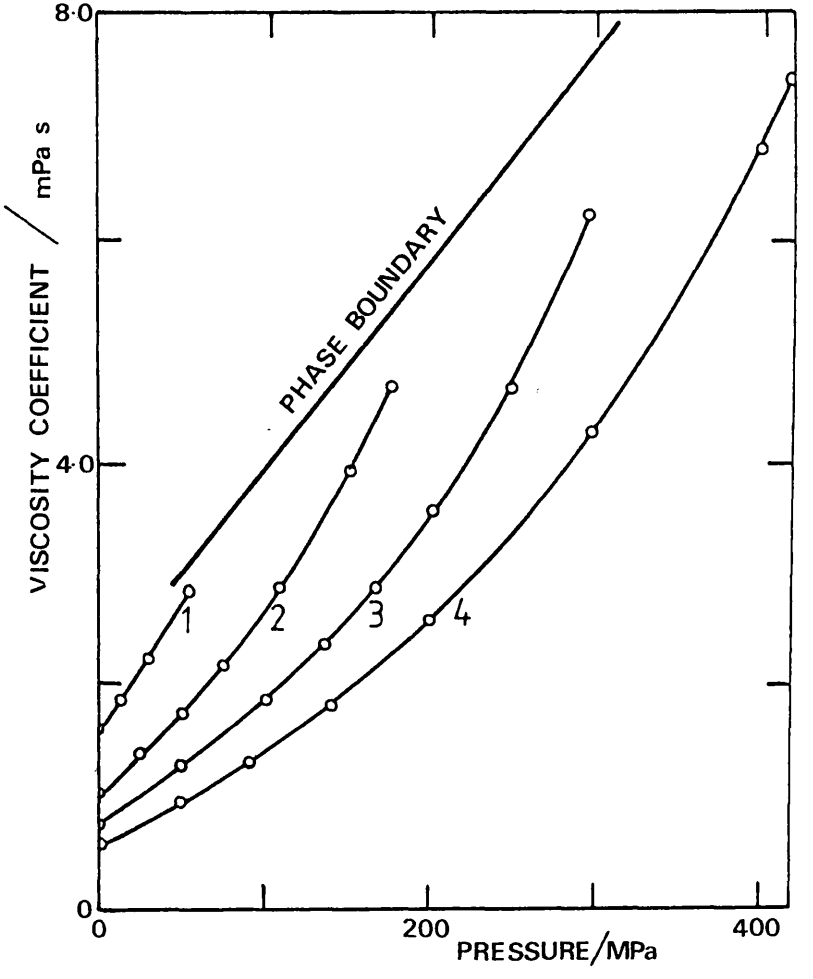

Figure 4.31 Viscosity Coefficients for the Mixture with a Mole Fraction of n-Hexadecane of 0.600. 1 = 298.15 K, 2 = 323.13K, 3 = 348.31 K, 4 = 373.18K.

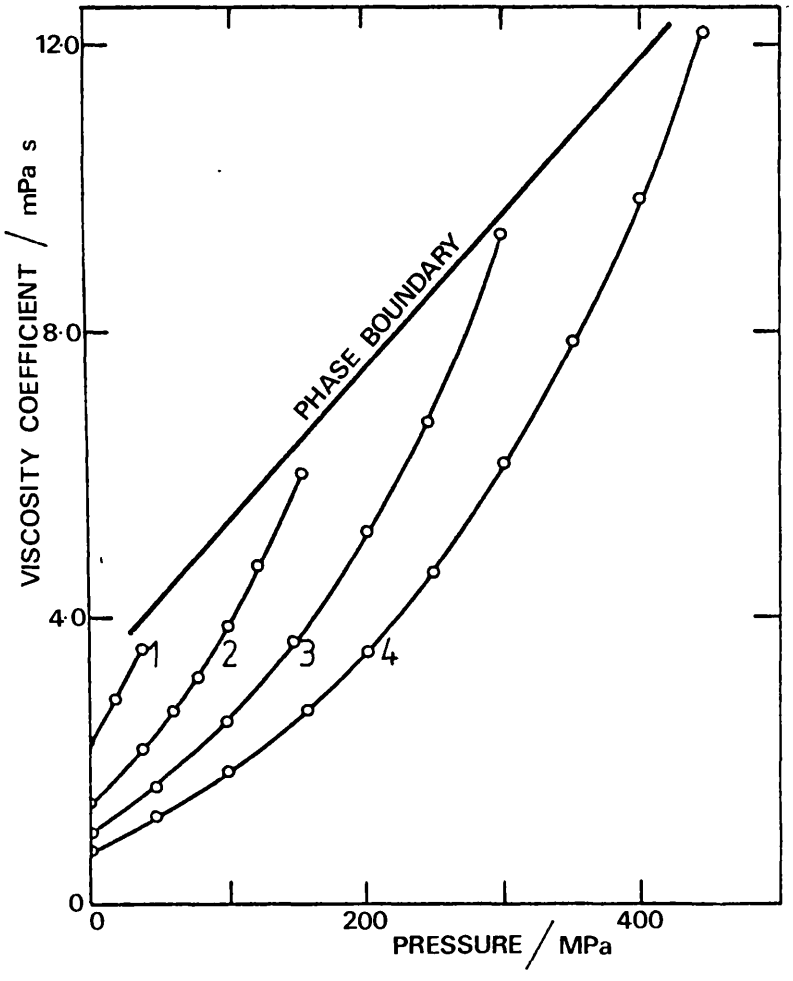

Figure 4.32 Viscosity Coefficients for the Mixture with a Mole Fraction of n-Hexadecane of 0.800.

1 = 298.09 K, 2 = 323.21 K, 3 = 348.09 K, 4 = 373.17 K.

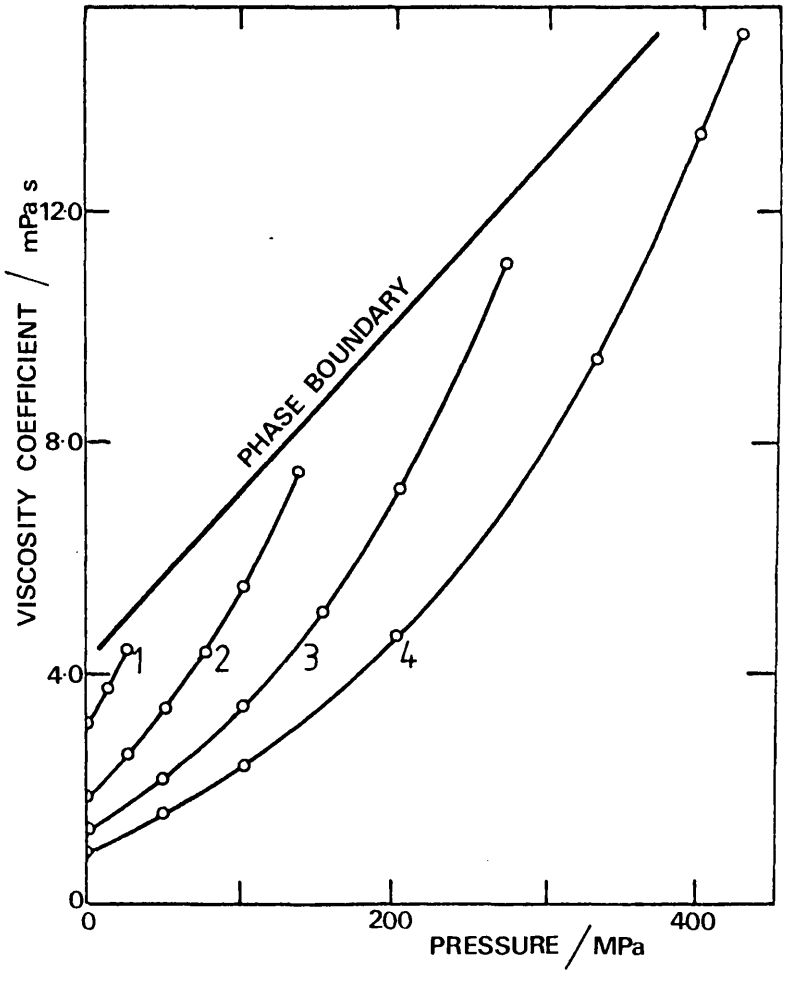

Figure 4.33 Viscosity Coefficients for n-Hexadecane.

1 = 298.08 K, 2 = 323.09 K, 3 = 348.11 K, 4 = 373.24 K.

point. Viscosity coefficients for n-hexane at 323 K and 348 K were also measured at elevated pressure in the new viscometer, hereafter referred to as viscometer 2 and results are presented in Table 4.12 and Figure 4.34. Also shown on Figure 4.34 are viscosity coefficient results from viscometer 1 for n-hexane at approximately the same temperatures.

This figure shows that the viscosity coefficient results for n-hexane at 323 K and 348 K obtained from the two different viscometer tube/sinker combinations agree to within $\pm$ 3 percent over pressure range 0.1 MPa to 400 MPa. If an uncertainty of $\pm$ 2 percent is assumed for the results from viscometer 2 (in line with the uncertainty from viscometer 1) then the value of $\pm$ 3 percent is well within the combined uncertainty of $\pm$ 4 percent for the two viscometers. This confirms the estimate of the uncertainty of the method as calculated in Section 4.4.7.

4.6.5 Comparison of Viscosity Coefficient Results with Literature Values

The ratio of viscosity coefficient at pressure, η_p, to the viscosity coefficient at atmospheric pressure, η_o, has been measured for n-hexane by Brazier and Freeman[134] at 273 K, 303 K and 333 K up to 400 MPa, by Bridgman[135] at 303 K and 348 K up to 980 MPa and by Isdale, Dymond and Brawn[23] at 298 K, 323 K, 348 K and 373 K up to 500 MPa using a similar National Engineering Laboratory high pressure viscometer with a different tube/sinker combination. The present viscosity coefficient results were converted to viscosity coefficient ratio and a comparison made with the literature values. The comparison is shown in Figures 4.35 and 4.36.

Table 4.12

Experimental Elevated Pressure Viscosity Coefficients for n-Hexane Measured Using Viscometer 2

Temperature (K)	Pressure (MPa)	Fall time (s)	Calculated density ($kg\ m^{-3}$)	Viscosity coefficient (mPa s)
323.21	0.1	28.43	631.6	0.2363
	99.2	62.12	703.6	0.5142
	202.6	104.45	742.0	0.8631
	300.0	156.09	766.9	1.289
	395.3	221.69	786.7	1.830
348.23	0.1	22.79	606.7	0.1896
	12.7	27.02	622.5	0.2246
	100.9	52.30	693.0	0.4327
	203.4	86.24	737.5	0.7116
	296.6	124.37	762.5	1.025
	395.0	174.42	788.8	1.436
	503.1	244.42	811.8	2.009

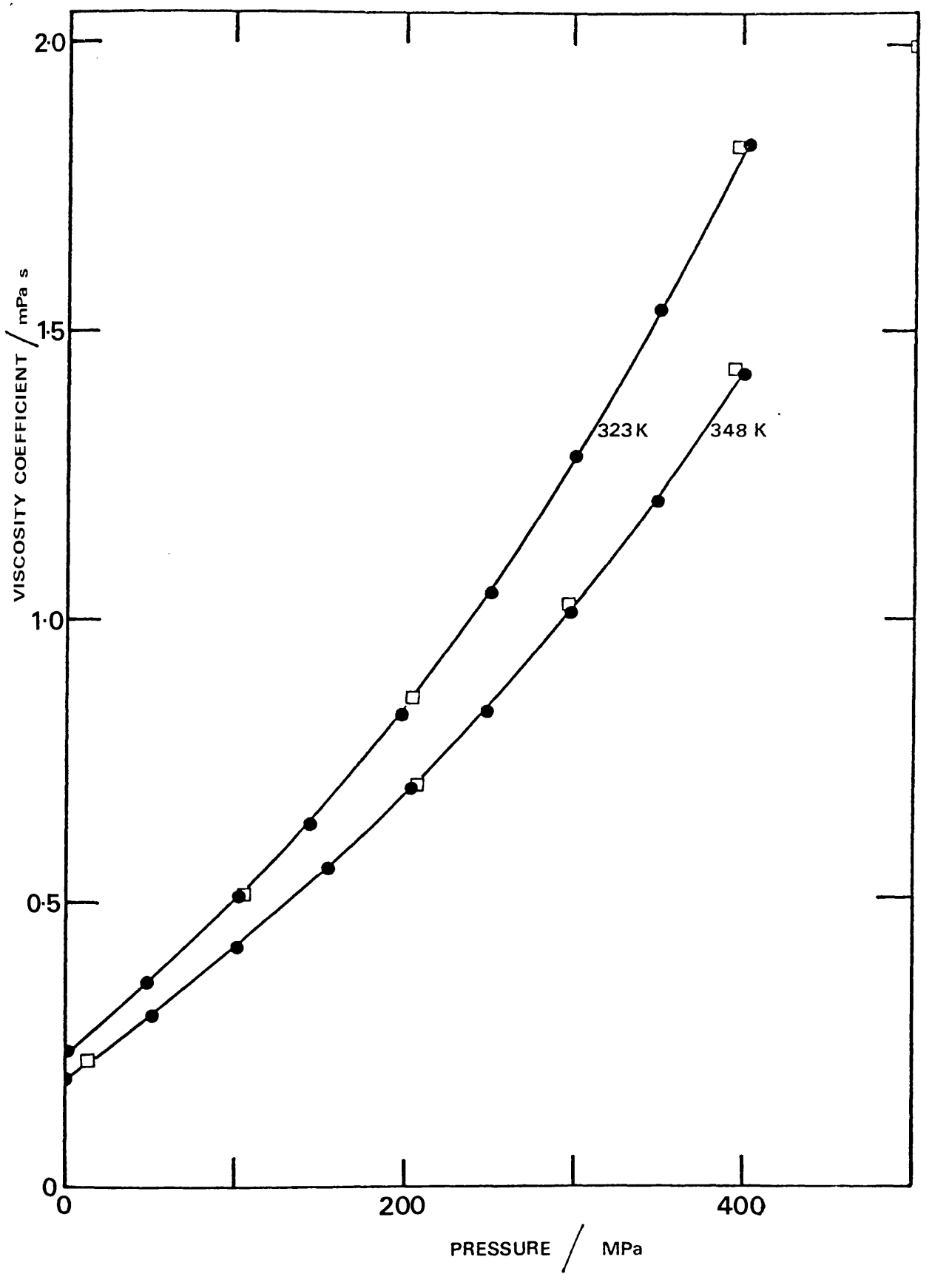

Figure 4.34 Viscosity Coefficient Results for n-Hexane at 323 K and 348 K Measured Using Viscometer 1 (●) and Viscometer 2 (□)

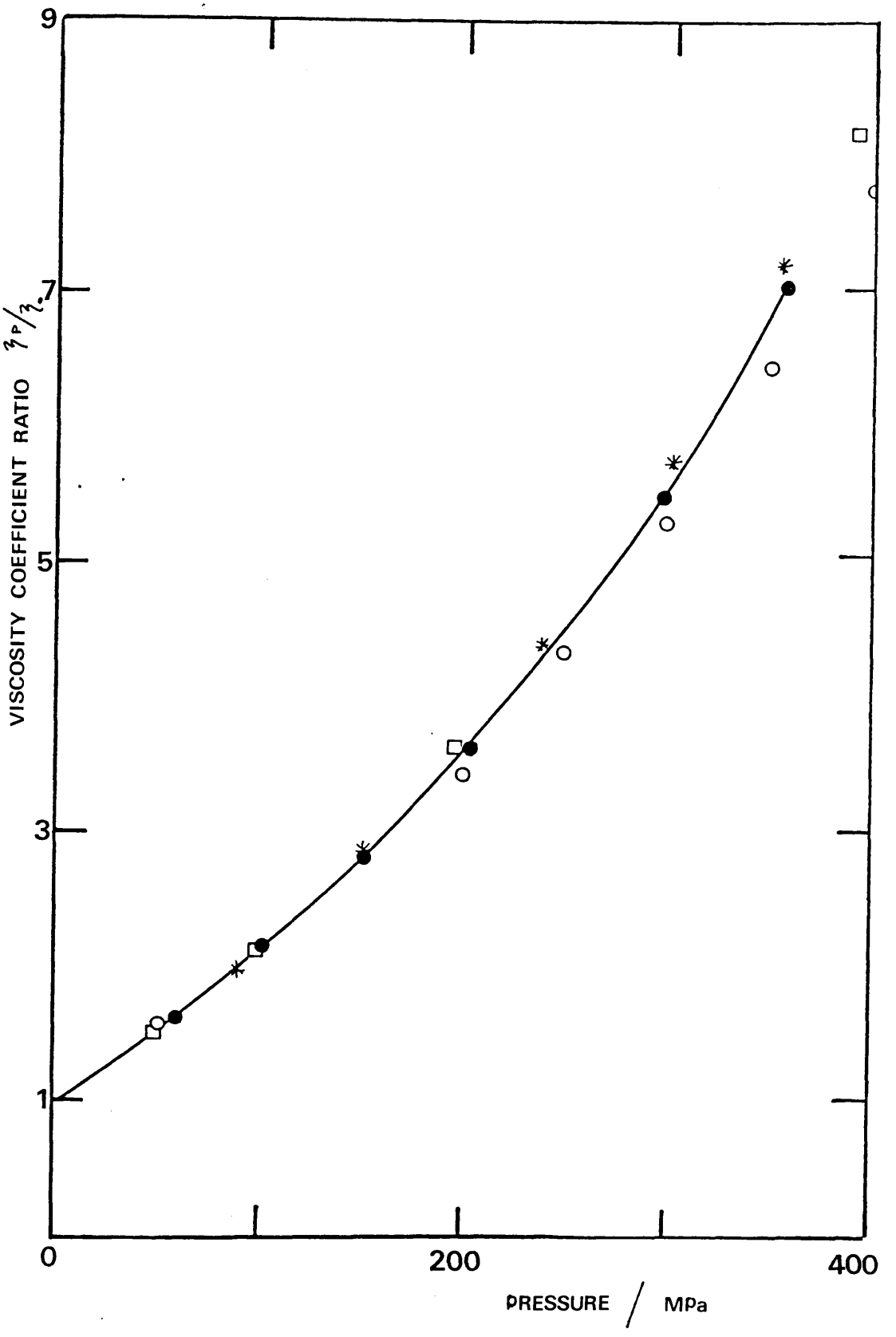

Figure 4.35 Comparison of Dynamic Viscosity Coefficient Ratios for n-Hexane with the Results of Isdale, Dymond and Brawn (23) at 298 K (✳), Brazier and Freeman (134) at 303 K (○) and Bridgman (135) at 298 K (□). ● This work, 298 K.

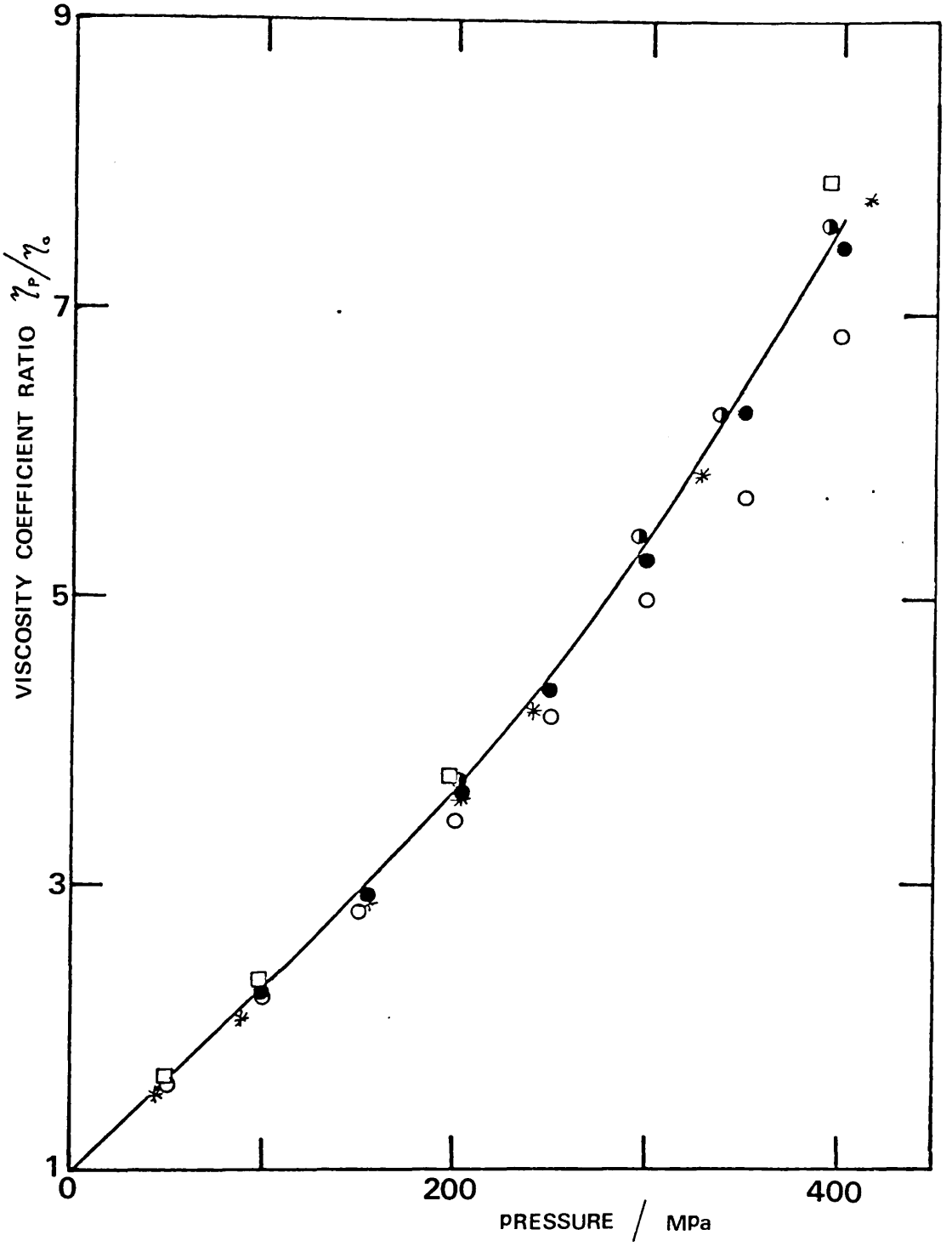

Figure 4.36 Comparison of Dynamic Viscosity Coefficient Ratios for n-Hexane with the Results of Isdale, Dymond and Brawn (23) at 348 K (✳), Brazier and Freeman (134) at 333 K (○) and Bridgman (135) at 348 K (□). ● Viscometer 1, 348 K; ◑ Viscometer 2, 348 K.

Figure 4.35 shows that at 303 K Brazier and Freeman[134] agree closely with Bridgman[135] up to 150 MPa but above this pressure the results become increasingly divergent to a maximum of 8 percent at the highest pressure. The present viscosity ratio results at 298 K fall between these two sources, as do results by Isdale, Dymond and Brawn[23]. Agreement with Isdale, Dymond and Brawn[23] over the full pressure range is within 2.5 percent, well within the combined uncertainty of 4 percent.

Figure 4.36 shows results obtained in viscometers 1 and 2 at 348 K together with results by Isdale, Dymond and Brawn[23] and Bridgman[135] at 348 K and Brazier and Freeman[134] at 333 K. At 350 MPa the results of Brazier and Freeman[134] extrapolated to 348 K disagree with the values given by Bridgman[135] by as much as 22 percent while the present values agree with Isdale, Dymond and Brawn[23] to within 1 percent and with Bridgman[135] to within 7 percent. Results for viscometer 2 agree with those from viscometer 1 to within 3 percent, within the combined uncertainty, and with Bridgman[135] to within 4 percent.

Brazier and Freeman[134] do not give an estimate of the accuracy of their results other than that the repeatability of measurement of fall time is within $\pm$ 0.3 percent. The very large difference between the results of Brazier and Freeman[134] and those of Bridgman[135] and the present measurements suggests the former at 333 K are in error. Bridgman estimates that his time of fall measurements are accurate to within $\pm$ 1.6 percent for n-hexane at 303 K and 0.1 MPa and within $\pm$ 2.5 percent at 348 K and 0.1 MPa with the various corrections to fall time under pressure amounting to 3 to 4 percent and as much as 10 percent in extreme cases. This suggests that the present results at 298 K and 348 K are in agreement with Bridgman[135] if an uncertainty of between

2 and 5 percent is assumed for Bridgman's[135] results. Agreement with Isdale, Dymond and Brawn[23] for the other isotherms (323 K and 373 K) is within 2 percent over the whole pressure range covered in this work.

Viscosity coefficients for n-hexadecane have been measured at 293.2 K, 298.2 K 310.9 K and 372.0 K from 0.1 MPa to the freezing pressure for each isotherm in the A.S.M.E. Pressure Viscosity Report, 1953[132]. At 298.2 K and 0.1 MPa the report gives a value of 2.988 mPa s while this research using the high pressure viscometer gave a value of 3.078 mPa s, a difference of 2.9 percent. Other literature values at 298 K and 0.1 MPa are 3.062 mPa s[54] and 3.086 mPa s[75] which suggests that the A.S.M.E.[132] value is too low by at least 2.5 percent. Since this is outside their estimate of the experimental error the most probable cause is that their calibration is slightly out at this point. However, if the ratios of viscosity coefficients at elevated pressures to viscosity coefficient at atmospheric pressure are calculated and compared with viscosity coefficient ratios obtained from this research, agreement is within 2.3 percent which is within the combined undertainty of 4 percent. At 372.0 K A.S.M.E.[132] results in the range of pressure 286 MPa to 450 MPa extrapolated to 373.2 K agree with the present results to within 6 percent. In this pressure range the A.S.M.E. results for n-hexadecane have a possible uncertainty of 2 to 5 percent. The agreement at 373 K is therefore within the combined experimental uncertainty. No literature values of viscosity coefficients under elevated pressure for mixtures of n-hexane with n-hexadecane were found.

4.6.6 Calculation of Viscosity Coefficients at Other Pressures

To obtain viscosity coefficients at rounded temperatures and pressures the experimental viscosity coefficients were first used to calculate viscosity coefficients at exact rounded pressures along a particular isotherm by use of the equation

$$\eta_i = \exp\left[\ln\eta_j - \ln(\eta_j/\eta_h)(P_j - P_i)/(P_j - P_h)\right] \qquad (4.18)$$

(η_h, P_h) and (η_j, P_j) are experimental points and $P_h < P_i < P_j$. η_i is the calculated viscosity coefficient at the rounded pressure P_i. In effect this equation is interpolating viscosity coefficients from a plot of $\ln\eta$ versus P and since in most cases the rounded pressure and experimental pressure are close together the additional uncertainty in viscosity coefficient is very small. By taking these calculated viscosity coefficients for each liquid along isobars at the experimental temperatures it was then possible to calculate viscosity coefficients at exact rounded temperatures by interpolating from a plot of $\ln\eta$ versus $1/T$ using equation (4.19).

$$\eta_l = \exp\left[\ln\eta_k - \ln(\eta_k/\eta_m)(T_k - T_m)/(T_k - T_l)\right] \qquad (4.19)$$

where $T_k < T_l < T_m$.

In this equation η_k and η_m are now the calculated values from equation (4.18) at the experimental temperatures T_k and T_m. η_l is the calculated viscosity coefficient at the rounded temperature T_l. Again the rounded temperature T_l is very close to the experimental temperature so the additional uncertainty in viscosity coefficients is small. It is estimated that the total uncertainty of the viscosity coefficients calculated in this way is $\pm$ 3.5 percent. Table 4.13 lists calculated viscosity coefficients for the n-hexane plus n-hexadecane system

Table 4.13

Viscosity Coefficients (in mPa s) for the n-Hexane plus n-Hexadecane System at 50 MPa Intervals

Pressure (MPa)	Mole fraction of n-hexadecane					
	0	0.200	0.400	0.600	0.800	1
Temperature : 298.15 K						
0.1	0.2980	0.5847	0.9909	1.518	2.233	3.073
50.0	0.4520	0.9381	1.634	2.684		
100.0	0.6262	1.365				
150.0	0.8155					
200.0	1.060					
250.0	1.324					
300.0	1.648					
350.0	2.032					
Temperature : 323.15 K						
0.1	0.2357	0.4428	0.7048	1.028	1.410	1.843
50.0	0.3702	0.7087	1.147	1.716	2.412	3.296
100.0	0.5061	1.011	1.714	2.638	3.840	5.323
150.0	0.6617	1.372	2.424	3.826	5.758	
200.0	0.8359	1.812				
250.0	1.036					
300.0	1.270					
350.0	1.529					
400.0	1.817					
Temperature : 348.15 K						
0.1	0.1915	0.3498	0.5226	0.7555	0.9876	1.241
50.0	0.3093	0.5584	0.8574	1.270	1.643	2.151
100.0	0.4228	0.7975	1.272	1.856	2.558	3.342
150.0	0.5477	1.064	1.740	2.571	3.701	4.907
200.0	0.6842	1.382	2.354	3.515	5.119	6.955
250.0	0.8384	1.744	3.043	4.680	6.859	9.580
300.0	1.012	2.172	3.870		9.311	
350.0	1.208	2.665				
400.0	1.419	3.282				
Temperature : 373.15 K						
0.1	0.1603	0.2802	0.4150	0.5686	0.7289	0.8964
50.0	0.2616	0.4616	0.6875	0.9607	1.226	1.535
100.0	0.3629	0.6522	0.9914	1.394	1.834	2.336
150.0	0.4676	0.8656	1.336	1.923	2.564	3.280
200.0	0.5805	1.101	1.762	2.565	3.471	4.582
250.0	0.7058	1.370	2.236	3.326	4.602	6.066
300.0	0.8434	1.693	2.813	4.304	6.093	8.002
350.0	0.9967	2.049	3.482	5.406	7.797	10.450
400.0	1.157	2.460	4.282	6.791	9.813	13.406
450.0		2.919	5.192			
500.0		3.475	6.281			

in steps of 50 MPa at 298.15 K, 323.15 K, 348.15 K and 373.15 K.

4.6.7 Calculations

A Fortran program incorporating equations (4.6), (4.8), (4.9), (4.16), (4.17), (4.18) and (4.19) was written to perform the calculation of density and secant bulk modulus from the raw experimental pressure and micrometer readings. The program tabulated values of density and secant bulk modulus and evaluated and tabulated the parameters in Equation (4.17) for secant bulk modulus.

Viscosity coefficients at the experimental temperatures and pressures and at rounded pressures were calculated from the raw experimental pressure and fall time readings using the densities calculated in the first part of the program.

Viscosity coefficients and densities so calculated were stored on magnetic tape to facilitate other calculations referred to in Chapter 6.

C H A P T E R 5

MOLAR EXCESS VOLUMES FROM DENSITY MEASUREMENTS

5.1 INTRODUCTION

This chapter describes the effects of temperature and pressure on the molar excess volume V_m^E, calculated from the measured densities of the binary hydrocarbon mixtures studied.

When two miscible liquids are combined to form a binary mixture the final volume is not usually the sum of the volumes of the pure components. The measurement of the resulting volume change, the molar excess volume, V_m^E, has been the object of much research in the past[136]. There are currently two general methods employed in the determination of V_m^E for binary mixtures. The first of these is an indirect method involving the measurement of the density of the pure components and a series of mixtures at the same temperature. Density has normally been measured by pyknometry[137] but more recently measurements have been made using vibrating tube densimeters[138,139]. Molar excess volume of the mixture, V_m^E, is calculated from the measured densities using the equation

$$V_m^E = \frac{x_1M_1 + x_2M_2}{\rho_m} - \left[\frac{x_1M_1}{\rho_1} + \frac{x_2M_2}{\rho_2}\right] \qquad (5.1)$$

where x is mole fraction, M is molecular weight and ρ is density.

The second general method determines the change in volume directly using a dilatometric technique[140] and is inherently capable of higher precision and accuracy. However, the density results obtained in this research are sufficiently accurate to illustrate the effects of temperature and pressure on V_m^E.

5.2 MOLAR EXCESS VOLUME FOR BINARY HYDROCARBON MIXTURES AT SATURATION PRESSURE

From the densities given in Chapter 3, values of V_m^E at saturation pressure can be calculated using equation (5.1). Although the main reason for measuring densities was to enable dynamic viscosity coefficients to be calculated, the densities are sufficiently accurate to show the variation of V_m^E with temperature. This exercise is worthwhile as very few studies of this kind have been made. Such studies that have been made are usually limited to a narrow range of temperature. For example recent measurements by Harrison and Winnick[141] on n-alkane mixtures cover the range of temperature 298 K to 318 K. Experimental values of V_m^E in the range of temperature 283 K to 393 K for the binary systems studied in this research are given in Table 5.1. This table shows that for the n-hexane plus n-hexadecane system the molar excess volumes are negative at 298.19 K and become increasingly negative as temperature is increased. For the benzene plus n-alkane systems studied, and for benzene plus cyclohexane, V_m^E is positive at temperatures from 283.15 K to 393.2 K. The effect of change in temperature on V_m^E is very much smaller for these systems but there is a definite trend towards larger positive values at higher temperatures, except for the benzene plus n-hexane system. For this system V_m^E is significantly lower than for the corresponding benzene plus cyclohexane system. Figure 5.1 shows the results plotted as V_m^E versus mole fraction of benzene for the benzene plus n-octane, benzene plus n-decane, benzene plus n-dodecane and benzene plus n-hexadecane systems at 298.19 K. In general there is an increase in V_m^E as the n-alkane chain length increases with a shift in the maximum towards mixtures more concentrated in benzene. This shift in the maximum is also apparent from the results of Diaz Pena and Nunez Delgado[87]

Table 5.1

Molar Excess Volume for Binary Hydrocarbon Mixtures at Saturation Pressure

System	Temperature (K)	x_1	V_m^E ($cm^3\ mol^{-1}$)	x_1	V_m^E ($cm^3\ mol^{-1}$)	x_1	V_m^E ($cm^3\ mol^{-1}$)	x_1	V_m^E ($cm^3\ mol^{-1}$)	x_1	V_m^E ($cm^3\ mol^{-1}$)
n-hexane plus n-hexadecane	298.19	0.1987	-0.28	0.3772	-0.46	0.5983	-0.64	0.7982	-0.59		
	318.25	0.1976	-0.33	0.3758	-0.55	0.5971	-0.81	0.7975	-0.76		
	338.36	0.1958	-0.41	0.3734	-0.69	0.5949	-1.04	0.7963	-0.99		
	358.28	0.1929	-0.48	0.3695	-0.87	0.5916	-1.34	0.7944	-1.34		
	378.28	0.1885	-0.48	0.3637	-1.06	0.5864	-1.78	0.7915	-1.84		
benzene plus n-hexane	283.15	0.4995	0.38								
	288.15	0.4995	0.37								
	298.19	0.4997	0.36								
	313.23	0.5002	0.30								
	333.36	0.5007	0.26								
	353.28	0.5013	0.21								
	373.28	0.5022	0.10								
benzene plus n-octane	283.15	0.2539	0.57	0.5041	0.83	0.6746	0.79	0.8255	0.52		
	288.15	0.2539	0.57	0.5041	0.84	0.6746	0.80	0.8255	0.51		
	298.19	0.2536	0.58	0.5037	0.85	0.6743	0.81	0.8253	0.52		
	313.23	0.2533	0.61	0.5034	0.87	0.6741	0.82	0.8252	0.52		
	333.36	0.2527	0.61	0.5027	0.90	0.6735	0.83	0.8249	0.51		
	353.28	0.2518	0.64	0.5016	0.87	0.6726	0.89	0.8243	0.53		
	373.28	0.2503	0.64	0.4999	0.83	0.6713	0.94	0.8236	0.58		
	393.2	0.2482	0.69	0.4975	0.77	0.6694	1.05	0.8244	0.65		
benzene plus n-decane	283.15	0.4991	0.79								
	288.15	0.4991	0.80								
	298.19	0.4986	0.82								
	313.23	0.4982	0.81								
	333.36	0.4972	0.91								
	353.28	0.4956	0.95								
	373.28	0.4931	0.99								
	393.2	0.4895	1.09								
benzene plus n-dodecane	283.15	0.2509	0.59	0.4994	0.92	0.7498	0.93				
	288.15	0.2509	0.68	0.4994	0.93	0.7498	0.93				
	298.19	0.2504	0.56	0.4988	0.92	0.7495	0.94				
	313.23	0.2500	0.58	0.4984	0.97	0.7492	0.94				
	333.36	0.2490	0.63	0.4973	0.98	0.7485	0.97				
	353.28	0.2473	0.63	0.4954	1.03	0.7474	1.00				
	373.28	0.2446	0.70	0.4925	1.04	0.7457	1.03				
	393.2	0.2408	0.84	0.4882	1.11	0.7431	1.10				
benzene plus n-hexadecane	298.19	0.1211	0.30	0.2858	0.61	0.5976	0.98	0.8497	0.87		
	313.23	0.1207	0.30	0.2852	0.59	0.5971	0.96	0.8495	0.85		
	333.36	0.1199	0.30	0.2839	0.63	0.5960	0.97	0.8491	0.85		
	353.28	0.1186	0.30	0.2817	0.71	0.5940	1.02	0.8493	0.87		
	373.28	0.1165	0.30	0.2782	0.70	0.5910	1.15	0.8472	0.90		
	393.2	0.1134	0.30	0.2730	0.67	0.5864	1.31	0.8454	0.98		
benzene plus cyclohexane	283.15	0.1991	0.46	0.4020	0.61	0.6004	0.59	0.7949	0.43	0.8779	0.29
	288.15	0.1991	0.45	0.4020	0.61	0.6004	0.58	0.7949	0.43	0.8779	0.28
	298.19	0.1989	0.46	0.4017	0.61	0.6001	0.60	0.7947	0.43	0.8778	0.29
	313.23	0.1987	0.47	0.4014	0.62	0.5998	0.60	0.7945	0.43	0.8777	0.29
	333.36	0.1982	0.48	0.4007	0.64	0.5991	0.60	0.7941	0.43	0.8774	0.29
	353.28	0.1975	0.51	0.3995	0.69	0.5980	0.65	0.7934	0.48	0.8769	0.26
	373.28	0.1969	0.59	0.3977	0.74	0.5963	0.68	0.7922	0.54	0.8762	0.26
	393.2	0.1944	0.54	0.3950	0.82	0.5936	0.68	0.7905	0.64	0.8750	0.25

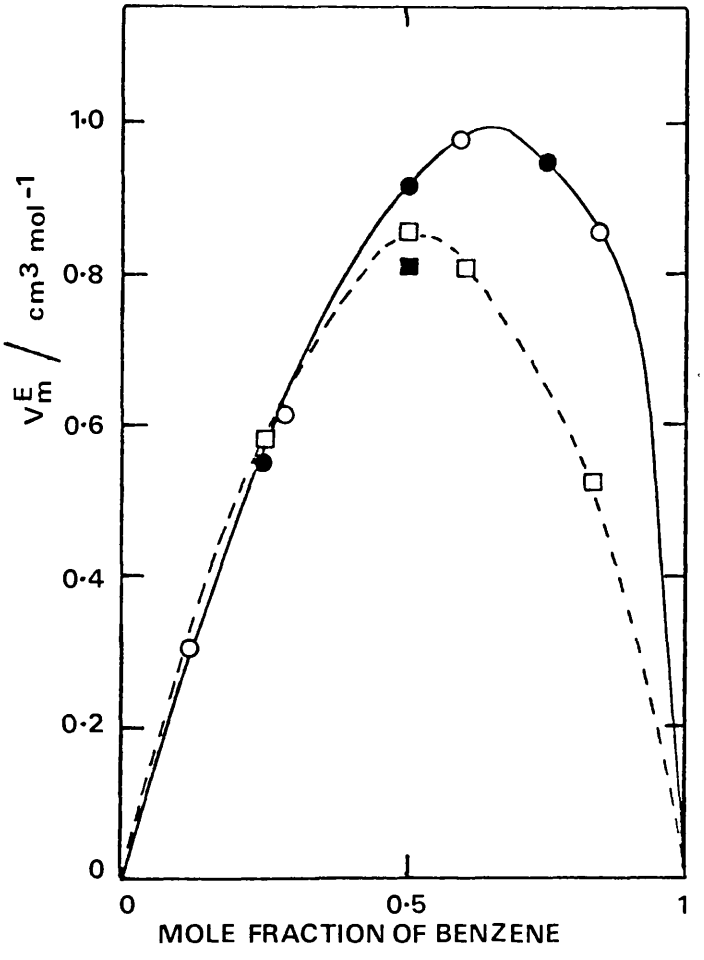

Figure 5.1 *Molar Excess Volumes for Benzene plus n-Alkane Systems at 298.19 K and Saturation Presure.* - - - - - - □ *plus n-Octane,* ■ *plus n-Decane,* ● *plus n-Dodecane,* ——○ *plus n-Hexadecane.*

on the benzene plus n-alkane systems at 323.15 K.

A comparison of the V_m^E values obtained in this research with recent literature values is given in Table 5.2. Apart from the n-hexane plus n-hexadecane system[54] these literature values have been obtained by the more accurate dilatometric technique[87,88]. The literature values were corrected to the same composition as the experimental values using the smoothing equations which appear in these references and the experimental uncertainties quoted have been calculated assuming an uncertainty in density of 0.1 kg m^{-3} at 298.19 K and 0.3 kg m^{-3} at 323.15 K. The table shows that agreement with the literature values is well within the experimental uncertainty.

Table 5.2

Comparison of V_m^E with Literature Values

System	Temperature (K)	x_1	V_m^E (cm^3 mol^{-1})	
			Literature	This work
n-hexane plus n-hexadecane	298.19	0.1987	-0.27 ± 0.02[a]	-0.28 ± 0.09
		0.3772	-0.48 ± 0.02	-0.46 ± 0.09
		0.5983	-0.60 ± 0.02	-0.64 ± 0.09
		0.7982	-0.49 ± 0.02	-0.59 ± 0.09
benzene plus n-hexane	323.15	0.5004	0.362[b]	0.28 ± 0.15
benzene plus n-octane	323.15	0.2530	0.474[b]	0.58 ± 0.17
		0.5030	0.696	0.89 ± 0.17
		0.6738	0.649	0.82 ± 0.17
		0.8250	0.475	0.52 ± 0.17
benzene plus n-decane	323.15	0.4977	0.810[b]	0.81 ± 0.18
benzene plus n-dodecane	323.15	0.2495	0.571[b]	0.60 ± 0.18
		0.4978	0.889	0.97 ± 0.18
		0.7489	0.843	0.96 ± 0.18
benzene plus n-hexadecane	323.15	0.1203	0.321[b]	0.32 ± 0.21
		0.2845	0.657	0.61 ± 0.21
		0.5965	0.989	0.96 ± 0.21
		0.8493	0.721	0.85 ± 0.21
benzene plus cyclohexane	298.19	0.1989	0.422[c]	0.46 ± 0.06
		0.4017	0.623	0.61 ± 0.06
		0.6001	0.614	0.60 ± 0.06
		0.7947	0.416	0.43 ± 0.06
		0.8777	0.274	0.29 ± 0.06

[a] Reference (54); [b] Reference (87); [c] Reference (88).

5.3 MOLAR EXCESS VOLUME FOR THE n-HEXANE PLUS n-HEXADECANE SYSTEM AT ELEVATED PRESSURES

Values of V_m^E have been calculated from the measured densities at elevated pressure reported in Chapter 4 for the n-hexane plus n-hexadecane system[142] and results are shown in Figure 5.2 for different pressures at a constant temperature of 373.15 K. At this temperature high pressures are attained before freezing occurs.

Although the results have an uncertainty which is significantly greater than that associated with direct measurements of excess volumes at elevated pressures[143] they indicate clearly that an increase in pressure at constant temperature causes V_m^E to become less negative and even positive. Snyder, Benson, Huang and Winnick[144] have observed that the V_m^E values for the n-decane plus n-tetradecane and n-dodecane plus n-hexadecane systems also become less negative and then positive as pressure is increased at constant temperature. These results can be contrasted with recent results by Jeschke and Schneider[143] for the toluene plus methyl cyclohexane system where V_m^E was positive and decreased as the pressure increased at constant temperature.

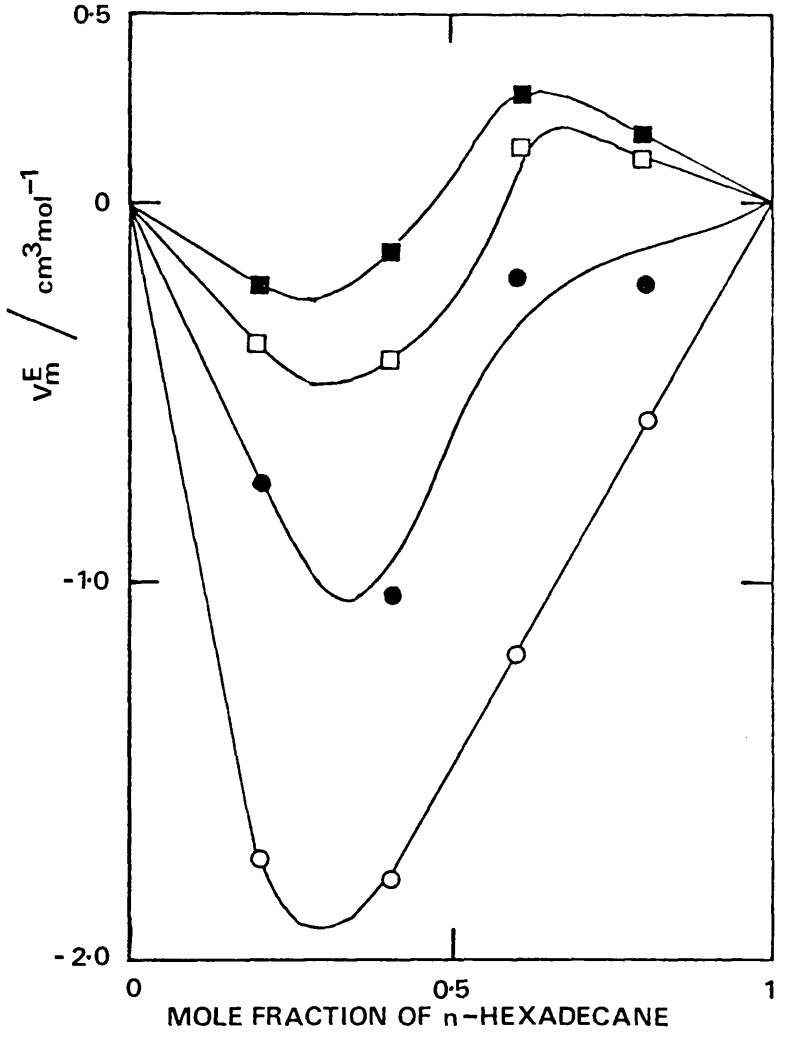

Figure 5.2 Molar Excess Volumes for the n-Hexane plus n-Hexadecane System at 373.15 K up to 400 MPa. ○ 0.1 MPa, ● 50 MPa, □ 200 MPa, ■ 400 MPa.

C H A P T E R 6

DISCUSSION OF MIXTURE VISCOSITY COEFFICIENT DATA

6.1 INTRODUCTION

The experimental viscosity coefficient data for hydrocarbon mixtures reported in Chapters 3 and 4 cover a wide range of temperature and pressure and provide a critical test for existing theoretical and empirical expressions. In Section 6.2 the results are considered in terms of the smooth hard sphere and rough hard sphere theories, and in Section 6.3 they are discussed on the basis of the Hildebrand equation. In the following section the effect of changes in temperature and pressure on $\Delta^* G^E$, the molar excess free energy of activation for flow in the Eyring theory, derived from the experimental data, is investigated. Values of $\Delta^* G^E$ are used to test the validity of the Principle of Congruence as applied to n-alkane mixtures at temperatures above 298 K. Finally the effectiveness of the Grunberg and Nissan equation for representing mixture viscosity coefficients is discussed.

6.2 HARD SPHERE THEORIES

The rough hard sphere model has recently been applied[145] to tracer diffusion studies in systems with n-hexane as one of the components. It is therefore of great interest to see how closely the present viscosity coefficient measurements for n-hexane at elevated pressure follow the rough hard sphere predictions. Dymond[146] has shown that the fluidity, $\frac{1}{\eta}$, of a smooth hard sphere system at temperature T can be represented by

$$\frac{1}{\eta} = 1.324 \times 10^{8}(V - 1.384\ V_o)/V_o^{1/3}(MRT)^{1/2} \qquad (6.1)$$

where V is the molar volume, V_o is the volume relative to the volume of close packing and M is the molecular weight. By combining this equation with the expression given by Chandler[12] for a rough hard sphere system

$$\eta_{RHS} \simeq C\eta_{SHS} \qquad (6.2)$$

the relationship between viscosity coefficient, molar volume and temperature becomes

$$\frac{1}{\eta_{RHS}} \simeq 1.324 \times 10^{8}(V - 1.384\ V_o)/CV_o^{1/3}(MRT)^{1/2} \qquad (6.3)$$

A plot of fluidity versus molar volume at constant temperature should therefore be linear if a system of real polyatomic molecules follows the rough hard sphere behaviour with respect to viscosity coefficients and if the translational-rotational coupling constant, C, is practically temperature and density independent. Experimental data for n-hexane at 298 K reported in Chapter 4 are plotted in this way in Figure 6.1. The plot is almost linear for pressures up to about 90 MPa though there is evidence even here of slight curvature. From this graph, a value for V_o of 78.9 $cm^3\ mol^{-1}$ is obtained. Since this theory is based on

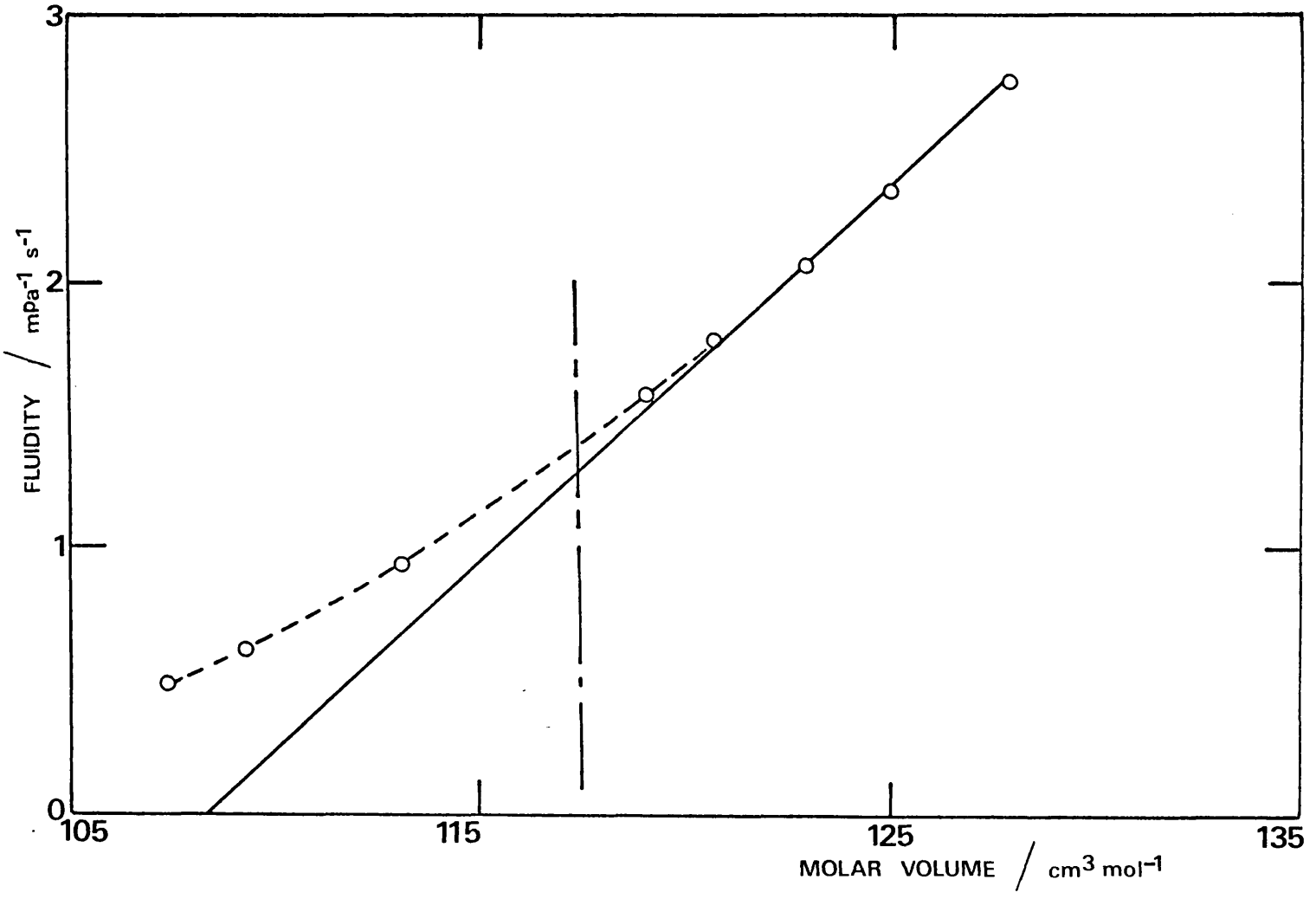

Figure 6.1 Molar Volume Dependence of the Fluidity of n-Hexane at 298.29K. The Vertical Line Denotes the Limiting Volume for which the Hard Sphere System Remains Fluid.

the smooth hard sphere theory it cannot be applied at V_o/V greater than 0.66, indicated by the broken line in Figure 6.1. This corresponds to a pressure of 120 MPa, but n-hexane remains liquid to pressures of at least 1000 MPa[122]. This approach is therefore only valid for the interpretation of viscosity coefficient data for liquids over a very restricted density range. It has severe limitations for the prediction of viscosity coefficients because values of the translational-rotational coupling constant can only be obtained from the viscosity coefficient data. For n-hexane, C has the value 1.48.

As a method of correlating viscosity coefficient data for pure liquids composed of polyatomic molecules, based on the rough hard sphere model Dymond and Brawn[30] have shown that curves of η' or of log η', where η' is defined as $\eta V^{2/3}/(MT)^{1/2}$, versus log V for each temperature should be superimposable by adjustment along the log V axis. From the values of log V at a point where two curves superimpose, the ratio $V_o(T_R)/V_o(T)$ corresponding to the ratio of molar volumes of close packing at the reference temperature T_R, and at temperature T can be determined. This approach was very satisfactory for the correlation of data for pseudo-spherical molecules and for rigid bicyclic hydrocarbons, indicating that it can be usefully applied to aspherical molecules also where the molecular shape is not expected to vary much with change of temperature and pressure[30].

This approach was extended to the n-hexane plus n-hexadecane system where the molecules are more flexible and where molecular shape would be expected to vary with changes in temperature and pressure. However, it was found that in the temperature and pressure range studied, which in some mixtures produced a fifteenfold increase in viscosity

coefficient on going from atmospheric pressure to the highest pressure, this provided a very satisfactory method for correlating the experimental data not only over the density range for which the hard sphere theory might be expected to apply, but over the whole density range. The results for n-hexane, n-hexadecane and for each of the mixtures are shown in Figures 6.2 to 6.7. η' is plotted versus log V' where $V' = V.V_o(T_R)/V_o(T)$, and T_R is the reference temperature. The 373 K isotherm was chosen as a reference isotherm for each liquid and liquid mixture, and even for mixtures the deviation from the curve of η' versus log V' at this temperature when the other isotherms were superimposed was in all cases less than 5 percent and usually considerably less than this. It is interesting to note that an uncertainty of 0.25 $cm^3\ mol^{-1}$ in the V_o values leads to a deviation of 5 percent from the reference curve.

Values derived for $V_o(T)/V_o(T_R)$ for the pure liquids and mixtures at the different temperatures are given in Table 6.1. This table shows that, as temperature is increased values for V_o, the volume of close packing, decrease. The relative change in V_o is greater for n-hexadecane and n-hexadecane rich mixtures than for n-hexane.

These results demonstrate that there is a definite relationship between the viscosity coefficient of a dense fluid and the molar volume, specifically the molar volume relative to the close packed volume. Values of $V_o(T)/V_o(T_R)$ for these mixtures at other temperatures can be interpolated from a graph of $V_o(T)/V_o(T_R)$ versus T and viscosity coefficients predicted for specific densities at these temperatures.

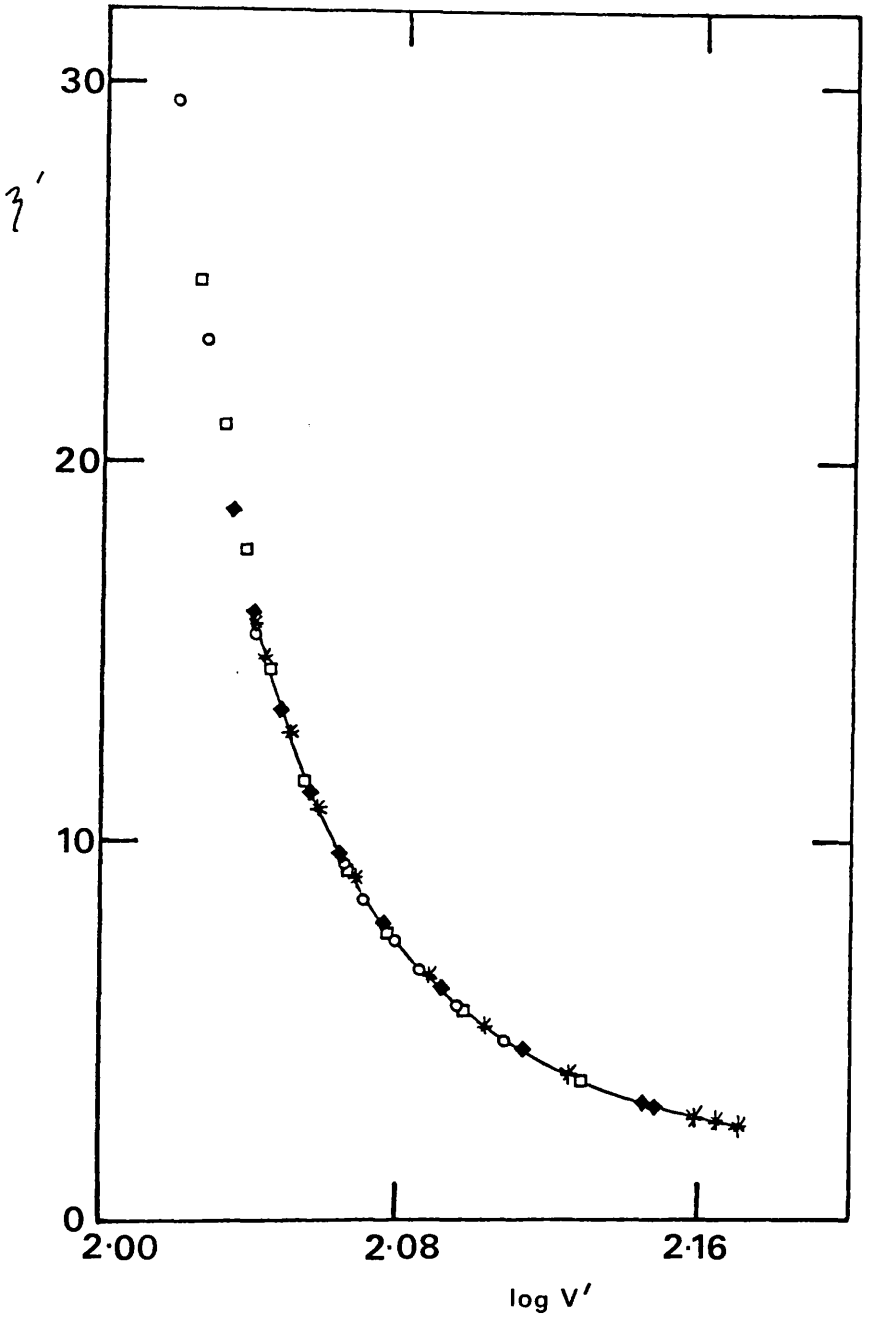

Figure 6.2 Correlation of Experimental Viscosity Coefficient Data for n-Hexane at Different Temperatures and Pressures.

○ 298.29 K, □ 323.15 K, ◆ 348.38 K, ✳ 373.36 K.

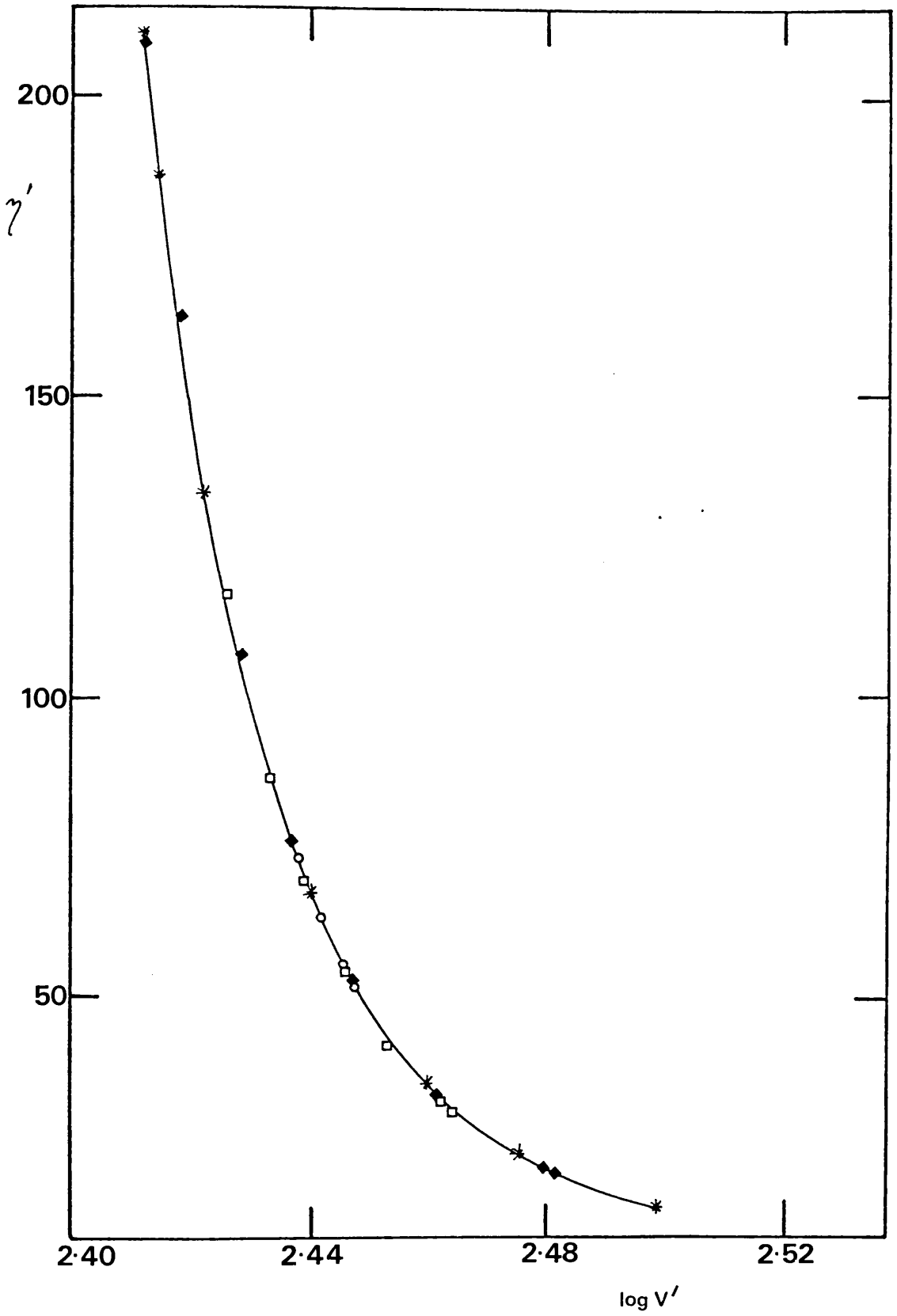

Figure 6.3 Correlation of Experimental Viscosity Coefficient Data for n-Hexadecane at Different Temperatures and Pressures.

○ 298.08 K, □ 323.09 K, ◆ 348.11 K, ✳ 373.24 K.

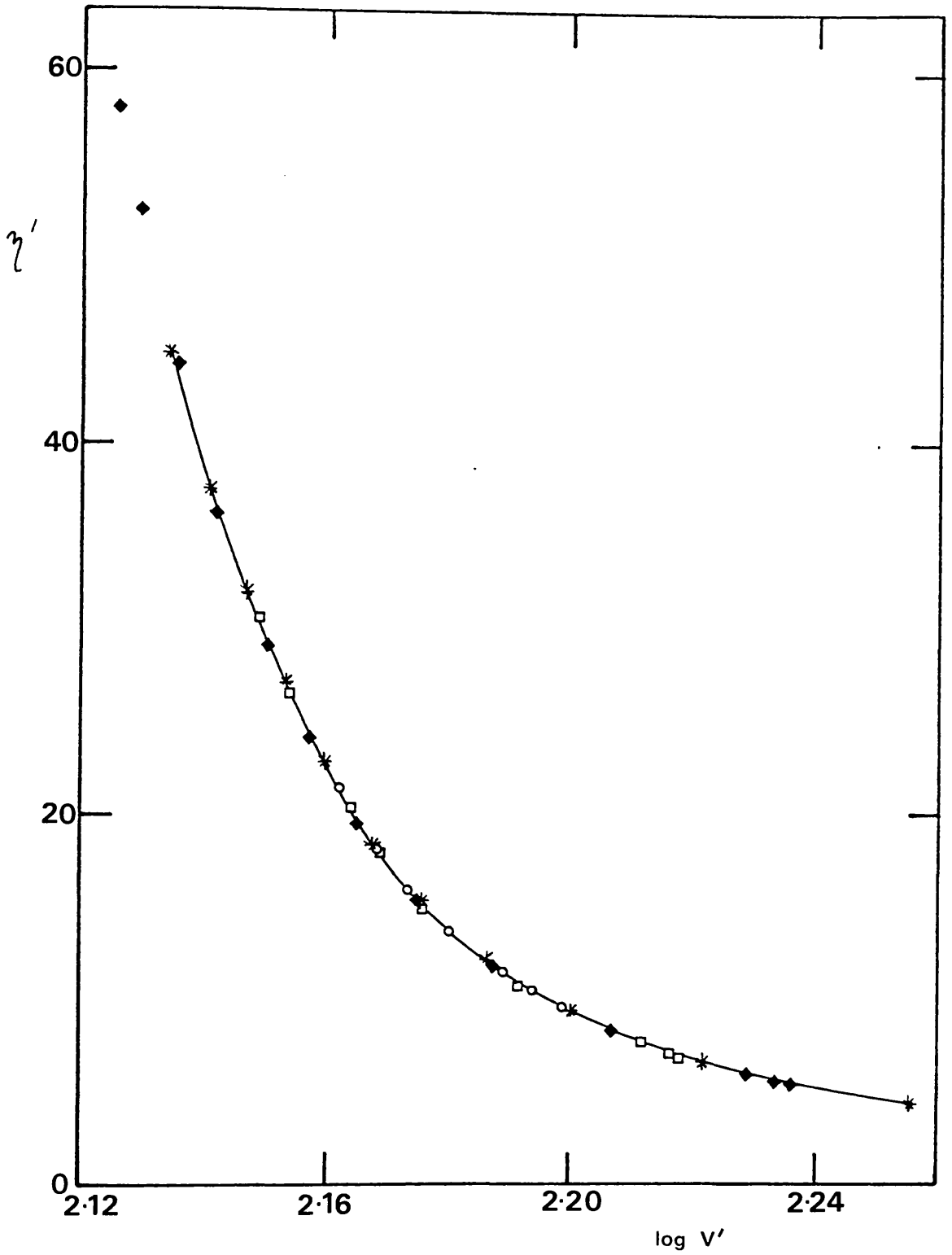

Figure 6.4 Correlation of Experimental Viscosity Coefficient Data for the Mixture with a Mole Fraction of n-Hexadecane of 0.200 at Different Temperatures and Pressures.

○ 298.22 K, □ 323.19 K, ◆ 348.07 K, ✳ 373.12 K.

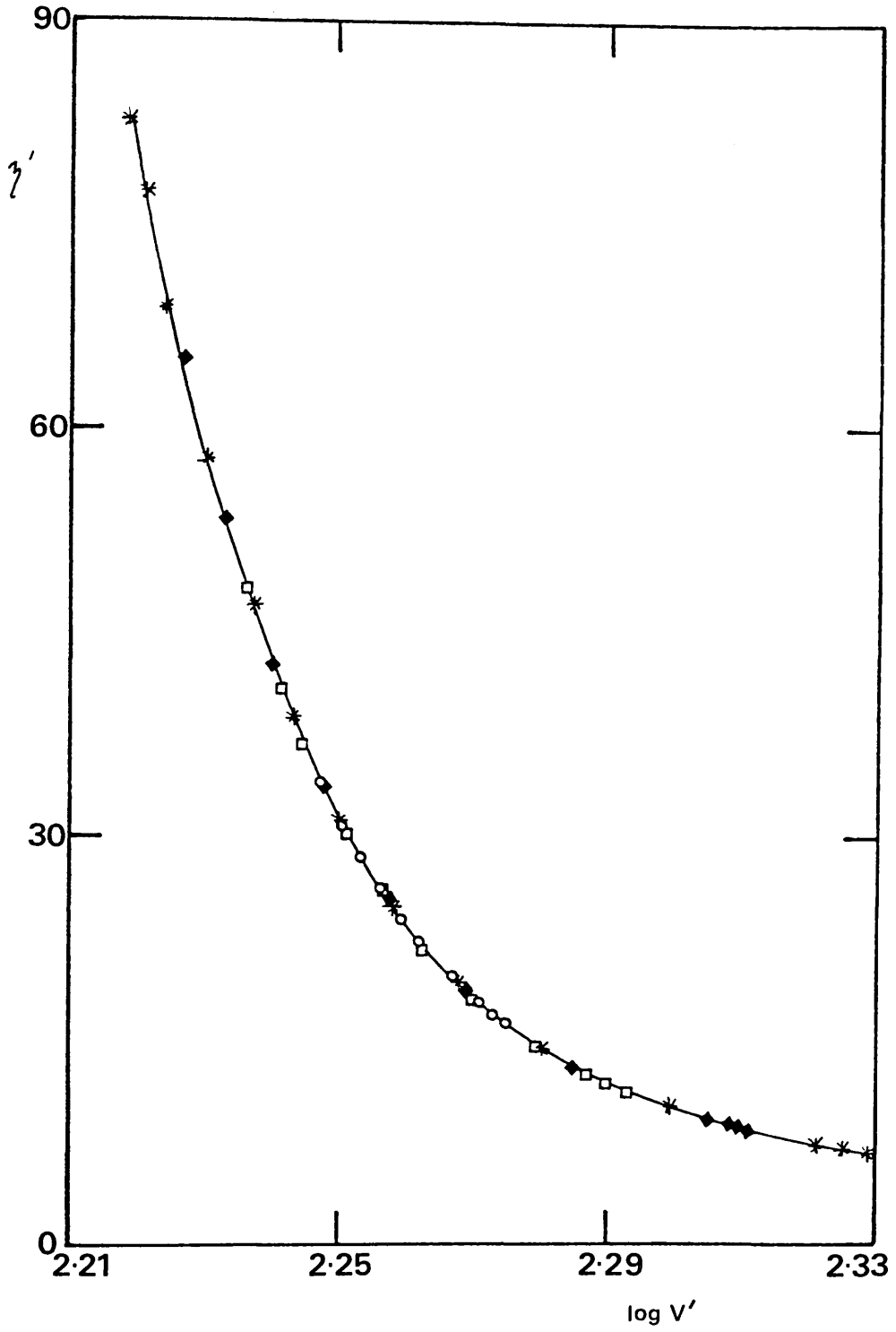

Figure 6.5 Correlation of Experimental Viscosity Coefficient Data for the Mixture with a Mole Fraction of n-Hexadecane of 0.400 at Different Temperatures and Pressures.

○ 298.12 K, □ 323.33 K, ◆ 348.29 K, ✳ 373.24 K.

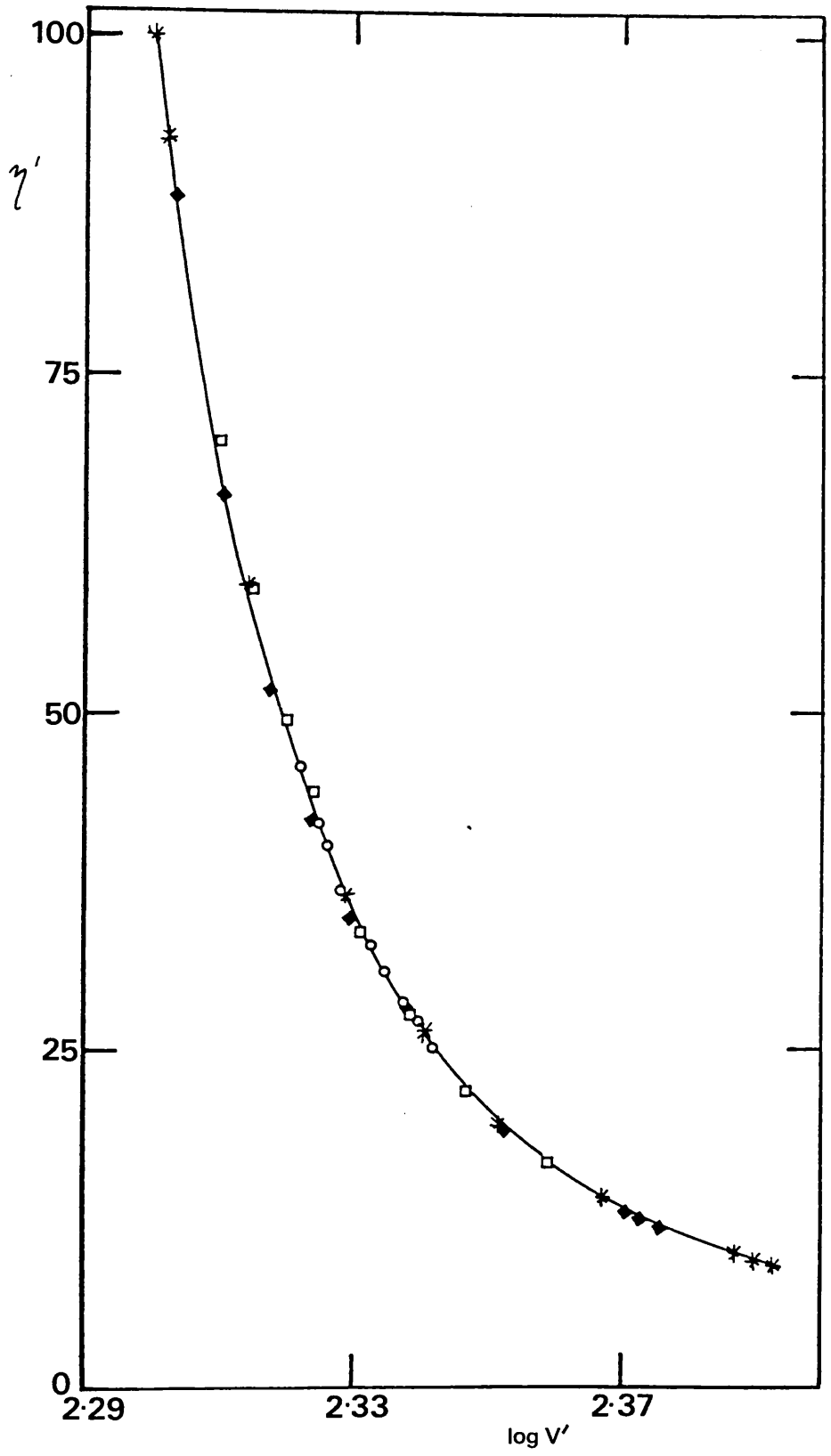

Figure 6.6 Correlation of Experimental Viscosity Coefficient Data for the Mixture with a Mole Fraction of n-Hexadecane of 0.600 at Different Temperatures and Pressures.

○ 298.15 K, □ 323.13 K, ◆ 348.31 K, ✳ 373.18 K.

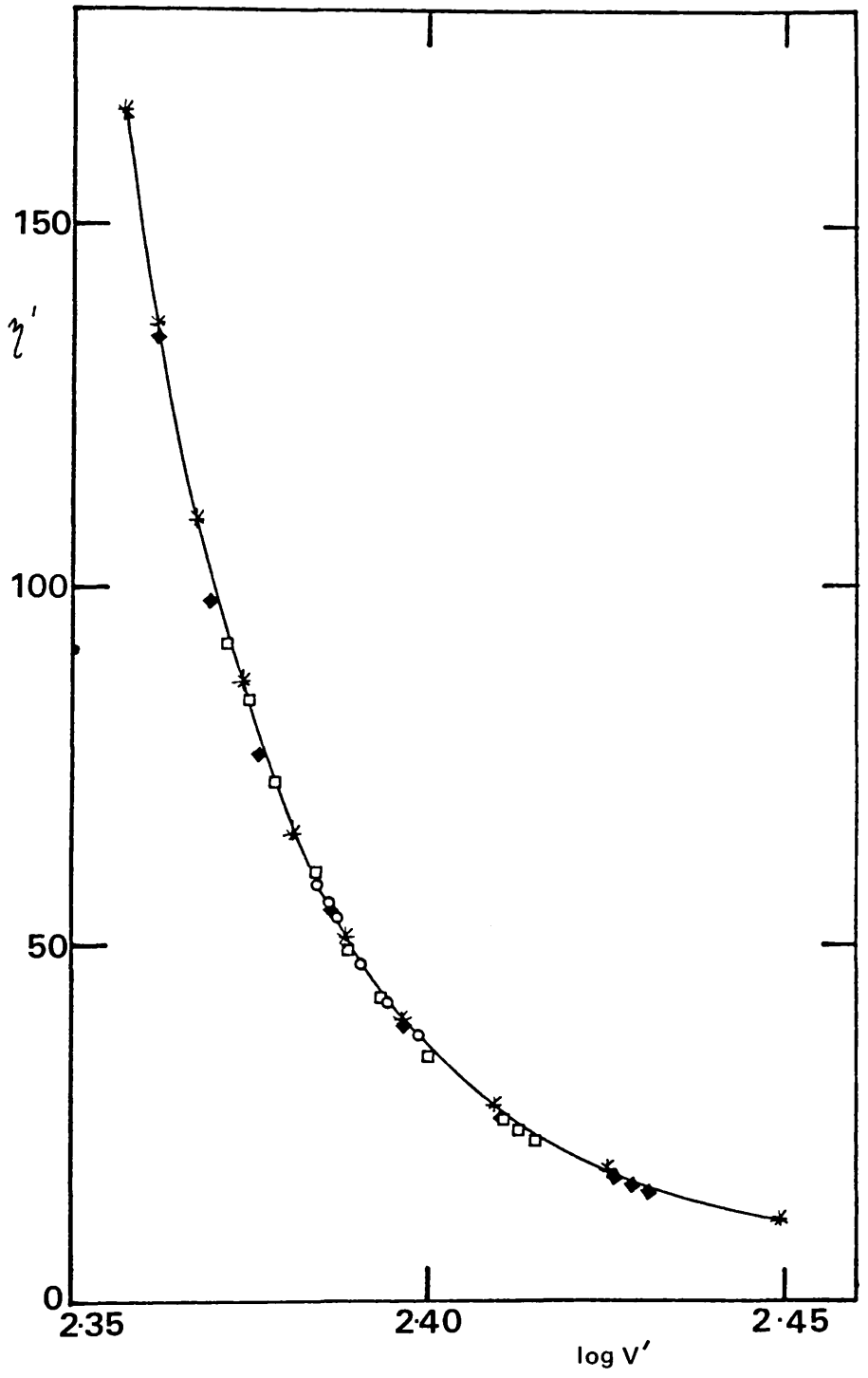

Figure 6.7 Correlation of Experimental Viscosity Coefficient Data for the Mixture with a Mole Fraction of n-Hexadecane of 0.800 at Different Temperatures and Pressures.

○ 298.09 K, □ 323.21 K, ◆ 348.09 K, ✳ 373.17 K.

Table 6.1

Values of $V_o(T)/V_o(T_R)$ for the n-Hexane plus n-Hexadecane System at Elevated Pressure

x_{HD}*					
0	T(K)	298.3	323.2	348.4	373.4
	$V_o(T)/V_o(T_R)$	1.027	1.016	1.009	1.000
0.200	T(K)	298.2	323.2	348.1	373.1
	$V_o(T)/V_o(T_R)$	1.034	1.021	1.011	1.000
0.400	T(K)	298.1	323.3	348.3	373.2
	$V_o(T)/V_o(T_R)$	1.039	1.026	1.012	1.000
0.600	T(K)	298.2	323.1	348.3	373.2
	$V_o(T)/V_o(T_R)$	1.040	1.025	1.012	1.000
0.800	T(K)	298.1	323.2	348.1	373.2
	$V_o(T)/V_o(T_R)$	1.044	1.029	1.016	1.000
1	T(K)	298.1	323.1	348.1	373.2
	$V_o(T)/V_o(T_R)$	1.048	1.033	1.015	1.000

* HD = n-hexadecane

Now for pseudospherical molecules and relatively rigid ring hydrocarbons Dymond and Brawn[30] have shown as has been discussed in Chapter 2, that viscosity coefficient data can be fitted within the estimated experimental uncertainty by the equation

$$\ln\eta' = A + BV_o/(V - V_o) \qquad (6.4)$$

where η' is defined as $\eta V^{2/3}/(MT)^{1/2}$. c.g.s. units were used and η was in units of 10^{-4} g cm^{-1} s^{-1}. V_o represents the close packed volume on the basis of the hard sphere model and A and B are adjustable parameters to take account of the effects of non spherical molecular shape and of translational-rotational coupling. For the liquids studied by Dymond and Brawn[30] A was found to be temperature independent and equal to -1.0. B was also found to be temperature independent. In a more general form

$$\ln \left[\frac{\eta V^{2/3}}{(MRT)^{1/2}}\right] = A + BV_o/(V - V_o) \qquad (6.5)$$

where A now has the value -19.328. The effectiveness of this equation in correlating the viscosity coefficient data for the n-hexane plus n-hexadecane system at elevated pressure was investigated for each of 24 isotherms.

By comparing viscosity coefficients calculated with different values of A, B and V_o with the experimental viscosity coefficients, values of A, B and V_o were obtained for each isotherm which fitted the data to within the estimated experimental uncertainty. It was found that an excellent fit to the experimental data was obtained when A was equal to -19.328. With this value of A it was found that the V_o values deviated to only a very small extent from a linear relationship with mole fraction over the whole mole fraction range. V_o was therefore set equal to $x_1V_{o1} + x_2V_{o2}$, with values of V_o for the pure components given in Table 6.2. Values of B were determined which gave the optimum fit to the experimental viscosity coefficient data and these values are also given in Table 6.2, and B and V_o are plotted versus mole fraction of n-hexadecane in Figures 6.8 and 6.9. Using these values, viscosity coefficients are fitted to within 3 percent for 216 out of the 230 experimental points with the remaining 14 points fitted to within 6 percent.

It is considered that agreement to within 3 percent is very satisfactory in view of the experimental uncertainties in the viscosity coefficents plus the possible uncertainties in the density data. A change in the molar volume of 0.2 $cm^3\ mol^{-1}$ where the molar volume is 254 $cm^3\ mol^{-1}$, B is 2.41 and V_o is 169 $cm^3\ mol^{-1}$ produces a variation in the

Table 6.2

Values of B and V_o in Equation (6.5) and B in Equations (6.6) and (6.7) for the n-Hexane plus n-Hexadecane System at Elevated Pressure

x^*_{HD}	Temperature (K)	V_o ($cm^3\ mol^{-1}$)	B (equation 6.5)	B (equation 6.6)	B (equation 6.7)
0	298.29	73.0	2.064	2.064	2.070
	323.15	72.0	2.084	2.084	2.087
	348.38	71.0	2.115	2.115	2.112
	373.36	70.0	2.144	2.144	2.145
0.200	298.22	98.2	2.153	2.150	2.142
	323.19	96.2	2.197	2.197	2.193
	348.07	94.2	2.239	2.254	2.240
	373.12	92.2	2.321	2.313	2.316
0.400	298.12	123.4	2.207	2.223	2.207
	323.33	120.4	2.287	2.292	2.283
	348.29	117.4	2.341	2.370	2.352
	373.24	114.4	2.447	2.455	2.458
0.600	298.15	148.6	2.258	2.281	2.264
	323.13	144.6	2.356	2.369	2.359
	348.31	140.6	2.458	2.463	2.447
	373.18	136.6	2.583	2.570	2.572
0.800	298.09	173.8	2.311	2.326	2.313
	323.21	168.8	2.413	2.427	2.419
	348.09	163.8	2.525	2.534	2.525
	373.17	158.8	2.651	2.653	2.657
1	298.08	199.0	2.356	2.356	2.353
	323.09	193.0	2.467	2.467	2.463
	348.11	187.0	2.583	2.583	2.586
	373.24	181.0	2.716	2.716	2.714

*HD = n-hexadecane

calculated viscosity coefficient of 1.2 percent.

Isdale, Dymond and Brawn[23] have suggested that as a means of summarising the viscosity coefficient data for the n-hexane plus cyclohexane system B values can be represented by the equation

$$B = x_1B_1 + x_2B_2 + 0.2\ x_1x_2\ (B_2 - B_1) \qquad (6.6)$$

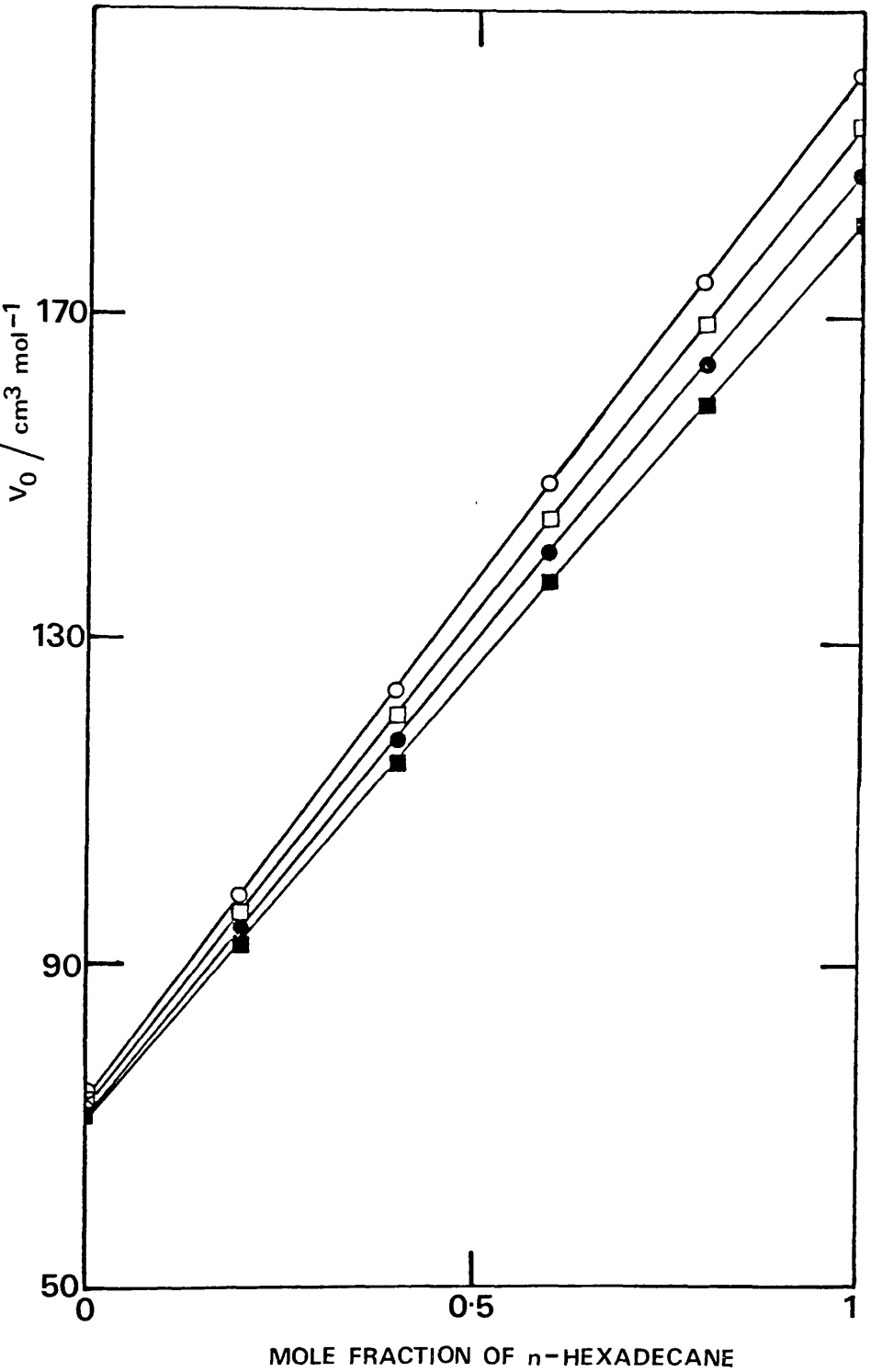

Figure 6.8 Dependence of V_o on Mole Fraction and Temperature.

○ *298 K,* □ *323 K,* ● *348 K,* ■ *373 K.*

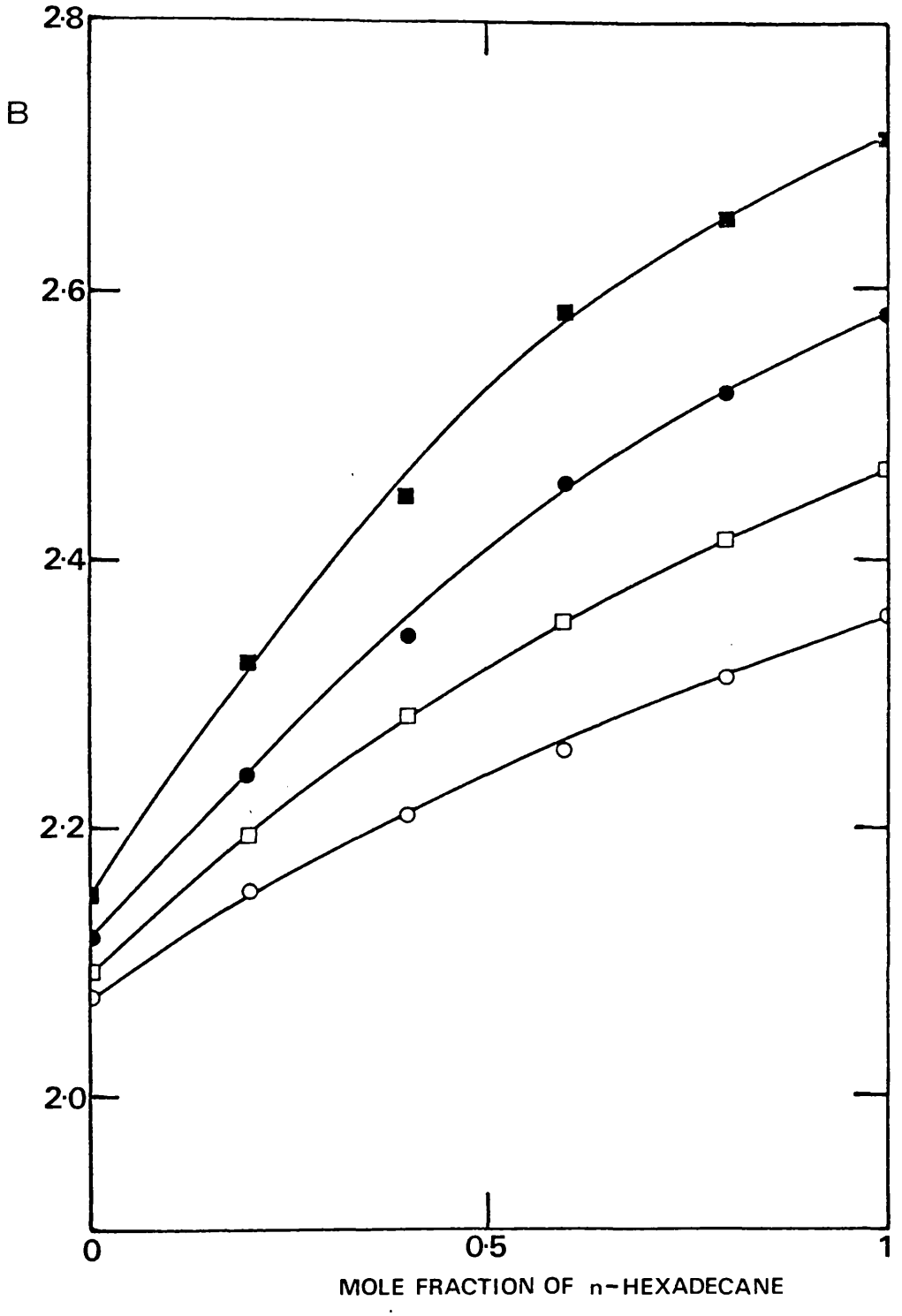

Figure 6.9 Dependence of B on Mole Fraction and Temperature.

○ *298 K,* □ *323 K,* ● *348 K,* ■ *373 K.*

This equation was applied to the n-hexane plus n-hexadecane results and reasonably close agreement with the optimised B values was obtained when the 0.2 was changed to 0.6. However, a more satisfactory representation was obtained by a quadratic equation in mole fraction

$$B = m + nx_2 - px_2^2 \qquad (6.7)$$

which gave closer agreement with the best B values obtained above. The values of m, n and p for each isotherm are given in Table 6.3.

Table 6.3

Values of m, n and p in Equation (6.7) for the n-Hexane plus n-Hexadecane System at Elevated Pressure

Temperature (K)	m	n	p
298.2	2.0697	0.3836	0.1000
323.2	2.0873	0.5666	0.1906
348.2	2.1121	0.6834	0.2098
373.2	2.1451	0.9230	0.3536

A comparison of the B values obtained from equations (6.6) and (6.7) together with the best B values from equation (6.5) for each mixture is given in Table 6.2. Table 6.4 compares the number of points fitted within prescribed limits using each of the three sets of B values.

Table 6.4

Comparison of 'Goodness of Fit' using Different B Values

Limits (%)	Number of points fitted		
	B (equation (6.5))	B (equation (6.6))	B (equation (6.7))
<1	99	74	89
1-2	77	66	76
2-3	40	31	40
3-4	8	22	13
4-5	2	19	6
5-6	4	11	6
6-7		3	
7-8		0	
8-9		2	
9-10		2	

Thus a simple quadratic equation involving only mole fraction gives B values which are accurate enough to reproduce viscosity coefficients for the mixtures almost to within the experimental accuracy of the measured values. Thus for the n-hexane plus n-hexadecane system viscosity coefficients can be calculated from equation (6.5) by specifying values of A, B and V_o if values of molar volume under these conditions are known. This equation thus provides a very convenient way of summarising the experimental data, and will provide a very reliable estimate of the viscosity coefficients under other conditions of composition, temperature and pressure. Furthermore, the fact that viscosity coefficient data for the n-hexane plus n-hexadecane system and for the n-hexane plus cyclohexane system[23] can be fitted to generally within 5 percent by the same equation with identical values of A, a linear relationship in mole fraction for V_o and a simple expression for B suggests that viscosity coefficients of other binary hydrocarbon mixtures may be similarly

represented. This should then form a basis for a satisfactory prediction of such data. Its one disadvantage already stated is that accurate values are required for the molar volume.

6.3 THE HILDEBRAND EQUATION

The Hildebrand equation, which is discussed in Chapter 2, relates the fluidity, $\frac{1}{\eta}$, and the molar volume, V, by the relationship

$$\frac{1}{\eta} = B\left(\frac{V - v_o}{v_o}\right) \qquad (6.8)$$

where v_o is the volume for which the fluidity is zero. The data obtained in this research provide a rigorous test of the range of validity of this equation as viscosity coefficients have been obtained above the normal boiling point for n-hexane and benzene, close to the freezing point for n-dodecane and n-hexadecane and up to high pressures for n-hexane and n-hexadecane. The relationship given by Bertrand[36] for mixtures, which was derived as an extension of the Hildebrand equation, has been tested using the saturation pressure viscosity coefficient data for the binary systems reported in Chapter 3.

To test the applicability of the Hildebrand Equation for the n-alkanes fluidity was plotted versus molar volume at saturation pressure. Straight lines were obtained for n-hexane and n-octane as predicted by equation (6.8) but for n-decane, n-dodecane and n-hexadecane increasing divergence from the straight line at the lower temperatures was observed as experimental temperatures came close to the freezing point. A similar observation was made by Eicher and Zwolinksi[34] for n-hexane below 253 K. Ertl and Dullien[35] have established that the Hildebrand equation is normally valid at reduced temperatures T/T_c, where T_c is the critical temperature, above 0.46. This is confirmed by the results of this work which show divergence from the straight line below this temperature.

Using the n-hexane and benzene viscosity coefficient data it was possible to test the validity of the Hildebrand equation above the normal boiling point. Figures 6.10 and 6.11 show the change in fluidity with increasing molar volume for n-hexane and benzene respectively. The Hildebrand equation holds to the maximum temperature of 393 K reached in this work which corresponds to a temperature of 0.77 T_c, where T_c is the critical temperature, for n-hexane and 0.70 T_c for benzene.

The effect of pressure on the applicability of equation (6.8) has been studied by Hildebrand and Lamoreaux[147] using data for n-decane[148] up to 41 MPa at 444 K. Their conclusion was that fluidity is uniquely determined by values of $V-v_o$, irrespective of whether changes in volume result from changes of temperature or of pressure. The present results for n-hexane and n-hexadecane at pressures up to 500 MPa provide a critical test of whether this conclusion is valid with respect to viscosity coefficients at temperatures significantly below the critical temperature. Figure 6.12 shows a plot of fluidity versus molar volume for n-hexane at 323 K and 373 K. Experimental points for the fluidity depart from the straight line predicted by equation (6.8) at a pressure of about 90 MPa. Similar behaviour was observed for n-hexadecane and the liquid mixtures studied.

Thus the Hildebrand equation is not valid for this system at pressures above 90 MPa.

The Hildebrand equation has recently been extended by Bertrand[36] in an attempt to relate mixture fluidity to the fluidities of the pure components.

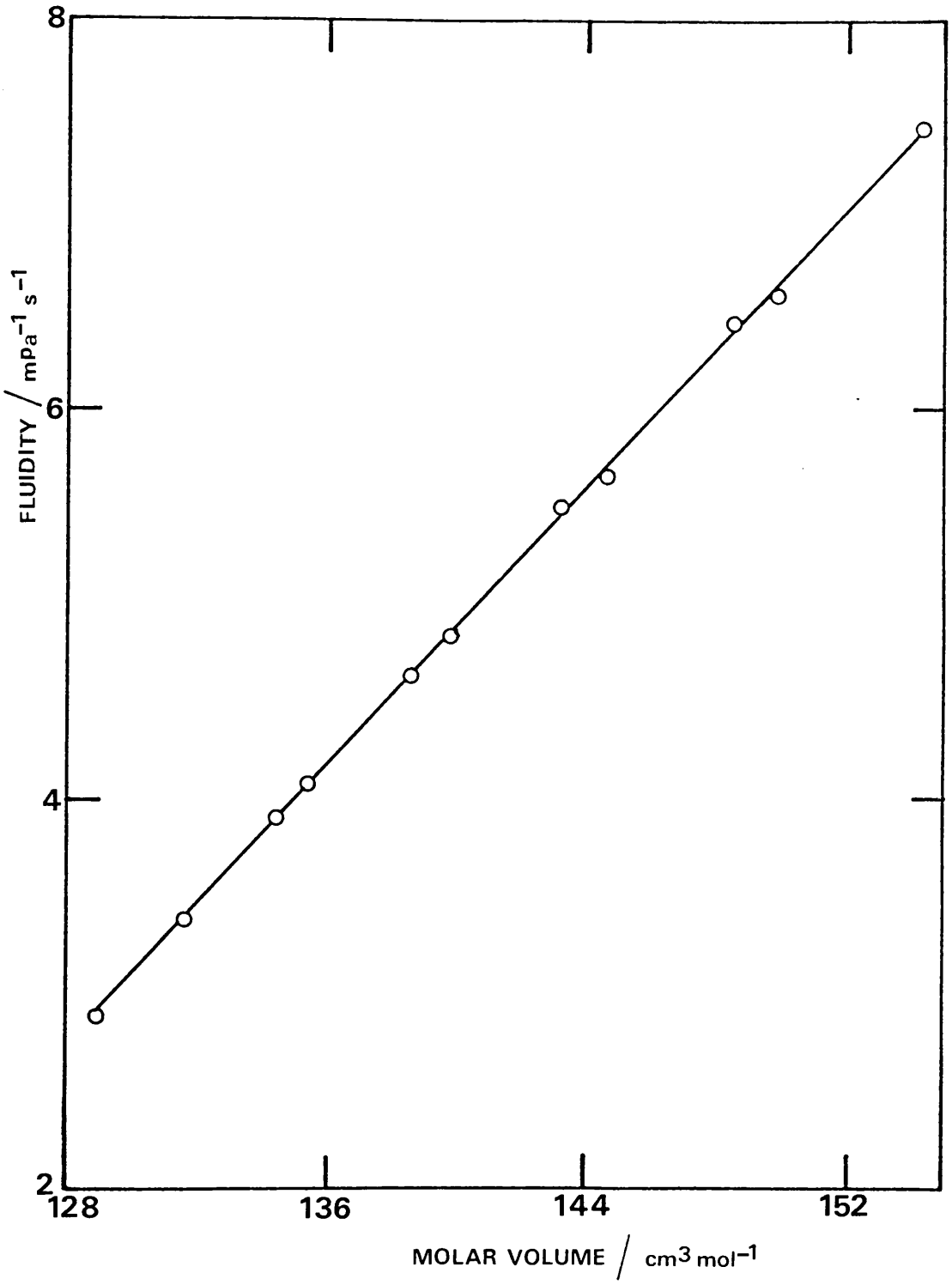

Figure 6.10 Dependence of Fluidity on Molar Volume for n-Hexane at Saturation Pressure and Different Temperatures.

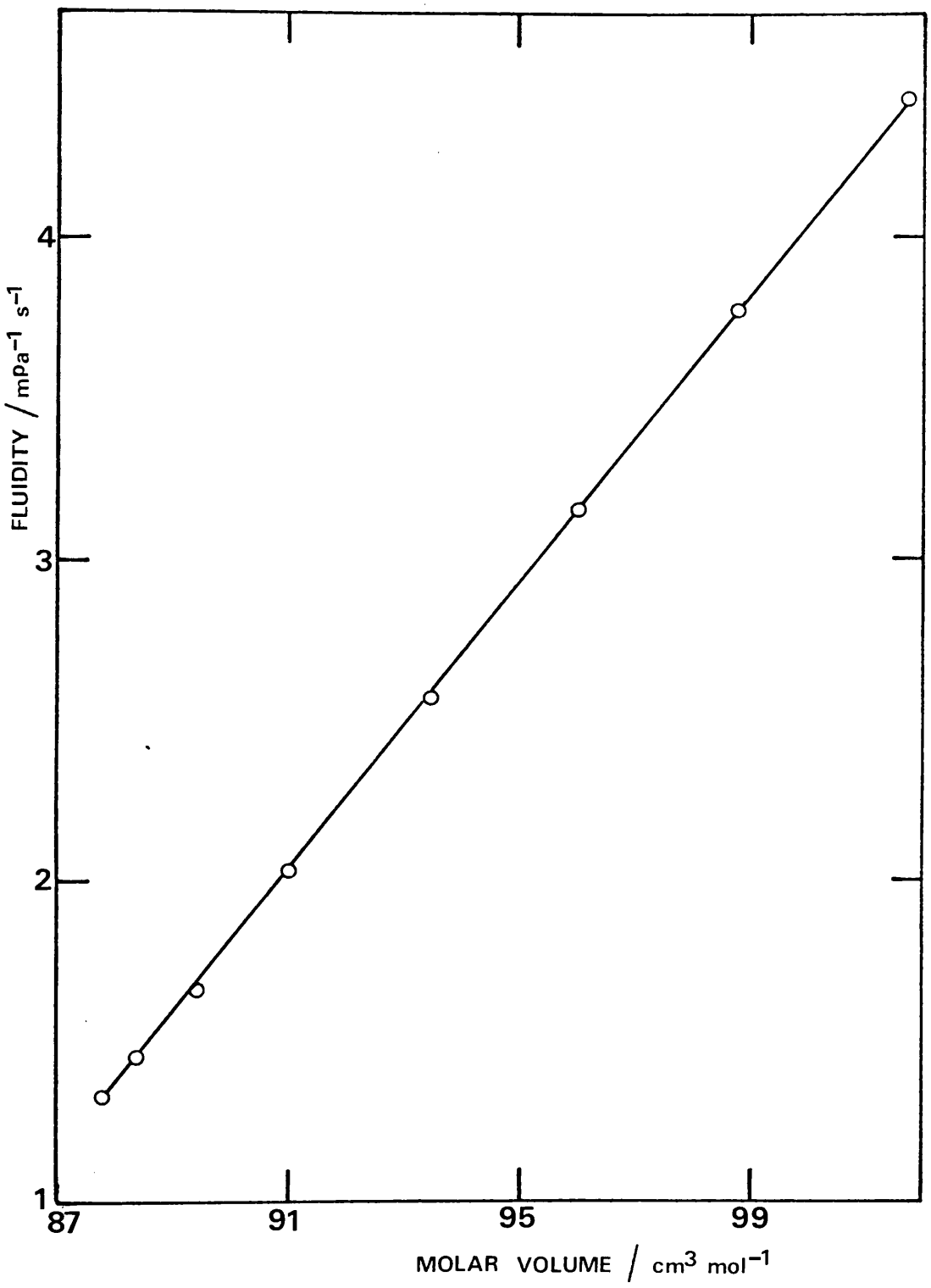

Figure 6.11 Dependence of Fluidity on Molar Volume for Benzene at Saturation Pressure and Different Temperatures.

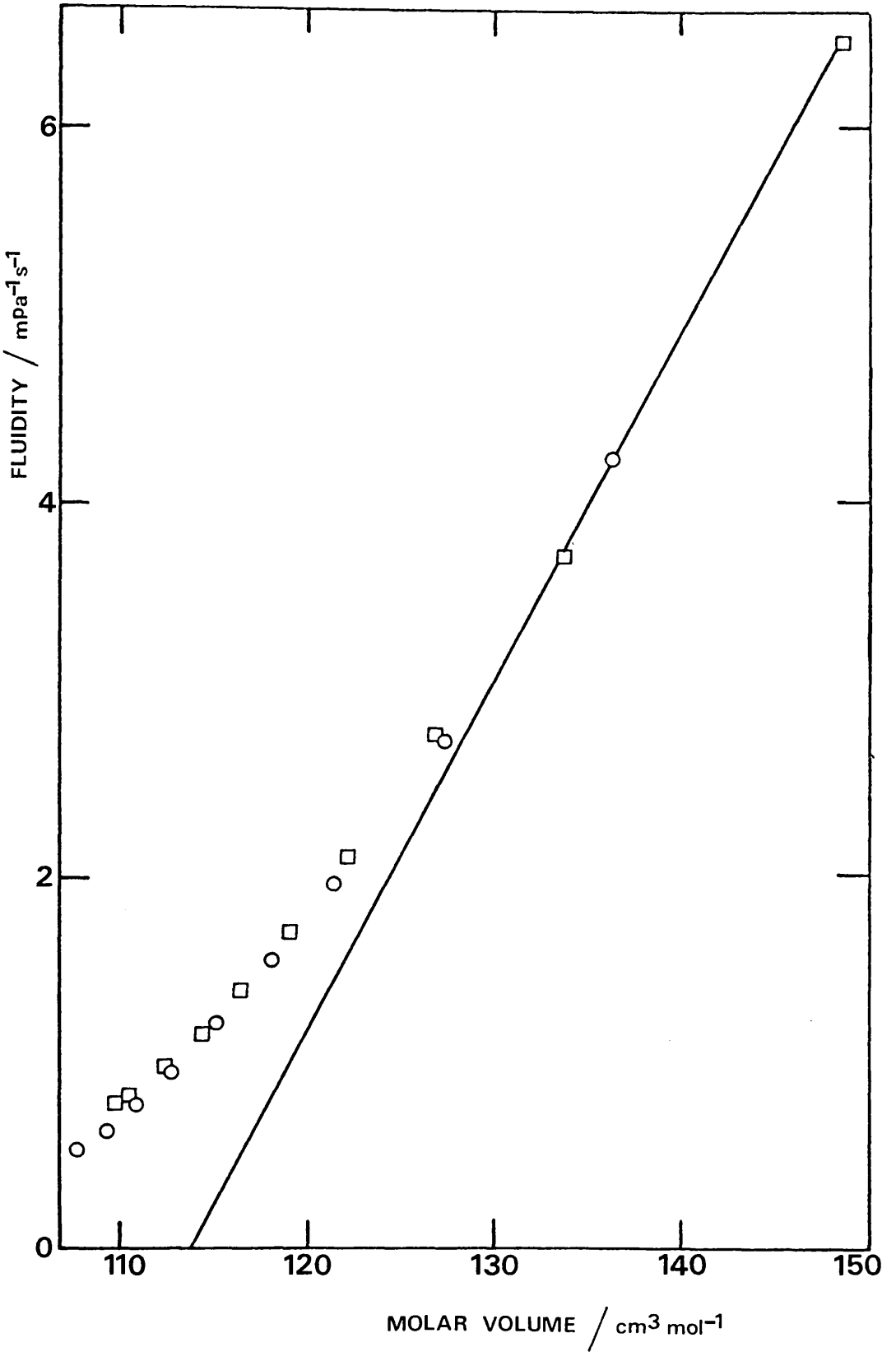

Figure 6.12 Dependence of Fluidity on Molar Volume for n-Hexane at Different Temperatures and Pressures. ○ 323.15 K, □ 373.36 K. The Straight Line Represents the Predictions of the Hildebrand Equation.

Bertrand[36] approximated the mixture parameters for equation (6.8) by

$$V_{mix} = x_1 V_1 + x_2 V_2 + \ldots \tag{6.9}$$

$$v_{o,mix} = x_1 v_{o,1} + x_2 v_{o,2} + \ldots \tag{6.10}$$

$$(BV)_{mix} = (B_1 V_1)^{\gamma_1} (B_2 V_2)^{\gamma_2} \tag{6.11}$$

where γ is volume fraction and x is mole fraction.

He then calculated mixture fluidity from

$$\frac{1}{\eta} = (B_1 V_1)^{\gamma_1} (B_2 V_2)^{\gamma_2} \ldots \left[(x_1 v_{o,1} + x_2 v_{o,2} + \ldots)^{-1} - (x_1 V_1 + x_2 V_2 \ldots)^{-1} \right] \tag{6.12}$$

Equation (6.12) was tested by Bertrand[36] using experimental data for 11 binary systems and two ternary systems at temperatures greater than 0.46 T_c for the pure components and found to be comparable to, or better than, the best predictions of four commonly used equations for mixture viscosity coefficients. However, this study only considered data at 293 K and 298 K and could not therefore test the validity of the individual approximations made. The present accurate measurements over a wide temperature range make possible a more searching test of the Bertrand equation. In Table 6.5, the present results are compared with the predictions of equation (6.12).

Table 6.5

Deviation of Mixture Fluidity from Equation (6.12)

System	Percentage Deviation [a] at $T > 0.46\ T_c$
benzene plus n-hexane	-0.8 to 4.3
benzene plus n-octane	1.0 to 9.1
benzene plus n-decane	0.2 to 5.4
benzene plus n-dodecane	-1.4 to 1.8
benzene plus n-hexadecane	-1.8 to -7.4
benzene plus cyclohexane	3 to 19
n-hexane plus n-hexadecane	-10 to -26

[a] $100\ (\frac{expt-calc}{expt})\%$

Clearly this equation does not predict mixture fluidity with an accuracy approaching that of the experimental measurements, although for the benzene plus n-dodecane system the deviations are small. For benzene plus n-alkanes of shorter chain length the predicted values are generally too low but for benzene plus n-hexadecane values given by equation (6.12) are too high. The discrepancies between the experimental and predicted values are greatest for benzene plus cyclohexane where the calculated results are significantly lower and for n-hexane plus n-hexadecane where the calculated values are much larger. In order to determine the reasons for the failure of equation (6.12) to represent the data satisfactorily, viscosity coefficient results for the two systems have been used to test the three approximations represented by equations (6.9), (6.10) and (6.11).

(i) The assumption in equation (6.9) is that values are strictly additive and it therefore does not take into account the actual volume change on mixing. For the benzene plus cyclohexane system

the largest value for the molar excess volume was found to be 0.82 $cm^3\ mol^{-1}$. The error in the calculated fluidity through neglect of this actual volume change is 3.7 percent. In the case of n-hexane plus n-hexadecane the maximum value of V_m^E was -1.84 $cm^3\ mol^{-1}$. This leads to a difference of 4.9 percent in the calculated fluidity.

(ii) The approximation introduced by equation (6.10) is that the parameter v_o varies linearily with mole fraction of the mixture. Values of v_o determined from experimental viscosity coefficient data using equation (6.8) are plotted in Figure 6.13 for benzene plus cyclohexane and in Figure 6.14 for n-hexane plus n-hexadecane.

For the benzene plus cyclohexane system the experimental v_o values deviate from a straight line between the v_o values for the pure components as the value of v_o for cyclohexane is higher than would be expected from the best line through the experimental v_o data for the mixtures. This may be due in part to the uncertainty in v_o for cyclohexane due to curvature from the straight line predicted by equation (6.8) at the lower temperatures. The difference between $v_{o,mix}$ calculated by equation (6.10) and the experimental value leads to a maximum uncertainty in viscosity coefficient of 11.5 percent for the benzene plus cyclohexane mixture with a mole fraction of benzene of 0.600 at 298.19 K. For the n-hexane plus n-hexadecane system however, the results lie very close to the straight line indicating that equation (6.10) is a reasonable approximation for this system.

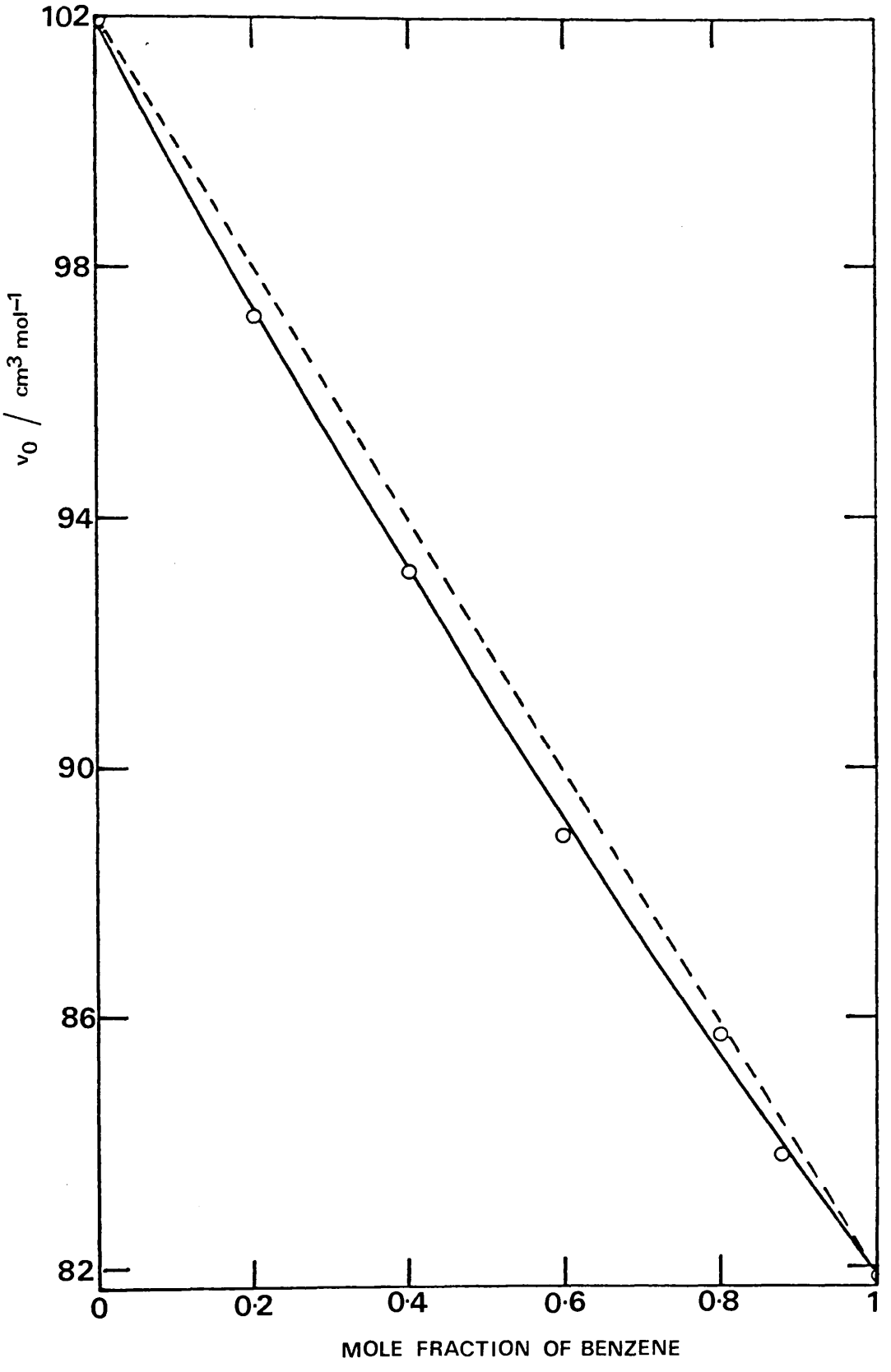

Figure 6.13 Dependence of v_o on Mole Fraction for the Benzene plus Cyclohexane System. The Dotted Line Represents the Predictions of Equation (6.10).

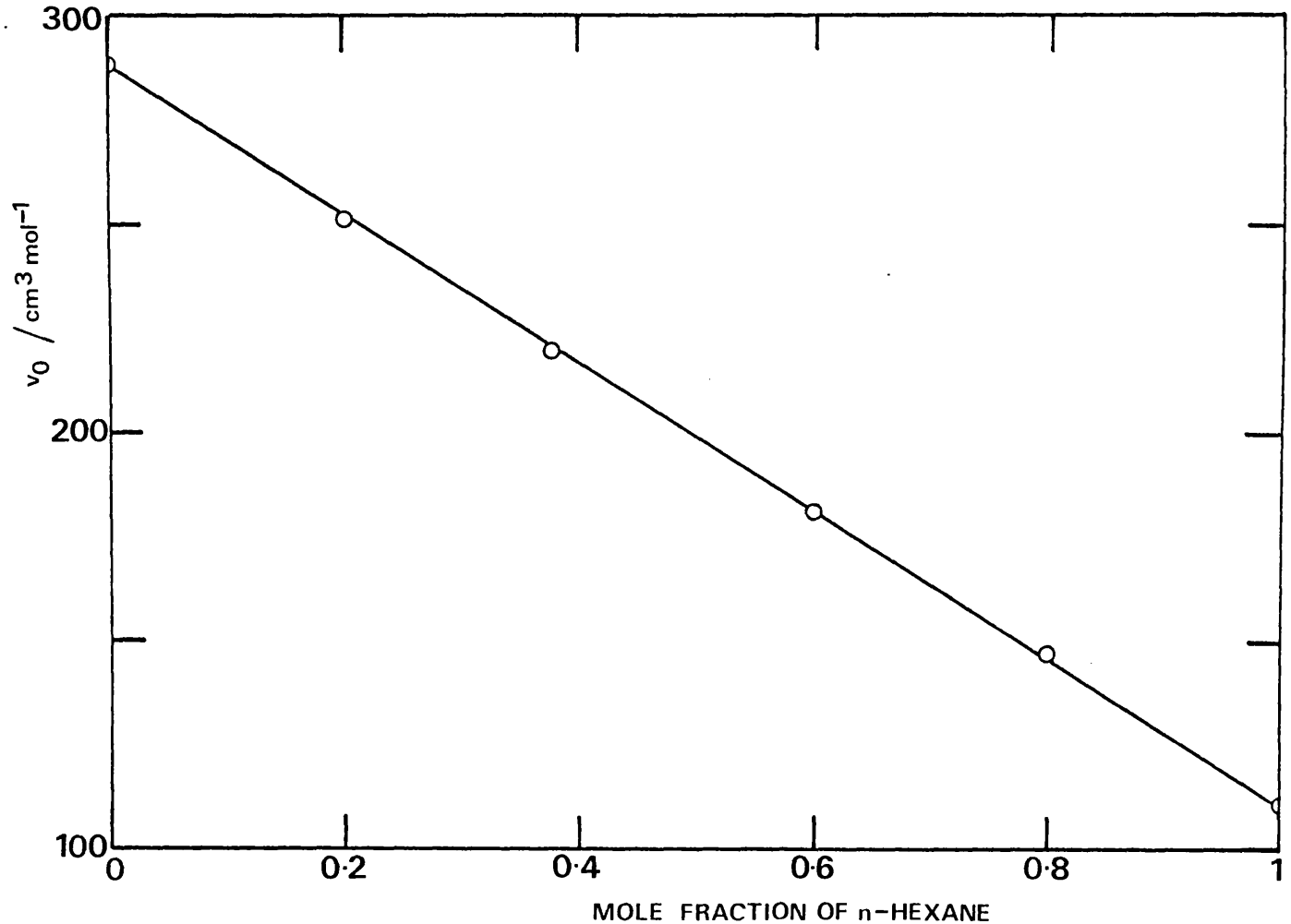

Figure 6.14 Dependence of v_o on Mole Fraction for the n-Hexane plus n-Hexadecane System.

(iii) The approximation that $(BV)_{mix}$ is given by equation (6.11) is tested in Figures 6.15 and 6.16 for the benzene plus cyclohexane and n-hexane plus n-hexadecane systems respectively. Figure 6.15 shows that this is a good approximation in the case of the benzene plus cyclohexane system. However, for the n-hexane plus n-hexadecane system the agreement between $(BV)_{mix}$ and the values calculated using equation (6.11) is very poor. Indeed it is the inadequacy of this approximation which leads to the poor agreement between the predicted viscosity coefficients and the experimental data for this system.

The conclusion is that for the binary hydrocarbon systems studied, the Hildebrand equation is only useful in correlating fluidities for temperatures greater than 0.46 times the critical temperature of the n-alkane, and in the range of pressure from atmospheric to approximately 90 MPa. Reasonably accurate prediction of mixture fluidity at saturation pressures from pure component fluidities using expressions based on the Hildebrand equation and given by Bertrand[36] is obtained for benzene plus n-dodecane but for other systems and especially for benzene plus cyclohexane and n-hexane plus n-hexadecane the agreement with experimental data is very poor. The problem lies in being able to predict the values of B, V and v_o for mixtures with sufficient accuracy.

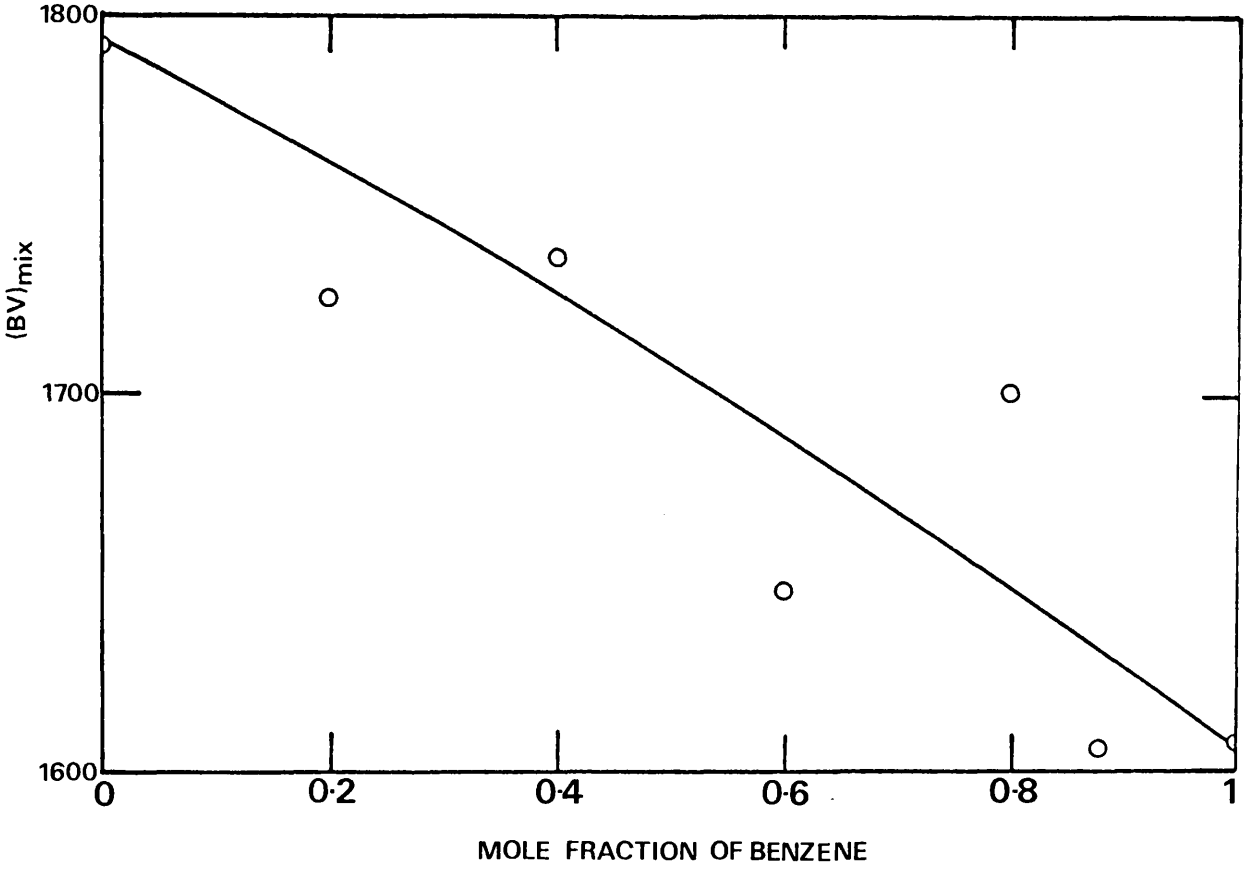

Figure 6.15 Dependence of $(BV)_{mix}$ on Mole Fraction for the Benzene plus Cyclohexane System at 298 K. The Line Represents the Predictions of Equation (6.11).

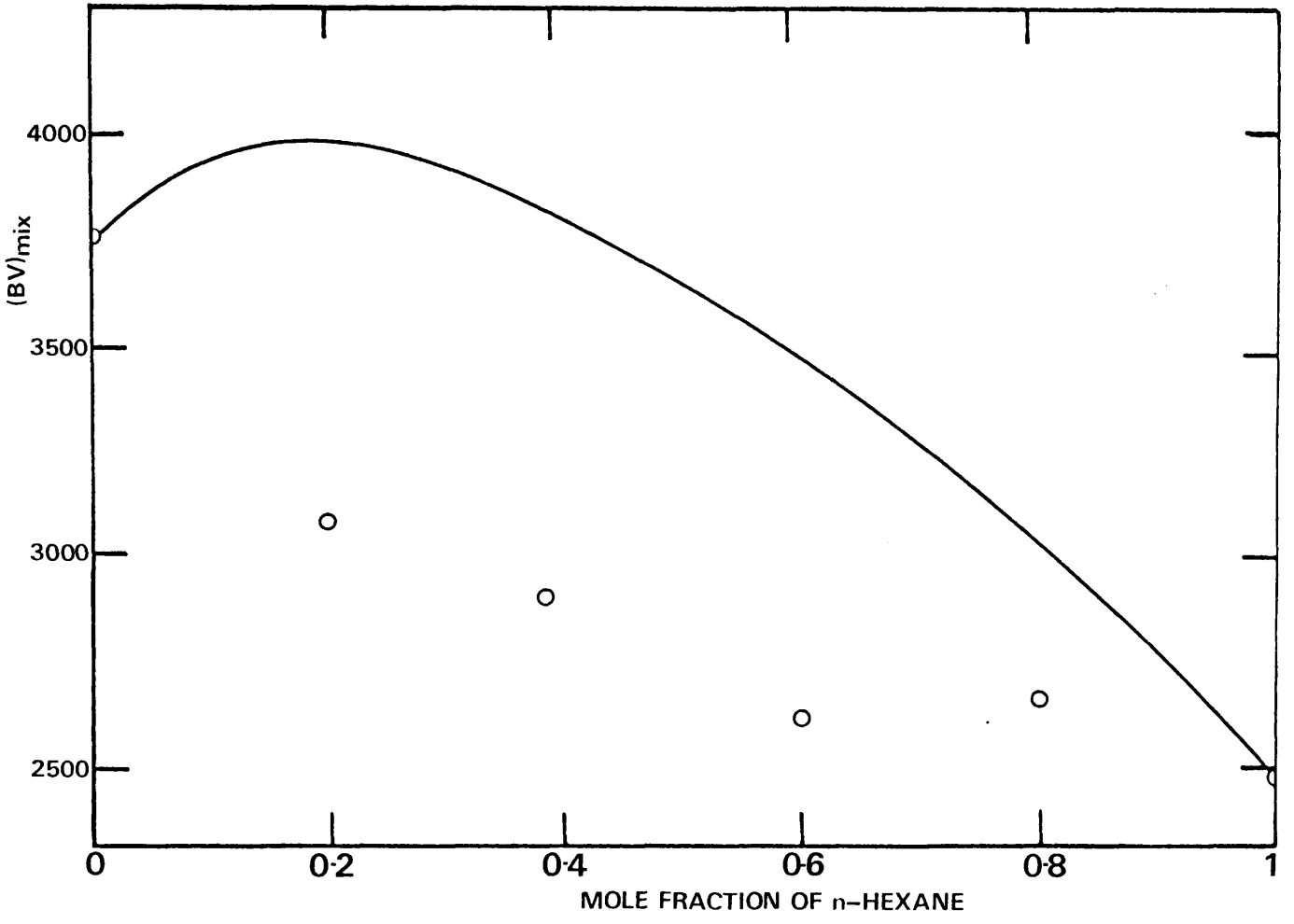

Figure 6.16 Dependence of $(BV)_{mix}$ on Mole Fraction for the n-Hexane plus n-Hexadecane System at 358 K. The Line Represents the Predictions of Equation (6.11).

6.4 EYRING ACTIVATION MODEL AND THE PRINCIPLE OF CONGRUENCE

Although there are reasons for considering that the Eyring activation theory of transport processes does not have a sound physical basis, as discussed in Chapter 2, it has proved extremely useful for the correlation and prediction of viscosity coefficients for n-alkane mixtures[56]. Values of the molar excess Gibbs free energy of activation for flow, $\Delta^* G^E$ at 298 K conform to the Principle of Congruence. For the prediction of mixture viscosity coefficients it is therefore necessary to establish the curve of $\Delta^* G^E$ as a function of average carbon chain length n of the mixture, which Coursey and Heric[56] determined from mixture viscosity coefficient data for the n-hexane plus n-hexadecane system at 298 K. Values of n are calculated from the expression

$$n = \sum_i x_i c_i \qquad (6.13)$$

where c_i is the number of carbons in the n-alkane chain of component i, and x_i is its mole fraction. The $\Delta^* G^E$ value for any other mixture of n-alkanes which have chain lengths from 6 to 16 is obtained from this reference curve. For example the $\Delta^* G^E$ value of a n-hexane plus n-octane plus n-dodecane mixture of average chain length n is given by

$$\Delta^* G^E{}_n = \Delta_{616:n} - x_6\Delta_{616:6} - x_8\Delta_{616:8} - x_{12}\Delta_{616:12} \qquad (6.14)$$

where $\Delta_{616:k}$ is the height from the X-axis to the curve at the point where n = k, and x_k is the mole fraction of n-alkane with carbon chain length k.

The viscosity coefficient of this n-alkane mixture is then calculated from the equation

$$\ln\eta V = x_1 \ln\eta_1 V_1 + x_2 \ln\eta_2 V_2 + \frac{\Delta^* G^E}{RT} \,. \qquad (6.15)$$

The results obtained by Coursey and Heric[56] indicate that the viscosity coefficients of n-alkane mixtures calculated by this method have an accuracy of 2.0 percent at 298 K and saturation pressure. The mixture viscosity coefficients given in Chapter 3 now allows the range of validity of the approach to be tested at temperatures from 298 K to 378 K and the mixture viscosity coefficients given in Chapter 4 allow the pressure dependence of $\Delta^* G^E$ to be determined. This is essential for determining whether the Principle of Congruence applies at elevated pressures also. In Table 6.6 a comparison is made between the $\Delta^* G^E$ values predicted[56] at 298 K on the basis of the Congruence Principle and values derived from the present experimental viscosity coefficient data at saturation pressure. The agreement is very satisfactory.

Table 6.6

Comparison of $\Delta^* G^E$ Values at 298 K with Reference (56)

System	$\Delta^* G^E$ expt. (J mol^{-1})	$\Delta^* G^E$ ref. (56) (J mol^{-1})
2 component mixtures		
n-hexane/n-hexadecane		
x = 0.1987/0.8013	474	456
0.3772/0.6228	755	753
0.5983/0.4017	886	886
0.7982/0.2018	698	694
3 component mixtures		
n-hexane/n-octane/n-hexadecane		
x = 0.3286/0.3297/0.3417	687	656
0.1093/0.1152/0.7755	408	377
4 component mixtures		
n-hexane/n-octane/n-dodecane/ n-hexadecane		
x = 0.2593/0.2997/0.2507/0.1903	483	484

The effect of an increase in temperature on $\Delta^* G^E$ at saturation pressure is shown in Figure 6.17, where the values of $\Delta^* G^E$ are plotted against average carbon chain length.

For the three and four component n-alkane mixtures, $\Delta^* G^E$ values from equation (6.15) are used to test the Congruence Principle by plotting values of $\Delta_{616:n}$ from equation (6.14) against n in the same figure. The curves show that the Principle of Congruence is obeyed not only at 298 K but also at higher temperatures. However $\Delta^* G^E$ is definitely temperature dependent, increasing as the temperature is raised for a given mixture as shown by the values given in Table 6.7. This is important for the calculation of viscosity coefficients of n-alkane mixtures at saturation pressure at temperatures above 298 K. If the 298 K reference curve is used to calculate $\Delta^* G^E$ for the mixture the predicted values of viscosity coefficient will be low for example by 4 percent for the three component mixture with a mole fraction of n-hexane of 0.3229, of n-octane of 0.3317 and of n-hexadecane of 0.3454 at 358 K.

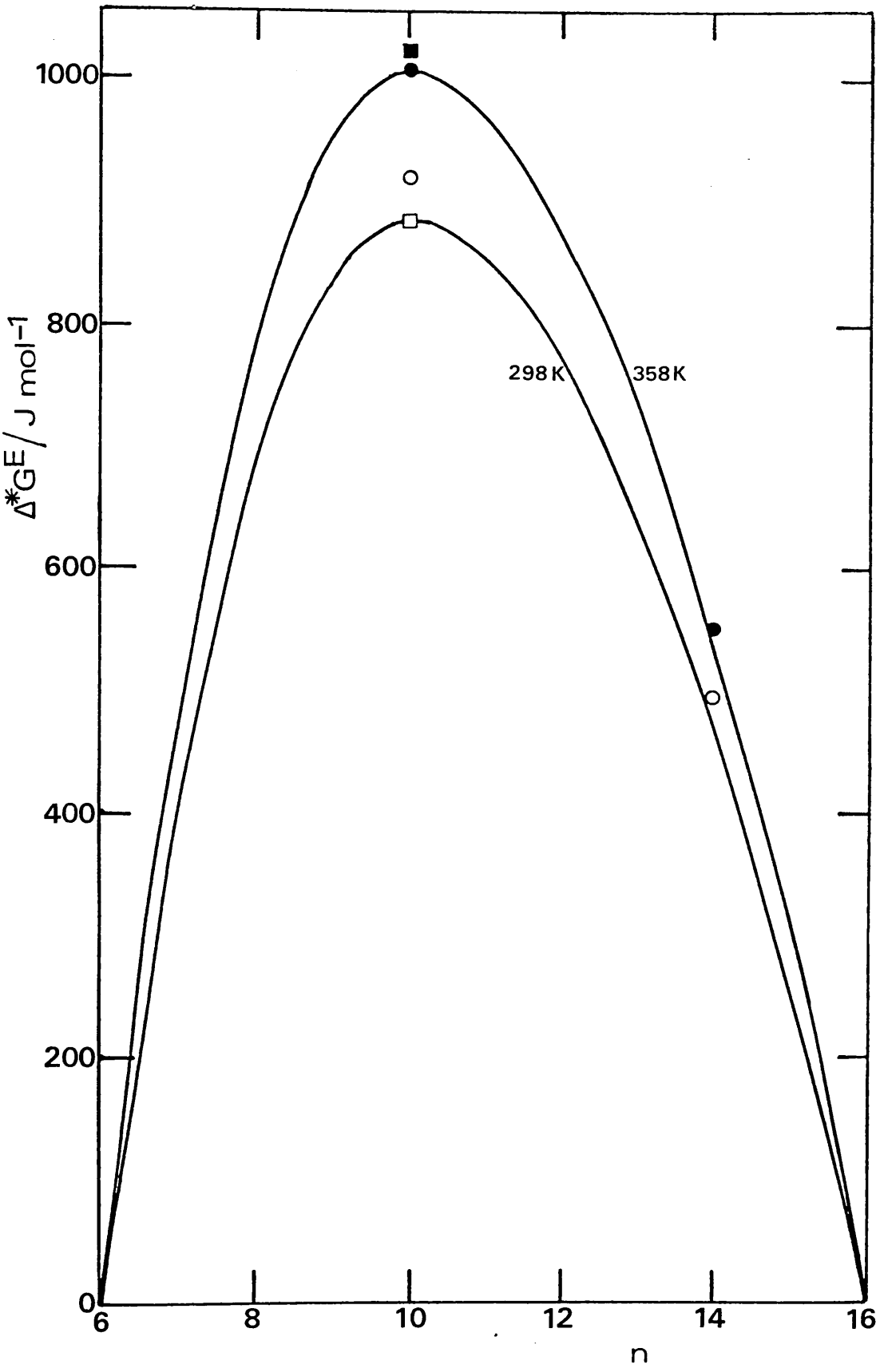

Figure 6.17 Effect of Temperature on $\Delta^* G^E$ for n-Alkane Mixtures. The Lines are Drawn Through the Present Results for the n-Hexane plus n-Hexadecane System. Ternary Mixtures ○ 298 K, ● 358 K. Quaternary Mixture □ 298 K, ■ 358 K.

Table 6.7

$\Delta^* G^E$ Values at Elevated Temperature

Temperature (K)	Mixture				$\Delta^* G^E$ expt. (J mol^{-1})	Mixture			$\Delta^* G^E$ expt. (J mol^{-1})
	$^*x_H$	x_O	x_{DD}	x_{HD}		x_H	x_O	x_{HD}	
318.26	0.1086	0.1152		0.7762	420	0.3276	0.3300	0.3424	711
338.36	0.1076	0.1151		0.7773	441	0.3259	0.3303	0.3438	749
358.28	0.1058	0.1149		0.7793	449	0.3229	0.3317	0.3454	768
318.26	0.2584	0.2997	0.2510	0.1909	497				
338.36	0.2569	0.3004	0.2517	0.1910	529				
358.28	0.2545	0.3009	0.2529	0.1917	551				

$^*H$ = n-hexane, O = n-octane, DD = n-dodecane

HD = n-hexadecane

The effect of an increase in pressure on the derived $\Delta^* G^E$ values is illustrated in Figure 6.18 where results are given at 373 K at saturation pressure and for pressures of 200 and 400 MPa. The points lie on smooth curves at each pressure but measurements on other n-alkane mixtures are required to establish that the Congruence Principle is obeyed. Such measurements as have been made on other n-alkane systems only extend to moderate pressures for example viscosity coefficient results have been reported, by Naziev, Guseinov and Badalov[21] for n-heptane plus n-decane at temperatures from 290 K to 591 K up to 49 MPa and by Aleskerov, Mamedov and Khalilov[22] for n-heptane plus n-octane from 291 K to 475 K up to 49 MPa.

For the accurate prediction of mixture viscosity coefficients the value of $\Delta^* G^E$ should be taken from the curve for the given pressure. If values are taken from the 0.1 MPa (saturation pressure) line then the calculated viscosity coefficients will be low, by up to 10 percent for the equimolar mixture of n-hexane plus n-hexadecane for a pressure of 400 MPa at 373 K. Thus, in order to calculate viscosity coefficients of n-alkane mixtures from equation (6.15) with an accuracy approaching that of the viscosity coefficients of the pure components, values for $\Delta^* G^E$ must be taken from the curve for the particular temperature and pressure (although it still remains to be shown that the Congruence Principle is obeyed at elevated pressures).

Two disadvantages of this method are, firstly, the need for accurate density data for the pure components and the mixture at the temperature and pressure of interest, and secondly that the relatively low freezing pressures of n-hexadecane limits the pressure range for which curves of $\Delta^* G^E$ versus average carbon chain number, n, can be established,

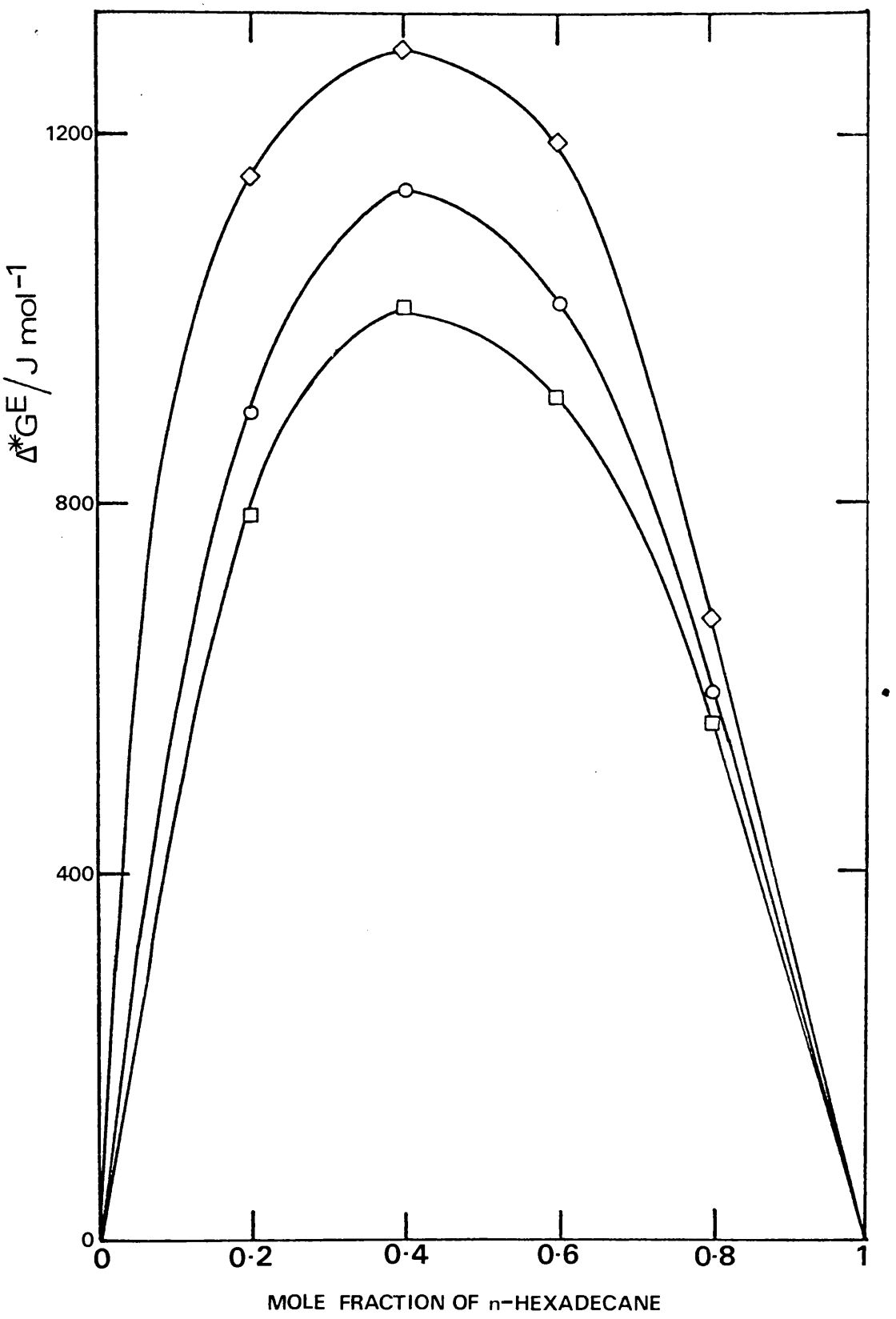

Figure 6.18 Effect of Pressure on $\Delta^* G^E$ for the n-Hexane plus n-Hexadecane System at 373 K. □ 0.1 MPa, ○ 200 MPa, ◇ 400 MPa.

especially at temperatures approaching the melting point.

It is not to be expected that the Congruence Principle will apply to the Gibbs free energy of activation for flow for the benzene plus n-alkane systems studied in this work but nevertheless it is instructive to determine the change in $\Delta^* G^E$ *with n-alkane carbon chain length.*

At 298.19 K, $\Delta^* G^E$ *values are negative for benzene plus n-hexane, benzene plus n-octane and benzene plus n-decane and become increasingly positive for benzene plus n-dodecane and benzene plus n-hexadecane as illustrated in Figure 6.19.* $\Delta^* G^E$ *values at 373.28 K are also included in this figure to illustrate the effect of temperature changes. It is found that an increase in temperature causes* $\Delta^* G^E$ *to become less negative for benzene plus n-hexane and benzene plus n-octane. For benzene plus n-dodecane and benzene plus n-hexadecane* $\Delta^* G^E$ *values increase with increasing temperature. For benzene plus n-decane there is a change in sign with increasing temperature. Although the Congruence Principle cannot be used to predict viscosity coefficients for other benzene plus n-alkane mixtures, it is possible to make accurate predictions by plotting* $\Delta^* G^E$ *versus n-alkane chain length at constant mole fraction. This is illustrated in Figure 6.20 for equimolar benzene plus n-alkane mixtures at 298.19 K and 373.28 K. Using plots such as this for different compositions, values of* $\Delta^* G^E$ *for binary mixtures at other temperatures, and with other n-alkanes as the second component, can be interpolated, and viscosity coefficients for benzene plus n-alkane mixtures predicted with an estimated accuracy of 1 to 2 percent.*

Equation (6.15) can thus provide a useful basis for the correlation and prediction of viscosity coefficient data although it has certain

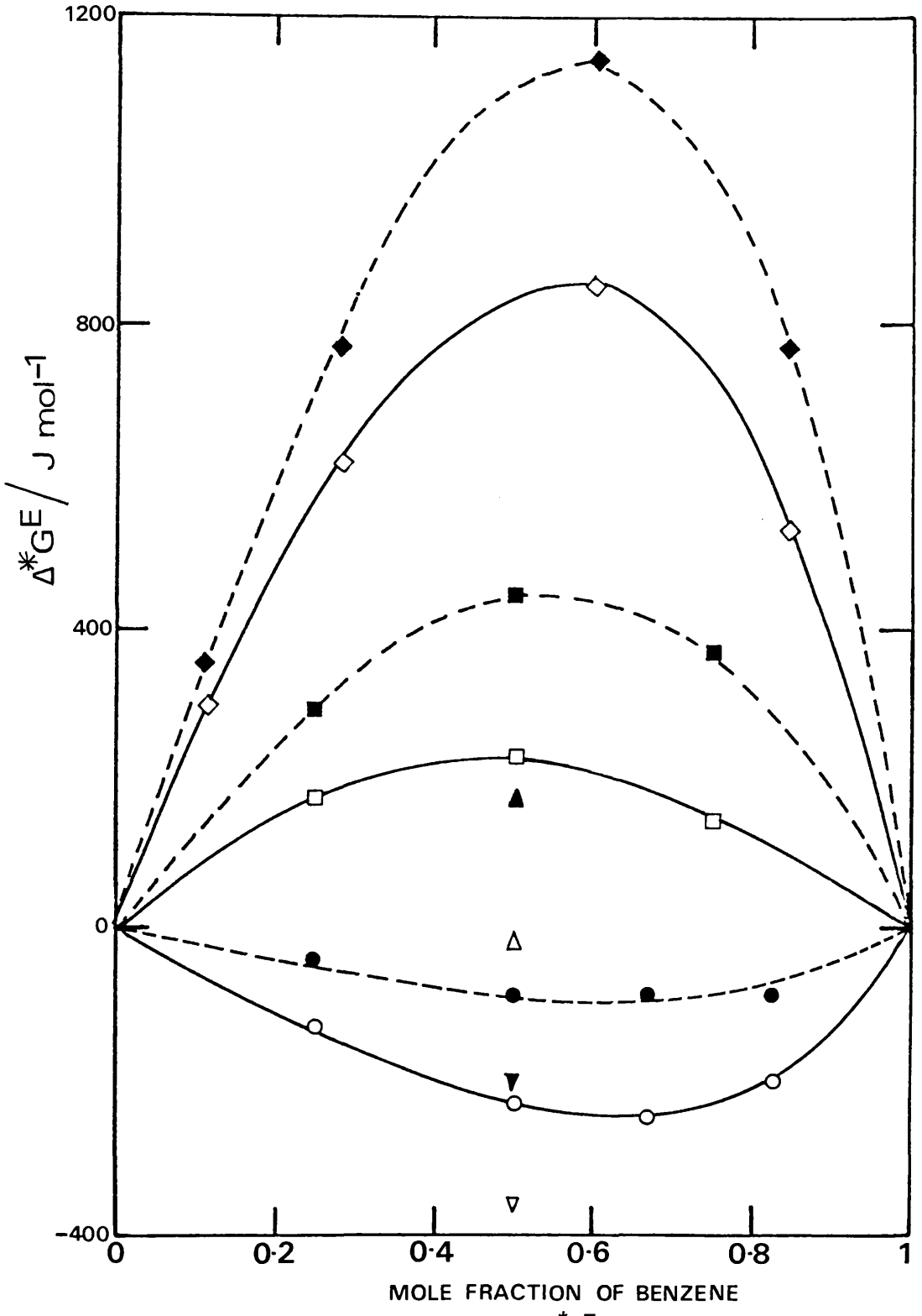

Figure 6.19 Effect of Temperature on $\Delta^* G^E$ for Benzene plus n-Alkane Mixtures. ——— 298 K, - - - - 373 K, ▽ plus n-Hexane, ○ plus n-Octane, △ plus n-Decane, □ plus n-Dodecane, ◇ plus n-Hexadecane.

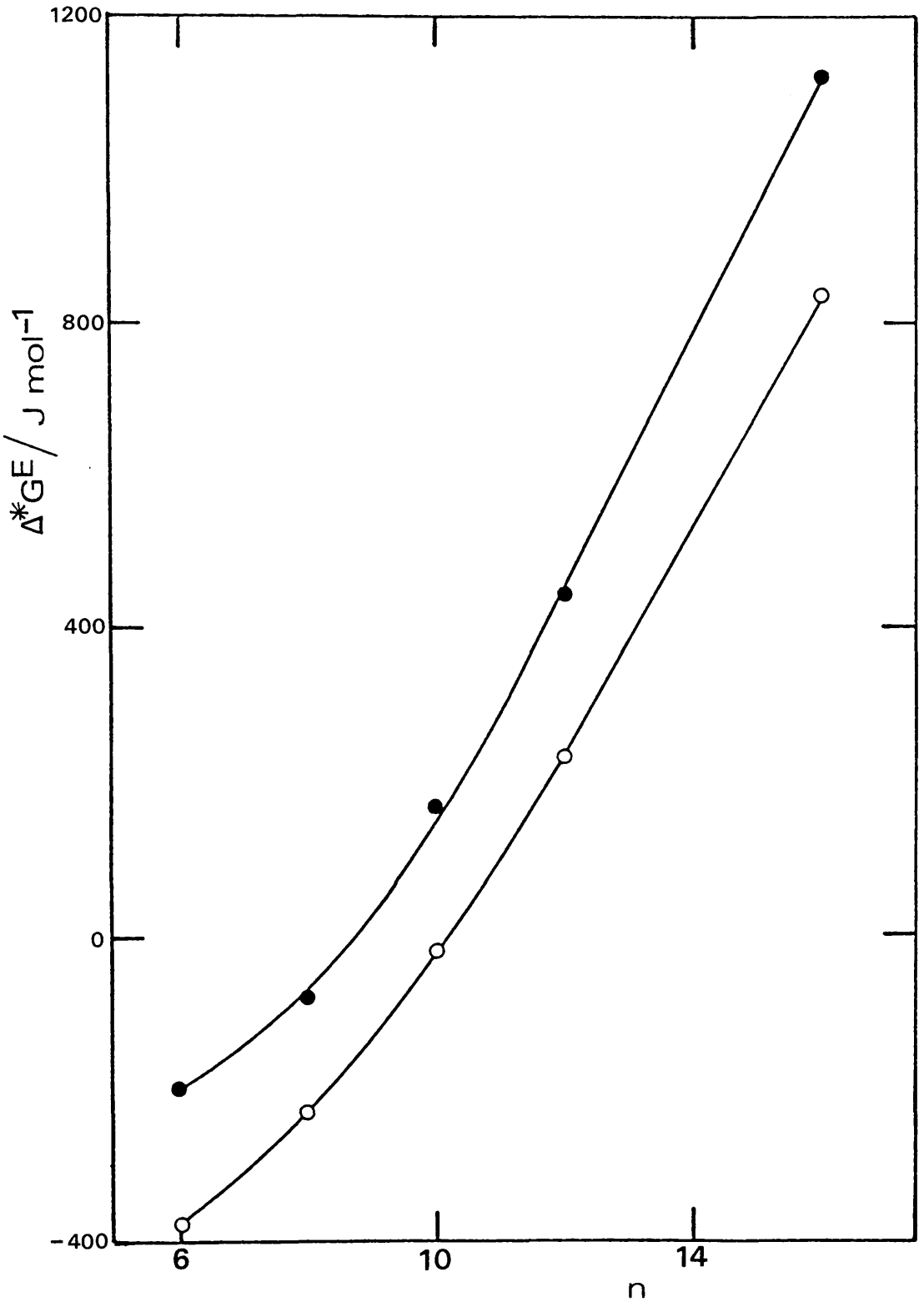

Figure 6.20 Variation in $\Delta^* G^E$ with n-Alkane Chain Length for Equimolar Benzene plus n-Alkane Mixtures.
○ 298 K, ● 373 K.

limitations. The most serious of these is that it is not possible to determine $\Delta^* G^E$ values, except from experimental viscosity data. Attempts to correlate $\Delta^* G^E$ with thermodynamic mixing properties, such as the molar excess volumes[54] *have proved unsuccessful.*

6.5 THE GRUNBERG AND NISSAN EQUATION

The Grunberg and Nissan[149] equation, originally proposed in 1949, has been recommended by Irving[150] after a study of more than 25 equations, as being the most effective equation in representing viscosity coefficient data for binary mixtures. This empirical expression may be written as

$$\ln\eta = x_1 \ln\eta_1 + x_2 \ln\eta_2 + x_1 x_2 G \qquad (6.16)$$

where η is the viscosity coefficient of the mixture, x_i the mole fraction of component i and η_i its viscosity coefficient. G is the Grunberg and Nissan constant, which Irving[150] recommended should be considered as a single disposable parameter even though, for the few systems for which viscosity coefficient data were available at elevated temperature, G was found to be temperature dependent.

It is now possible with the experimental viscosity coefficient data obtained in this research and reported in Chapters 3 and 4 to make a more critical assessment of the effectiveness of the Grunberg and Nissan[149] equation as applied to viscosity coefficient data for binary hydrocarbon mixtures. As a first step, the effect on G of changes in composition, temperature, and pressure was determined. Figure 6.21 shows values of G versus mole fraction of benzene at 298.19 K and 373.28 K for the systems studied at saturation pressure with benzene as one of the components. In general G is not constant for these systems, but varies with both temperature and composition. For mixtures of benzene plus n-alkanes up to n-dodecane G is negative at 298.19 K for a mole fraction of benzene of 0.25 and becomes more negative for mixtures richer in benzene. An increase in temperature leads to a larger value of G and reduces the effect of change in composition on G. For binary

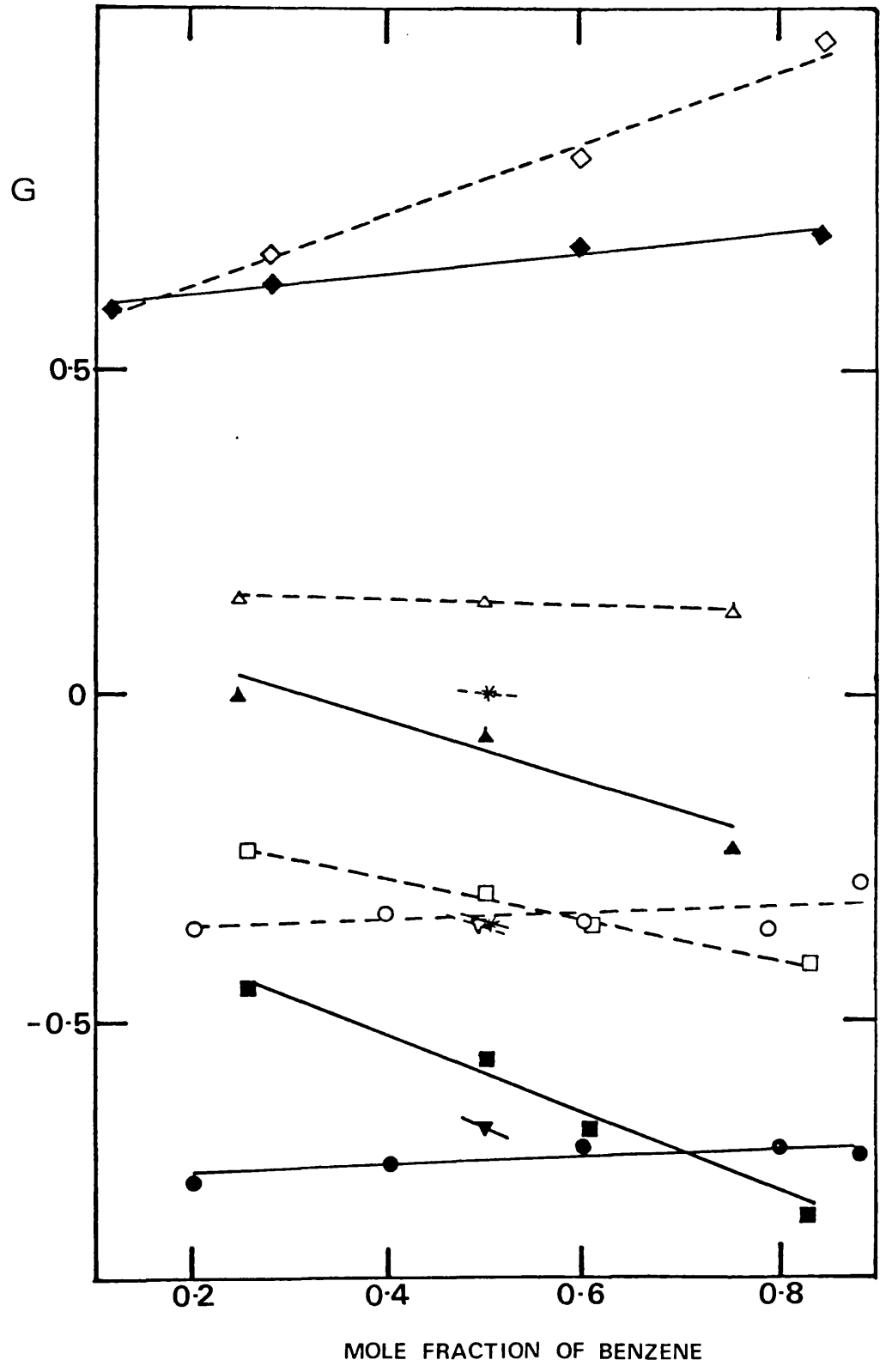

Figure 6.21 Dependence of G on Mole Fraction and Temperature for Binary Mixtures Containing Benzene. ——298 K, ----373 K. ○ plus Cyclohexane, ▽ plus n-Hexane, □ plus n-Octane, ✳ plus n-Decane, △ plus n-Dodecane, ◇ plus n-Hexadecane.

benzene plus n-alkane mixtures where the carbon chain length is greater than 12, G is positive at 298.19 K and for benzene plus n-hexadecane becomes increasingly positive for mixtures richer in benzene. The effect of an increase in temperature is to give a more positive value of G and for the composition dependence to be greater. By contrast, for the benzene plus cyclohexane system the composition dependence of G is almost zero at each temperature but again there is a marked temperature dependence, G becoming less negative as the temperature is raised.

Thus, for the accurate representation of viscosity coefficients of benzene plus n-alkane and benzene plus cyclohexane mixtures by the Grunberg and Nissan[149] equation it is essential to take into account the composition and temperature dependence of G. For example, if a single value is taken for G corresponding to the equimolar mixture at 348 K for each of the benzene plus n-alkane systems studied, the calculated mixture viscosity coefficients differ from the experimental values by up to 8 percent.

Since the Grunberg and Nissan[149] equation is empirical any physical significance which may be attached to the parameter G is obscure and attempts to relate its values to other defined physical properties have not been successful. However, systematic variations with chemical structure have been observed in limited groups[151]. Figure 6.22 illustrates the variation of G with carbon chain length for equimolar mixtures of benzene plus n-alkanes at 298.19 K and 373.28 K. There is a smooth variation in G with increasing carbon chain length, and above C_{10} this becomes effectively linear. From such a plot of G versus n-alkane chain length for the benzene plus n-alkane systems for a given mole fraction

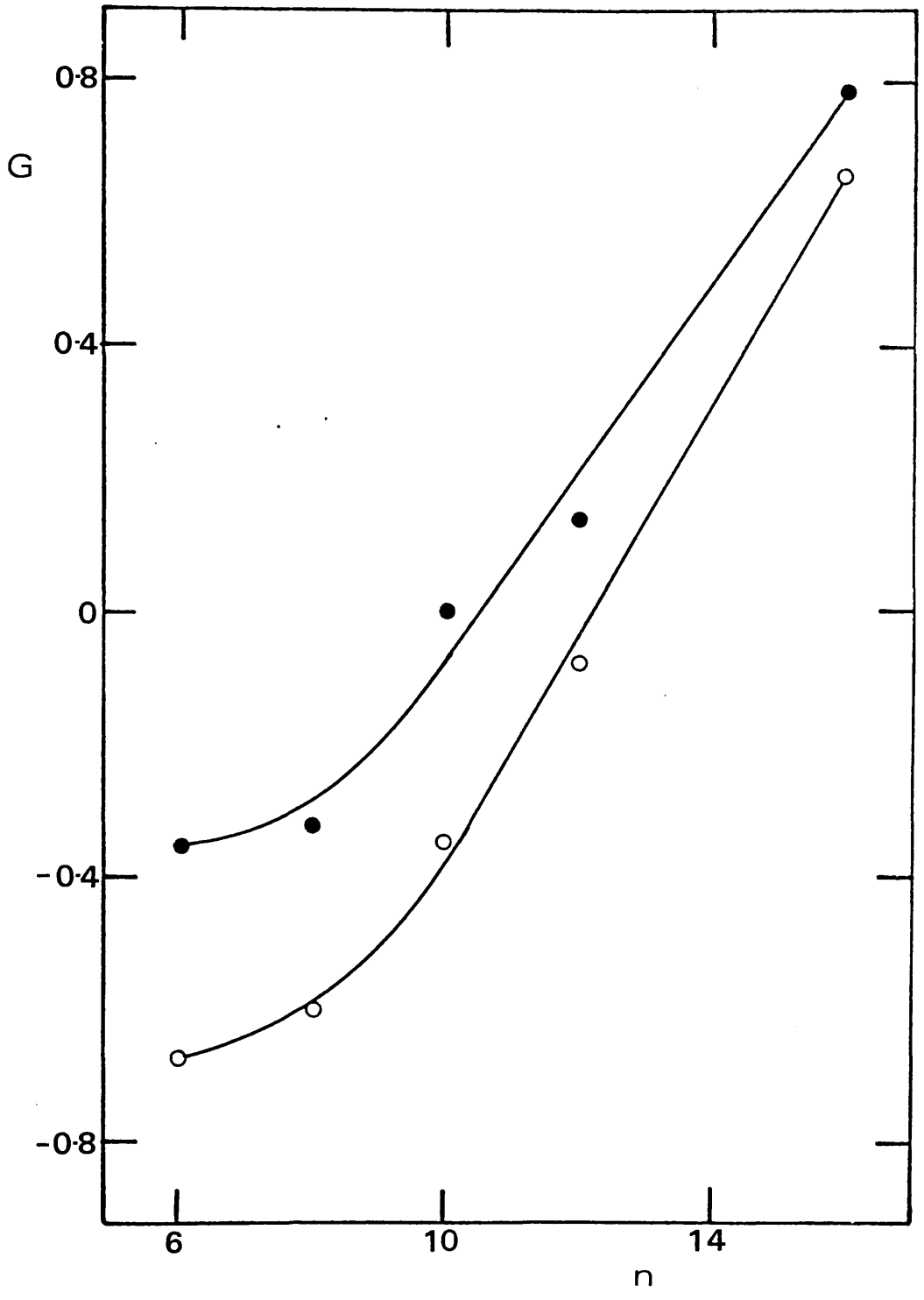

Figure 6.22 Variation in the Grunberg and Nissan Constant with n-Alkane Chain Length for Equimolar Benzene plus n-Alkane Mixtures. ○ *298 K,* ● *373 K.*

of benzene at a particular temperature a value for G can be read for any system of interest and the viscosity coefficient calculated to within an estimated accuracy of $\pm$ 1 percent.

The effect of pressure on the value of G was determined using the mixture viscosity coefficients reported in Chapter 4 for the n-hexane plus n-hexadecane system.

In Table 6.8, values of G are presented for this system up to 400 MPa. For a particular mixture the effect of an increase in temperature at constant pressure on the G values is negligible and G is constant within the accuracy of the measurement of the viscosity coefficients. For a particular isotherm the effect of an increase in pressure on G is first to reduce its value up to a pressure of 50 to 100 MPa after which the value increases with increase in pressure. This is illustrated in Figure 6.23 which presents G versus pressure at 373.2 K.

For pressures up to 100 MPa, mixture viscosity coefficients can be calculated to within $\pm$ 2 percent of the experimental values using equation (6.16) if values of G at atmospheric pressure are used. However, for pressures of 100 MPa and above the effect of pressure on G must be taken into account. The effect of change in composition and change in pressure on G under these conditions can be summarised by equation (6.17).

$$G = 1.58 - 1.7\, x_2 + 0.9\, x_2^2 + 0.001\, P \qquad (6.17)$$

where x_2 is the mole fraction of n-hexadecane and P is in MPa. Mixture viscosity coefficients calculated using equations (6.16) and (6.17) agree with the experimental values to within $\pm$ 2 percent.

Table 6.8

G Values for the n-Hexane plus n-Hexadecane System at Elevated Pressure

Temperature (K)	Pressure (MPa)	x^*_{HD}			
		0.200	0.400	0.600	0.800
298.2	0.1	1.29	1.12	0.95	0.92
323.2	0.1	1.37	1.14	1.00	0.90
	50.0	1.33	1.07	0.92	0.78
	100.0	1.38	1.16	0.99	0.90
348.2	0.1	1.43	1.07	1.05	0.91
	50.0	1.27	1.02	1.04	0.74
	100.0	1.38	1.14	0.99	0.92
	150.0	1.41	1.16	0.96	0.98
	200.0	1.50	1.28	1.02	0.98
	250.0	1.53	1.31	1.08	0.96
373.2	0.1	1.34	1.10	0.98	0.86
	50.0	1.34	1.08	1.00	0.81
	100.0	1.34	1.08	0.95	0.81
	150.0	1.41	1.13	1.02	0.90
	200.0	1.42	1.18	1.03	0.85
	250.0	1.46	1.22	1.08	0.96
	300.0	1.54	1.27	1.17	1.11
	350.0	1.57	1.30	1.17	1.11
	400.0	1.65	1.37	1.25	1.11

*HD = n-hexadecane

Thus it is possible to calculate the viscosity coefficient of any n-hexane plus n-hexadecane mixture at the temperatures and pressures of this work to within the estimated accuracy of the experimental measurements. To predict mixture viscosity coefficients at other temperatures and pressures it is first necessary to obtain the pure component viscosity coefficients under these conditions by interpolation. It is estimated that mixture viscosity coefficients calculated in this way will be

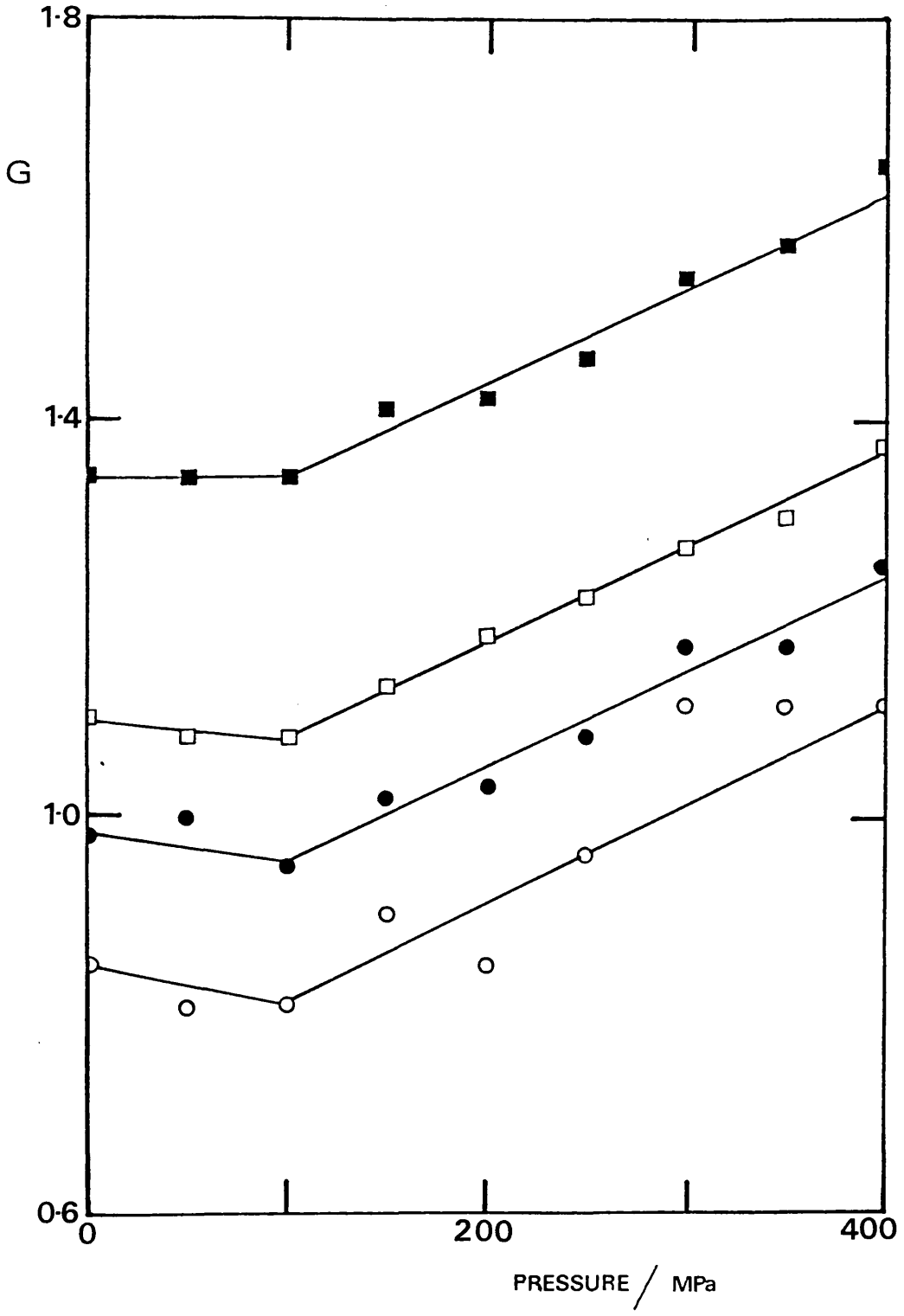

Figure 6.23 Dependence of G on Mole Fraction and Pressure for the n-Hexane plus n-Hexadecane System at 373 K. Mole Fraction of n-Hexadecane: ■ 0.200, □ 0.400, ● 0.600, ○ 0.800.

accurate to ± 4 percent.

CHAPTER 7

CONCLUSIONS

CHAPTER 7 - CONCLUSIONS

For the most satisfactory interpretation of transport property data for liquids and liquid mixtures, a rigorous theory based on a sound molecular model is required. At the present time the only successful molecular theory of transport is for dilute gases composed of structureless spherical particles. For molecular liquids and liquid mixtures it is necessary to take into account non-spherical molecular shape and the many-body interactions. Even with the advent of fast electronic computers it has proved possible to calculate viscosity coefficients only for certain model systems. Moreover, even if it were possible to represent molecular interactions in real polyatomic liquids correctly, the computer time involved in the calculation of viscosity coefficients is so great that other methods of prediction and correlation of viscosity coefficients would still be of the greatest importance.

In order to test the effectiveness of empirical and of semi-theoretical expressions, that is those which are based on a molecular model but which involve certain approximations in their derivation, for representing viscosity coefficient data it is essential to have accurate experimental data over a wide range of temperature and pressure. However, there are few measurements at elevated pressures and even at one atmosphere the data generally cover a very restricted range of temperature. For this reason, one of the aims of this research was the measurement at saturation pressure of viscosity coefficients for hydrocarbon mixtures specifically for two-component, three-component and four-component n-alkane mixtures from 285 K to 378 K and for binary benzene plus n-alkane mixtures, where the alkane was n-hexane, n-octane, n-decane, n-dodecane and n-hexadecane, and for benzene plus cyclohexane from 283 K to 393 K.

The estimated accuracy of these results is 0.5 percent. The specially designed viscometer and volume change apparatus allowed measurements to be made of the kinematic viscosity coefficient and density at temperatures above the boiling point of benzene and the lower n-alkanes. In order to investigate the effect of increased pressure, viscosity coefficients have been measured for n-hexane, n-hexadecane and four binary mixtures using a self-centring falling body viscometer from 298 K to 373 K at pressures up to the freezing pressure or 500 MPa with an estimated accuracy of 2 percent for the pure liquids and 3 percent for the mixtures. To overcome certain limitations in the viscometer, a new viscometer was designed, built and tested. An improved method for measurement of density at elevated pressure increased the accuracy to 0.2 percent.

These accurate measurements have been used to test the adequacy of the hard-sphere theories for representing viscosity coefficient data for real single component liquids. The density dependence of the results for n-hexane at any given temperature does follow closely the behaviour expected on the basis of the rough hard-sphere model for pressures up to 150 MPa. The derived value for the translational-rotational coupling constant was 1.48. The serious disadvantages of this approach are firstly that it can be applied only for densities up to the point where the system, considered as an assembly of hard-spheres, becomes solid. This occurs when the molar volume has decreased to one and a half times the volume of close packing which in practical terms for n-hexane corresponds to a pressure of about 150 MPa. However, n-hexane itself remains liquid over the whole pressure range covered in this work, up to 500 MPa and indeed up to much higher pressures. The model can therefore only be considered adequate over a very limited density range. The second point is that there is at present no method for calculating the trans-

lational-rotational coupling constant, except from viscosity coefficient data.

However, based on the rough hard-sphere model, a method for correlation of viscosity coefficients which has previously been applied to pseudo-spherical molecular liquids and rigid ring hydrocarbons was shown to work successfully for n-hexane, n-hexadecane and their binary mixtures. From a curve of η'*, defined as* $\eta V^{2/3}/(MT)^{1/2}$*, versus log* V' *obtained from experimental data on a given mixture at one temperature, it is possible to calculate viscosity coefficients for that mixture at any pressure at any other temperature, with an estimated accuracy of better than 5 percent, knowing the saturation pressure viscosity coefficient at that temperature. The one disadvantage is that it is necessary to know the molar volume at the pressure and temperature considered, but this method is very useful in that it satisfactorily correlates data for mixtures of given composition at different temperatures over the whole available pressure range.*

These results indicate that viscosity coefficients depend on molar volume and particularly on the volume relative to some reference volume which, in the case of hard-spheres, is the volume of close packing.

The free-volume expression proposed on the basis of hard-sphere theories and previously shown to account satisfactorily for viscosity coefficient data for pseudo-spherical molecular liquids and rigid ring hydrocarbons was applied to the data for the n-hexane plus n-hexadecane system. It was found that this form of equation was very satisfactory for representing viscosity coefficient data not only for these pure liquids but also for their mixtures. Moreover, the adjustable parameters in this

expression had values for the mixture which simply related to the values given by the pure liquids. The only disadvantage of this expression is that values are required for the molar volume of the system under the given experimental conditions. However, it correlates all the data very satisfactorily, and can be used for calculation of viscosity coefficients of any mixture for any density with an accuracy which is probably better than 3 percent. This semi-theoretical approach is most strongly recommended for the correlation and prediction of viscosity coefficients.

The idea that the viscosity coefficients depend on the molar volume is embodied also in the Batschinski equation recently modified by Hildebrand and the present accurate measurements provide a rigorous test of this equation. The results at saturation pressure confirm the findings of other workers that deviations from the equation occur at reduced temperatures below 0.46. Measurements above the normal boiling-point for benzene and n-hexane show that the equation is still valid at reduced temperatures up to 0.8. Consideration of the data for n-hexane and n-hexadecane at elevated pressure show that the fluidity is the same for a given liquid under different conditions of temperature and pressure, providing the molar volume is constant, only up to pressures of about 90 MPa. The Hildebrand equation is not valid for this system at higher pressures. Experimental viscosity coefficient data on mixtures at saturation pressure were used to test Bertrand's extension of the Hildebrand equation. For benzene plus n-dodecane the experimental results were in good agreement with values predicted from the data for the pure liquids. However, for benzene plus cyclohexane and for n-hexane plus n-hexadecane the results were significantly different.

A method which has proved successful for the correlation and prediction of viscosity coefficients of n-alkane mixtures at saturation pressure at 298 K involves the application of the Congruence Principle to the molar excess Gibbs free energy of activation of flow, $\Delta^{*}G^{E}$, which appears in the Eyring activation model. The present measurements show that the Congruence Principle does apply similarly at other temperatures but that increase in temperature leads to an increase in $\Delta^{*}G^{E}$. For accurate calculation of mixture viscosity coefficients it is essential to take values of $\Delta^{*}G^{E}$ from the curve for the temperature of interest. Increase in pressure also produces an increase in $\Delta^{*}G^{E}$ for the n-hexane plus n-hexadecane system and this also must be taken into account in the calculation of viscosity coefficients for n-alkane mixtures. For the benzene plus hydrocarbon systems studied the Congruence Principle does not apply but $\Delta^{*}G^{E}$ varies regularly from one member of a series to another where the second component is a n-alkane, at a given mole fraction at a given temperature. This makes it possible to determine $\Delta^{*}G^{E}$ for other benzene plus n-alkane mixtures and hence calculate the viscosity coefficient with an accuracy approaching that of the results for the pure liquids. This approach also requires knowledge of the molar volume and extensive measurements have to be made to establish the curves for $\Delta^{*}G^{E}$ as a function of composition, temperature and pressure. There is also some doubt concerning the validity of the underlying molecular model.

In view of the difficulties of developing a successful rigorous theory based on a sound molecular model, it is appropriate also to consider purely empirical relationships for the representation of mixture viscosity coefficients. The Grunberg and Nissan equation, a simple relation containing one adjustable parameter, which has been shown by

Irving to be most effective in representing viscosity coefficient data for mixtures was found to reproduce the present data practically to within the estimated experimental uncertainty provided that the Grunberg and Nissan constant was allowed to vary with temperature, pressure and composition. The outstanding advantage of this expression is that knowledge of the molar volumes is not required.

REFERENCES

REFERENCES

1. *J.O. Hirschfelder, C.F. Curtiss and R.B. Bird, 'Molecular Theory of Gases and Liquids' (Wiley, New York, 1954), Ch.8.*

2. *R.A. Aziz and H.H. Chen, J.Chem.Phys., 1977, 67, 5719.*

3. *Ref.(1), Section 8.2.*

4. *J.V. Sengers, M.H. Ernst and D.T. Gillespie, J.Chem.Phys., 1972, 56, 5583.*

5. *J. Weinstock, Phys.Rev., 1965, 140, A460.*

6. *S.Chapman and T.G. Cowling, 'The Mathematical Theory of Non-Uniform Gases' (Cambridge University Press, 1939), Ch.16.*

7. *M.K. Tham and K.E. Gubbins, J.Chem.Phys., 1971, 55, 268.*

8. *H.J.M. Hanley, R.D. McCarty and E.G.D. Cohen, Physica, 1972, 60, 322.*

9. *J.F. Ely and D.A. McQuarrie, J.Chem.Phys., 1974, 60, 4105.*

10. *B.J. Alder, D.M. Gass and T.E. Wainwright, J.Chem.Phys., 1970, 53, 3813.*

11. *J.H. Dymond, Physica, 1974, 75, 100.*

12. *D. Chandler, J.Chem.Phys., 1975, 62, 1358.*

13. *H.J. Parkhurst, Jr. and J. Jonas, J.Chem.Phys., 1975, 63, 2705.*

14. *H.J. Parkhurst, Jr. and J. Jonas, J.Chem.Phys., 1975, 63, 2698.*

15. *D.W. Rebertus and K.M. Sando, J.Chem.Phys., 1977, 67, 2585.*

16. *W.B. Streett and D.J. Tildesley, Proc.Roy.Soc.Lond., 1977, A 355, 239.*

17. *P.S.Y. Cheung and J.G. Powles, Mol.Phys., 1975, 30, 921.*

18. *J. Kushick and B.J. Berne, J.Chem.Phys., 1976, 64, 1362.*

19. *K. Nakanishi , K. Toukubo and N. Watanabe, J.Chem.Phys., 1978, 68, 2041.*

20. *K. Singer, J.V.L. Singer and A.J. Taylor, Mol.Phys., 1979, 37, 1239.*

21. Ya.M. Naziev, S.O. Guseinov and Yu.A. Badalov, Rev.Roum.Chim., 1975, 20, 55.

22. M.A. Aleskerov, A.A. Mamedov and Sh.Kh.Khalilov, Izv.Vyssh. Uchebn.Zaved., Neft Gaz., 1979, 22, 58.

23. J.D. Isdale, J.H. Dymond and T.A. Brawn, High Temp.-High Press., 1979, 11, 571.

24. J.D. Isdale and C.M. Spence, N.E.L. Report No.592 (National Engineering Laboratory, East Kilbride, Glasgow, 1975).

25. N.F. Carnahan and K.E. Starling, J.Chem.Phys., 1969, 51, 635.

26. B.J. Alder and T.E. Wainwright, 'The Many Body Problem' (Interscience Publishers, Inc., New York, 1963), p.511.

27. J.H. Dymond and B.J. Alder, J.Chem.Phys., 1966, 45, 2061.

28. J.H. Dymond, Proc.Symp.Thermophys.Prop., 6th 1973, 143-57. Edited by P.E. Liley, ASME: New York, N.Y.

29. T. Wainwright and B.J. Alder, Nuovo Cimento Suppl. 1958, 9, 116.

30. J.H. Dymond and T.A. Brawn, Proc.Symp.Thermophys.Prop., 1977, 7, 660.

31. A.J. Batschinski, Z. Physik.Chem., 1913, 84, 643.

32. J.H. Hildebrand, Science, 1971, 174, 490.

33. J.L. Dejardin, R. Marrony, C. Delseny and S. Brunet, Rheol. Acta, 1977, 16, 523.

34. L.D. Eicher and B.J. Zwolinski, Science, 1972, 177, 369.

35. H. Ertl and F.A.L. Dullien, J.Phys.Chem., 1973, 77, 3007.

36. G.L. Bertrand, Ind.Eng.Chem., Fundam., 1977, 16, 492.

37. A.K. Doolittle, J.Appl.Phys., 1951, 22, 1471.

38. A.K. Doolittle and D.B. Doolittle, J.Appl.Phys., 1957, 28, 901.

39. M.H. Cohen and D. Turnbull, J.Chem.Phys., 1959, 31, 1164.

40. D.L. Hogenboom, W. Webb and J.A. Dixon, J.Chem.Phys., 1967, 46, 2586.

41. J.A. Dixon and W. Webb, Proc.Am.Petrol.Inst.Section 8, 1962, 42, 146.

42. J.H. Dymond, Chem.Phys., 1976, 17, 101.

43. J.H. Dymond, Physica, 1976, 85A, 175.

44. W.M. Haynes, Physica, 1973, 67, 440.

45. W.M. Haynes, Physica, 1974, 76, 1.

46. W.M. Haynes, Physica, 1977, 89A, 569.

47. B.E. Eakin, K.E. Starling, J.P. Dolan and R.T. Ellington, J.Chem.Eng. Data, 1962, 7, 33.

48. L.T. Carmichael, V.M. Berry and B.H. Sage, J.Chem.Eng. Data, 1964, 9, 411.

49. S. Glasstone, K.J. Laidler and H. Eyring, 'Theory of Rate Processes' (McGraw-Hill, New York, 1941), Ch.9.

50. R.B. Bird, W.E. Stewart and E.N. Lightfoot, 'Transport Phenomena' (John Wiley & Sons, New York, 1960), p.28.

51. J.F. Kincaid, H. Eyring and A.E. Stearn, Chem.Rev., 1941, 28, 301.

52. J.H. Hildebrand and B.J. Alder, Ind.Eng.Chem., Fundam., 1973, 12, 387.

53. B.J. Alder and T. Einwohner, J.Chem.Phys., 1965, 43, 3399.

54. E.L. Heric and J.G. Brewer, J.Chem.Eng. Data, 1967, 12, 574.

55. T.M. Reed III and T.E. Taylor, J.Phys.Chem., 1958, 63, 58.

56. B.M. Coursey and E.L. Heric, Mol.Phys., 1967, 13, 287.

57. J.N. Bronsted and J. Koefoed, K.danske.Vidensk.Selsk.Skr., Mat.-fys.Medd, 1946, 22, 1.

58. I. Newton, Principia Lib.II., Sect.IX, 1685.

59. J.L.M. Poiseuille, Ann.Chim., 1843, 3 Serie 7, 50.

60. Methods for Determination of the Viscosity of Liquids. B.S.188: 1977 (British Standards Institution, British Standards House, 2, Park Street, London W.1).

61. A. Korosi and B.M. Fabuss, Anal.Chem., 1968, 40, 157.

62. J. Kestin, M. Sokolov and W. Wakeham, Appl.Sci.Res., 1973, 27, 241.

63. L. Korson, W. Drost-Hansen and F.J. Millero, J.Phys.Chem., 1969, 73, 34.

64. M.M. Couette, Ann.d.Chim.et Phys., 1890, 21, 433.

65. A. Finkener and R. Gartenmeister, Zeit.physik.Chem., 1890, 6, 524.

66. E.C. Bingham and G.F. White, Zeit.physik.Chem., 1912, 80, 684.

67. D.J. Kingham, W.A. Adams and M.J. McGuire, J.Chem.Eng. Data, 1974, 19, 1.

68. L.D. Eicher and B.J. Zwolinski, J.Phys.Chem., 1972, 76, 3295.

69. M.R. Cannon, R.E. Manning and J.D. Bell, Anal.Chem., 1960, 32, 355.

70. R.E. Wellman, R. DeWitt and R.B. Ellis, J.Chem.Phys., 1966, 44, 3070.

71. W.A. Caw and R.G. Wylie, Brit.J.Appl.Phys., 1961, 12, 94.

72. J. Kestin, M. Sokolov and W.A. Wakeham, J.Phys.Chem. Ref. Data., 1978, 7, 941.

73. G.D. Wedlake, J.H. Vera and G.A. Ratcliff, Rev.Sci.Instrum., 1979, 50, 93.

74. Chemical Rubber Company Handbook of Chemistry and Physics, 57th Edition (CRC Press, Inc., Cleveland, Ohio, 1977), p.D-179.

75. American Petroleum Institute Research Project 44, Texas A. and M. University, 1942, corrected 1953, 1955, 1973.

76. J.R. Coe, Jr. and T.B. Godfrey, J.Appl.Phys., 1944, 15, 625.

77. R.C. Hardy and R.L. Cottington, J.Res.Nat.Bur.Stand., 1949, 42, 573.

78. A. Nagashima, J.Phys.Chem.Ref.Data, 1977, 6, 1133.

79. Release on Dynamic Viscosity of Water Substance. The Eighth International Conference on the Properties of Steam, Giens, France, September 1975.

80. J.F. Swindells, J.R. Coe, Jr. and T.B. Godfrey, J.Res.Nat.Bur. Stand., 1952, 48, 1.

81. R.S. Marvin, J.Res.Nat.Bur.Stand., 1971, 75A, 535.

82. L.D. Eicher and B.J. Zwolinski, J.Phys.Chem., 1971, 75, 2016.

83. A. Weissberger, 'Physical Methods of Organic Chemistry, Part 1' (Interscience, New York, 1959), Ch.4.

84. G.W.C. Kaye and T.H. Laby, 'Tables of Physical and Chemical Constants and some Mathematical Functions, 14 Ed.' (Longman Group Ltd, London, 1973), p.173.

85. J.L. Hales and R. Townsend, J.Chem.Thermodyn., 1972, 4, 763.

86. R.M. Tennent, 'Science Data Book' (Oliver and Boyd, Edinburgh, 1971), p.61.

87. M. Diaz Pena and J. Nunez Delgado, J.Chem.Thermodyn., 1975, 7, 201.

88. T.M. Letcher, J.Chem.Thermodyn., 1975, 7, 205.

89. International Data Series, Selec.Data Mixtures, Ser.A., 1973, 100.

90. M. Diaz Pena and G. Tardajos, J.Chem.Thermodyn., 1978, 10, 19.

91. M. Diaz Pena and C. Menduina, J.Chem.Thermodyn., 1974, 6, 387.

92. O. Kiyohara and G.C. Benson, Can.J.Chem., 1973, 51, 2489.

93. International Data Series, Selec.Data Mixtures, Ser.A, 1975, 11.

94. N. Radojković, A. Tasić, D. Grozdanić, B. Djordjević and D. Malić, J.Chem.Thermodyn., 1977, 9, 349.

95. E. Alcart, G. Tardajos and M. Diaz Pena, J.Chem.Eng.Data, 1980, 25, 140.

96. S.-S. Chen and B.J. Zwolinski, J.Chem.Soc., Faraday Trans. II, 1974, 70, 1133.

97. J. Brunet and K.E. Gubbins, Trans.Faraday Soc., 1969, 65, 1255.

98. International Data Series, Selec.Data Mixtures, Ser.A, 1974, 124.

99. International Data Series, Selec.Data Mixtures, Ser.A, 1974, 132.

100. International Data Series, Selec.Data Mixtures, Ser.A, 1974, 203.

101. J. Jonas, D. Hasha and S.G. Huang, J.Phys.Chem., 1980, 84, 109.

102. J.D. Isdale, Engineering Sciences Data Item No.79027 (ESDU, 251-259, Regent St., London W1R 7AD).

103. D.L. Bidlack and D.K. Anderson, J.Phys.Chem., 1964, 68, 3790.

104. Kh.M. Khalilov, Zh.Eskp.Teor.Fiz., 1939, 9, 335.

105. P.E. Parisot and E.F. Johnson, J.Chem.Eng.Data, 1961, 6, 263.

106. Landolt Borenstein, Group II, Vol.5A, 1969.

107. F. Mato and J.L. Hernández, Anal.Quimica, 1969, 65B, 9.

108. L. Grunberg, Trans.Faraday Soc., 1954, 50, 1293.

109. R.J. Fort and W.R. Moore, Trans.Faraday Soc., 1966, 62, 1112.

110. H.M.N.H. Irving and R.B. Simpson, J.Inorg.Nucl.Chem., 1972, 34, 2241.

111. M.J. Mussche and L.A. Verhoeye, J.Chem.Eng.Data, 1975, 20, 46.

112. M.S. Medani and M.A. Hasan, Can.J.Chem.Eng., 1977, 55, 203.

113. J. Robertson, internal communication.

114. J.D. Isdale, Ph.D. Thesis, Glasgow: University of Strathclyde, 1976.

115. C.-Y. Wang, Rev.Sci.Instrum., 1967, 38, 24.

116. M.D. Boren, S.E. Babb, Jr. and G.J. Scott, Rev.Sci.Instrum., 1965, 36, 1456.

117. P.W. Bridgman, Proc.Am.Acad.Arts Sci., 1911, 47, 321.

118. P.W. Bridgman, Proc.Am.Acad.Arts Sci., 1940, 74, 1.

119. L.H. Adams, R.W. Goranson and R.E. Gibson, Rev.Sci.Instrum., 1937, 8, 230.

120. A. Michels and M. Lenssen, J.Sci.Instrum., 1934, 11, 345.

121. S.E. Babb, Jr., 'High Pressure Measurement' (Butterworth Scientific Publications, Washington, D.C., 1963), pp.115-124.

122. P.W. Bridgman, Proc.Am.Acad.Arts Sci., 1930, 66, 185.

123. T.A. Brawn, internal communication.

124. T. Grindley and J.E. Lind, Jr., J.Chem.Phys., 1971, 54, 3983.

125. G.S. Kell and E. Whalley, J.Chem.Phys., 1975, 62, 3496.

126. W.G. Scaife, C.G.R. Lyons, J.K. Vij and S. Ruttle, J.Phys.E: Sci. Instrum., 1977, 10, 874.

127. P.W. Bridgman, Proc.Am.Acad.Arts Sci. 1942, 74, 399.

128. M.S. Benson and J. Winnick, J.Chem.Eng.Data, 1976, 21, 432.

129. F.I. Mopsik, J.Res.Nat.Bur.Stand., 1967, 71A, 287.

130. H.E. Eduljee, D.M. Newitt and K.E. Weale, J.Chem.Soc., 1951, 3086.

131. A.K. Doolittle, J.Chem.Eng.Data, 1964, 9, 275.

132. A.S.M.E. Pressure Viscosity Report, New York, 1953, Vol.1.

133. A.T.J. Hayward, N.E.L. Report No.295 (National Engineering Laboratory, East Kilbridge, Glasgow, 1967).

134. D.W. Brazier and G.R. Freeman, Can.J.Chem., 1969, 47, 893.

135. P.W. Bridgman, Proc.Am.Acad.Arts Sci., 1926, 61, 57.

136. J.S. Rowlinson, 'Liquids and Liquid Mixtures' (Butterworth Scientific Publications, London, 1959).

137. R. Battino, Chem.Rev., 1971, 71, 5.

138. P. Picker, E. Tremblay and C. Jolicoeur, J.Solution Chem., 1974, 3, 377.

139. J.R. Goates, J.B. Ott and J.F. Moellmer, J.Chem.Thermodyn., 1977, 9, 249.

140. J.S. Brennan, R.J. Hill and F.L. Swinton, J.Chem.Thermodyn., 1978, 10, 169.

141. C. Harrison and J. Winnick, J.Chem.Eng.Data, 1967, 12, 176.

142. J.H. Dymond, K.J. Young and J.D. Isdale, J.Chem.Thermodyn., 1979, 11, 887.

143. P. Jeschke and G.M. Schneider, J.Chem.Thermodyn., 1978, 10, 803.

144. P.S. Snyder, M.S. Benson, H.S. Huang and J. Winnick, J.Chem. Eng. Data., 1974, 19, 157.

145. L.A. Woolf and K.R. Harris, Chem.Phys., 1978, 32, 349.

146. J.H. Dymond, J.Chem.Phys., 1974, 60, 969.

147. J.H. Hildebrand and R.H. Lamoreaux, J.Phys.Chem., 1973, 77, 1471.

148. A.L. Lee and R.T. Ellington, J.Chem.Eng.Data, 1965, 10, 346.

149. L. Grunberg and A.H. Nissan, Nature, 1949, 164, 799.

150. J.B. Irving, N.E.L. Report No.631 (National Engineering Laboratory, East Kilbride, Glasgow, 1977).

151. J.D. Isdale, Symposium on Transport Properties of Fluids and Fluid Mixtures: Their Measurement, Estimation, Correlation and Use, 10-11 April, 1979. Issued by N.E.L., East Kilbride, Glasgow, G75 0QU.